August 2016

The Function of Renalase

Brett Allen Beaupre
University of Wisconsin-Milwaukee

THE FUNCTION OF RENALASE

by

Brett A. Beaupre

A Dissertation Submitted in

Partial Fulfillment of the

Requirements for the Degree of

Doctor of Philosophy

in Chemistry

at

The University of Wisconsin-Milwaukee

August 2016

ABSTRACT

THE FUNCTION OF RENALASE

by

Brett A. Beaupre

The University of Wisconsin-Milwaukee, 2016
Under the Supervision of Professor Graham R. Moran

Renalase was originally reported to be an enzyme secreted into the blood by the kidney to lower blood pressure and slow heart rate. Despite multiple reports claiming to confirm this activity *in vivo* there has been considerable discord in regards to the reaction catalyzed by renalase. The structural topology of renalase resembles that of known flavoprotein oxidases, monooxygenases and demethylases, but the conserved active site residues are unique to renalase. It has been reported that the catalytic function of renalase is to oxidize circulating catecholamines, however *in vitro* studies have failed to demonstrate a catalytic activity in the presence of such molecules. We have identified renalase as a novel oxidase enzyme which catalyzes the oxidation of both 6-dihydro NAD(P) and 2-dihydro NAD(P) to β-NAD(P)$^+$ delivering the electrons harvested to dioxygen forming hydrogen peroxide. Catalysis involves the oxidation of the dihydropyridyl ring of the substrate by transferring two electrons to the flavin cofactor, followed by release of the oxidized β-NAD(P)$^+$ product, and then the reoxidation of the reduced cofactor. Renalase substrates, 2-dihydro and 6-dihydro NAD(P) are thought to arise from non-specific reduction of NAD(P)$^+$ or tautomerization of NAD(P)H. These aberrant nicotinamide isomers are potent inhibitors of dehydrogenase enzymes including those of glycolysis and the TCA cycle. It would therefore appear that the function of renalase is to eliminate this inhibitory threat to primary metabolism. In addition to identifying the true catalytic substrates and proposing a metabolic function we have also identified verifiably active forms of renalase from

Psuedomonas phaseolicola and *Pseudomonas aeruginosa, as well as* crystal structures of renalase from *P. phaseolicola* in complex with β-NAD^+ and β-NADH. The data presented in this dissertaion chronolog the discovery of a genuine catalytic role for renalase that is likely an important housekeeping function for all life forms.

To my wife,

Your love and support made this possible.

TABLE OF CONTENTS

LIST OF FIGURES

LIST OF TABLES

LIST OF SCHEMES

LIST OF ABREVIATIONS

Abbreviation	Meaning
ACP	acyl carrier protein
2DHNAD	2-dihydronicotinamide[a] adenine dinucleotide
6DHNAD	6-dihydronicotinamide adenine dinucleotide[a]
β-ME	beta-mercaptoethanol
β-NAD^+	oxidized nicotinamide adenine dinucleotide
β-NADH (4DHNAD)	reduced nicotinamide adenine dinucleotide
β-NADPH	reduced nicotinamide adenine dinucleotide phosphate
CS	chorismate synthase
DLD	lipoamide dehydrogenase
DMAP	dimethylallyl monophosphate
DMSO	dimethyl sulfoxide
Dopamine	4-(2-Aminoethyl)benzene-1,2-diol; Epinephrine, (*R*)-4-(1-Hydroxy-2-(methylamino)ethyl)benzene-1,2-diol
EPSP	5-enol-pyruculshikimate 3-phosphate
FAD	flavin adenine dinucleotide
$FADH_2$	reduced flavin adenine dinucleotide
fdc1	ferulic acid decarboxylase
FMN	flavin mononucleotide
$FMNH_2$	reduced flavin mononucleotide
HEPES	4-(2-hydroxyethyl)-1-piperazineethanesulfonic acid

HsRen	renalase from *Homo sapien*
HPLC	high pressure liquid chromatography
IC50	50% inhibitory concentration
IPTG	isopropyl-β-thiogalactopyranoside
ITC	isothermal titration calorimetry
L-DOPA	L-3,4-Dihydroxyphenylalanine
LB	Luria Bertani media
LDH	lactate dehydrogenase
MAO	monoamine oxidase
MDH	malate dehydrogenase
NAD	nicotinamide adenine dinucleotide
NADP	nicotinamide adenine dinucleotide phosphate
NADPH	reduced nicotinamide adenine dinucleotide phosphate
NESGC	North East Structural Genomics Consortium
NMR	nuclear magnetic resonance
OYE	old yellow enzyme
pad1	phenylacrylic acid decarboxylase
PCR	polymerase chain reaction
PDB	Protein Data Bank
PpRen	renalase from *Pseudomonas Syringae* (van Hall pathovar *phaseolicola* strain 1448A)
$prFMNH_2$	prenylated flavin mononucleotide
$prFMN_{imminium}$	immium prenylated flavin mononucleotide

$prFMN_{radical}$	radical prenylated flavin mononucleotide
Renalase	human renalase variant 1
SSM	secondary-structure matching
TMG	trimethylglycine
ubiD	3-otcaprenyl-4-hydroxybenzoate carboxy-lyase
ubiX	3-otcaprenyl-4-hydroxybenzoate carboxy-lyase
UDP	uridine diphosphate
UDP-galp	UDP-galactopyranose
UDP-galf	UDP-galactofuranose
UGM	UDP galactopyranose mutase

a – The naming convention used throughout this article is based on common usage for reduced nicotinamide bases. Early naming of reduced NAD(P) molecules used 1,2-, 1,4-, or 1,6-dihydroNAD. However, reduced nicotinamides gain only a single hydrogen at the position of reduction and are therefore formally 2, 4, or 6-monohydronicotinamides. We have chosen instead the descriptive hybrid name of n-dihydronicotinamide (n-DHNAD) based on the current convention of describing the reduced pyridyl ring of NAD as a dihydropyridyl moiety.

ACKNOWLEDGEMENTS

First and foremost I would like to thank my thesis advisor Dr. Graham R. Moran, your enthusiasm propelled my curiosity and your shared knowlegde allowed me to apply this curiosity to sound discovery. Dr. Moran is a gifted mentor that shares his scientific passion to motivate everyone that enters the laboratory.

I would also like to thank the member of my thesis comittee, Dr. Andy Pacheco, Dr. Nicholas Silvaggi, Dr. Gilherme Indig and Dr. Alan Schwabacher. Their combined knowledge has helped guide my research and provided creative solutions for a multitude of research related conundrums. Thank you all for your help and support.

Furthermore, science is a team effort and without the support and collaboration of other gifted scientists progression is difficult. With that in mind I would like to thank all those that have contributed to this project, Dr. John Conrad, Dr. Dhara Shah, Matt Hoag, Joseph Roman, Brenton Carmicheal, Holger Foersterling and Neal Korfhage.

Chapter I.

New Chemistry for an old Cofactor: Recent Advancements in the Study of Flavoproteins

Brett A. Beaupre and Graham R. Moran

Abstract

Flavin cofactors are commonly recruited by enzymes know as flavoproteins where the cofactor plays an important role catalyzing many diverse reactions in a multitude of different organism. Most commonly, flavins are employed to mediate redox reactions involving both one- or two-electron chemistries but have also been observed to catalyze many unique and unprecedented reactions. In this article we present recent advancements involving six unique flavoproteins; 1) chorismate synthase and 2) UDP-galactorpyranose, which catalyze redox neutral reactions, 3) UbiD/Fdc1, which require a unique 4-ringed modified flavin supplied by UbiX/Pad1, 4) EncM, which requires a unique "super oxidized" flavin-N(5)-oxide species for catalysis, 5) renalase, which uses a tradition flavin redox chemistries to oxidize a unique substrate and 6) choline oxidase, which catalyzes a set of two reactions that normally requires two separate enzymes.

Introduction

Enzymes catalyze chemical reactions and as such are integral to life. Collectively, enzymes exhibit a myriad of strategies to promote specific chemistries. While many enzymes are formed only from polymerization of the twenty known proteinogenic amino acids, some reactions require more specialized entities to facilitate chemistry. It is common for

enzymes to contain an organic or inorganic prosthetic group that forms an association with the apoenzyme and is required for catalytic function. These groups are described collectively as cofactors. One of the most intensively studied cofactors is the flavin, a riboflavin derived cofactor that acts as a precursor for two nucleotide forms, flavin adenine dinucleotide (FAD), and flavin mononucleotide (FMN)

Flavins are most often employed to mediate in oxidation/reduction reactions where the isoalloxazine ring system acts as both an oxidizing and reducing participant. This chemical capacity is made more versatile by the fact that the isoalloxazine can stabilize three redox states: oxidized, one-electron reduced (semiquinone) and two-electron reduced.

In addition to redox chemistries, flavins have been shown to be involved in catalysis where no net redox change occurs. In this scenario the reduced isoalloxazine ring acts as an acid or a base to facilitate rebounding electron transfer or generate covalent intermediates. In this article we present relatively recently identified oddities in the spectrum of known catalytic chemistries facilitated by flavin cofactors. These include enzymes that utilize a flavin-N(5)-oxide (EncM), another that requires a four-ringed prenylated flavin (UbiD/Fdc1), two examples of redox neutral flavin reactions (chorismate synthase and UDP galactopyranose mutase), an enzyme that takes advantage of traditional flavin redox roles to recognize, bind and react a unique substrate (renalase), and also a flavin dependent enzyme that undergoes two redox reactions to catalyze a reaction normally requiring two enzymes (choline oxidase).

Renalase

In 2005 a new gene product was discovered whose expression was prominent in the kidney. The primary structure of this protein, named renalase, bore a minor resemblance to monoamine oxidase enzymes (13 - 17% amino acid identity). This low level of sequence similarity and an tenuous account of catecholamine oxidase activity was all that was offered to categorize renalase as the third monoamine oxidase, MAO C (*1*). Through the ensuing decade the renalase literature record has accrued an exponential increase in articles. These reports have purported multifarious claims of native catalytic activity and associated physiological effects (*2-35*). This had occurred despite a near complete lack of verified *in vitro* catalytic activity. The current prevailing belief is that renalase is an enzyme/hormone that is secreted by the kidney to slow the heart and diminish vascular tone by oxidizing circulating catecholamine neurotransmitters (*1-29, 31, 35-47*). Attempts to challenge this notion have largely gone unheeded (*48-58*). However, more recent evidence for an unexpected catalytic role for renalase undermines the prevalent notions of its function. In this newly discovered role, renalase has an apparent intracellular housekeeping function that ameliorates the threat of specific toxic isomers of NAD(P)H. The substrates identified were 2-dihydroNAD(P) and 6-dihydroNAD(P) both of which are highly isosteric with NADPH and inhibit enzymes that require reduced nicotinamide nucleotides as substrates (*55*). Despite the dissonance in literature the true substrates (*53, 55*) and the newly proposed metabolic role (*55, 56*) for renalase represent an odd variant of what is otherwise common flavin/nicotinamide hydride transfer redox chemistry. This synopsis of the renalase literature is offered as a retrospective analysis of the bases of the misconceptions that have arisen and persisted for this enzyme.

Renalase was originally identified from a 2003 genomic library in an attempt to find novel kidney secreted factors. The screen located a 37.8 kDa, apparently FAD- dependent protein that could also be detected in heart skeletal muscle, and liver tissue (*1*). Claims of catecholamine oxidase activity highlight the inherent limitations of assigning function from sequence. The overall motif structure and length of the protein was reminiscent monoamine oxidases, and this otherwise isolated correlation resulted in a functional conclusion that in turn led directly to claims of a hemodynamic influence that was further compounded by corresponding claims. The initial work asserted that a single bolus injection of renalase decreased both systolic and diastolic pressure 23-33% in Sprague-Dawley rats within 30 sec. This, now inexplicable claim led directly to the notion that renalase must function by eliminating catecholamines and presumably, based on the primary structure, by oxidation (*1*).

Catalytic catecholamine oxidase activity was determined using a generic oxidase assay that employs Amplex red and peroxidase to report hydrogen peroxide (H_2O_2) concentration. In an incubation of catecholamines in the presence of renalase, 0.25% of the dye was converted resulting from 1.8 to 3.2 nmol H_2O_2 mg^{-1} min^{-1} or 0.004 s^{-1}. Multiple reports cite such minimal rates of H_2O_2 evolution as resulting from non-enzymatic redox chemistry (*48, 50, 59*). Both catecholamines and $FADH_2$ are able to participate in autoxidative single electron chemistries with dioxygen resulting in the generation of H_2O_2. Unfortunately, no control reactions were included in the experiments that initially claimed renalase's function. The reply to the criticism that the exceeding low rate of hydrogen peroxide production was likely non-enzymatic autooxidation of catecholamines was that the claimed activity was observed in the absence of the co-substrate β-NAD(P)H and was

therefore not the true chemistry (*13*). The Desir group referred to the presence of a GXXXG or Rossman fold motif close to the N-terminus that would be available to bind the nicotinamide dinucleotide and reported that the addition of β-NADH caused a pronounced increase in activity compared to earlier reports (*2*). A proposed overall reaction (Scheme 1.1) was offered claiming as the aminochrome product (*2*). The reaction was said to be comprised of the renalase FAD cofactor being reduced by electrons received from β-NADH and subsequently delivered to dioxygen generating a flavin semiquinone and a superoxide anion that exclusively oxidizes catecholamines in multiple one-electron steps.

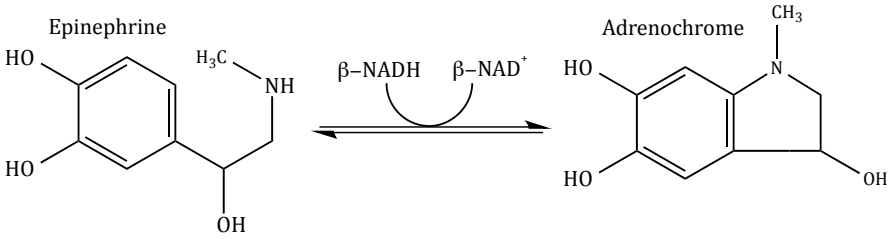

Scheme 1.1. The initial proposal for the reaction catalyzed by renalase

The Aliverti group published a crystal structure of renalase from *Homo sapiens* (PDB code 3QJ4) in 2011. In this structure it was revealed that the function of the GXXXG Rossman fold motif was to bind the adenosine moiety of the FAD and there was no classical site for β-NADH interaction (*60*). This group also conducted the first independent attempt to verify renalase activity with catecholamines concluded that compared to the appropriate control reactions, renalase did not oxidize catecholamines and the interaction between the renalase FAD and β -NADH is due to the slow promiscuous redox chemistry of the two molecules (*61*). They also demonstrated that under anaerobic conditions prolonged

incubation of renalase with β-NADH results in the reduction of the FAD cofactor and that this was the rate limiting process in the experiments described by Desir et al. (*2*). Aliverti et al. also reported that renalase possesses diaphorase activity when incubated with either β-NADH and β-NADPH with a preference for β-NADPH, and described kinetic parameters that parallel initial observations made by Desir et al. (*2*) in the presence of a variety of electron acceptors, concluding that this interaction is actually a predicted, non-enzymatic side reactions facilitated by the large solvent exposed active site cavity which facilitates access for the redox interaction between the flavin and β-NADH(*51*).

Despite this apparently sound refutation, the prevalence of the belief in a physiological role for renalase's activity and function has remained and stands as an interesting example of the lasting influence of erroneous data in science. This synoposis of renalase will not focus further on the multifarious claims for the function of renalase. For a more comprehensive reviews of this topic see, Moran 2016(*58*), Malyszko et al 2014 (*52*), and Baroni et al 2013 (*51*) and Li et al 2014 (*7*). The focus of this section will be the discovery of what appears to be a true catalytic function of for this enzyme.

Our group presented the first report of genuinely catalytic activity for renalase in 2013. We showed that under anaerobic conditions the renalase FAD cofactor could undergo rapid reduction (~40 s^{-1}) when reacted with a contaminant found in β-NADH (1.3%) or β-NADPH (4%) (*53, 54*) solutions. This rate was four-orders of magnitude more rapid than prior activity reports (*36*). These apparent substrate molecules induce multiple enzymatic turnovers converting the contaminant β-NAD(P)$^+$ and delivering two electrons to dioxygen resulting in the production of H_2O_2 with 1,1:1,1 stoichiometry. The fleeting nature of the β-NAD(P)H contaminant substrates required the establishment of regimented

separation and purification techniques to obtain pure, quazi-stable substrate. Initially only one form of the substrate was described (contaminant species), but guided by a literature trail dating back to the 1950's (*62-66*) we determined that incubation of β-NAD(P)$^+$ with a strong reductant (sodium borohydride) results in the formation of 3 distinct products with an observed extinction coefficients and absorbance maxima of, ε_{340nm} = 6220 $M^{-1}cm^{-1}$, ε_{345nm} = 6580 $M^{-1}cm^{-1}$ and ε_{394nm} = 5360 $M^{-1}cm^{-1}$. NMR and mass spectrometry confirmed that the species with 340 nm λmax was β-NAD(P)H (4-dihydroNAD(P)), that the 345 nm λmax species was 6-dihydroNAD(P) and the 394nm λmax species was 2-dihydroNAD(P). Interestingly, both 6-dihydroNAD(P) (the initial contaminant identified) and 2-dihydroNAD(P) were substrates for renalase and both yield β-NAD(P)$^+$ as product (*55*). These substrates induced reduction of the renalase cofactor with respective rate constants of 230 s^{-1} and 860 s^{-1} with associated dissociation constants (K_d) of 166 μM and 173 μM for the E•S complexes. The observed rate constant for flavin re-oxidation by reducing dioxygen (k_{ox}) was 5 x 10^3 $M^{-1}s^{-1}$. To determine if flavin re-oxidation was contingent on product release, reduction potential measurements were conducted and revealed similar reduction potentials (~150 mV) for both the oxidized enzyme and the β-NAD$^+$ (or product) complex suggesting that the propensity for re-oxidation of the flavin cofactor is not influenced by the presence of the product. Moreover, it was shown that exogenous addition of β-NAD$^+$ could not suppress the reoxidation rate constant even at near saturating concentrations, establishing that the free reduced enzyme and the enzyme product complex were equally able to reduce dioxygen. These results allowed us to construct a proposed mechanism for human renalase (Scheme 1.2).

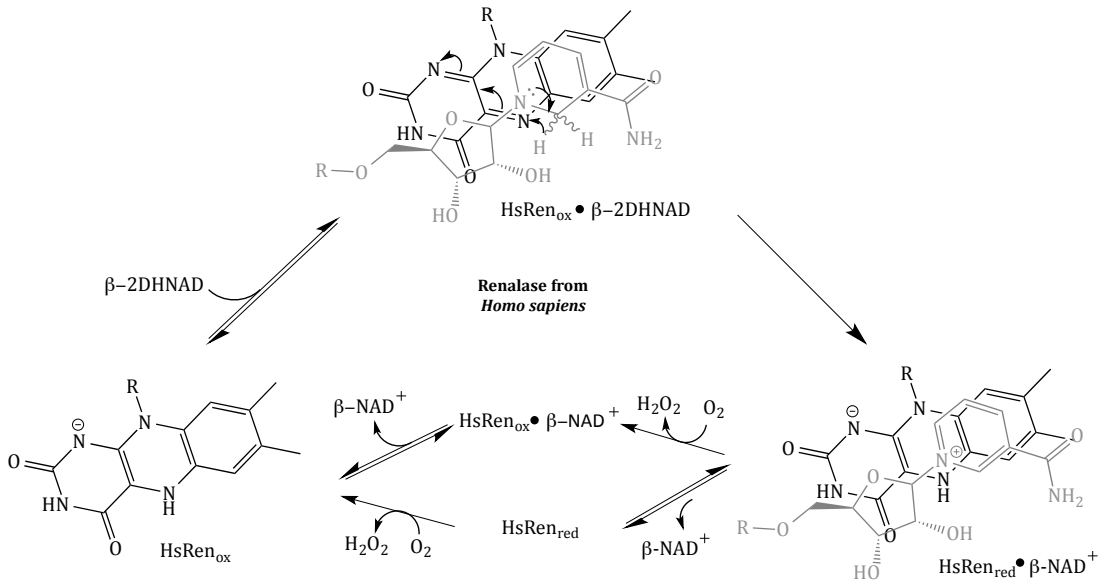

Scheme 1.2. Proposed chemical and kinetic mechanism of human renalase. (shown 2-dihydroNAD(P) as substrate).

Collectively, these observations permitted the proposal that renalase functions as a oxidase enzyme whose purpose is to recycle erroneous reduced forms of reduced nicotinamide nucleotides that are generated in non-specific reduction reactions of β-NAD(P)$^+$ (Scheme 1.3).

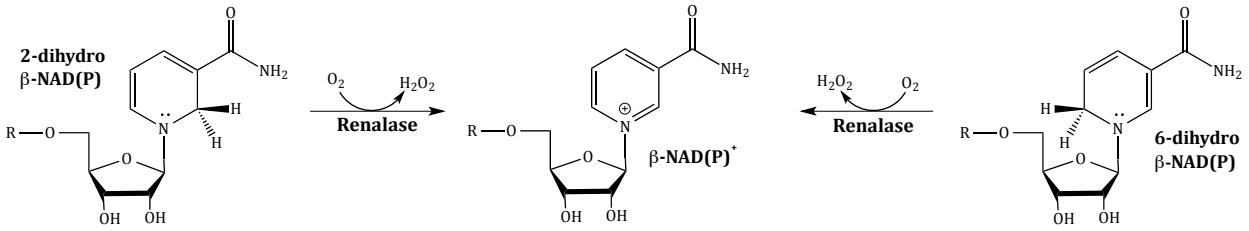

Scheme 1.3. Reactions catalyzed by renalase.

The observations made in 1961 by Lowry et al, and Godtfredsen (*67, 68*) not only aided our substrate identification, but they also prompted an investigation into the potential physiological function of renalase. We monitored turnover of malate dehydrogenase, lactate dehydrogenase, and dihydrolipoamide dehydrogenase in the presence of either 2- or 6-dihydroNAD. The data suggested that 2- and 6-position isomeric forms of β-NAD(P)H pose a significant threat to primary metabolism dehydrogenase enzymes with inhibition constants (Ki) values in the nMolar range(*55*). Not only was this the first evidence for alternate configurations/isomers of β-NAD(P)H being biologically active and the first evidence for their occurence in metabolism.

The identification of apparent true substrates for renalase also verified that the enzyme was fully active and thus presented the opportunity to revisit the initial renalase observations and conduct the conclusive control reactions for claimed catecholamine oxidase activity. These experiments definitively demonstrated that renalase does not catalyze the oxidation of catecholamines to aminochromes and the accumulation of H_2O_2 is a result of non-enzymatic interactions between β-NAD(P)H, FAD and dioxygen (*57*). The results also indicated that the generation of aminochrome is higher when renalase is replaced with FAD alone, supporting the idea that binding of FAD to renalase actually shelters the cofactor against NAD(P)H reduction. In this article it was also concluded that renalase does not have a prorenalase form that is only active in blood as previously proposed (*11*). The catalytic activity is not modulated in 50% blood plasma and/or by the presence of catecholamines.

The proposed amelioration of the threat posed by NAD(P)H isomers suggests that renalase should be found in other forms of life. However, BLAST sequence alignments do

not recover sequences from Kingdoms other than the *animalia*. If renalase could be identified in an organism without a pulmonary system this would be at least partially antithetical to physiological claims for the role of renalases catalytic function. To this end, Hoag et al., recently discovered a bacterial form of renalase from *P. phaseolicola (56)*. This enzyme was previously labeled generically as an "amine oxidase" (from *Psuedomonas syringe* VanHall pathovar *phaseolicola* strain 1448A) and the crystal structure of this protein had been solved by the NESGC in 2009 (PDB cod KKJ). While this enzyme displayed only 19% sequence identity to renalase from *H. sapiens* the active site constellation was highly similar. It was confirmed that this putative bacterial renalase was indeed able to rapidly oxidize the same isomers of β-NAD(P)H. The crystal stuctures of this enzyme bound to β-NAD^+ (2.0 Å, PDB code 4ZCD), the enzyme•product complex, and β-NADH (1.66 Å, PDB code 4ZCC) which is representative of the enzyme•substrate complex gave the first insights into renalase active site interactions (*vide infra*) (*56*).

The kinetic parameters obtained from transient state analysis of the reductive and oxidative half reactions of this bacterial renalase with all four known substrates (NAD and NADP derived) indicated unique substrate preferences with rate constants for reduction of 130 s^{-1}, 4 s^{-1}, 0.4 s^{-1} and 0.5 s^{-1} and dissociation constants of 36 μM, 468 μM, 28 μM and 1380 μM for 2-dihydroNAD, 2-dihydroNADP, 6-dihydroNAD and 6-dihydroNADP respectively. As such renalase from *P. phaseolicola* displays a preference for β-NAD^+ derived substrates binding them 10 to 50-fold more tightly then β-$NADP^+$ derived substrates as described by their dissociation constants. However, it also has a marked preference in terms of reduction rate constant for 2-dihydro- over 6-dihydro- substrates.

This observation is in contrast to observed dissociation constants for renalase from *H. sapiens* where only a 2-fold preference for 6-dihydroNAD when compared to 6-dihydroNADP and no pronounced isomer preference. The ratio of the reduction rate constant of the dissociation constant (k_{red}/K_d) indicates that the bacterial enzyme has a 20 (2-dihydroNADP) to 10000 (6-dihydroNADP)-fold preference for 2-dihydroNAD.

While crystal structures did not provide a full explanation for β-NAD versus β-NADP-derived isomer selectivity they did offer insight into isomer selectivity for the rates of reduction. β-NADH binds to the active site in a conformation where the 4-dihydro-nicotinamide moiety stacks above flavin isoalloxazine ring placing the 2'-hydrogen directly adjacent (3.6 Å) to the flavin N5. This orientation is aided by Threonine 185 that forms a hydrogen bond with the nicotinamide amide. While the active site can accommodate the "flipped" conformation that would place the -6-position of the nicotinamide adjacent to N5, no evidence for this binding mode was observed in the E•β-NADH structure. The basis for discrimination against the 4-dihydroNA(P) species was apparent as this position is not sufficiently proximal to flavin isoalloxazine N5 to aid hydride transfer (in either binding mode) (Figure 1.1).

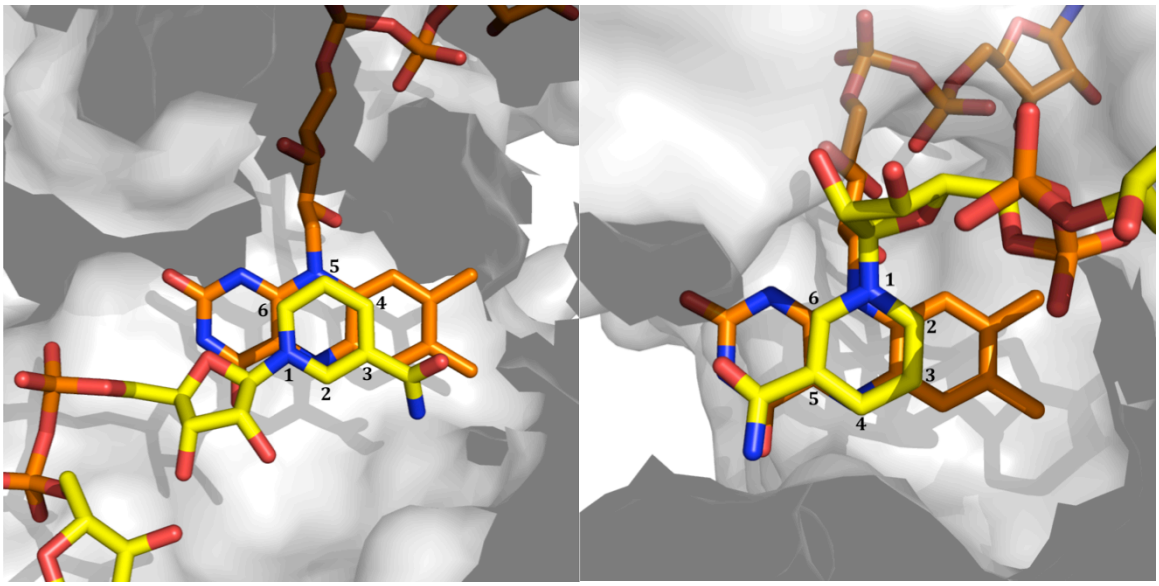

Figure 1.1. Enzyme substrate complexes. **A**. Renalase from *P. phaseolicola* in complex with β-NADH. **B**. Glutathione reductase from *H. sapiens* in complex with β-NADH.

Comparisons of Ppren and Hsren active sites revealed that multiple conserved residues lined the internal cavity of the binding pocket where W276 (HsRen W288), Y57 (HsRen Y62) and H232 (HsRen H245) are conserved and residues T185 (HsRen R193), W212 (HsRen F223) and F204 (HsRen Y214) present a similar functional groups in conserved locations yet these residues arise from different portions of the secondary structure. (Figure 1.2)

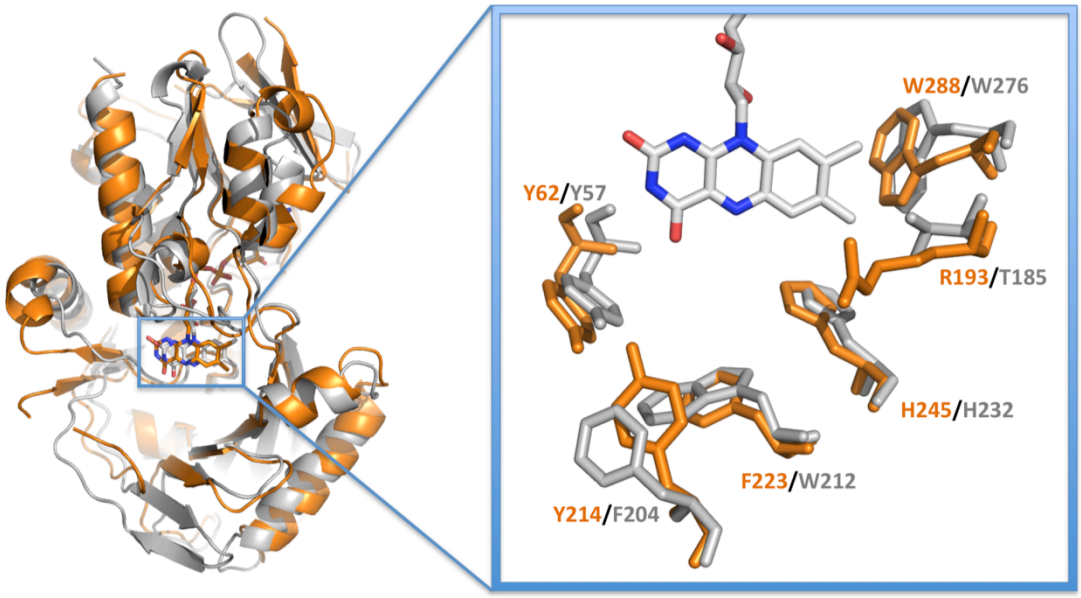

Figure 1.2. Overlay of crystal structures of renalase from *P. phaseolicola* (grey) and *H. sapiens* (orange) and overlay of partially conserved active site residues.

Though the bacterial form of renalase shows active site similarities and paralleled catalytic activity it was determined that the mechanism of action was slightly deviated from its human counterpart. The bimolecular rate constant (k_{ox}) for reoxidation of the flavin cofactor of renalase from *P. phaseolicola* (5 x 10^{-3} $M^{-1}s^{-1}$) was similar to that of the human enzyme (2.9 x 10^{3} $M^{-1}s^{-1}$). However, the reoxidation of bacterial renalase was inhibited by exogenous β-NAD^+ yielding a dissociation constant (K_d) of 230 μM for the reduced enzyme•β-NAD^+ complex. This observation is indicative of a ordered product release where the β-$NAD(P)^+$ product must dissociated from the reduced enzyme before reoxidation of the flavin cofactor can occur. The proposed mechanism of renalase from *P. phaseolicola* is presented in Scheme 1.4.

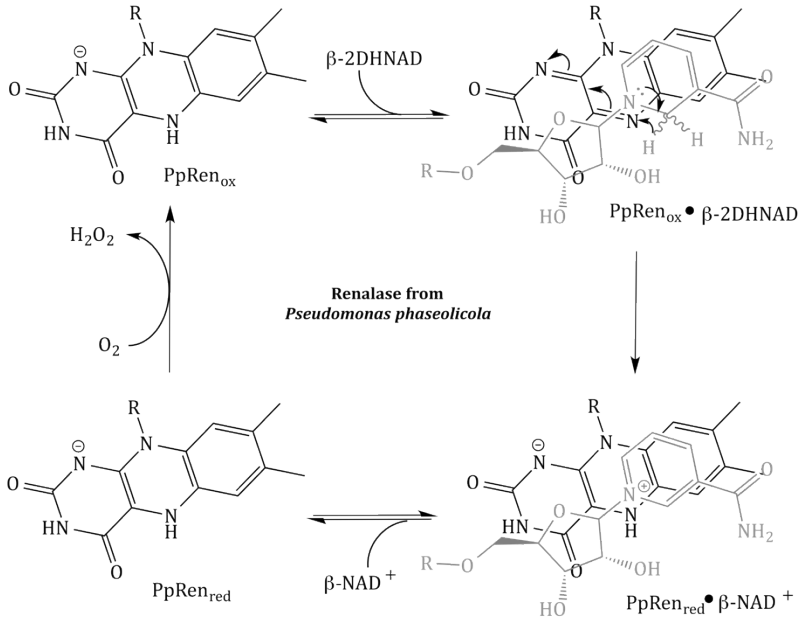

Scheme 1.4. Proposed mechanism of bacterial renalase shown with 2- dihydroNAD(P) as substrate.

A decade of discord has preceded the identification of a substantiated catalytic mechanism and metabolic function of enzyme renalase. Isomeric forms of reduced nicotinamide species pose an inhibitory threat to primary metabolism and renalase can alleviate this simply by oxidation to form β-NAD(P)$^+$. The observations made by the Moran group represent the first evidence for the in vivo occurrence of 2-dihydroNAD(P) and 6-dihydroNAD(P) which are presumably generated from nonspecific reduction reactions of β-NAD(P)$^+$. The catalytic mechanism is a simple oxidase reaction where the true genius lies in the ability for renalase to accommodate hydride transfer from 2 different positions (2' and 6') on the nicotinamide ring while discriminating against a 3rd position (4') and couple this to the reduction of dioxygen providing a very high driving force (an therefore scavenging capacity) for the chemistry.

Choline oxidase

The 4-electron oxidation of choline to glycine betaine (trimethylglycine, TMG) is an important transformation for many forms of life. TMG plays an important role in osmoregulation where it is utilized as an organic osmolyte in both eukaryotes and prokaryotes in response to various sources of external stress including extreme temperature fluctuations and changes in osmotic pressure (*69-79*). In bacteria omsomlytic control of the cytoplasm is imperative to survival and is largely controlled by the intercellular solute concentration failure to do so would result in plasmolysis or cytolysis as a result of the water flux. Studies have shown a large influx of choline and its precursors at sites of infection (*80, 81*) and have also demonstrated that multiple infectious bacteria including *Escherichia coli, vibrio cholera, Klesiella pneumonia, Enterococus faecalis, Listeria monocytogenes* and *Pseudomonas aeruginosa* modulate cytoplasmic concentrations of TMG which allows for growth in hyperosmotic media (*82-86*). Furthermore observations have correlated high intracellular osmolarity with up regulation of the genes associated with virulence and cellular invasion in multiple human pathogens (*87-92*). These observations have prompted investigations into the mechanism of enzymes involved in the oxidation of choline, specifically focusing on inhibition of choline oxidase to enhance susceptibility to conventional treatments (*87*).

In plants TMG is found in the chloroplast where it is responsible for modulation of the thylakoid membrane in order to maintain photosynthetic efficiency in response to external stresses (*93, 94*). It was shown that over-production of the genes responsible for the regulation of TMG biosynthesis in transgenic species was shown to increase tolerance to osmotic fluctuations and temperature extremes (*94, 95*). The implications of these

observations have resulted in exploration enhancing TMG production as a method for bioengineering stress tolerant crops species (*74, 75, 87*).

TMG is formed in three unique ways; in one pathway choline initially undergoes a 2-electron oxidation by choline dehydrogenase, which is found in mammals bacteria and fungi, resulting in the formation betaine aldehyde which is then gives a pair of electrons to betaine aldehyde dehydrogenase forming TMG. Plants lack choline dehydrogenase and thus utilize choline monooxygenase for the initial oxidation of choline to betaine aldehyde that is further oxidized to glycine betaine by betaine aldehyde dehydrogenase. The third pathway is found in *Arthrobacter globiformis* and is unique requiring only a single enzyme, choline oxidase to catalyze the 4-electron oxidation required to convert choline to glycine betaine. (Scheme 1.5)

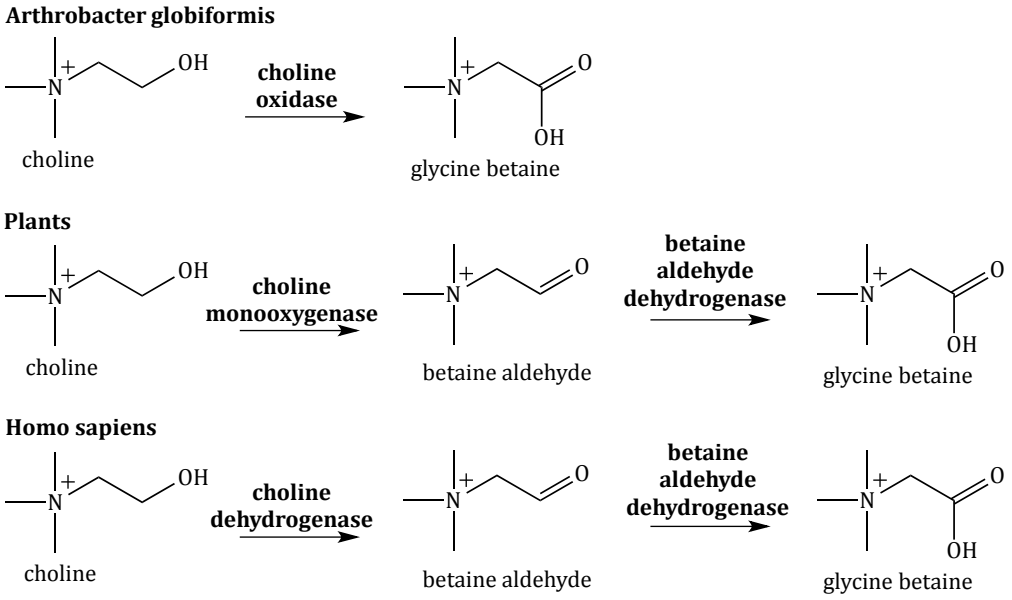

Scheme 1.5. Known pathways of oxidation of choline to glycine betaine.

Despite the multiple pathways that utilize collectively four enzymes to oxidize choline to TMG the primary focus of the enzymology community has been the reaction of choline oxidase. Choline oxidase is a unique flavoprotein that catalyzes the 4-electron oxidation of choline, involving two separate, rate-limiting hydride transfer steps (Scheme 1.6). The biochemical function and mechanism of choline oxidase have been extensively investigated (*87, 96-121*) and have revealed a two-step oxidation reaction involving two separate hydride transfers bridged by an aldehyde intermediate species (*97, 102, 109*).

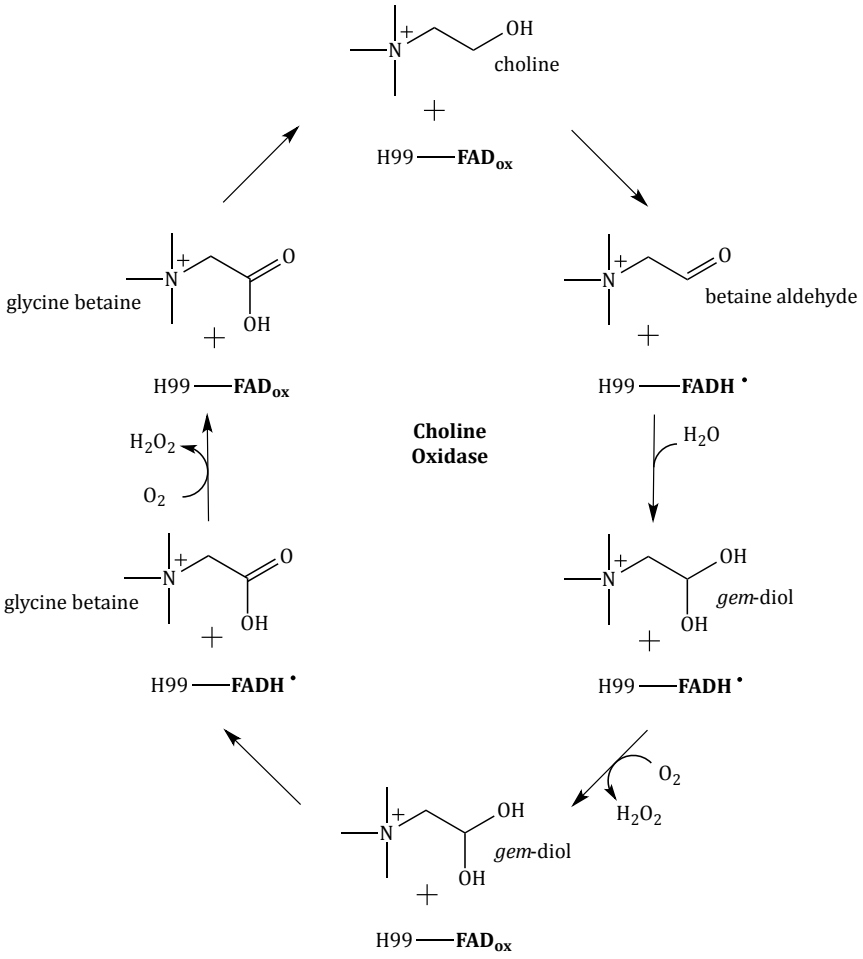

Scheme 1.6. Proposed steps in the oxidation of choline to glycine betaine by choline oxidase from *Arthrobacter globiformis.*

Initially, choline enters the active site via a small tunnel, lined with hydrophobic residues, extending from the active site to the solvent exposed surface of the enzyme mediated by a gated mechanism (*114*). Optimal positioning of the substrate is chaperoned by an electrostatic interaction between the side chain of E312 and the trimethylammmonium group of choline (*108*) during a preorganization of the enzyme-substrate complex required for efficient quantum mechanical tunneling of the hydride ion from the α-carbon of choline to the flavin N5-position (*104*). Both electrostatic interactions between side chains of multiple residues (E312 and H466) and the oxygen of the alkoxide and a covalent linkage between H99 and the flavin contribute to the preorganization of the binary complex (*104, 107, 108, 112, 113*). The hydride transfer reaction is assisted by His466, which acts as the catalytic base that abstracts a proton from the hydroxyl resulting in the formation of betaine aldehyde and anionic flavin hydroquinone (*120*). The bound betaine aldehyde intermediate (*102, 104*) is rapidly hydrated to the *gem*-diol form (*105*) while the anionic flavin hydroquinone is oxidized by dioxygen generating hydrogen peroxide (*104*). Oxygen accessibility to the reduced flavin is mediated by a gating mechanism that employs the phenyl ring of F357 to block or allow access to the hydrophobic tunnel extending into the active site (*121*) (Figure 1.3). Oxidation of the reduced flavin by dioxygen results in the generation of hydrogen perioxide (*104*).

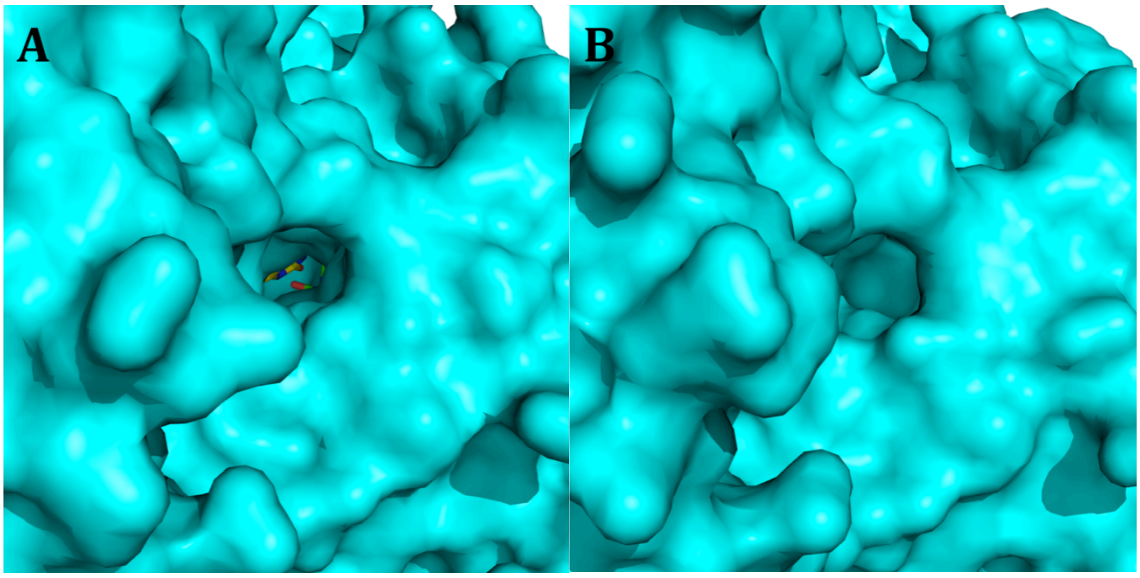

Figure 1.3. Open and closed conformations of choline oxidase. Open (A) conformation of choline oxidase from *Anthrobacter globiformis* in complex with glycine betaine (PDB code 4MJW). Closed (B) conformation of choline oxidase from *Anthrobacter globiformis* with DMSO bound in the active site (PDB code 2JBV).

The *gem*-diol aldehyde intermediate is further oxidized to the glycine betaine product in a second flavin mediated hydride transfer reaction where the reduced flavin is reoxidized by a second dioxygen utilizing a mechanism that mimicks the first flavin reoxidation (*105*). The *gem*-diol intermediate has been observed to remain bound to the active site during turnover of choline oxidase from bacteria (*101*) in contrast to fungal choline oxidase where the *gem*-diol intermediate is released to bulk solvent after the initial hydride transfer (*122*).

The first structural insights into the mechanism of choline oxidase came in 2008 when a crystal structure of wild type choline oxidase from *Anthrobacter globiformis* was solved at 1.86Å (PDB code 2JBV) (*108*) and revealed that choline oxidase forms a homodimer where monomers displayed a fold analogous to other members of the glucose-methanol-choline

(GMC) oxidoreductase enzyme superfamily (*123-133*) and included a loop domain (residues 64 to 95) observed to enclose the proposed substrate domain in other members of the GMC family (*126, 129, 133*). The dimer interface is composed of 2 identical sets of intersubunit contacts (Asp72 to Lys398, Asp250 to Glu53, Arg255 to Glu370, Asp358 to Arg396, Arg363 to Asp394 and Arg363 to Asp397) near opposite poles of the interface and a central portion lacking any substantial intersubunit contacts (*108*). Since 2008 multiple other crystal structures of choline oxidase from *A. globiformis* been solved including two active site mutant variants, Ser101Ala (2.47Å, PDB code 3NNE) (*134*) and Val464Ala (2.20Å, PDB code 3LJP) (*135*) and a wild type variant in complex with the reaction product glycine betaine (1.95Å, PDB code 4MJW) (*136*) and had revealed many structural and mechanistic details.

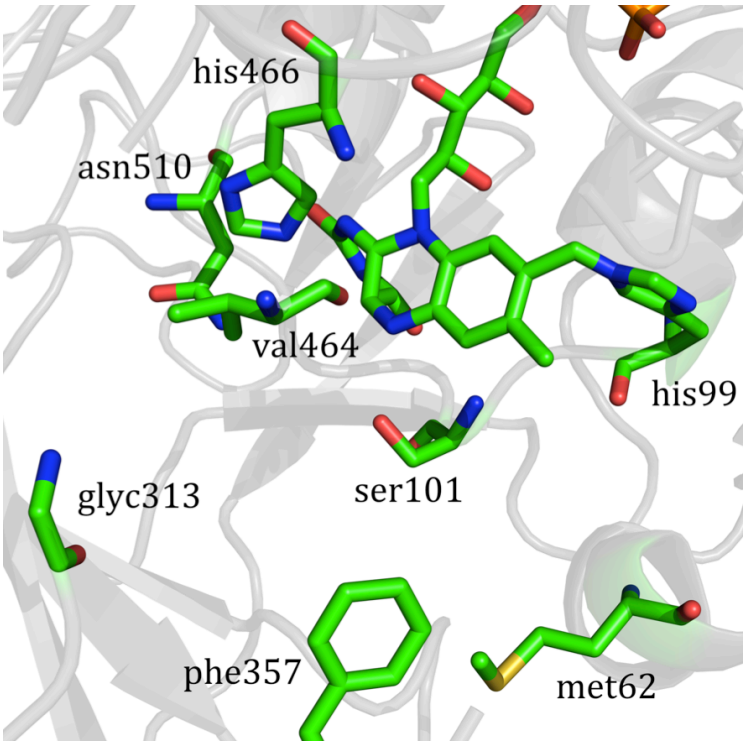

Figure 1.4. Active site residues of choline oxidase predicted to play a role in catalysis.

The FAD binding domain (residues 1 to 159, 201 to 311 and 464 to 527) is composed of a 3-stranded anti parallel β-sheet on one end and a 6-stranded parallel β-sheet at the apposing end surrounded by 8 α-helices (*108*). A covalently bound FAD molecule was observed in crystal structures where the 8α-methyl of the FAD isoalloxazine ring is linked to the 1 position π nitrogen of histidine 99 (*108*) that was contrary to earlier reports that had proposed that histidine 87 was responsible for the covalent interaction with FAD (*137*). The covalently bound FAD cofactor is almost completely devoid of solvent exposure where only 21.5 $Å^2$ (2.1%) is solvent exposed (*117*) and is positioned such that the re-face of the isoalloxazine moiety is exposed to the substrate binding pocket.

The substrate binding domain (residues 160 to 200 and 312 to 463) is composed of a 6-stranded antiparallel β-sheet in a distorted conformation positioned near one pole of the binding domain and a set of 3 α-helices that extend out into bulk solvent are positioned on the opposite pole. This topology frames a 125 $Å^3$, solvent excluded, substrate-binding pocket adjacent to the re-face of the FAD isoalloxazine ring. The crystal structure of the TMG complex had the oxygen atom of the product carboxylate moiety within 2.7 Å of the N(5) position of the isoalloxazine ring and also making interactions with the four position oxygen of the FAD, the side chain of Asn510 and the 2-position (π) nitrogen of His466 (*136*). It was also noted that the proximity and position of His466 near the carboxylate of glycine betaine suggest that this residue is the active site base responsible for catalyzing the cleavage of alcohol O-H bond(*136*).

Comparative analysis of the crystal structures of WT choline oxidase product/glycine betaine complex and the WT enzyme with bound DMSO in the active site confirmed the existence of two differing protein conformations that exhibit substantial positional rearrangement of a loop found at each pole the dimer interface consisting of residues 250 to 255 from each monomer (*118*). The terms “closed” and “open” were coined to describe the orientation of residues associated with the glycine betaine-bound and DMSO-bound conformations respectively (Figure 1.*3*). Overlay of the these two crystal structures revealed that disorder in the interface loop in the presence of glycine betaine results in the proximal rotation of Phe253 positioning this residue within 3.6 Å of Tyr330. In contrast the *open* conformation, as displayed by the DMSO-bound complex, stacks the aromatic ring of Phe253 with the side chains of Met359, Phe357, Leu65, Met62 of the other monomer(*118*). Both *open* and *closed* conformations were also observed in the in the

crystal structure of Val464Ala mutant enzyme (*135*), but not the Ser101Ala mutant (*134*) where all monomers where observed in the *closed* conformation.

The observed rotation of phenyl of Phe253 results in a closed conformation that appears to block access to the entrance of the tunnel extending to the active site. Xin et al first predicted the tunnel in 2009, where they describe a tunnel with a radius of 1 Å composed of hydrophobic residues (Met62, Leu65, Val355, Phe357 and Met359) and predicted that these serve as a gating mechanism controlling access to the active site of the adjacent subunit (*138*). Site directed mutagenesis studies of multiple residues (Met62Ala, Phe357Ala and the Met62Ala-Phe357Ala double mutant) of the hydrophobic tunnel confirmed that Phe357 is the residue responsible for modulation of the reduced enzyme prior to reoxidation and controls dioxygen accessibility to the active site (*121*).

Analysis of active site mutants revealed the function of multiple residues involved directly in catalysis. Residue Glu312 was determined to be responsible for binding and proper positioning of the choline substrate for hydride transfer (*108*). It was reported that the hydroxyl of Ser101 was demonstrated to stabilize the transition state for the proton transfer reaction that oxidizes choline and that mutation of Ser101 to threonine, alanine, valine or cysteine results in at least a 15-fold decrease for the rate constants for the proton extraction/hydride transfer steps (*139*). Asp510 was also determined to play an important role in catalysis where kinetic analysis of Asn510Ala variant displayed a 4300-fold decrease in $k_{cat}/K_{choline}$, a 600-fold decrease in k_{red}, a 660-fold decrease in k_{cat}, and a 50-fold decrease in k_{cat}/K_{O2} (*116*). These data suggest that that Asn510 participates in both the oxidative and reductive half reactions where it is involved in relative timing of cleavage of choline OH and CH bonds. It was also demonstrated that mutation of Asn510 could disrupt

the covalent interaction between the FAD molecule and His99 (*116*). Interestingly mutations of Val464 had no effect on the reductive half reaction but Val464Ala and Val464Thr mutations resulted in a ~50-fold decrease in rate constant for flavin reoxidation (k_{ox}) (*135*). Researchers suggested that hydrophobic character of Val464 was responsible for the positioning of the oxygen atom with respect to the C(4a) atom of the reduced flavin (*135*).

The identity of the active site base has been the subject to discord since the involvement of an active site catalytic base with an apparent pka = 7.5 described for both wild type and various mutant variants using multiple kinetic techniques(*103-105, 108, 110*). His466 was originally suggested to play the role of the active site base because it is completely conserved in the GMC oxidoreductase superfamily (*140-143*). Despite the conserved nature of this residue, results of initial experiments using His466Ala variant enzyme (*103*) paralleled those of His351Ala mutant choline oxidase (*110*) and it was concluded that neither His466 or His351 act as the catalytic base (*103, 110, 144*). Inspection of crystal structure of choline oxidase in complex with glycine betaine revealed that the only residues that are in close enough proximity to the ligand carboxylate oxygen to function as the catalytic base are His466 and His351(*136*) forcing re-evaluation of the role of these residues. In 2015 variants His466Gln and His351Gln of choline oxidase were kinetically analyzed and revealed that although mutation of His351 to Gln causes significant decreases in k_{cat} and k_{cat}/K_m, mutation of His466 to Gln completely abolishes catalytic activity and thus is a prime suspect for the catalytic base (*120*).

EncM

Flavins are one of the most intensively studied enzymatic cofactors and are found across all forms of life where they are required for catalysis by numerous classes of enzyme and participate in what is generally regarded as a defined set of reaction categories (*145-149*). Flavin dependent monooxygenases identify as one of these classes and utilize a flavin cofactor to mediate oxygenation via a stabilized well documented C(4a)-hydroperoxyflavin intermediate. Until recently the C(4a)-peroxyflavin mechanism was thought to be the most common method of flavin mediated oxygenation where the distal oxygen atom is transferred from the electrophilic hydroperoxyflavin intermediate to an activated nucleophilic organic substrate (*145, 150, 151*). In 2013, a unique bacterial enzyme, EncM, was described to catalyze the peroxyflavin independent oxygenation and dehydrogenation to promote the Favorskii-like rearrangement of the poly(β-carbonyl) substrate to the rearranged desmethyl-5-deoxyenerocin using a stable flavin oxygenating species proposed to be a flavin-N5-oxide(*152, 153*). (Scheme 1.7)

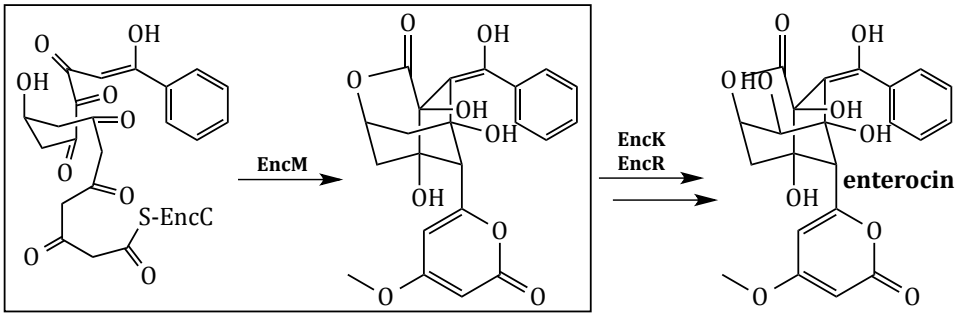

Scheme 1.7. Reaction catalyzed by EncM and subsequent conversion to enterocin by EncK and EncR

Flavoprotein EncM plays an important role in the biosynthesis of enterocin in multiple streptomycete bacteria (*154-157*). The dual oxidation reactions of the highly reactive poly(β-carbonyl) substrate promote the subsequent Favorskii-type rearrangement responsible for the formation of the lactam ring of enterocin (*152, 158*). This highly unusual reaction is the first example of a "superoxidized" or four-electron oxidized flavin species (*152*).

The crystal structure of EncM was solved (PDB code 3W8W, 1.95 Å) in the presence of 4mM NADPH (PDB code 4XLO, 1.67 Å). This structure revealed that, consistent with in solution oligomer determinations, EncM crystallizes as a homodimer where the subunits are almost identical (0.19Å RMSD for Cα atoms)(*152*). Structures also revealed that residues 2-210 and 419-461 form FAD-binding domain where covalent binding of the C8-methyl of the isoalloxazine moiety to His78 positions the reactive isoalloxazine moiety adjacent to the substrate binding domain forming the internal face of the active site. The active site resides at the end of an L-shaped (~30 Å) tunnel the extends to the surface of the enzyme near the dimer interface and studies suggest that the shape of this tunnel is largely complementary to the conformation of acyl carrier protein (ACP)-derived phosphopantetheine arm, the octaketide chain and the terminal benzene moiety of the proposed 1,3-diketone substrate (*152*). Interestingly, a group of positively charged residues the forms a basic patch on the surface of the enzyme that is complementary to the negative surface area of ACP (*157, 159*). On this basis it was proposed that this patch mediates a protein-protein interaction between EncC and EncM where acyl carrier protein EncC transfers its product, elongated (1,3-diketone) polyketide intermediates to EncM limiting deleterious side reactivity of the poly(β-carbonyl) chain (*152, 154*). Protein-protein

interaction between EncC and EncM is supported by computational docking simulations using an EncM homology model (*152*). Additionally, mutagenesis studies designed to disrupt the protein-protein interface by mutating Arg210 to glutamic acid resulted in ~40% decrease activity compared to wild type (*152*).

Additional crystal structures of EncM where solved in complex with substrate analogs trifluorotriketide (PDB code 3W8X, 1.82 Å) and hydroxytetraketide (PDB code 3W8Z, 1.80 Å) (*152*). These structures revealed binding representative of the enzyme-substrate complex where the terminal benzene group of the substrate analog forms multiple van der Waals and pi-stacking interaction with the hydrophobic residues of EncM. These interactions position the enol at C1 of the substrate analogs within hydrogen bonding distance (2.4 Å) of the 4-oxygen of flavin cofactor. It was proposed that the L shaped binding tunnel of EncM is composed of 2 orthogonal sections whose function is to separate the triketide head from the pantothenate-linked tetraketide tail of the highly reactive substrate that would otherwise undergo deleterious cyclization/aromatization reactions if not stabilized (*152*). The chemical and physical stabilization of the substrate provided by the enzyme scaffold also promotes the specific Favorskii rearrangement that is proposed to follow substrate oxidation(*152*).

In initial biochemical analysis of EncM it was observed that enzyme activation occurred after several turnovers where inactivation results in large changes in the absorbance spectrum of active form of EncM and it was proposed that spectral changes occurred as a result of the loss of a flavin oxygenating species (*152*). As mentioned above, conventional flavin chemistry utilizes a flavin-C4a-peroxide (*151, 160, 161*) as an oxygenating species. However, this intermediate was ruled out due to distinct spectral

characteristics and greatly increased stability of the EncM oxygenating species (*152*). It was also observed that the generation of EncM flavin oxygenating species from anaerobically reduced enzyme required reoxidation by oxygen where anoxic chemical reoxidation resulted in inactive oxidized EncM (*152*). Additionally, ^{18}O-labeling studies carried out using EncM that was reoxidized with ^{18}O and substrate analog that significantly resembles the proposed substrate but has a shortened polyketide tail described a 1:1 conversion to diastereomeric mixture of product identified by NMR and MS as the ring open derivatives of lactone (*152*). These studies also revealed that the substrate-binding tunnel of EncM is specifically tailored to accommodate only the (R)-enantiomer of the substrate supporting the observed retention of the configuration of the c4-hydroxyl in the enterocin product (*152*). Based on these observations the identity of the EncM flavin oxygenating species was proposed to be the flavin-N5-oxide; a species introduced as a possible new flavin intermediate species of monoxygenases (*152, 162, 163*).

Until recently intensive biochemical analysis required an arduous effort due to the high reactivity of the proposed substrate where substrate analogs where used to mimic catalysis (*152*). Biochemical analysis using multiple techniques including HPLC, UV-Vis spectroscopy, NMR, and MS revealed many details about the mechanism of EncM turnover with a substrate analog and allowed researchers to propose a catalytic mechanism of EncM (*152*). In this mechanism the N5-oxide of the flavin undergoes initial protonation by the C5-enol hydroxyl of the substrate promoting tautomerization of the N5-hydroxylamine and would result in the formation of the electrophilic oxoammonium species. The oxoammonium then oxygenates the enolate moiety of the substrate resulting in oxidation of the flavin cofactor and generation of a C4-hydroxylated intermediate (shown as H2O),

which is dehydrogenated to produce the C4-ketone product in a reaction that is coupled to the reduction of the flavin cofactor to its reduced ($FADH_2$) form. The C4-ketone product would then undergo EncM mediated Favorskii rearrangement and would be susceptible to *retro*-Claisen transformation to produce the 2 sets for diastereomer products formed in the presence of glycerol or H_2O (*152*).

Direct evidence for the active N(5)-oxide flavin came in 2015 when researchers analyzed peptide fragments generated by EncM digestion by protein kinase K using high resolution electrospray ionization liquid chromatography mass spectrometry (HR-ESI-LCMS) and identified a His78 bound flavinN(5)-oxide fragment (*153*). Psuedo-MS^3 confirmed the presence of a flavin bound oxygen molecule (*153*). To definitively correlate the observed mass signal with the addition of a flavin-bonded oxygen molecule chemically reduced EncM was reoxidized by ^{18}O and subject to digestion by protein kinase K and analyzed the fragments as discussed above and confirmed the generation of the flavin-N(5)-^{18}oxide (*153*).

Utilizing all the available biochemical, mechanistic and structural data a proposed mechanism of flavin-N(5)-oxide formation was presented where the N5-position of the flavin undergoes a direct reaction with dioxygen (*153*) (Scheme 1.8). In this mechanism the net equivalent of a hydrogen atom is transferred from the N5-position of the reduced flavin to dioxygen resulting in a flavin-N5-peroxide that immediately undergoes water elimination to form the flavin-N5-oxoammonium, the resonance form of flavin-N5-oxide. The authors noted that the initial hydrogen transfer reaction could occur in a one step

hydrogen transfer reaction or in a series of two steps where single electron transfer is preceded by proton transfer.

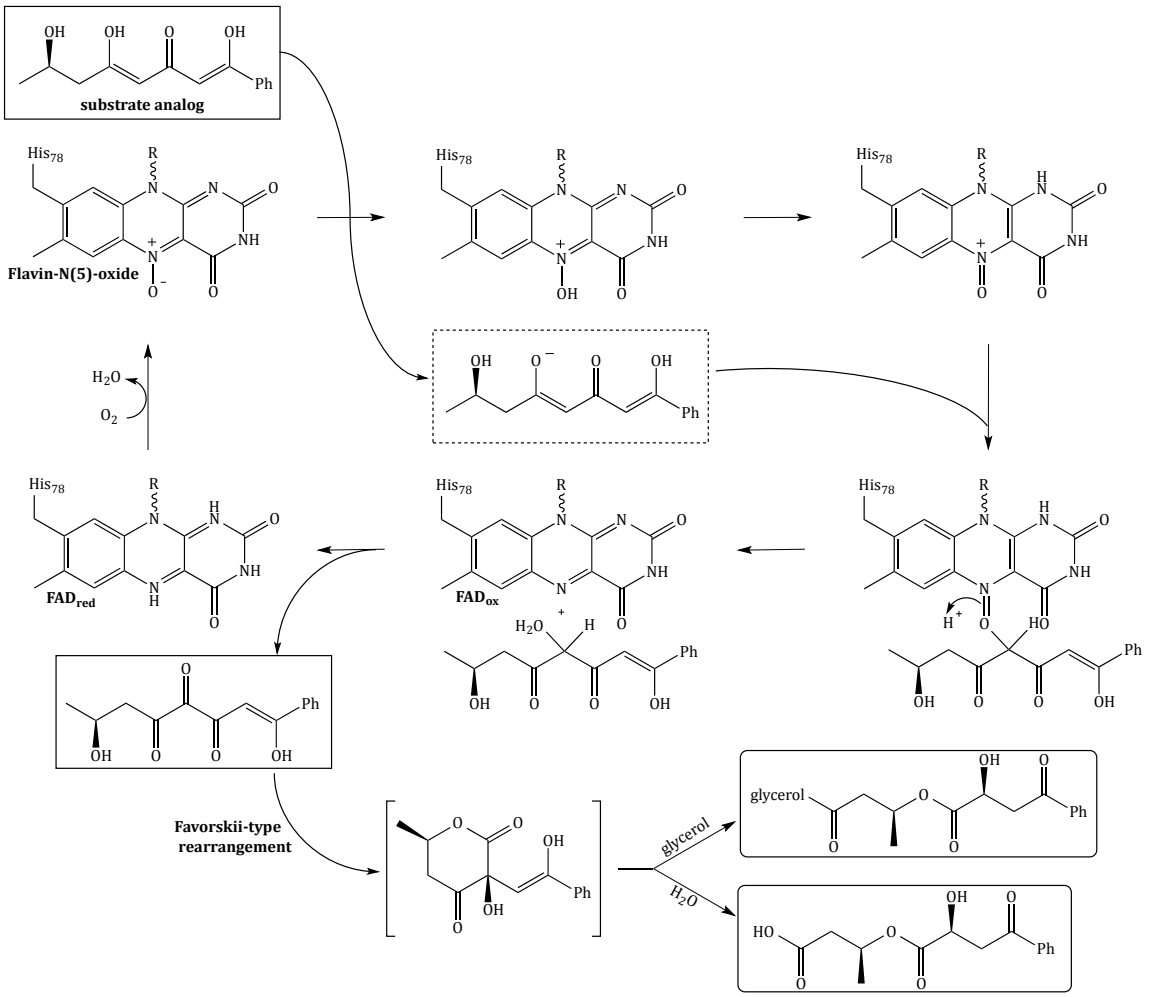

Scheme 1.8. Proposed catalytic mechanism of EncM with substrate analog.

As previously discussed EncM does not have a catalytic requirement for NADPH and lacks a formal NADPH binding domain, however it was suggested that NADPH did have a biological role in regards to its relationship with this enzyme (*153*). NADPH was described to recover EncM that had undergone auto-oxidation resulting in inactive, oxidized EncM

and re-reduce it so that it can undergo the desired activation by dioxygen. This proposal is supported by data that describes ~36-fold lower binding affinity for NADH compared to NADPH while maintaining similar rate constants for flavin reduction (~0.100 s^{-1}) where EncM displays a distinct selectivity for NADPH in the absence of formal NAD(P)H binding domain (*153*).

EncM presents the first example of a flavoprotein that requires a "superoxidized" flavin cofactor (flavin-N(5)-oxide) for proper catalytic functioning. This new flavin cofactor role emerges from one of the most studied classes of enzyme, flavoprotein and hints at the immense diversity of biological systems. This begs the question, is EncM an extremely unusual flavoprotein that displays unique chemistry or is this just the first identified example of a class of as yet unidentified flavoproteins?

UbiX UbiD, Pad1 Fdc1

The bacterial genes *ubiX (164)* and *ubiD (165)* and fungal homologs pad1 and fdc1 encode for a pair of enzymes associated with a reversible, non-oxidative decarboxylation of an aromatic substrate (*166, 167*), an essential step in the biosynthesis of prokaryotic ubiquinone (or Coenzyme Q) (*164, 165, 168-170*) or fungal degradation of phenylacrylic/aromatic acids (*171-174*) which can cause the accumulation of volatile phenols in yeast containing food products. Until recently, proteins encoded by *ubiX* (UbiX, 3-otcaprenyl-4-hydroxybenzoate carboxy-lyase) and *ubiD* (UbiD, 3-otcaprenyl-4-hydroxybenzoate carboxy-lyase) or *pad1* (Pad1, phenylacrylic acid decarboxylase) and *fdc1* (Fdc1, ferulic acid decarboxylase) were believed to be isofuctional though they have no

amino acid sequence similarities. However, both proteins where expressed together and thought to have redundant catalytic activity where bacterial UbiX and UbiD catalyze the decarboxylation of 3-octaprenyl-4-hydrozybenzoate to 2-octaprenylphenol (*169, 173, 175-179*) and eukaryotic Pad1 and Fdc1 catalyze the decarboxylation of cinnamic acid, coumaric acid and ferulic acid to styrene, 4-vinyl phenol and 4-vinyl benzene respectively (*171, 173, 174, 180*). It was recently determined that UbiX and isofunctional pad1 do not exhibit decarboxylase activity (*181*) and instead functions as a prenyltransferase catalyzing the formation of a 4 ring prenylated flavin mononucleotide that is required for the non-oxidative reversible decarboxylation catalyzed by UbiD and Pad1 enzymes (*182, 183*). (Scheme 1.9*)*

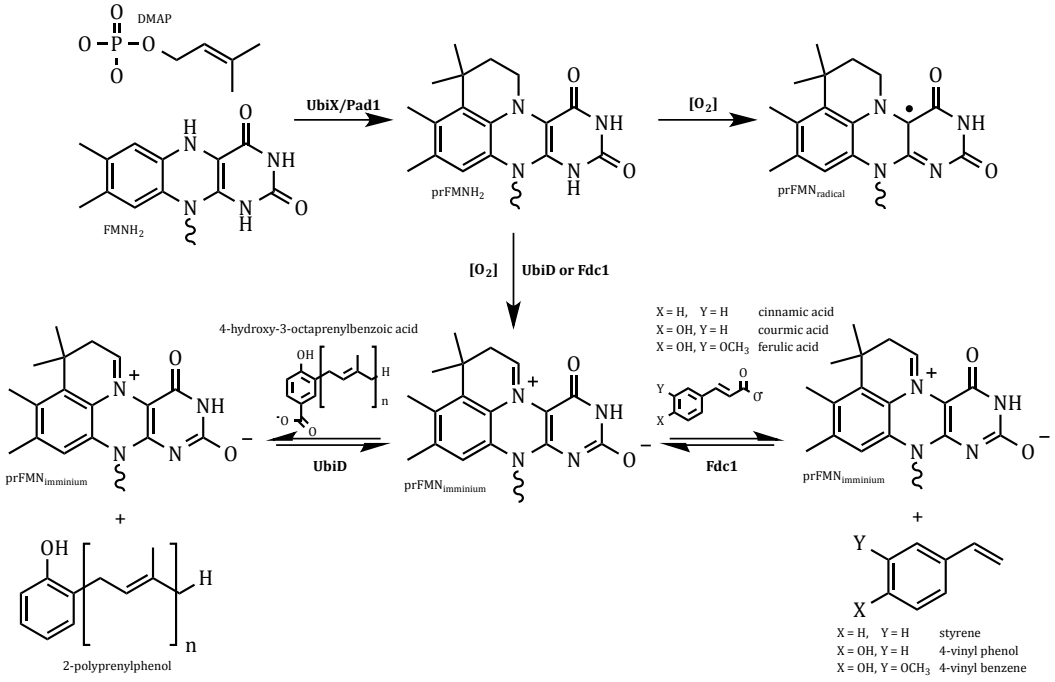

Scheme 1.9. Overview of the proposed reactions of UbiX, Pad1, UbiD, and Fdc1.

Reduced flavin monophosphate ($FMNH_2$) is prenylated by UbiX in bacteria and Pad1 in yeast. The N5-C6 prenylated flavin mononucleotide ($prFMNH_2$) can undergo oxidation via molecular oxygen to form a radical species ($prFMN_{radical}$) or is utilized as a cofactor by apoUbiD/apoFdc1 and oxidized to the catalytically active prenylated flavin mononucleotide imminium ($prFMN_{imminium}$) form which catalyzes the prokaryotic (UbiD) decarboxylation of 4-hydroxy-3-octaprenylbenzoic acid to 2-polyprenylphenol or the eukaryotic (Fdc1) decarboxylation of cinnamic acid, courmic acid or ferulic acid to styrene, 4-vinyl phenol and 4-vinyl benzene respectively. Decarboxylation reactions are not uncommon in the chemistries of living organisms and there are even multiple examples of the enzymatic use of flavin mononucleotides for decarboxylation (*184-186*) but the use of a prenylated FMN (*182*) is for this chemistry is novel.

Initial reports of 3-octaprenyl-4-hydroxybenzoate carboxy-lyase activities in *Escherichia coli* biosynthesis of ubiquinone suggest that optimal activity of the decarboxylase enzyme(s) require the presence of Mn^{2+} and a reductant (methanol or dithiothreitol) (*165*). It was later proposed that decarboxylase activities in the biosynthesis of ubiquinone in *E. coli* was the result of two isofunctional enzymes, UbiX and UbiD (*164*) and that 80% of this activity is correlated to UbiD as a result of weak promoter strength of the *ubiX* gene (*187, 188*). Despite being assigned isofuntional catalytic activities these enzymes display no sequence similarities where UbiX is 21 kDa and UbiD is 55 kDa and in 2007 it was suggested that UbiX and UbiD are not isofunctional but rather act together in the decarboxylation step of ubiquinone biosynthesis where UbiD induces the decarboxylation activity of UbiX (*169*).

Homologous eukaryotic/yeast genes *pad1* and *fdc1* and their respective enzyme transcripts Pad1 and Fdc1 were first associated with *Saccharomyces cerevisiae* resistance to cinnamic acid through decarboxylation to styrene in 1994 (*174*). Overexpression of the pad1 gene resulted additional resistance to ferulic acid (*180*) and in 2007 it was discovered that deletion of the *pad1* gene resulted in the inability to decarboxylate cinnamic acid and sorbic acid, adding sorbic acid to the list of potential substrates of Pad1 (*171*). The homologous nature of pad1/fdc1 and ubiX/ubiD was identified in 2009 and researchers demonstrated that both Pad1 and Fdc1 are required for the decarboxylation of phylacrylic acids in *S. cerevisiae (172)*. Though homologous UbiX/UbiD and Pad1/Fdc1 do not share a physiological function.

The first crystal structure of a 3-octaprenyl-4-hydroxybenzoate decarboxylase (UbiD) from *Escherichia coli* (PDB code 2IDB) was solved in 2006 by the Northeastern Structural Genomics Consortium revealing a hexameric quaternary structure, however the due to the resolution of the structure (2.9 Å) specific details in regards to residue identity and position could not be determined. In 2013 a 1.9Å crystal structure of the dimeric PA0254 (UbiD) from *Psuedomonas aeurginosa* (PDB code 4IP2) was solved and the associated electron density maps displayed clear difference electron density indicative of a metal center, in this case Mg^{2+} (*177*). A large cleft on the face of the structure extends from the metal binding site across 2 domains and terminates near a pocket of conserved residues Arg170, Glu273 and Glu278 (Asp278 in UbiD from *Escherichia coli*) and could represent a putative active site. Crystal structures have provided valuable information about the

structure however *in vitro* attempts to verify carboxy-lyase activity with shorter length substrate analogs vanillic acid cinnamic acid and ferulic acid but suggested this was due to the absence of a long polyprenyl tail found on the suspected true physiological substrate 3-octaprenyl-4-hydroxybenzoate which would interact with the surface cleft in a way required for correct positioning of the substrate (*177*). It was also noted that residues Glu229 and His188 from PA0254 were structurally conserved with Glu105 and His68 from FMN-binding protein from *Methanobacterium thermoatuotrophicum* (*189*) (PDB code 1EJE) believed to be involve with the binding of flavin mononucleotide whose phosphate is bound to a metal ion similar to the Mg^{2+} found in PA0254, however binding of FMN to PA0254 could not be demonstrated by conventional methods *(177)*.

The first structural insights into functionality of UbiX/Pad1 came in when a 1.5Å crystal structure of UbiX from *Psuedomonas aeruginosa* was solved (*190*) and it was determined that Ubix assembles in to a deodecamer exhibiting a Rossman fold that harbors a FMN molecule located at the interface between two subunits where the ribityl moiety interacts with residues from 2 adjacent subunits. Crystal structures reveal a small hydrophilic pocket adjacent to the re face of the flavin isoalloxazine moiety constructed of residues from 3 separate subunits; neither face of the flavin isoalloxazine is accessible to bulk solvent. This suggests that incorporation of additional substrates would require large conformational changes, which is not consistent with current crystal structure data (*190*). These findings allowed researcher to classify UbiX and homologous Pad1 as a FMN-dependent decarboxylase enzymes. Despite structural similarities to multiple enzymes

associated with classifications related to decarboxylase activity (*185, 186, 191-193*) no activity was seen when UbiX from *Psuedomonas aeruginosa* was incubated with substrate analogs 4-hydroxybenzoic acid, vanillic acid and 3-carboxymethyl amino-methyl-4-hydroxybenzoic acid (*190*) suggesting inactivity is due to substrate specificity, researchers did not have access to the true physiological substrate 3-octaprenyl-4-hydroxybenzoate. The redox role for FMN in the decarboxylation of benzoic acid derivatives (substrate of UbiD/UbiX) could not be established unless used as an acid-base catalyst, however chemistries of phenylacrylic decarboxylases (Pad1/Fdc1) could accommodate the presence of a flavin mononucleotide(*190*). The crystal structure of UbiX form *Colwellia psychrerythraea* (PDB code 4RHE) was reported as solved along with the structure of a stable FMN-free mutant (V47S) apo-UbiX (PDB code 4RHF) further confirming the presence of a UbiX/Pad1 FMN cofactor (*178, 179*).

In 2009 Mukai et al examined a study (Ago, S., Kawasaki, H., and Kikuchi Y., Abst. 50th Annu. Meet. Soc. Biothechnol. p.24, 1998) that demonstrated that sake yeast, normally devoide of ferulic acid decarboxylase activity due to lack of the *fdc1* gene, could exhibit resistance to ferulic acid when the gene *fdc1* (YDR539W) from wine yeast was incorporated into its genome which suggests that Pad1/fdc1 (UbiX/UbiD) are not isofunctional and that expression of both genes is required for decarboxylation activity. Confirmation came when it was demonstrated that decarboxylase activity in Saccharomyces cerevisea could be ceased with the deletion of either the *fdc1* or *pad1* gene and that the resulting phenotype of both knockouts was identical to the double knockout (*Δpad1fdc1*) (*172*), however how their respective enzyme transcripts function together remains unknown.

Researchers form the University of Michigan proposed Pad1 and Fdc1 are part of a two component decarboxylase system where Pad1 activates Fdc1 and suggested it does so by providing Fdc1 with a covalently modified flavin mononucleotide cofactor necessary for catalytic activity (*181*). On this basis UbiX was incubated with oxidized FMN and dimethylallyl monophosphate (DMAP) and perturbation of the FMN UV-visible spectrum was observed (*182*) suggesting that DMAP binds in close proximity to the flavin. The binding of dimethylallyl monophosphate was confirmed by solving a crystal structure of the UbiX-oxidized FMN-DMAP (PDB code 4ZAF) (*182*) complex where the DMAP binds to adjacent to the re face of the isoalloxizine moiety of the flavin monophosphate in a hydrophobic pocket that resembles that of terpene synthases and prenyl transferases (*194-196*).

The identity of the modified flavin mononucleotide produced by UbiX and Pad1 was determined when UbiX from *Psuedomonas aeruginosa* was incubated with oxidized flavin mononucleotide (FMN) and dimethylallyl monophosphate resulting in the formation of a prenylated flavin monocleotide ($prFMNH_2$) (*182*). (Scheme 1.9)

Crystals of UbiX from *Psuedomonas aeruginosa* could undergo active turnover allowing researchers to use kinetic crystallography matched with mass spectroscopy and/or UV visible spectroscopy to confirm the binding of DMAP to the oxidized UbiX flavin monophosphate (UbiX-FMN-DMAP)(PDB code 4ZAF) (Scheme 1.10, **1**), reduction of the UbiX flavin cofactor (E49Q mutant UbiX-$FMNH_2$-DMAP complex)(PDB code 4ZAL) (Scheme

1.10, **2**), the initial formation of N5-C1' alkyl adduct (PDB code 4ZAV) (Scheme 1.10, **3**), the formation of the UbiX-reduced prenylated FMN product complex (UbiX-prFMNH_2) (PDB code 4ZAW) (Scheme 10.1, **7**) and the oxidization of the reduced prenylated FMN to the purple shifted oxygen dependent radical species (UbiX-prFMN$_{radical}$)(PDB code 4ZAX) formed at 1-5, 20-30, or 30+ seconds respectively when UbiX-FMN-DMAP where incubated with sodium dithionite using rapid freeze quench techniques to capture desired time points (*182*). Active site mutations of *Psuedomonas aeruginosa* UbiX revealed species (Scheme 1.10, **5a**) and revealed that large conformational changes occur after the reduction species (Scheme 1.10, **3**) to the stable N5 adduct (Scheme 1.10, **4**) and again during product formation (Scheme 1.10, **7**), which could be the key to understanding UbiX catalysis (*182*). However no direct evidence of species (Scheme 1.10, **5b**) or species (Scheme 1.10, **6**) has been obtained.

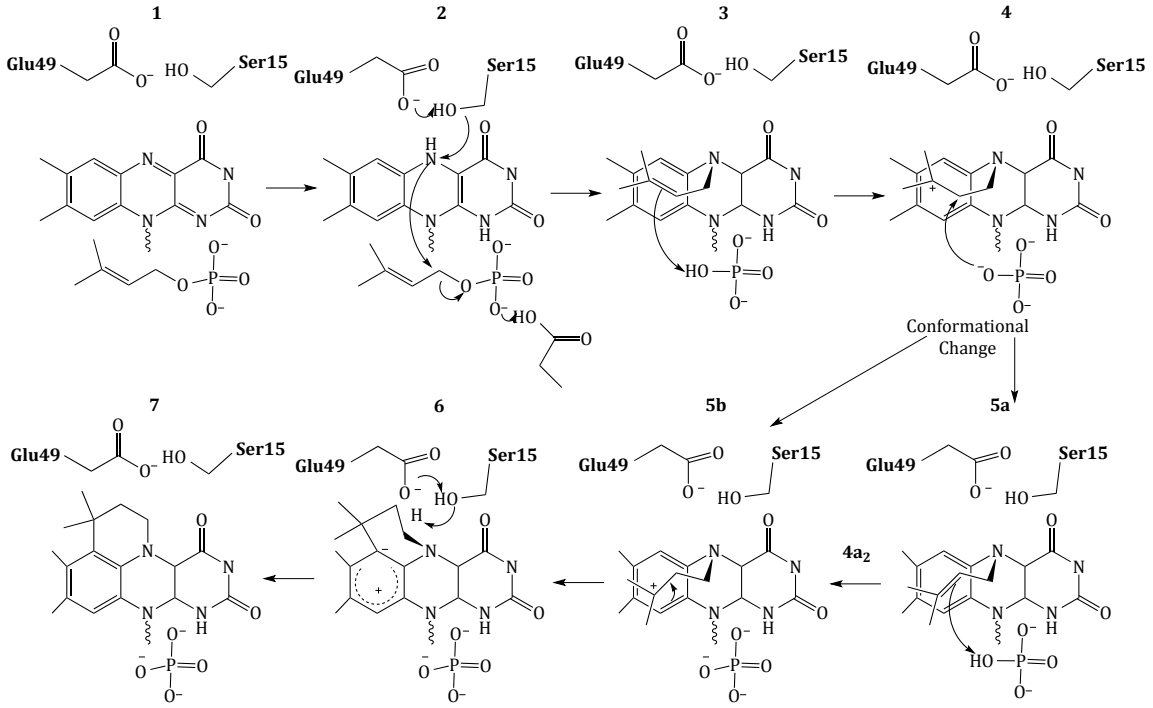

Scheme 1.10. Proposed catalytic mechanism of UbiX/Pad1. Reduced flavin mononucleotide ($FMNH_2$) is prenylated by UbiX/Pad1 untilizing the cosubstrate dimethyl monophosphate to bridge the N5 to the C6 of the flavin.

Ubix/Pad1 offers the first example of a flavin monophosphate dependent prenyl transferase and the first description of a new flavin cofactor, a dimethyl four-ring prenylated flavin linked at the N5 and C6 atoms of the isolalloxizine moiety. The enzymes UbiX and Fdc1 have also found a unique way to ensure a stable N5-alkyl adduct flavin species ($prFMNH_2$) is favored over the N5-imminium adduct ($prFMN_{imminium}$) by utilizing the reduced from of the flavin monophosphate ($FMNH_2$) to act as a nucleophile. This strategy ensures that the reduced prenylated flavin monophosphate ($prFMNH_2$) product of UbiX/Pad1 can be transferred to apo-UbiD/fdc1 before undergoing hydrolysis.

Though no direct interactions have been observed between UbiX/Pad1 and UbiD/Fdc1, when the *fdc1* gene from *Aspergillus niger* and the gene *ubiX* from *E. coli* were coexpressed in *E. coli* the resulting enzyme ($Fdc1_{UbiX}$) displayed distinct spectral properties when compared to single express Fdc1 and $Fdc1_{UbiX}$ catalyzed the decarboxylation of multiple aromatic carboxylic acids *in vitro (183)*. This is the first genuine evidence of catalytic activity demonstrating that enzymes UbiD and homologous Fdc1 are exclusively responsible for non-oxidative reversible decarboxylation their of aromatic substrates. Researchers also demonstrated that decarboxylation activity requires a heavily modified flavin cofactor, product of UbiD/Pad1 catalysis obtained in reduced form ($prFMNH_2$) and they solved crystal structures of $Fdc1_{UbiX}$ using Fdc1 from *A. niger* (1.22 Å, PDB code 4ZA4), *Camidida dubliensis*(2.46 Å, PDB code 4ZAD) *and Sacchromyces cerevisiae* (1.65 Å, PDB code 4ZAC) confirming the identity of the prenylated flavin mononucleotide (prFMN) where an isopentenyl adduct is formed bridging N_5 to C_6 effectively forming a 4^{th} ring represented in an oxidized imminium form ($prFMN_{imminium}$) (*183*). The crystal structures also revealed the presence of metal ions in complex with the phosphate tail of the prenylated flavin cofactor which were suggested based on electron density, to be Mn^{2+}(confirmed by EPR) and K^+ (unconfirmed) (*183*) confirming earlier reports of the dependence of UbiX/Pad1 and UbiD/Fdc1 on Mn^{2+} (*165*). To further probe for binding and mechanistic details crystals of$Fdc1_{UbiX}$ from *A. niger* were soaked with various trans-cinnamic-acid-related compounds, 4-vinyl guaiacol (PDB code 4ZAA), penta-fluorocinnamic acid (PDB code 4ZA8), phenyl pyruvate (PDB code 4ZA9) and alpha-fluoro cinnamic acid (PDB code 4ZAB) (*183*). Structures were solved and revealed the substrates enoic acid double bonds stack directly above the oxidized prenylated flavin (prFMN) cofactor occupying the active site in one of

two configurations, an isoalloxazine N_5 imminium adduct ($prFMN_{imminium}$) or a N_5 ketamine species ($prFMN_{ketamine}$) (*183*).

Because of the presence of two species of oxidized prFMN cofactor were found 2 possible mechanisms, where reduced prenylated flavin mononucleotide is derived from UbiX/Pad1 and transferred to UbiD/Fdc1 (*182*) in the reduced form ($prFMNH_2$) which then requires activation by oxidation via dioxygen to either oxidized form isomer, the imminium ($prFMN_{imminium}$) (Scheme 1.11, **3**) or ketamine ($prFMN_{ketamine}$) (Scheme 1.11, **7**) form (*183*). Acid base chemistry could utilize the N5 of the secondary ketamine of the $prFMN_{ketamine}$ as a catalyst taking advantage of the positioning of the substrates α,β-unsaturated carbonyl above the $prFMN_{ketamine}$ C4a and undergo a Michael addition-like chemistry seen in other flavin containing enzymes (*197, 198*), forming a transient C4a-substrate adduct (Scheme 1.11, **8**) preceding decarboxylation.

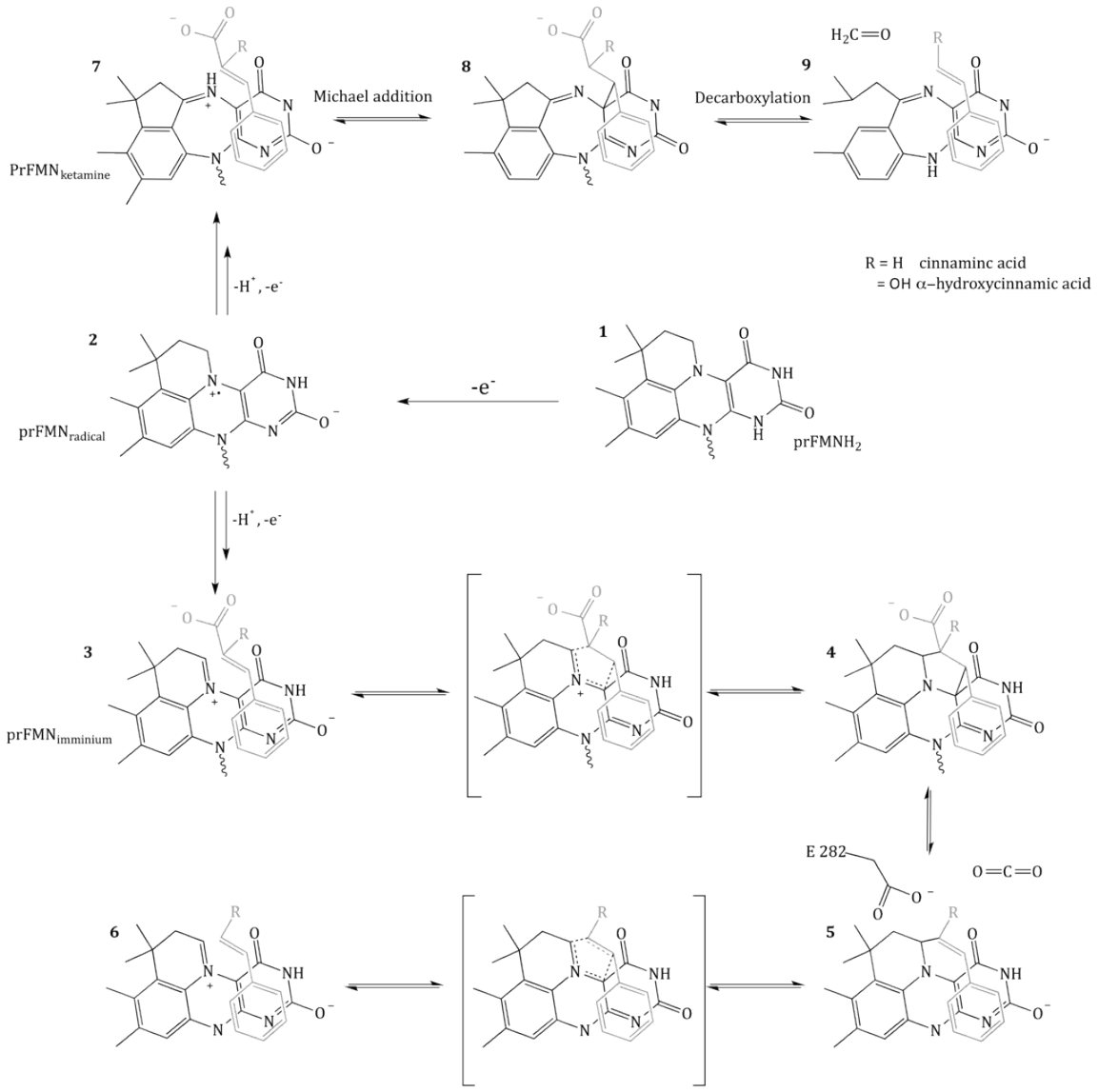

Scheme 1.11. Proposed catalytic mechanisms of $Fdc1_{UbiX}$ using both the $prFMN_{ketamine}$ and $prFMN_{imminium}$.

The second proposed mechanism utilizes $prFMN_{iminium}$ (Scheme 1.11, **6**) as the catalytically relevant form of the enzyme, where the substrate α,β-unsaturated carbonyl, a dipolarophile, takes advantage of the 1,3-dipole arrangement of $prFMN_{imminium}$, a configuration known to facilitate this type of reaction (*199*), undergoing what would be the

first biological example of a 1,3 dipolar cycloaddition leading to the formation of a substrate-prFMN$_{imminium}$ adduct bridging both the C4a and C1' of the prFMN$_{imminium}$ cofactor (Scheme 1.11, **4**). The double-bridged substrate-prFMN$_{imminium}$ could then undergo a Grob-like decarboxylative fragmentation(*200*) of the pyrrolidine adduct (Scheme 1.11, **4**) could be coupled to cleavage of the C4a-substrate bond resulting in a single-bridged prFMN$_{iminium}$ C1'-substrate adduct (Scheme 1.11, **5**) where protonation via E282 leading to the formation of the second double-bridged pyrrolidine adduct (Scheme 1.11, **5a**). This adduct would then be subject to *"retro 1,3-dipolar cycloaddition"* resulting the formation of the product complex (Scheme 1.11, **6**). In an attempt to determine which pathway is utilized, Fdc1$_{UbiX}$ from *A. niger* was incubated phenylpyruvate resulting in reversible inhibition of the enzyme by the enol tautomer of phenylpyruvate, α-hydroxycinnamic acid and crystal structure solutions of this complex revealed a α-hydroxystyrene prFMN$_{imminium}$ adduct (*183*). The α-hydroxystyrene adduct is the result of keto-enol tautomerization of the single-bridged prFMN$_{iminium}$ C1'-substrate adduct (Scheme 1.11, **5**) confirming prFMN$_{imminium}$ is the active form of the enzyme and suggests that the reversible non-oxidative decarboxylation occurs via a 1,3-dipolar cycloaddition.

It must be noted that in 2004 a 2.0Å crystal structure of a tentative Pad1 for *Escherichia coli* Q157: H7 in complex with FMN (PDB code ISBZ) was solved (*188*). Even though Pad1 is most commonly found in eukaryotic species this possible prokaryotic PAD1, a UbiX paralog with similar sequence identity to UbiX from *Escherichia coli* (51%) and Pad1 from *Saccharomyces cervisiae* (54%) has been identified in pathogenic strains of *Escherichia coli*.

Although this prokaryotic Pad1 displayed high sequence identity to other members of the HFCD superfamily no decarboxylase activity of phenylacrylic acids was ever demonstrated.

Chorismate Synthase

Chorismate synthase is a unique FMN dependent flavoprotein that plays an essential role as the catalytic terminus of the shikamate pathway. The shikamate pathway is a seven step, seven enzyme, metabolic pathway found in bacteria, plants, fungi and anticomplexan parasites (*201*) responsible for the biosynthesis of a precursor (chorismate) for multiple essential compounds including multiple quinone species including ubiquinone, plastiquinone and vitamin K, tocopherols, folates, aromatic amino acids tryptophan, phenylalanine, and tyrosine as well as a number of secondary metabolites. (Scheme 1.12) The absence of the shikimate pathway in mammalian metabolism has meant that the enzymes of this pathway are targets for neoteric antibiotics, herbicides and antiparasitic agents (*201, 202*).

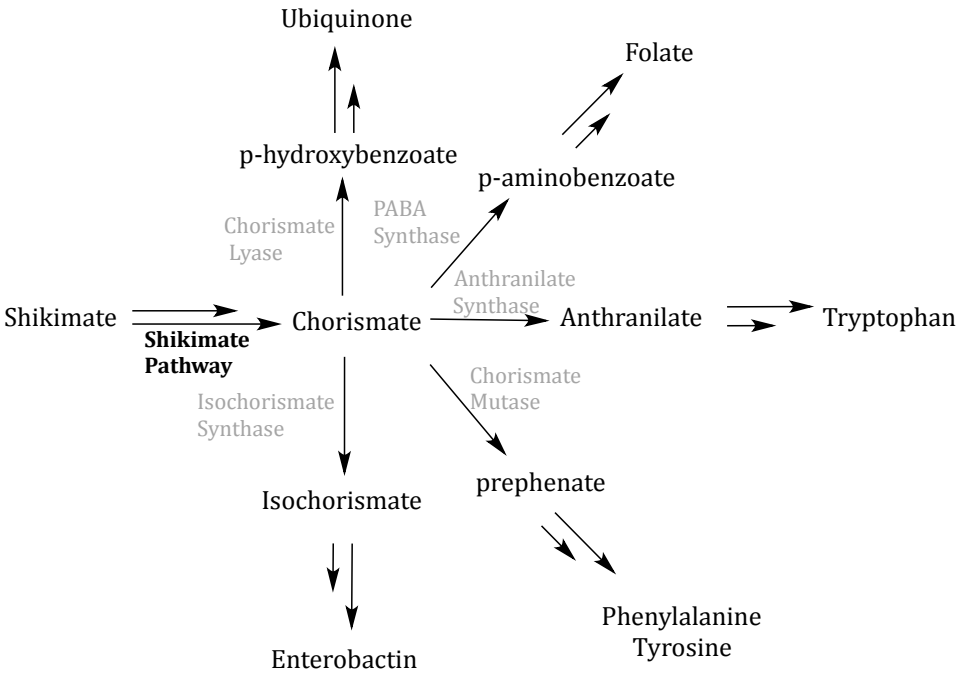

Scheme 1.12. Reactions involving chorismate.

Chorismate synthase (CS) is responsible for a novel FMN dependent enzymatic 1,4-*anti* elimination of the 3-phosphate and cleavage of the C6-(proR)-hydrogen from 5-enol-pyruculshikimate 3-phosphate (ESPS) generating chorismate (*203, 204*) (Figure 1.5). CS displays an absolute requirement for reduced FMN for normal catalysis (*205-207*); despite the reduced state of the flavin, turnover of this enzyme does not result in a net redox change (*203, 204, 208, 209*). The classification of chorismate synthase is dictated by the acquisition of the required $FMNH_2$ cofactor; mono-functional chorismate synthases acquire exogenously reduced FMN (Figure 1.5) and are examples are found in bacteria and plants (*202, 205, 210-222*), *bi*-functional chorismate synthases exhibit β-NADPH dehydrogenase activity and are able to intrinsically reduce FMN (Figure 1.5) and are found in Neurospora *crassa* and *Saccharomyces cerevisiae (206, 218, 223, 224)*. Despite differences in the means

of FMN reduction both *mono*-functional and *bi*-functional chorismate synthases display similar phosphate elimination and hydrogen cleavage chemistries. One explanation for similarity is that all chorismate synthases share a common mono-functional ancestor (*218*).

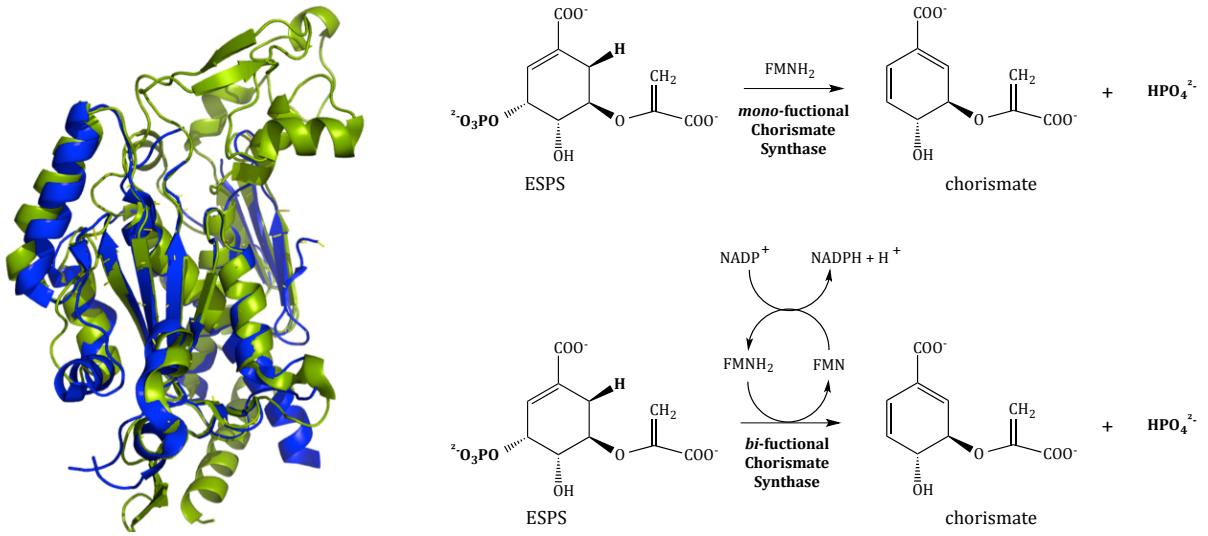

Figure 1.5. Comparison of *mono*- and *bi*-functional CS. Overlay of *mono*-functional CS from *S. pneumonia* (green) and *bi*-functional CS from *S. cerevisiae* (blue). Reactions catalyzed by chorismate synthase.

This intriguing catalytic activity has been the target of extensive studies to determine the mechanism of action (*203, 204, 208*). This unusual chemistry was novel to any known flavin dependent enzymes where the flavin traditionally participates in single or double electron redox chemistries (*150, 225, 226*). Macheroux and colleagues noticed that *mono*-functional chorismate synthase from *E. coli* binds oxidized FMN (K_d = 30 μM) three orders of magnitude (1000-fold) tighter in the presence of EPSP (K_d = 20 nM) indicative of an ordered binding mechanism (*215, 227*).

Product analysis of the conversion of ESPS to chorismate by chorismate synthase

revealed that catalysis involves an *anti*-1,4- elimination of the 3-phosphate and removal of the C6-(proR)-hydrogen (*201*). The *anti* stereochemistry of the product excludes the possibility of a concerted mechanism, supported by both theoretical and experimental data where the product of a concerted 1,4 elimination has *syn* stereochemistry (*204, 208, 228-230*). To determine if cleavage of the C6-(proR)-hydrogen occurs previous or subsequent to the *anti*-1,4- elimination of the 3-phosphate researchers measured the isotope effects when (6R)-[6-2H]-EPSP was used as the substrate and observed a small effect (~1.3) interpreted to be a secondary isotope effect where the C6 deuterium only slightly influenced the rate of C-O bond cleavage (*202*). This interpretation implies that cleavage of the C-O bond/elimination of the phosphate occurs before the liberation of the C6-(proR)-hydrogen and was supported by tritium-isotope studies ([4-2H]-EPSP) using chorismate synsthase from both *E. coli (*S. Bornemann and R.N.F. Thorneley, personal communication) and confirmed by transient kinetic analysis (*214*).

The non-redox role of the reduced FMN cofactor in chorismate synthase catalysis was further invested by Macheroux where the FMN of chorismate synthase was replaced with multiple flavin derivatives (*216*) and results show that modulation of the microenvironment surrounding the reduced FMN cofactor is induced by the binding of EPSP results in a more negative redox potential, promotes the protonation of the N1 position of isoalloxazine moiety and stablizes the flavin semiquinone (*216*). The neutral reduced FMN is an important intermediate species and its presence in turnover supports a role for the reduced flavin in catalysis participating in an electron transfer step (*209, 214*). Kinetic studies conducted with (6S)-6-flouro-EPSP and (6R)-flouro-EPSP where FMN is reduced using dithionite, demonstrate a slow product formation and in both cases a long-

lived semiquinone intermediate is observed (*216*). Interestingly, the reaction with (6R)-flouro-EPSP resulted in stable FMN semiquinone*product complex claimed to be essentially irreversible. These results provide evidence in support of a non-concerted mechanism where the reduced flavin plays a role as an electron donor subsequent to activation induced by substrate binding (*216*). The lack of catalytic activity demonstrated with 1,5-dihydro-5-deaza-FMN further supports this conclusion (*217*).

The first structural insights into the catalytic mechanism of came in 2003 when Maclean et al. solved the 2.0Å resolution crystal structure of *mono*-functional chorismate synthase from *Streptococcus pneumonia* in complex with oxidize FMN and EPSP (PDB code 1QXO) (*219*). Structural analysis suggests chorismate synthase forms a tetramer, composed of a pair of dimers, where each monomer displays a novel β-α-β fold. This structural topology was also observed in crystal structures of *mono*-functional chorismate synthase from *Aquifex aeolicus* (2.05Å, PDB code 1Q1L) (*231*) and *bi*-functional chorismate synthase from *Saccharomyces cerevisiae* (2.2Å, PDB code 1R53) (*232*). However, it must be noted that electron density is missing from 23% of the structure from *S. cerevisiae*. Monomer structure is dominated by a single large core domain, consisting of 4 long a-helices sandwiched between a pair of antiparallel β-sheets (*219*) (Figure 1.5). Multiple structural search methods could not locate any similar structures demonstrating this fold (*233, 234*). Many hydrogen bonding interactions contribute to dimerization such as the β-sheet extends from each monomer to form an eight-stranded antiparallel b-sheet forming 4 hydrogen bonds to equivalent sheet on the adjacent dimer but only a single ionic interaction occurs. This ionic interaction one of the monomers utilizes Lysine 238 to form a water-bridge, contacting the phosphate of the FMN of an adjacent monomer. The

predominantly hydrophobic tetramerization interface contains multiple hydrogen bonding interactions and salt-bridges are formed between Arg 13 and Asp 57 on both dimers (*219*). Structural assessment of quaternary structure is consistent with a series of ultracentrifugation/ chromatography studies done by Fitzpatrick et al (*218*).

Further analysis revealed that three monomers in each tetramer represented a conformation deemed as "closed", where loops from each monomer extend across the active site isolating it from bulk solvent (*219*). The fourth of the protomers was found to be in an "open" conformation where the position of the a loop near the active site involving residues 332 through 338 are in a position that makes the active site more accessible (*219*) (Figure 1.6). The active site of *mono*-functional chorismate synthase is formed by residues extending from multiple positions of secondary structure creating a hydrophobic pocket at the interface of the helical domain and a β-sheet (β-sheet 2).

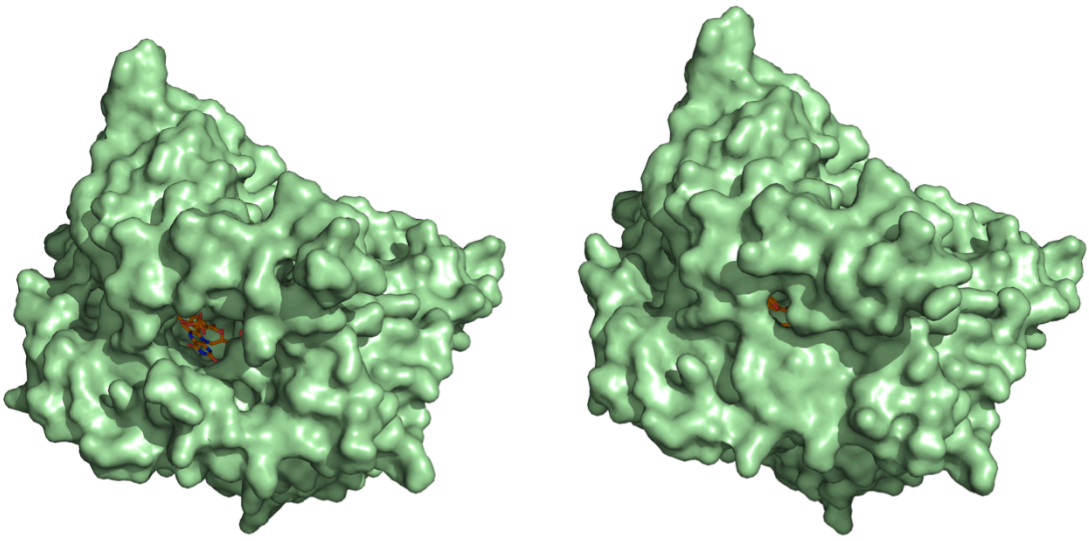

Figure 1.6. Monomer conformations displayed by crystal structures of chorismate synthase from *S. pneumonia*. Left structure represents the "open" conformation and the right structure represents the "closed" conformation.

The crystal structure data has also provided a structural explanation for the observations made by macheroux et al. where binding of FMN and EPSP are said to be ordered as the presence of EPSP causes a 1000-fold decrease in the dissociation constant for oxidized FMN (*215*). The phospho group of the FMN is buried deep within the secondary structure packing the *re*-face against the binding cavity exposing the *si*-face of the isoalloxazine to bulk solvent. EPSP stacks with the *si*-face of the FMN isoalloxazine closing off the active site and excluding solvent physically hindering the dissociation of FMN from the tertiary complex.

The binding of FMN is the result of multiple polar interactions between the hydroxyl and phosphate oxygen of the ribityl moiety of the FMN with the loop domain of the protein. The FMN phospho group resides at the dimer interface and interacts with the main chain nitrogen of Alanine 252, the side chain of Lys 311 and the main chain nitrogen of Glycine 296 from the neighboring monomer. A multitude of well-ordered water molecules surround the FMN phospho-ribityl and are responsible for bridging interactions to surrounding residues. The hydrophobic isoalloxazine appears to stack with a hydrophobic pocket of the protein.

The binding of EPSP to the *si*-face of the FMN involves a significant number of polar interactions with the enzyme and induces in a large conformational change that completes further interactions between members of the oligomer (*219*). The hydrophilic EPSP binding pocket is lined with 3 clusters of basic residues (2 histidine and 6 arginine residues) to form an environment complementary to EPSP. Site directed mutagenesis studies of his17 to alanine mutants from *Neurospora crassa* displayed a five-fold increase in the dissociation constant (K_d) for EPSP implying his17 is involved with the binding of EPSP (*220*).

Interestingly, there are no amino acid residues in the proximately of the C6-position of EPSP leaving the 5-position nitrogen on the isoalloxazine ring of the FMN as the only candidate close enough to act as a base (*219*).

The conformational change induced by the binding of EPSP positions His110 proximal to the N1 atom of the FMN close enough to promote protonation of the neutral reduced FMN, which suggests that His110 plays an important role in catalysis. This was later confirmed but site directed mutagenesis where a histidine106 (his110 in *S. pneunomiae*) to alanine mutant of *bi*-functional chorismate synthase from *Neurospora crassa* displayed a twenty-fold reduction in elimination activity when compared to wildtype (*220*). His110 was found in two different conformations in the crystal structure of enzyme from *S. pneunomiae*; in the *open* conformation his110 is coordinated with 2-oxygen of the FMN and in the *closed* conformation his110 contact both the 5-oxygen of EPSP and the main chain amide nitrogen of ala111. The mobility and the specific interactions of His110 suggest that it is the functional active site acid responsible for protonation of the FMN 2-oxygen resulting in a neutral $FMNH_2$ (*219*).

Based on these observations Maclean et al. proposed 2 possible mechanisms for chorismate synthase that differ in the role of the 5-nitrogen of the FMN during C6-(pro-R) hydrogen abstraction (*219*). (Scheme 1.13) One proposed mechanism utilizes radical intermediates of both EPSP and FMN where the flavin N5 hydrogen is involved in C6-(pro-R) hydrogen abstraction. In contrast, the cationic mechanism utilizes a proton from the 5-nitrogen of the FMN in C6-(pro-R) hydrogen abstraction and involves a cationic EPSP intermediate.

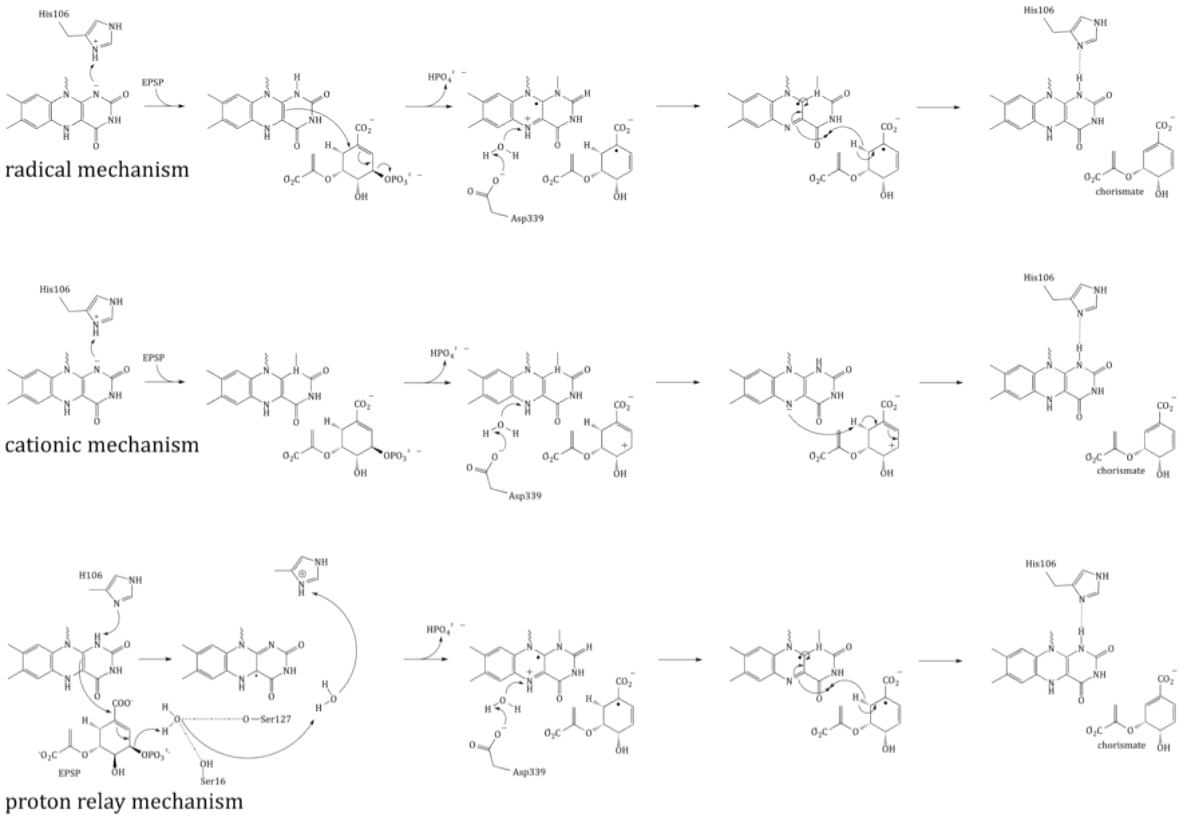

Scheme 1.13. Proposed mechanisms for the conversion of 5-enol-pyruculshikimate 3 phosphate (EPSP) to chorismate by chorismate synthase.

Both of these proposed mechanisms utilize the 5-nitrogen of the flavin as the active site base where hydrogen abstraction from the dephosporylated substrate is contingent upon deprotonation of this position (Scheme 13). A proximal aspartate (Asp339 in *S. pneumonia*, Asp367 in *N. crassa*) residue was proposed to be responsible for the water-mediated deproptonation of the 5-position nitrogen of the acid FMN semiquinone (*219*). Analysis of asp367ala and asp367asn mutant chorismate synthases from *N. crassa* revealed a 300 to 600 fold decrease in activity and the mutations had no significant effect on the binding of EPSP or oxidized FMN when compared to wild type further supporting the role of this residue in catalysis (*221*). Rauch et al carried out additional mutagenesis exploring

the role of two invariant active site serine residues (16 and 127) where both Ser16Ala and Ser127Ala mutants displayed a marked decrease in activity, 70- and 6- fold respectively compared to wild type and the Ser16ala-Ser127Ala double mutant was completely inactive (*222*). On this basis a third mechanism was proposed, where residues ser16, ser127 and his110 along with multiple water molecules form a "proton relay system" responsible for the formation of the observed radical intermediate (*222*) (Scheme 13). In this mechanism His106 is responsible for abstracting a proton from the N(1)-C(1)=O locus of the isoalloxazine ring using a two water shuttling system mediated by residues ser16 and ser127, resulting in protonation of the phosphate ester oxygen facilitating elimination.

UDP-galatopyranose mutase

UDP galactopyranose mutase (UGM) is a flavin dependent protein that catalyzes the 6 to 5 member sugar ring contraction of UDP-galactopyranose (UDP-galp) to UDP-galactofuranose (UDP-galf) (Scheme 1.14). This reaction has an equilibrium position that favors UDP-galp (11:1) as a result of the increase ring stain generated by the compression of the sugar (*235*). Much like CS, the UGM-dependent turnover of UDP-galp is redox neutral.

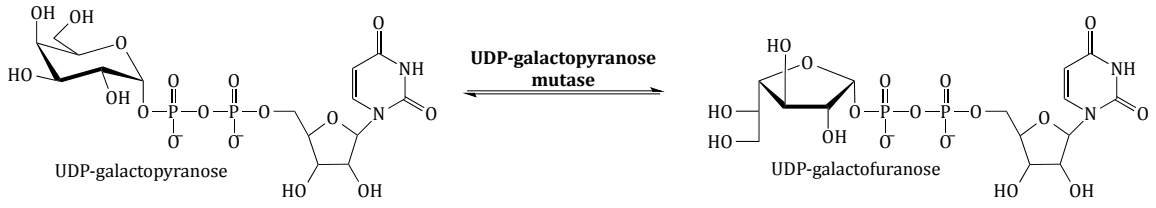

Scheme 1.14. Reaction catalyzed by UDP-galactopyranose mutase.

UDP-galf is a required precursor for the biosynthesis of galactofuranose dependent glycoconjugates found in bacteria, fungi, and protists (*236-239*). In *Mycobacterium* species UGM is responsible for the biosynthesis of precursors used for glycoconjugates which function in anchoring the out mycolic acid layer to the peptidoglycan of the cell wall. Mutant *Mycobacterium smegmatis* lacking the gene *glf* which codes for UGM lacked the ability to grow at non-permissive temperatures confirming that UGM in these organisms is essential for growth (*240*). UGM was also shown to have importance in the fungi *Aspergillus fumigatus* the causative agent of a condition that poses a lethal threat to immunocompromised individuals (*241*). Deletion of UGM in *A. fumigatus* resulted in attenuated virulence in a low dose mouse model and attributed to a decrease in the thickness of the cell wall correlating to an increased susceptibility to antifungal agents (*242*). In kinetoplastids such as the protozoan species *Leishmania major* the monosaccharide product of UGM catalysis serves as a precursor for galactofuranose, which anchor lipophosphoglycans and glycoinositolphopholipids to the cytosolic surface of the cell(*243*). Mutant *L. major* devoid of UGM activity paralleled growth of wild type species *in vitro* but displayed attenuated virulence (*244*). These observations have spurred scientific investigation into the catalytic and structural characterization of UGM in these organisms as this activity is absent in higher eukaryotic species such as humans making UGM is an ideal target for anti-microbial, -fungal and -parasitic agents (*240, 245*). Several recent studies have presented several UGM inhibitor candidates with significant (μM) inhibition constants (K_I) utilizing both substrate mimics (*246-250*), transition state mimics (*251*) and novel designs (*252-254*).

Initial reports indicated that UGM is FAD-dependent (*235*). It was later determined that UGM is only active in when the flavin is in the reduced form (*255-259*), though earlier reports suggested that the oxidized form of the enzyme does exhibit activity (*260*). Eukaryotic UGMs from fungi (*A. fumigatus)* and the protozoa *T. cruzi, L. Mexicana and L. infatum* utilize NADPH as a co-substrate and can stabilize the reduced form of the enzyme even under aerobic conditions (*261-263*). It was also demonstrated that once reduced eukaryotic UGMs can complete several hundred turnovers before reoxidation (inactivation) occurs as a result of the rate of oxidation (k_{ox}) occurring 200 to 1500-fold slower than rate of reduction (k_{red}) (*262-264*). Bacterial UGM can also utilize NADPH as reducing equivalents for enzyme activation but requires a large excess of NADPH and extended incubation times (10,000 fold reduction in k_{red} compared to eukaryotic UGM (*262*)), suggesting that alternative physiological substrates exist (*265*). It was proposed that this is indicative of promiscuous activation where oxidized UGM could accept a hydride/reducing equivalent from multiple types of reduced donors (*266*). Kinetic analysis demonstrated that UGM from multiple eukaryotic species undergo reduction of the flavin cofactor by NADH 7 to 17-fold slower than by NADPH but exhibit dissociation constants that bind NADH 5 to 10 fold more tightly than NADPH for UGM from *T. cruzi* and *A. fumigatus* respectively (*264*).

The most widely accepted chemical mechanism for UGM utilizes the flavin as a nucleophile to facilitate an attack on the anomeric carbon of the substrate displacing UDP. In this mechanism the binding of the substrate (UDP-galp) to the reduced (active) form of UGM results in a local reorganization of the active site resulting in positioning of the N(5) FAD proximal (3.4Å) to the C(1)-Galp (*262, 267-271*). The new conformation facilitates a

direct attack of the substrate anomeric carbon by the reduced flavin N(5) position in a proposed SN2-like mechanism (*272*). (Scheme 1.15) Direct attack by the flavin is also supported by studies where substitution of UGM-FAD with 5-deaza-FAD resulted in inactive enzyme (*273*). Inactivity of 5-deaza-FAD substituted UGM would be expected under such a mechanism as 5-deaza-FAD would be unable to offer the 5-Nitrogen as a nucleophile. It must be noted that the results of 5-deaza-FAD substitution studies were initially proposed to be evidence in support of a mechanism involving single electron transfer (*273*). Additionally, the kinetic linear free energy relationship of k_{cat} to the nucleophiliicity of the N(5) position of UGM substituted with various flavin analogs resulted in a $\rho = -2.4$, consistent with a direct attack mechanism (*254*).

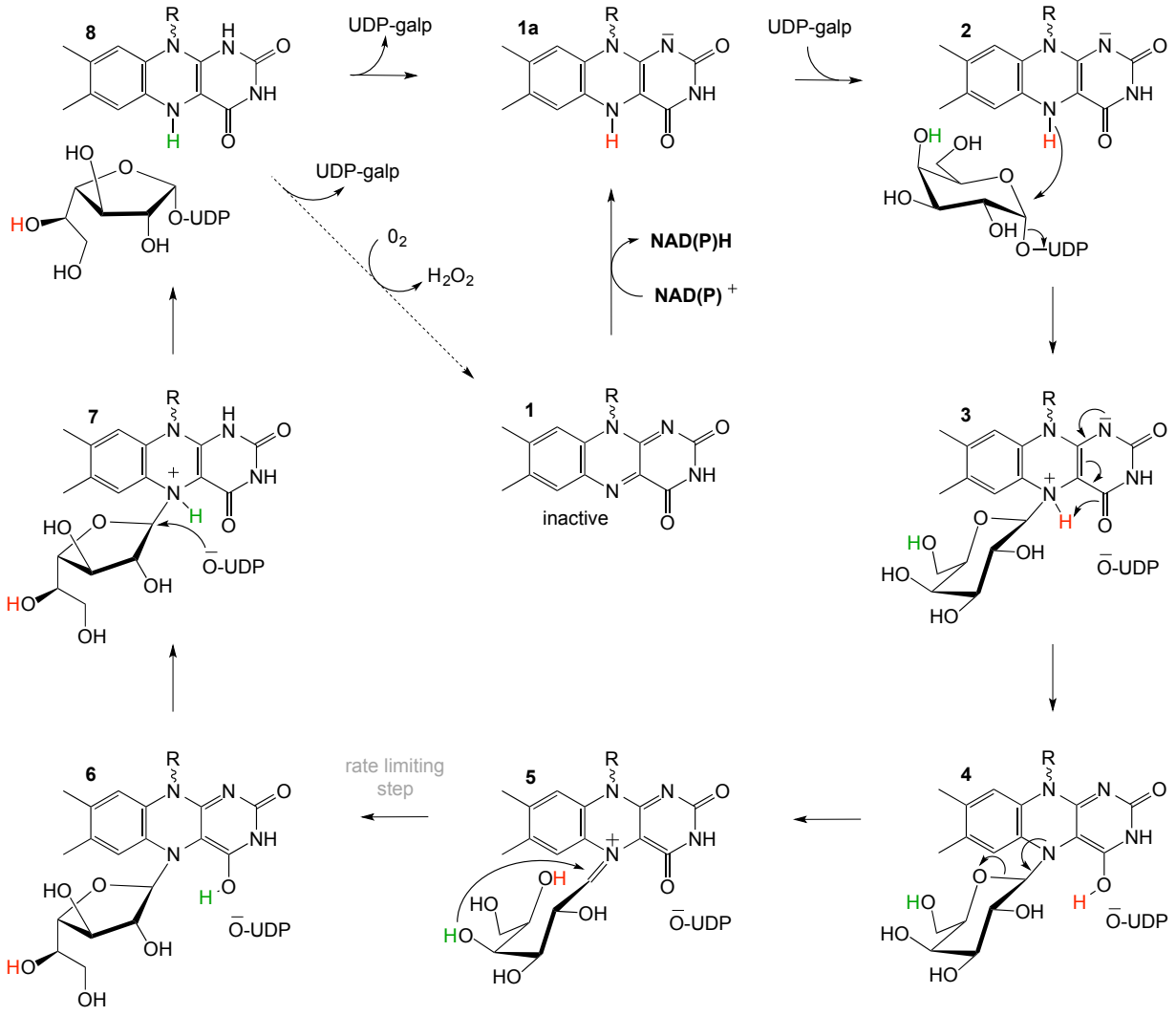

Scheme 1.15. Proposed mechanism of UDP-glactopyranose to UDP-galactofuranose by UGM.

The nucleophilic attack of the FAD N(5) of UGM on the C(1) of UDP-galp results in the formation of a covalently bonded FAD-sugar adduct and the displacement of the UDP. (Scheme 15, **3**) The formation of a covalent bound FAD reaction intermediate was confirmed in eukaryotic UGMs by UV/vis spectrophotometry and mass spectrometry (*261*). The covalent FAD-galactose intermediate was also confirmed in prokaryotic UGMs by mass spectrometry, NMR and most recently a solved crystal structure of *M. tuberculosis*

(structure not yet deposited in PDB) (*268, 274, 275*). It was suggested that the sugar-FAD adduct would facilitate ring opening and activation of the C(1) of galp where the flavin would act as a structural scaffold providing the dimensional constraints required for ring contraction (*148, 264, 276*). This mechanistic progression is also consistent with positional isotope exchange (PIX) studies that determined that the glycosidic bond of UDP-galp is cleaved during catalysis (*277, 278*). The exact identity of the captured covalent sugar adduct in crystal structures from *T. cruzi* could not be identified however researchers concluded it must be either species **3** or **4** of Scheme 15 (*274*).

Kinetic studies conducted with UGM from *Trypanosoma cruzi* showed no evidence of the formation of a flavin semiquinone species during turnover (*261*) despite earlier reports suggesting the flavin semiquinone is stabilized by substrate binding (*279*). Absence of a flavin semiquinone during catalysis does not offer support for the mechanism involving single electron transfer. Interestingly, these kinetic studies did reveal the formation of a possible flavin imminium ion intermediate (Scheme 15**, 5**) during the turnover of UGM from *T. cruzi (261)*. Hybrid quantum/classical calculations preformed at the density function theory level suggest that C(4)=O of the FAD accepts a proton from N(5) (Scheme 15**, 4**) of the FAD and subsequently donates it to the O(5) of Galp (*280*). FAD imminium ion formation would require deprotonation of the N(5)-FAD of the covalent FAD-sugar adduct thereby facilitate opening of the ring of galp between C(1) and the ether oxygen (Scheme 15**, 5**) (*264*). Hybrid simulations also predict that the proton for the C(4)-OH of Galp is shuttled to the C(4)=O of FAD during the contraction of the ring resulting in a covalent FAD-galf adduct (Scheme 15**, 6**) (*280*). To date there is no biochemical information on the

mechanisms of cleavage of the covalent FAD-galf complex or reconstruction of the galf-UDP molecule or the order in which they occur.

Kinetic analysis of UGM from *T. cruzi* demonstrated that the rate of the formation of the FAD imminium species (300 s^{-1}) occurs much more rapidly than the observed rate of catalysis ($k_{cat} \sim 10\ s^{-1}$) (*261, 264*). Viscosity effects studies have also ruled out product release as the rate-limiting step (*261, 264*). On this basis it was proposed that rate of catalysis is governed by either the ring contraction or reattachment of UDP (*261*).

The 3-demensional structure of UGM has been extensively characterized. In all 46 structures from 8 different species including prokaryotic strains from; *Camplobacter jejuni, Corynebacterium diphtheriae, Dienococcus radiodurans, Klebsiella pnuemoniae, Mycobacterium tuberculosis* and *Escherichia coli* as well as eukaryotic strains from *A. fumigatus* and *T. cruzi* have been solved *(246, 255, 262, 264, 267-269, 271, 275, 281-286).* These structures included examples of UGM in both the oxidized and reduced forms and in complex with multiple ligands including NADH, NADPH, flavin mononucleotide (FMN), UDP-phosphono-galactopyranose, UDP-galactose, UDP, UDP-galp and dideoxy-tetrafluorinated analogoues both the substrate and product, UDP-F_4-galp and UDP-F_4-galf as well as the potential inhibitor 2-[4-(4-chlorophenyl)-7-(2-thienyl)-2-thia-5,6,8,9-tetrabicyclo[4.3.0]nona-4,7,9-trien-3-yl]acetic (*246, 262, 268-271, 275, 283, 284*). Single site directed mutant UGM structures of F66A, Y317A, N207A, Q107A, Y104A and H63A mutants from *A. fumigatus* have also been determined (*264, 267, 285, 286*).

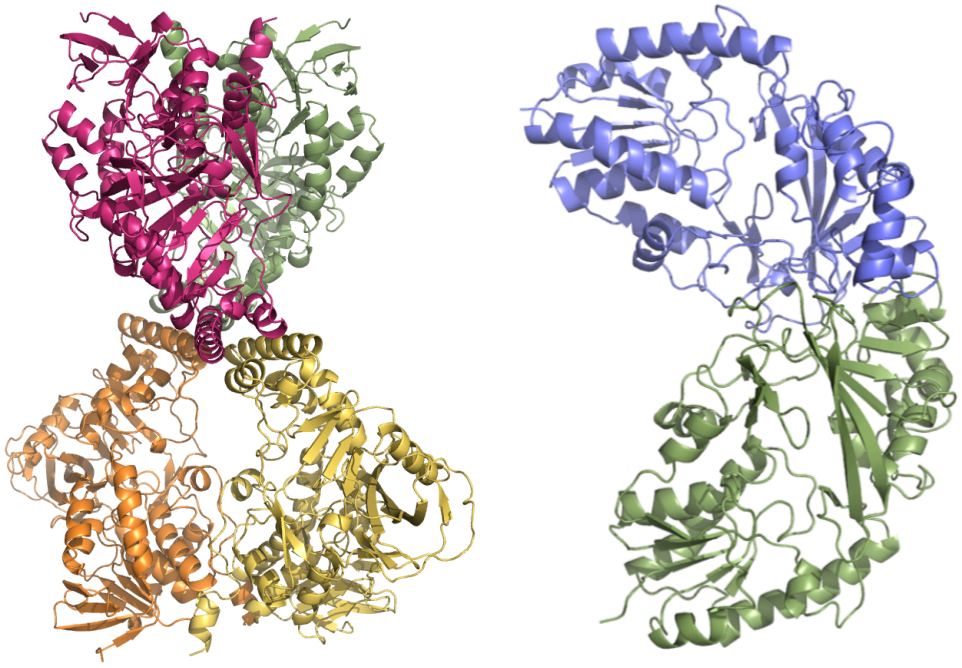

Figure 1.7. Crystal structures of UGM. Three-dimensional cartoon representation of tetrameric UGM from eukaryotic *A. fumigatus* (left) and dimeric UGM from prokaryotic *M. tuberculosis* (right).

The first crystal structure of prokaryotic UGM from Escherichia coli (PDB code 1I8T) was solved in 2001 and revealed a complex topology consisting of three domains, two of which are non-contiguous (*255*). The structure of domain 1 is non-contiguous tripartite domain containing an abbreviated Rossman fold responsible for FAD binding. The motif is commonly required to bind a FAD molecule however, in UGM from *E. coli* it lacks the terminal strand of the 6-stranded sheet found In classic examples of the Rossman fold (*287*). Domain 2 is contiguous and is composed of a cluster of 5 alpha helices and contains the binding site the uridine group, the active site flap 1 (residues 167 to 177 in *K. pneumoniae*) that undergoes UDP-galp dependent conformational changes and also plays a

role in dimerization (*284*). The third domain is bipartite and non-contiguous and consists of a 6-stranded antiparallel β-sheet. The structures of all bacterial UGMs are topologically similar where secondary-structure matching (SSM) analysis revealed that 73 to 96 % of secondary structure elements found in UGM from *E. coli* are completely conserved across all other known bacterial UGMs (*288*) despite substantial variation in primary structure (37 to 44 % pairwise identity with UGM from *E. coli) (264).*

Multiple challenges in structure determination were encountered using UGM from eukaryotic species both *A. fumigatus (270, 283, 289)* and *L. major (271)* including translational psuedo-symmetry and crystal twinning. It was later determined that mutagenesis of long charged surface residues, specifically lysine and glutamine allowed for reproducible crystal growth that were free of crystallographic pathologies (*283, 290, 291*). Two independent groups solved the mutant crystal structures of UGM from *A. fumigatus* using either the double mutant K344A/K345A(*283*) or the single mutant R327A (*271*) strains where the two structures produced are almost identical. These structures revealed that eukaryotic UGM consists of 3 domains similar to UGMs from prokaryotes with noticeable variations. Domain one retains the shortened Rossman fold described for prokaryotic UGMs but has an additional 4-stranded antiparrellel β-sheet that sits adjacent to the Rossman fold and an extended (~30 residues) C-terminus that play a role in the tetrameric assembly of UGM from *A. fumigatus.* Domain two consists of a bundle of α-helices similar to prokaryotic enzymes but contains an additional α-helix and a helical extension (~7 residues), which are involved in tetramer formation. The extra α-helix forms the scaffold for a additional mobile active site flap (flap 2) absent in prokaryotic UGMs.

Domain three contains a twisted, seven-stranded antiparallel β-sheet compared to the six-stranded β-sheet seen in prokaryotes.

More recently the crystal structure of UGM from *T. cruzi* was solved in both oxidized (PDB code 4DSG) and reduced (PDB code 4DSH) form (*282*). The protomer structure obtained from crystals of *T. cruzi* was nearly identical to the protomers of UGM from *A. fumigatus* (RMSD 1.10 Å) however the overall topology of the two differs greatly as a result of differences in oligomeric state (*264*). UGM from *T. cruzi* crystallized as a monomer as opposed to tetrameric UGM from A. fumigatus. The tetrameric state of crystal structures UGM from *A. fumigatus* are consistent with results of small angle X-ray scattering that describe the formation of a dimer of dimers (*282*).

Additionally, crystal structures of eukaryotic UGM from *A. fumigatus* were solved in complex with NADH (PDB code 4GDD) and NADPH (PDB code 4GDC) and provided a valuable description of the unique NAD(P)H binding site and interactions (*262*). The NAD(P)H molecule is sandwiched between domain one and three, forming interactions with both and is positioned in an unusually constrained conformation positions the adenine moiety within hydrogen bonding distance of the ribose hydroxyl (*286*) which is vastly different than the Rossman dinucleotide binding fold common described for most enzymes utilizing NAD(P)H as a substrate (*292, 293*). Multiple conserved residues (N57, I65, F66, H68, R91, S93, Y 104 and Y317) are involved in stabilizing the E•NAD(P)H complex where hydrogen bonding between Y104 and 2' phosphoryl group of NADPH is responsible for the ~180- fold preference (k_{cat}/K_D) for NADPH over NADH seen in UGM from *A. fumigatus* (*262*). However, binding of NAD(P)H molecules does not invoke conformational changes in either of the 2 active site flaps, flap 1 (residues 179 to 187 in

UGM from *A. fumigatus*) or flap 2 (residues 203 to 209 in UGM from *A. fumigatus*) responsible for closure of the active site (*262*). Interestingly, the bound NAD(P)H molecule extends into the UPD-galp binding pocket and implies that binding of NAD(P)H and UDP-galp are mutually exclusive (*264*). Prokaryotic UGM lack all of the conserved residues that contact the ADP moiety of NAD(P)H seen in eukaryotic UGM indicating that prokaryotic UGM does not contain a NAD(P)H binding domain which is consistent with biochemical data (*264*).

Chapter II.
Renalase is an α-NAD(P)H Oxidase/Anomerase

Brett A. Beaupre, Brenton R. Carmichael, Matthew R. Hoag, Dhara D. Shah and Graham R. Moran

Abstract

Renalase is a protein hormone secreted into blood by the kidney that is reported to lower blood pressure and slow heart rate. Since its discovery in 2005, renalase has been the subject of conjecture pertaining to its catalytic function. While it has been widely reported that renalase is the third monoamine oxidase (monoamine oxidase C) that oxidizes circulating catecholamines such as epinephrine, there has been no convincing demonstration of this catalysis *in vitro*. Renalase is a flavoprotein whose structural topology is similar to known oxidases, lysine demethylases and monooxygenases, but whose active site bears no resemblance to that of any known flavoprotein. We have identified the catalytic activity of renalase as an α-NAD(P)H oxidase/anomerase, whereby low equilibrium concentrations of the α-anomer of NADPH and NADH initiate rapid reduction of the renalase flavin cofactor. The reduced cofactor then reacts with dioxygen to form hydrogen peroxide and releases nicotinamide dinucleotide product in the β-form. These processes yield an apparent turnover number (0.5 s^{-1} in atmospheric dioxygen) that is at least two-orders of magnitude more rapid than any reported activity with catechol neurotransmitters. This highly novel activity is the first demonstration of a role for naturally occurring α-NAD(P)H anomers in mammalian physiology and the first report of a flavoprotein catalyzing an epimerization reaction.

Introduction

Human renalase was first discovered in 2005 by Xu et al. (*1, 294*) and its discovery spurred considerable interest as the protein was reported to be secreted into blood by the kidney as a hormone to down-modulate blood pressure and cardiac output. (*61*) These observations have since been associated with the high incidence of cardiovascular disease in patients with end-stage renal disease (*4*), emphasizing that diminishment of the endocrine function of the kidney is wholly detrimental to cardiac function. (*1, 25, 295*) In addition, mice deficient in renalase have been reported to exhibit elevated blood pressure (*4*) and human renalase polymorphisms have been linked with an increased incidence of diabetes and stroke. (*296, 297*) Since its discovery a definitive demonstration of the catalytic function of renalase has remained elusive. While it has been widely reported that renalase lowers blood pressure and modifies heartbeat by catabolizing circulating catecholamines (*2, 3, 5, 12, 14, 16, 36*), neither the specific substrate(s) and product(s) nor the overall stoichiometry for the reaction has been convincingly established. *In vivo* studies in rodents show that the concentration of circulating catecholic neurotransmitters is lowered by intravenous injection of renalase. (*1, 4, 36*) However, *in vitro* studies have failed to demonstrate significantly catalytic consumption of catecholic neurotransmitters (or their precursors). (*36, 51*) It has been claimed that renalase mobilizes four electrons by acquiring two electrons from NAD(P)H in order to catalyze a net two-electron oxidation and cyclization of epinephrine to form adrenochrome. (*2*) Such a transformation for epinephrine is, however, facile in the absence of an enzyme catalyst and readily observed in oxygenated solutions under a variety of conditions. (*298, 299*) Similarly, the observation of apparent slow oxidation of reduced pyridine nucleotide cofactors in the presence of

renalase is complicated by the inherent instability of these molecules at pH values near or below neutral pH. (*300*) As a consequence, claims of renalase directly catalyzing the breakdown of catecholamines has been challenged in both letters and research articles. (*48, 51, 301*)

The discord in regard to the activity of renalase has developed both from its reported physiological function and from its structural similarity to known redox enzymes. The primary structure of the protein has at least 4 forms that result from RNA splicing patterns for seven exons. Only the two longest sequences that include protein derived from at least six exons show direct similarity to known flavoproteins. (*12, 301*) The three-dimensional structure of renalase isoform 1 (342 amino acids) was published by Milani et al. 2011. (*60*) This structure indicated a fold consistent with a large structural family of flavoproteins that include oxidases, lysine demethylases, and monooxygenases. (*302-306*) The apparent active site of renalase was observed to be a clearly delineated pocket in the surface of the protein that provides access to the *si*-face of a non-covalently bound flavin adenine dinucleotide (FAD) cofactor. Within this cavity, the constellation of residues that are conserved in renalase primary structures gave no clear indication for any known activity of a flavoprotein. However, renalase was observed to readily form an adduct with sulfite ions at the FAD isoalloxazine N5 position, a curious characteristic that is most commonly associated with oxidase activity. (*60, 307, 308*)

In this article we identify renalase as an α-NAD(P)H oxidase/anomerase whereby the substrate α-dihydropyridyl ring is oxidized by transferring two electrons to the flavin cofactor and the configuration of the ribose C1 is converted from α to β. The reduced FAD cofactor then reoxidizes by reacting with dioxygen to yield hydrogen peroxide (Scheme

2.1). This highly novel transformation is both unprecedented catalytic chemistry and the first physiological link to α-pyridine nucleotides in higher organisms.

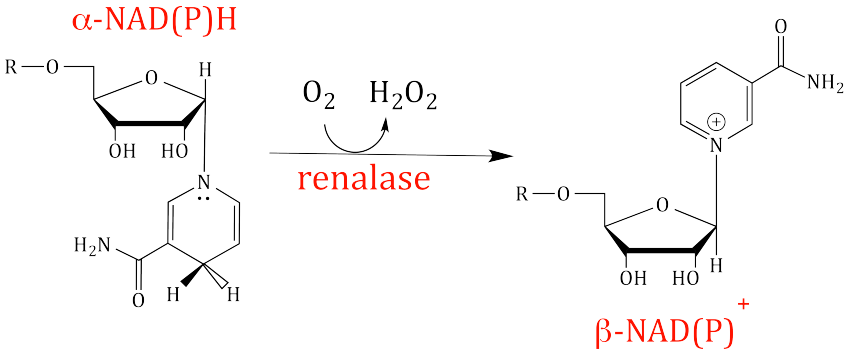

Scheme 2.1. Reaction catalyzed by renalase.

Materials and Methods

Materials: Plasmids were purified using the Qiagen Midi-Prep plasmid preparation kit. Oligonucleotides were synthesized by Operon. Vector pET28a(+) was obtained from Novagen. Restriction enzymes, DNA modification enzymes and competent (DH5α and BL21 (DE3)) *E. coli* were obtained from New England Biolabs. FAD, (4-(2-hydroxyethyl)-1-piperazineethanesulfonic acid (HEPES), potassium phosphate, isopropyl-β-thiogalactopyranoside (IPTG) and sodium chloride were from ACROS. Electrophoretic grade agarose was obtained from ICN Biomedicals. Luria Bertani broth (Lennox) powder was from Fisher Scientific. Kanamycin and β-NADPH were purchased from Alexis. β-$NADP^+$ was purchased from Calbiochem. β-NADH, β-NAD^+ and epinephrine were from Sigma-Aldrich.

Cloning and expression of Human Renalase: The gene encoding full length WT Human renalase (isoform 1) optimized for expression in *E. coli* and incorporating Nde I and Xho I sites at the 5' and 3' ends was purchased from Enzymax. The gene was supplied in plasmid pUC57 and subcloned into the Nde I and Xho I restriction sites of pET-28a(+) expression vector (Novagen). The Nde I insertion of pET-28a(+) plasmid incorporates an N-terminal His-Tag fusion. This plasmid (pHSRENHT) was transformed into chemically competent *E. coli* BL21 (DE3) cells (Novagen). All media used with transformed cells included 100 μg/mL kanamycin. Transformants were plated onto LB agar and a single isolated *E. coli* colony was cultured in LB broth. Individual 1 mL cell stocks were made by adding sterile glycerol to a final concentration of 20% to cells grown to early log phase and these were then stored at -80°C.

Renalase Expression and Purification: For expression, 1 mL cell stocks were thawed, plated onto LB agar, 100 μg/mL kanamycin, and grown overnight at 37°C (50 μL/plate). The lawn of cells obtained were then transferred to LB broth (two plates/L of broth) and grown at 37°C in a shaking incubator (220 rpm) to mid-log phase (OD_{600nm}=0.5) and the temperature lowered to 22°C. The culture was then grown to ~ OD_{600nm}=1.0 (~1 hr) and induced with 0.1 mM IPTG and left to express renalase for 20 hrs before the cells were harvested by centrifugation (4,000 g for 30 min). Unless otherwise stated, all subsequent purification steps were performed at 4°C. Cell pellets were resuspended in 20 mM HEPES buffer pH 7.5 (approximately 10 mL/L culture) and lysed by sonication using a Branson 450 sonicator (3 x 240 seconds at 50 W). The temperature of the cell suspension was

maintained below 10°C by immersing the sample vessel in a slurry of ice and water. Lysed cells were centrifuged at 32,800 x g for 30 min, the pellet was discarded and the supernatant loaded onto a 12.5 x 150 mm Co^{2+} Talon column (BD Biosciences) equilibrated with 20 mM HEPES buffer pH 7.5. Protein was eluted with a 1 mL/min two-step protocol. Initially contaminating proteins were eluted with 150 mL of 10 mM imidazole, 50 mM HEPES buffer pH 7.5, then a gradient from 10 mM to 150 mM imidazole in the same buffer was used to elute renalase. Distinctly yellow fractions were pooled. Imidazole was removed and the buffer exchanged to PBS (10 mM Na_2HPO_4, 2 mM KH_2PO_4, 2.7 mM KCl, 137 mM NaCl, pH 7.4) by repeated concentration and dilution using 10 kDa nominal molecular weight cut-off centrifugal concentrator (Millipore, Amicon) to achieve a net ≥1000-fold exchange. Aliquots of purified concentrated renalase were then stored at -80°C.

Quantitation: The concentration of NADPH and NADH solutions were determined using the published 340 nm extinction coefficient of 6200 $M^{-1}cm^{-1}$ (*309*). The extinction coefficient for Renalase was determined by liberating the FAD cofactor from the protein. Initially, the absorption spectrum of 9 μM renalase was recorded using a Hewlett Packard 8453 spectrophotometer. SDS to 1% final concentration was then added to denature the protein and release the flavin and the spectrum was again recorded. The spectrum of the unbound flavin was then corrected for dilution and the known extinction coefficient for this molecule at 450 nm (e_{450nm} = 11,300 $M^{-1}cm^{-1}$) was used to calculate the extinction coefficient of renalase (e_{458nm} = 11,330 $M^{-1}cm^{-1}$). Epinephrine was quantified by weight.

Substrate/Product Analysis: The apparent substrate for renalase was detected as a contaminant of β-NAD(P)H stocks that caused rapid reduction of the renalase flavin cofactor. The proportion of the substrate in NAD(P)H solutions was determined by two methods. First, relatively high concentrations of β-NADPH were mixed with renalase using a Hi-Tech (now TgK) stopped-flow spectrophotometer under anaerobic conditions. Prior to the experiment, the instrument was scrubbed of residual dioxygen for ~16 hrs using a solution of 50 mM glucose and 15.5 U/mL glucose oxidase. Renalase in PBS buffer was prepared in a tonometer by adding 8 μM enzyme with 1 mM glucose in the body of the vessel and 16 U of glucose oxidase in a side arm (U is defined as 1 unit of enzymatic activity or 1 μmole/min). The tonometer was then subject to 45 cycles of low vacuum followed by argon gas with mild agitation to exchange all dissolved dioxygen. Once anaerobic, the renalase/glucose solution was mixed with the glucose oxidase from the tonometer side arm and the vessel was mounted onto the stopped-flow instrument. NADPH solutions were prepared with 1 mM glucose and made anaerobic by sparging with argon for 5 minutes and then adding in 8 U of glucose oxidase immediately prior to mounting onto the instrument. Renalase and NADPH were then mixed and the extent of flavin cofactor reduction was recorded at 458 nm. The second method used to determine the proportion of substrate in NAD(P)H solutions was to observe the change in molecular oxygen concentration when high concentrations of NAD(P)H were added to low μMolar concentrations of renalase in PBS buffer using a Hansetech dioxgen electrode. Assuming 1:1 substrate to dioxygen reaction stoichiometry (*vide infra*), the concentration of substrate could be determined from the amplitude of the observed change in molecular oxygen concentration.

Evidence for the identity of the substrate was obtained from HPLC analysis. NAD(P)H solutions (10 mM) were diluted by a factor of 50 and filtered using a Millipore 0.5 mL 10 kDa nominal molecular weight centrifugal filter device. 50 μL of this solution was then injected onto a Waters Xterra C18 cartridge column (4.6 x 150 mm) run isocratically at 0.5 mL/min with 10 mM NaPi pH 7.5 coupled to a waters 600E pump and Waters 2487 detector. The elution of components was observed at both 260 and 340 nm. The dominant components having absorbance at 340 nm were collected and their spectra recorded. A second sample was then prepared in an equivalent manner but with the addition of renalase to 5 μM. After incubation for 2 min this sample was filtered to remove the enzyme and subject to HPLC analysis.

HPLC identification of the product of the renalase reaction was based on co-elution. Chromatography conditions were as described above. Initially, a 50 μL control sample from a solution of 340 μM NADH in PBS buffer was separated into its α and β-NADH components. A second 50 μL sample was then reacted with 5 μM renalase for 2 minutes and filtered using a Millipore 0.5 mL 10 kDa nominal molecular weight centrifugal filter device before being chromatographed in an equivalent manner. A third 340 μM sample was then prepared with the addition of 15 μM β-NAD^+ and chromatographed. The retention time of the product of the renalase reaction was compared to that of the sample spiked with β-NAD^+ to identify the product.

The nicotinamide product of a renalase/NADPH reaction was identified as β-$NAD(P)^+$ by nuclear magnetic resonance (NMR). A 40 mM solution of NADPH was prepared in 10 mM NaPi buffer pH 7.4 in deuterium oxide solvent. The ^1H NMR spectrum was then

recorded by collecting and transforming 256 FIDs soon after preparing the sample on a Bruker 300 MHz NMR instrument. Renalase (10 μM – 0.3 U) and catalase (0.2 U) were then added to the NMR tube and mixed by repeated pipetting with a Pasteur pipette. Further spectra were then recorded at specific times over the next 100 minutes. A control NADPH sample was then prepared at the same concentration in the same buffer and monitored similarly. Prior to each spectrum (sample and control) the contents of the NMR tube were re-equillibrated with atmospheric molecular oxygen by repeatedly drawing the solution into a Pasteur pipette. The concentration of the product was approximated from the relative integrations of known resonances for β-NADPH and the singlet resonance for proton N2 (2 position of the nicotinamide) of the species observed to accumulate in the reaction. These spectra were compared to the proton spectra of 1 mM β-$NADP^+$ alone and 1 mM β-$NADP^+$ in the presence of 40 mM β-NADPH.

Evaluation of Epinephrine as a Substrate for Renalase: Epinephrine was tested as a substrate for renalase using four approaches. In the first, the reported accumulation of adrenochrome in the presence of renalase was evaluated. The concentration dependence of the formation of adrenochrome was observed by adding varied concentrations of epinephrine (0-400 μM) (prepared in 10 mM HCl) to a solution of PBS buffer and then observing the increase in absorbance at 480 nm at 25°C. The initial rate at each epinephrine concentration was measured by fitting the first 200 seconds to a straight line and dividing the slope by the extinction coefficient for adrenochrome (4020 $M^{-1}cm^{-1}$). (*299*) To determine if renalase and/or NADPH accelerates this process, 10 μM renalase and then

10 μM renalase with freshly prepared β-NADPH to 400 μM was added to 400 μM epinephrine (final) and the initial rate recorded.

In the second approach the effect of epinephrine on the observed single-turnover kinetics was assessed by stopped-flow spectrophotometry. Non-pseudo first order single-turnover reactions were initiated by mixing a limiting concentration of the α-NADPH (~6 μM in 400 μM β-NADPH) in PBS buffer equilibrated with atmospheric dioxygen (~250 μM) with 11.4 μM aerobic renalase in the same buffer. The reaction was monitored by observing the reduction and reoxidation of enzymes' flavin cofactor at 458 nm. Epinephrine (400 μM) was then added to the α-NADPH solution and the observation repeated. In order to evaluate if some soluble component of blood modulated or reacted with renalase, this observation was repeated with the α-NADPH/epinephrine solution prepared in fresh cell free blood plasma. Solely for comparison the data were fit to Equation 2.1 that describes three successive first order events. In this equation k_1 is the rate apparent constant for reduction, k_2 is an additional unassigned phase and k_3 is the apparent rate constant for reoxidation, $DA_{1\text{-}3}$ are the respective absorbance amplitudes for the phases observed, and C is the endpoint absorbance.

Equation 2.1. $$A_{458nm} = \Delta A_1 e^{-k_1 t} + \Delta A_2 e^{-k_2 t} + \Delta A_3 e^{-k_3 t} + C$$

Isothermal titration calorimetry was used to assess if epinephrine associates with renalase. Renalase (350 μL of 339 μM in PBS buffer at 25°C) was injected into a TA instruments Nano ITC Model 5303 microcalorimeter. This sample then had 21, 2 μL

additions of 1.84 mM epinephrine injected over 2 h. The pattern of heat liberated was then fit to a single independent site model correcting for constant cell volume and injection dilution using NanoAnalyze Data Analysis software (TA instruments) to obtain a measure of the binding constant for the renalase•epinephrine complex. (*310*)

Perturbation of the renalase flavin absorption and fluorescence emission spectra in the presence of epinephrine was used as a qualitative measure to evaluate if the ligand formed a complex with the enzyme that had close association with the FAD isoalloxazine. Absorption spectra of renalase (30 μM) were measured at 25^{o}C in PBS buffer in the presence and absence of epinephrine (100 μM) using a Cary 3 dual beam spectrophotometer. The free enzyme spectrum was then subtracted from the spectrum obtained in the presence of the ligand to obtain the difference spectrum and accentuate changes. Similarly, fluorescence emission spectra were obtained under the same conditions with excitation at 450 nm. The emission spectrum (475-650 nm) of 4 μM renalase in PBS buffer was recorded in the absence and presence of 40 μM epinephrine using an Hitachi F-4500 spectrofluorometer at 25^{o}C.

Results

Expression and purification: Human N-terminally His-tagged renalase isoform 1 was expressed in BL21 DE3 *E. coli* to highest yield at 22 ^{o}C. Typically the yield of purified enzyme was 6 mg/L of culture. The enzyme was purified to homogeneity using a cobalt affinity column from which it eluted at approximately 30 mM imidazole and was assessed to be greater than 95% pure by SDS polyacrylamide gel electrophoresis. Consistent with prior reports, the renalase flavin spectrum was red-shifted compared to that of free flavin

(Figure 2.1) . (*60, 61*) The two visible maxima of the enzyme bound flavin spectrum occur at 387 and 458 nm with extinction coefficients of ε_{387nm} = 10,750 $M^{-1}cm^{-1}$ and ε_{458nm} = 11,330 $M^{-1}cm^{-1}$. The purified enzyme was stable in PBS buffer, could be stored indefinitely at -80°C and did not exhibit diminished activity with thawing. Heterologous expression of renalase in *E. coli* resulted in significant inclusion body accumulation at all temperatures tested. Attempts were made to refold this peptide to form active renalase following the methods of Desir et al. 2012. (*36*) The refolded peptide acquired FAD and was soluble to high concentration, but had a cofactor spectrum ostensibly unchanged from free FAD (Figure 2.1). Moreover, the refolded material did not have the activity described hereafter and was deemed to be misfolded inactive protein.

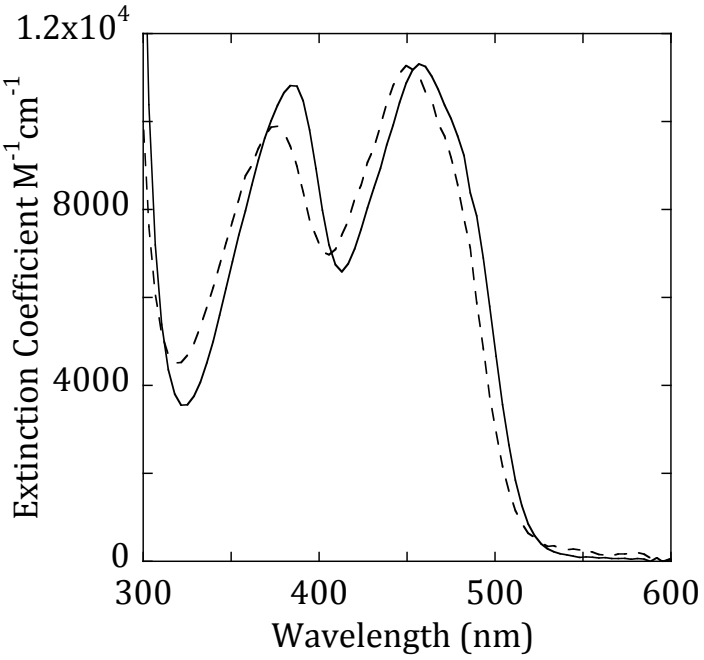

Figure 2.1 Flavin Spectra of Native and Refolded Renalase. Spectra shown are for heterologously expressed renalase from the soluble (solid line) and refolded from the insoluble or inclusion body (dashed line) fractions. The insoluble fraction was refolded using the methods of Desir et al. 2012.(*36*) The extinction coefficients of both forms were determined as described in the methods section.

Identification of a Renalase Substrate in NAD(P)H Stock Solutions: A substrate for renalase was detected whilst validating prior claims that β-NAD(P)H can serve as a renalase reductant in the production of adrenochrome from epinephrine. (*2*) Figure 2.2 depicts quantitative evidence for a renalase substrate occurring as a 1-4% impurity in β-NAD(P)H solutions. Figure 2.2A shows that rapid fractional reduction of renalase occurs when the enzyme is mixed with relative high concentrations of NADPH under strict anaerobic conditions. The measured $\Delta\varepsilon_{458nm}$ value (7945 $M^{-1}cm^{-1}$) for reduction, obtained when the substrate contaminant was added in apparent excess (449 μM NADPH reduction trace), permitted the concentration of the actual substrate at all limiting values to be calculated. When the concentration of fractionally reduced renalase was plotted against the NADPH stock concentrations a slope of 1.3% was determined (Figure 2.2B). In a separate experiment, high concentrations of NADPH were added to 5 μM renalase in a dioxygen electrode and the concentration of oxygen consumed was measured (Figure 2.2C). The amplitude measured in this experiment indicated that the substrate contaminant was present to 1.5% of the total NADPH concentration. Higher apparent substrate fractions (4-5%) were observed with NADH stock solutions (Figure 2.2D). When catalase was included in these assays close to one half of the dioxygen consumed by renalase was regained from the catalase disproportionation reaction indicating that hydrogen peroxide is a product of renalase activity. Collectively these data establish multiple characteristics of the renalase reaction. In regard to the contaminant substrate, the proportion in NAD(P)H solutions is small and can vary with the parent molecule suggesting degradation and/or equilibrium processes result in the substrate accumulation. The complete and monophasic reduction of the flavin cofactor in excess substrate under anaerobic conditions (Figure 2.2A – 449 μM

NADPH trace) suggests that one substrate molecule transfers two electrons to the flavin. The dioxygen electrode assays define that dioxygen is also a substrate for renalase with an observed rate of dioxygen consumption in solutions equilibrated with atmospheric dioxygen (~250 μM) of ~0.5 s^{-1}. The total dioxygen consumption also indicated that multiple (Figure 2.2 C&D) turnovers occurred in the presence of the substrate component of both NADPH and NADH solutions. That the reduction (Figure 2.2A) and dioxygen uptake (Figure 2.2C) experiments indicate a similar proportion of substrate in the NADPH stocks suggests that the stoichiometry of the reaction is 1:1 for dioxygen and the NADPH contaminant. Moreover, that we regain 0.5 equivalents of O_2 in the presence of renalase and catalase suggests that the product stoichiometry is also 1:1; product:H_2O_2.

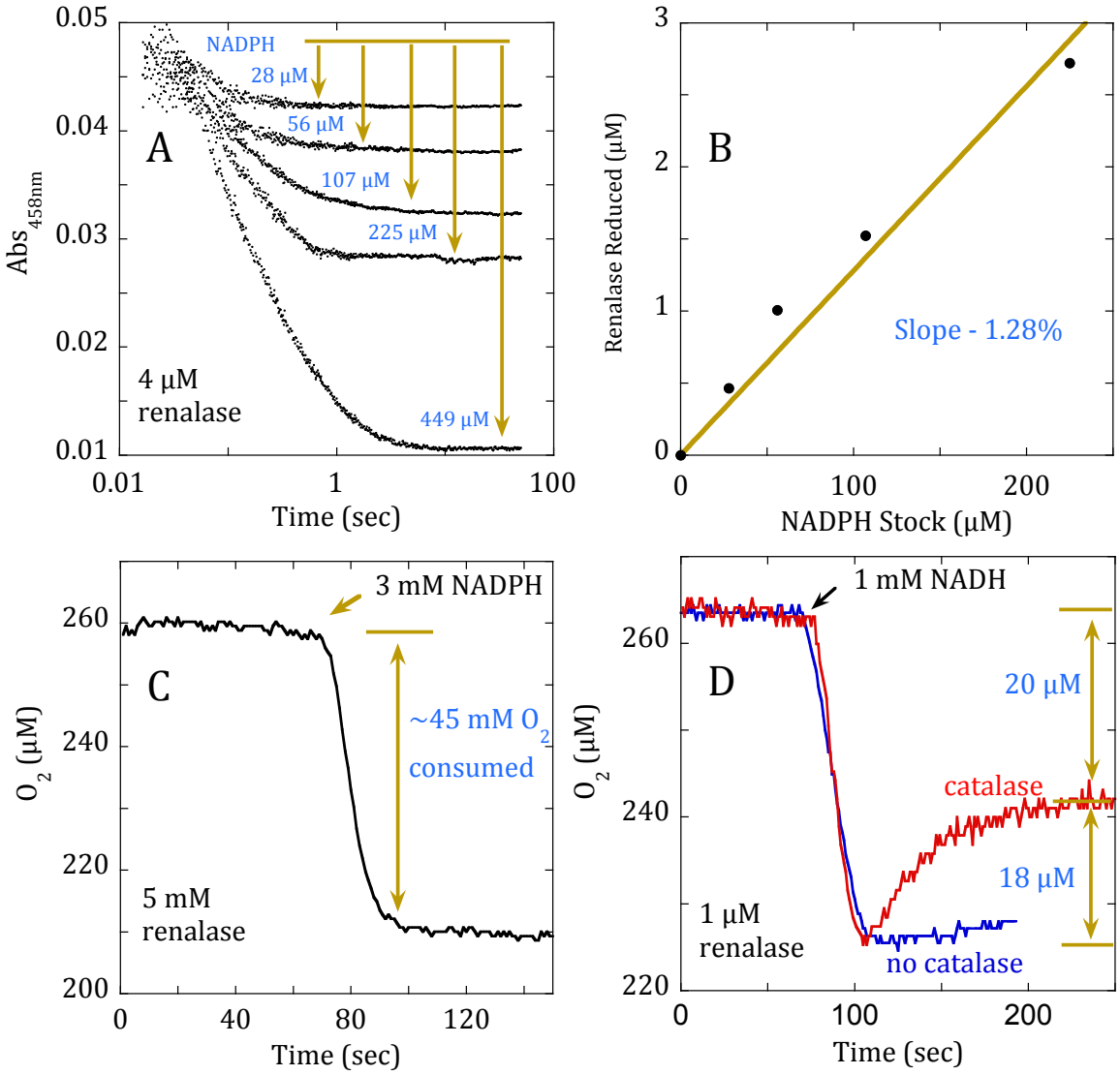

Figure 2.2. Evaluation of the Renalase Active Fraction in NAD(P)H Stock Solutions. **A**: Stopped-flow traces of fractional reduction of renalase as observed at 458 nm. Renalase (4.0 µM) was mixed under anaerobic conditions with varied concentrations of NADPH as shown. **B**: The fraction of NADPH consumed in the reduction in A based on the change in extinction coefficeint of the renalase flavin cofactor at 458 nm vs the stock concentration of NADPH. **C**: Demonstration of multiple turnovers with excess substrate. 5 µM renalase was added to PBS buffer in a dioxygen electrode and 3 mM of NADPH was added at the arrow. **D**: Stoichiometry of the renalase reaction with respect to dioxygen. Renalase (1 µM) was mixed with 1 mM NADH with and without 1 U of catalase. The traces shown in C and D are representative traces of typically 3-5 replicates for each observation.

HPLC product analysis was used to separate the components present in NADPH solutions and identify the substrate component (Figure 2.3). HPLC chromatograms were collected at known maxima for NADPH and NADH (340, 260 nm). Chromatograms collected at 340 nm indicated respective ~1.5% and 4% contaminants (by area) for NADPH and NADH solutions (Figure 2.3A & B). This component was largely consumed when the sample was incubated with renalase for two minutes (Figure 2.3A and B – red chromatograms) while the area of the major components (β-NADPH and β-NADH) remained unchanged. This indicated that the reactive component absorbed light at 340 nm and that this absorption was lost when reacted with renalase. An increase in absorption at 260 nm coinciding with a component already present in the NADH solution was observed in the sample to which renalase was added (Figure 2.3A lower). Coinjection of 15 μM of β-NAD^+ in the control sample identified the product of the renalase reaction as β-NAD^+ and indicated that the substrate concentration in the unreacted sample was ~13 μM (4.0%). For NADPH and NADH samples, the spectra of the substrate components (Figure 2.3C) exhibited maxima at 260 and 346 nm suggesting that the nicotinamide and adenine bases are intact in the substrate molecule. The loss of the 346 nm absorption of the substrate component when reacted with renalase is consistent with the dihydropyridyl base transferring a hydride equivalent to enzyme cofactor.

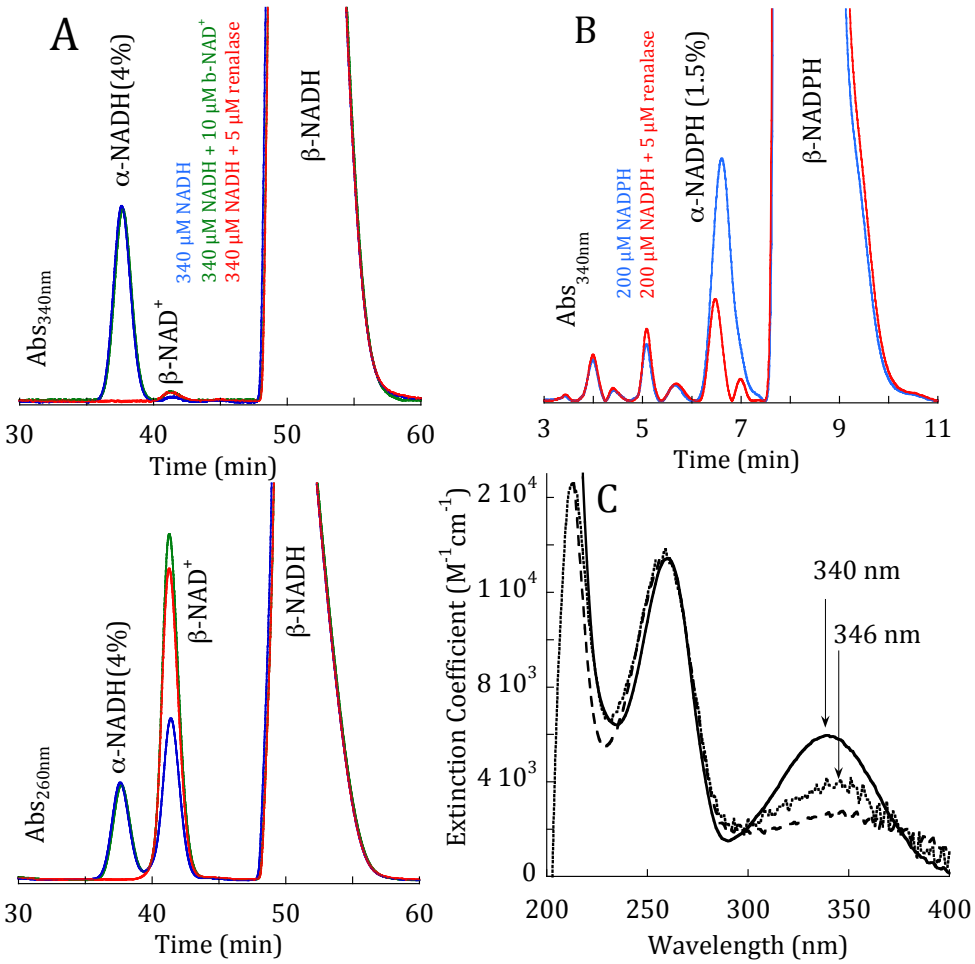

Figure 2.3. HPLC Identification of α-NAD(P)H as the Substrate for Renalase Occuring as a Contaminant of β-NAD(P)H Solutions. **A**&**B**: Species were separated using a Xterra reverse phase C18 column running isocratically in 10 mM sodium phosphate buffer, pH 7.5. In each the blue line is the control β-NAD(P)H stock while the chromatograms depicted as a red line were prepared identically to the control sample but were reacted with 5 µM renalase and then filtered to remove the enzyme. The chromatogram depicted with a green line in **A** is the same as the control sample but with 15 µM β-NAD+ added. **A**: Chromatographic separation of NADH solutions detected at 340 nm (upper) and 260 nm (lower-7-fold smaller scale) **B**: Chromatographic separation of NADPH solutions detected at 340 nm. **C**: Spectra of the renalase substrate species resolved in A&B. The spectrum represented with an unbroken line is β-NADPH and was included for reference. The dotted line spectrum was of the substrate peak in A. The dashed line spectrum was of the substrate peak in **B**. Spectra were normalized at 260 nm for clarity.

Red-shifted nicotinamide spectra of the active components of NADPH and NADH solutions is characteristic of α-NAD(P)H molecules. (*309, 311*) In amongst the numerous decay paths possible for pyridine nucleotides are anomerization equilibria that bring about the accumulation of a small fraction of the α-dihydronicotinamides in dissolved β-NAD(P)H solutions (*312*) (Scheme 2.1). Anomerization is only possible for the reduced form as the ribose ring-open Schiff base intermediate can form only when electrons are delocalized from the electron-replete dihydropyridyl ring; the oxidized forms are thus configurationally stable. Reduced nicotinamide nucleotides are one of the two naturally occurring nucleotides that exhibit anomerization in solution, the other being pseudouridine nucleotide.(*313*) The α/β equilibrium constants for NADPH and NADH are reported as 0.015 and 0.11 respectively (*309*), largely consistent with the ~1.5% and ~5% fractions observed for the experiments described above.

NMR was used to confirm the product of the renalase reaction. The oxidized nicotinamide proton resonances of the α and β forms of NAD(P) are readily discerned by NMR. (*300*) With respect to β-NAD(P), the resonances of protons of the α-nicotinamide moiety move to higher field while the discriminating proton attached to the anomeric carbon of the nicotinamide ribose moves downfield. Figure 4A depicts proton NMR spectra for the accumulation of β-$NADP^+$ from a stock solution (40 mM) of β-NADPH in the presence of renalase (blue spectra). In such a reaction α-NADPH is expected to be consumed by renalase as a burst of product formation before the reaction becomes limited by both available dioxygen and/or the rate of anomerization. What is observed is an ~200 μM burst in product accumulation that did not occur in the absence of renalase (Figure 4B).

That the observed product nicotinamide resonances are shifted upfield relative to those of β-NADP+ alone (Figure 4A green and blue spectra) indicates only the influence of the high concentration of β-NADPH in these samples. When the proton resonances and coupling constants are compared to those of a control sample having the same ratio of β-NADP+ to β-NADPH, the product and control spectra coincide (Figure 2.4A orange and blue spectra), indicating that the product of the reaction is β-NADP+.

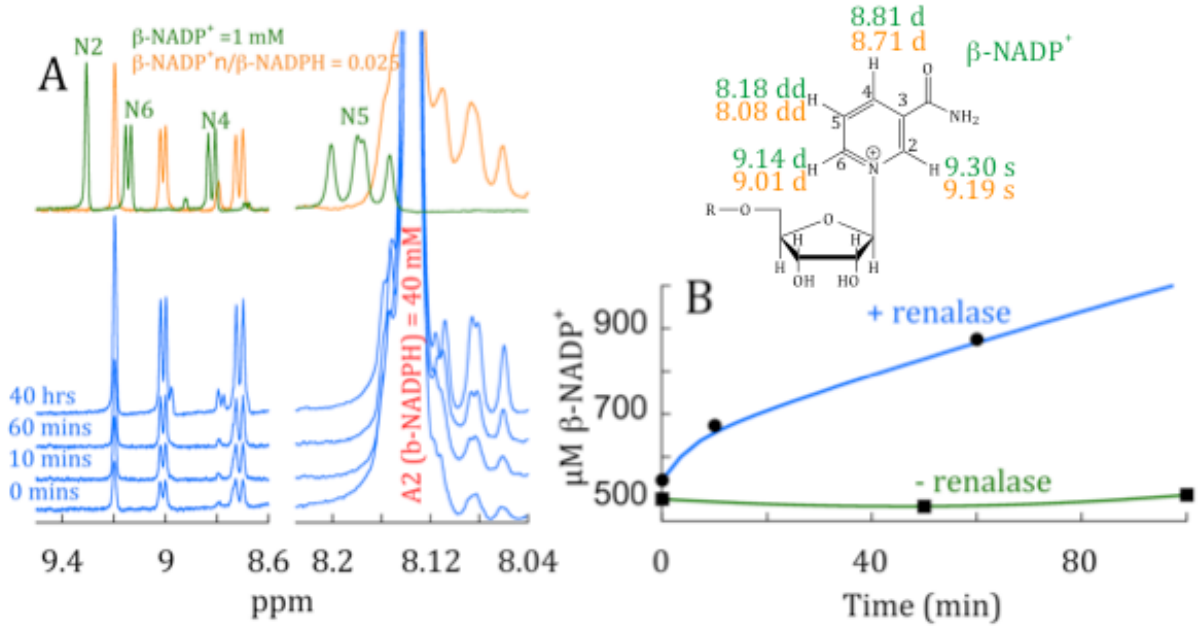

Figure 2.4. Identification of β-NAD(P)H as the Nicotinamide Product of the Renalase Reaction. **A**: 300 MHz ^{1}H NMR spectra. Blue spectra show the accumulation of resonances when 10 μM renalase was added to a freshly prepared solution of 40 mM β-NADPH in 10 mM sodium phosphate buffered deuterium oxide, pH 7.4. The upper spectra are control samples. For positional assignments the N designation refers to the nicotinamide base, while A references the adenine base. The green spectrum is that of 1 mM β-NADP+ and the orange spectrum is that of 1 mM β-NADP+ in the presence of 40 mM β-NADPH (both control samples prepared in 10 mM sodium phosphate buffered deuterium oxide, pH 7.4). Assignments of the shifts of the nicotinamide are shown to the right of the control spectra. **B**: Relative accumulation of β-NADP+ in the presence and absence of renalase based on the integration of the N2 proton and the known concentration of the β-NADPH in the sample.

Evaluation of Epinephrine as a Substrate for Renalase: The substrate for renalase has been the subject of some dispute since the discovery of the enzyme in 2005. (*48, 51, 59*) Figure 2.5 summarizes the data obtained for three approaches used to assess the response of renalase to the presence of epinephrine. In Figure 2.5A, non-pseudo-first order single turnover reactions of renalase with limiting α-NADPH and atmospheric dioxygen (observed at 458 nm) indicated reduction and reoxidation of the flavin cofactor. Under the conditions used these data could be fit to three exponential phases without significant systematic error in the residuals (11.6 s^{-1}, 1.63 s^{-1}, 0.54 s^{-1}). However, the number of phases, the values for rate constants and absorbance amplitudes are only apparent measures of the single turnover kinetics that provide a means to compare the data in the presence of and absence of epinephrine. It has been suggested that renalase obtains reducing equivalents from β-NADPH and then catalyzes a net two-electron oxidation of epinephrine to form adrenochrome, a process that would mobilize four electrons. (*2*) The addition of 200 μM epinephrine to single turnover reactions with α-NADPH and dioxygen did not change the observed kinetics (11.0 s^{-1}, 1.82 s^{-1}, 0.66 s^{-1}) indicating that no rate constant is significantly altered and no new intermediates accumulate in response to the catechol. It has been suggested that renalase is only activated in blood and is isolated as a relatively inactive pro-renalase. (*12*) In order to assess if some additional soluble component of blood is required to activate renalase to consume epinephrine the experiment was repeated in 50% fresh cell-free human blood plasma. This condition also did not significantly alter the observed single turnover kinetics (12.1 s^{-1}, 1.90 s^{-1}, 0.64 s^{-1}). The conclusion is that epinephrine is not catalytically consumed by renalase as isolated and that no soluble ligand in blood activates the enzyme to display this activity.

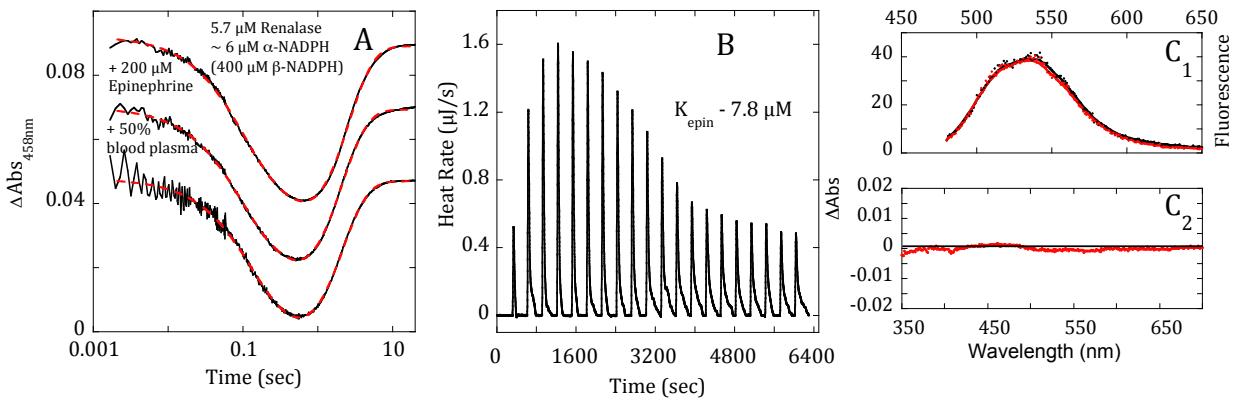

Figure 2.5. Evaluation of Epinephrine as a Substrate for Renalase. **A**: Single Turnover of renalase with limiting α-NADPH. Traces were observed at 458 nm when 5.7 μM renalase was reacted with with ~6 μM α-NADPH at atmospheric concentrations of molecular oxygen (~250 μM). Dashed red lines indicate fits to Equation 1. **B**: Isothermal titration calorimetry of 339 μM renalase with 21, 2 μL injections of 1.84 mM Epinephrine. **C**: The extent of spectrophometric perturbation of the flavin spectrum by epinephrine. **C_1**: Black line - flouresence emission spectrum of 4 μM renalase when excited at 450 nm. Red line - flouresence emission spectrum of 4 μM renalase plus 40 μM Epinephrine when excited at 450 nm. **C_2**: Absorption difference spectra. Black line – zero perturbation difference spectrum of 20 μM renalase. Red line – difference spectrum (sample-control) for 20 μM renalase plus 200 μM epinephrine.

To evaluate if renalase binds epinephrine, the enzyme was titrated with epinephrine in an isothermal titration calorimeter (Figure 2.5, B). The data obtained suggest an exothermic binding event with a dissociation constant for the renalase•epinephrine complex of ~8 μM. This complexation is either adventitious (and coincidental) or is a binding event whose link to physiology is yet to be established. The lack of influence of epinephrine on the observed kinetics of reduction and reoxidation of renalase by α-NADPH implies that the binding of epinephrine does not occur in the active site of the enzyme. To test this hypothesis, spectrophotometric observations using the flavin absorption and emission spectra as sensitive measures of ligand proximity were

undertaken (Figure 2.5C). These experiments show no appreciable perturbation of the flavin environment in the presence of epinephrine concentrations at least 4-fold higher than the measured binding constant, suggesting that the binding site for epinephrine is distant from the active site.

The accumulation of adrenochrome from epinephrine can be observed at 480 nm. (*299*) Our experiments indicated that the initial rate of oxidation of epinephrine to form adenochrome in atmospheric oxygen at 25 ^{o}C oxygen in PBS buffer was ostensibly zero for all concentrations tested. The addition of freshly dissolved β-NADPH did not bring about adrenochrome formation nor did the addition of 10 μM renalase (data not shown). As such it was concluded that renalase does not utilize β-NAD(P)H (or α-NAD(P)H) to catalyze a reaction that forms adrenochrome.

Discussion

Eight years after its initial discovery, we have identified an activity for human renalase as an α-NAD(P)H oxidase/anomerase. This activity is the first demonstration of a potential physiological role for α-NAD(P)H in mammals and the first example of a flavoprotein catalyzing an anomerization reaction. This discovery runs contrary to the persistent assertion that renalase catabolizes adrenergic catecholamines. Renalase has often been described as "MAO C"; the third monoamine oxidase (*2, 11, 36*) that oxidizes the catechol ring rather than the distal amine. We suggest that epinephrine and other catechols have most often been reported as the substrate for renalase as they exhibit instability at or above neutral pH values and form chromophoric products (aminochromes) that may be

easily taken for slow catalytic activity. (*2*) Our data suggest that epinephrine has no influence on the activity of the enzyme.

It may be possible to reconcile our observations with the majority of earlier reports of adrenochrome formation by renalase. *In vitro* catalytic adrenochrome production by renalase are solely for the refolded renalase peptide. (*36*) In our hands, this form of the protein exhibits none of the α-NADPH oxidase/anomerase activity described herein. It is thus tentatively proposed that the refolded form may have a solvent exposed flavin isoalloxazine ring (Figure 2.1) that due to the difference in reduction potentials (-320 vs -207mV) will be reduced by NADPH in a slow steady-state reaction that forms H_2O_2 autocatalytically. This molecule will readily oxidize epinephrine to initially form a quinone species prior to nucleophilic attack by the distal amine of the side chain to yield the adenochrome product. The natively folded renalase enzyme does not promote this chemistry to any significant extent as it selects against binding of the β-form from the NAD(P)H reductant pool (Figures 2.1, 2.2 and 2.3). Moreover, it may be possible to observe the accumulation of aminochromes with natively folded renalase in the presence of reduced nicotinamide dinucleotides when long incubations are employed as non-enzymatic anomerization will form α-NAD(P)H as a minor component resulting in the formation of product H_2O_2 and hence promote the ensuing non-enzymatic oxidation and cyclization of the catechol.

From an experimental perspective α-NAD(P)H molecules are highly elusive. The apparent rate constants to attain equilibrium from the α-NAD(P)H anomer on the order of 10^{-5}-10^{-6} s^{-1}. (*309*) As such the concentration of pure α-NADPH is altered within hours of a

solution being prepared, to some extent undermining the systematic use of the pure substrate in activity assays. The use of the β-anomer to obtain the α-form requires prolonged incubation to reach anomer equilibrium and verification of the α-fraction before use as a stock solution but has the advantage of supplying a constant α/β ratio throughout the period of observation. While α-NAD(P)H will invariably be the minor component it must be assumed that renalase is highly discriminatory for the α-anomer given that it was destined to function in an environment in which the β-anomer is predominant.

More evidence is needed to define the means by which the activity of renalase transmits a signal to the circulatory system to induce the reported vasodilation. However, this oxidase/anomerase activity may have a core physiological role that is separate and more pervasive than blood pressure modulation. The necessity for renalase to harbor two functionalities may arise from the fact that α-NAD(P)$^+$ molecules are metabolically isolated. In Scheme 2.2 the α/β equilibria are depicted with the redox pathways for both anomers of NAD(P)H molecules. The inherently lower reduction potential of α-NAD(P) molecules and the lack of participation in other metabolic pathways dictates that there would be an inexorable loss of nicotinamide dinucleotide cofactors as a-NAD(P)$^+$. Without considering other redox partners, the anomer equilibrium and redox potential difference would predict that ~50% of the β-NAD(P)H would ultimately accumulate as α-NAD(P)$^+$. (*300*) If renalase were not to catalyze oxidation in addition to anomerization these molecules would accumulate and deplete both the total concentration of NAD(P)H molecules and the normal NAD(P)H/NAD(P)$^+$ ratio. The α-NAD(P)H oxidation couples the reaction to dioxygen reduction providing a large driving force that in concert with the anomerization activity

recycles α-NAD(P)H molecules back to the β-pool maintaining the α-NAD(P)H concentration near zero.

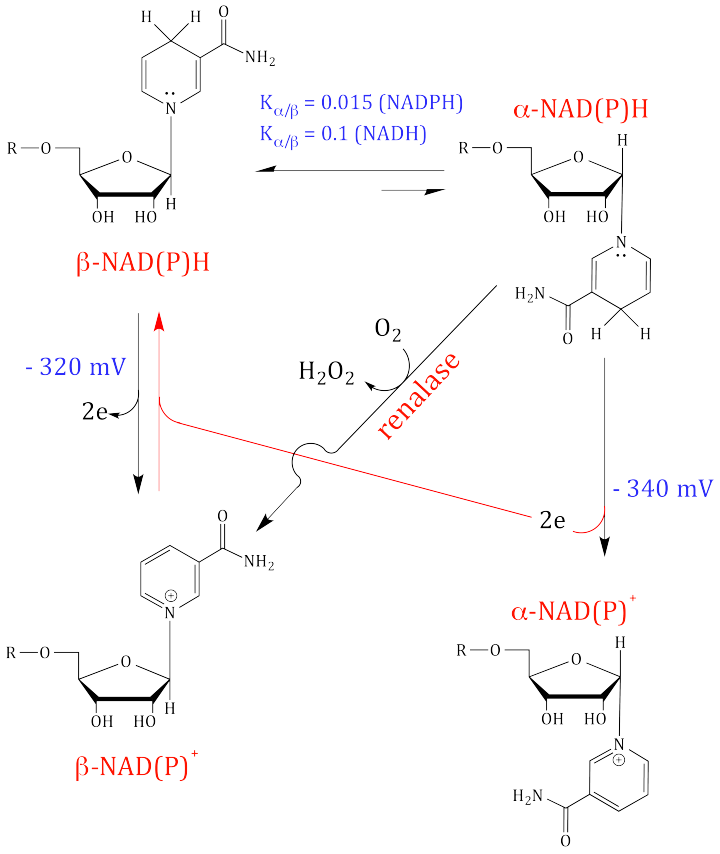

Scheme 2.2. Initial proposed physiological function of renalase.

This activity for renalase raises numerous chemical and physiological questions. From an enzyme chemistry perspective, hydride transfer to a flavin is not unusual, though the timing of this process with respect to the anomerization reaction is highly intriguing. While it may be reasonable to conclude that anomerization occurs after reduction of the FAD cofactor in order that the enzyme be selective for α-NAD(P)H, this raises the question as to what redox state of renalase catalyzes the anomerization. That is, is α-NAD(P)$^+$ (or β-

NAD(P)$^+$) a substrate for the reduced or oxidized enzyme and if the reduced enzyme catalyzes anomerization of the oxidized nicotinamide dinucleotide how is the ribose ring cleaved if the otherwise requisite schiff base/ring open intermediate can no longer form? A hypothetical mechanism that circumvents these apparent conundrums is depicted in Scheme 2.3. In this mechanism the oxidized enzyme is selective for the α-NAD(P)H substrate and first promotes the formation of a ring open ribose/Schiff base intermediate. It is then this intermediate that reduces the flavin, concomitantly forming the β-NAD(P)$^+$ product prior to reoxidation.

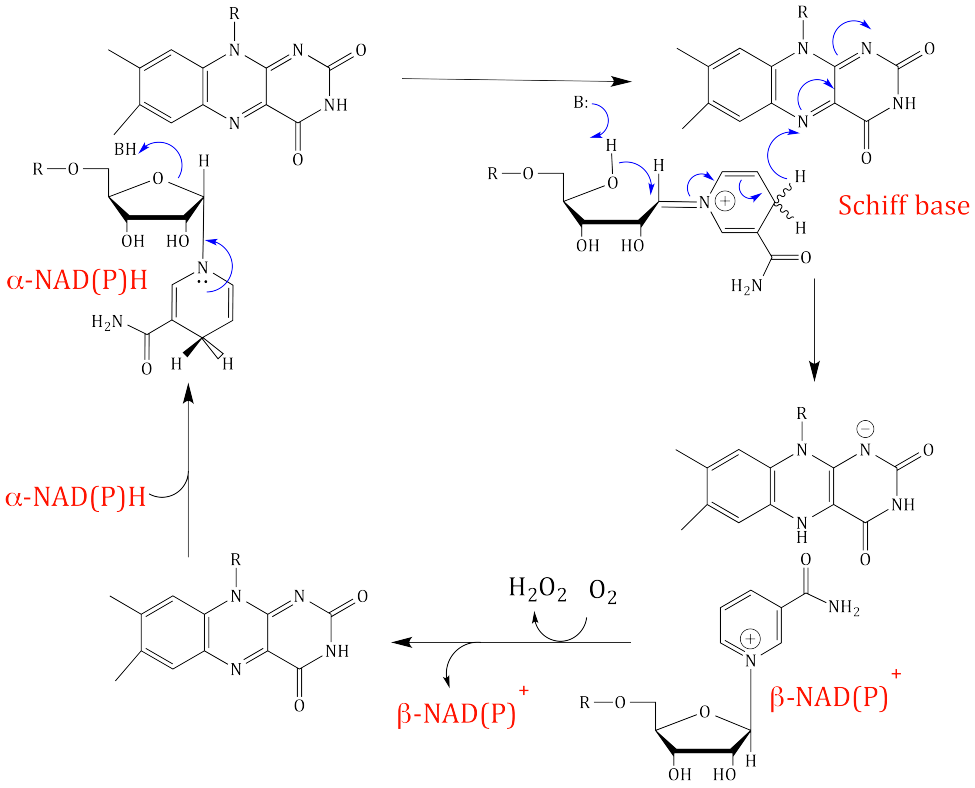

Scheme 2.3. Initial proposed mechanism of renalase

This research does not address the manner in which this newly identified activity of renalase is imparted *in vivo* in regard to vasodilation. It may be ventured that the observed

decrease in blood pressure and slowing of the heart rate is not a result of diminishment of either of the substrates or the accumulation of the β-NAD(P)$^+$ product as each of these molecules are ubiquitous in mammalian circulation. It therefore seems reasonable to implicate H_2O_2 as the signal for vasodilation arising from renalase activity. (*314-316*)

CHAPTER III
Kinetics and Equilibria of the Reductive and Oxidative Half-Reactions of Human Renalase with α-NADPH

Brett A. Beaupre, Matthew R. Hoag, Brenton R. Carmichael and Graham R. Moran

Abstract

Renalase is a recently discovered flavoprotein that has been reported to be hormone produced by the kidney to down-modulate blood pressure and heart rate. The consensus belief has been that renalase oxidizes circulating catecholamine neurotransmitters thereby attenuating vascular tone. However, a convincing *in vitro* demonstration of this activity has not been made. We have recently discovered that renalase has α-NAD(P)H oxidase/anomerase activity. Unlike most naturally occurring nucleotides, NAD(P)H can accumulate small amounts of the α-anomers that once oxidized are configurationally stable and unable to participate in cellular activity. Thus anomerization of NAD(P)H would result in a continual loss of cellular redox currency. As such, it appears that the root purpose of renalase is to return α-anomers of nicotinamide dinucleotides to the β-anomer pool. In this article we measure the kinetics and equilibria of renalase in turnover with α-NADPH. Renalase is selective for the α-anomer that binds with a dissociation constant of ~20 ± 3 μM. This association precedes monophasic two-electron reduction of the FAD cofactor with a rate constant of 40.2 ± 1.3 s^{-1}. The reduced enzyme then delivers both electrons to dioxygen in a second order reaction with a rate constant of ~2900 $M^{-1}s^{-1}$. Renalase has modest affinity for its β-$NADP^+$ product (K_d = 2.2 mM), and the FAD cofactor has a reduction potential of -155 mV that is unaltered by saturating β-$NADP^+$. Together these

data suggest that the products are formed and released in a kinetically ordered sequence (β-$NADP^+$ then H_2O_2), however, the reoxidation of renalase is not contingent on the dissociation of β-$NADP^+$. Neither the oxidized nor the reduced form of renalase is able to catalyze anomerization, implying that the redox and anomerization chemistries are inextricably linked through a common intermediate.

Introduction

Reported initially in 2005, renalase was said to be a new renal hormone that is secreted into blood by the kidney to induce lower blood pressures and slowed heart rate. (*1, 317*) In subsequent studies it has been reported that mice deficient in renalase have elevated blood pressures and that renalase polymorphisms result in a higher incidence of stroke and diabetes. (*10, 296, 297*) The consensus belief has been that renalase imparts its physiological response by catabolizing circulating catecholamine neurotransmitters (chiefly adrenaline) thereby attenuating vascular tone. (*1, 4, 36*) The expression of renalase has been reported in additional tissues (*1, 12, 301*) with at least four variants arising from altered splicing of seven exons. (*12, 301*) The X-ray structure of the longest variant, isoform 1, (342 amino acids) was published in 2011, revealing a protein whose structural topology was similar to known flavoprotein oxidases, monooxygenases and demethylases, but whose activity could not be readily discerned from conserved active site residues. (*51, 60, 302-305*) Given the similarity of the structural fold of renalase to monoamine oxidases A & B, catabolism of catecholamines would appear to be a reasonable, albeit contextual, function for renalase. However, there has been considerable difficulty establishing this activity *in vitro,* leading to the assertion that renalase as isolated is “prorenalase”; a form

that must be activated in blood by catecholamines or other modifiers. (*11*) Slow accumulations of adrenochrome in the presence of renalase, epinephrine and NADPH have been offered as evidence that renalase catalyzes the oxidation of the catecholamines and promotes nucleophilic attack by the side-chain distal amine. (*2*) The difficulty is that this is a facile, well-established degradative reaction for catecholamines that exhibits measureable rates under mildly oxidizing conditions in the absence of an enzyme catalyst. (*298, 299, 318*) Moreover, the stoichiometry of such a reaction in regard to the fate of the mobilized electrons has not been established. (*2*) As such, the claim that renalase catabolizes circulating catecholamines has been questioned by a number of researchers. (*48, 51, 59*)

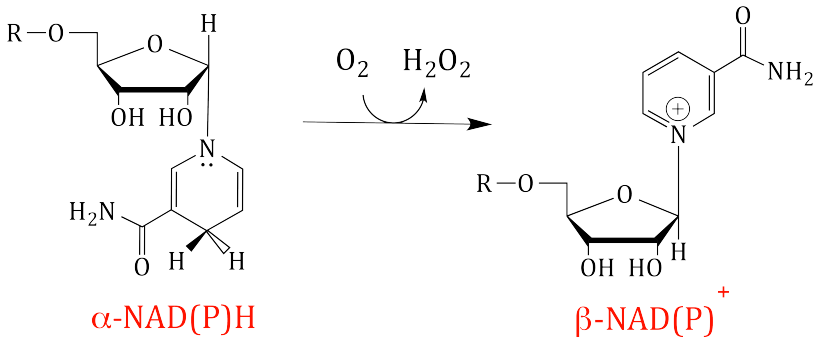

Scheme 3.1. Initial proposed activity of renalase.

We have recently discovered an activity for renalase as a bifunctional α-NAD(P)H oxidase/anomerase. (*319*) Renalase oxidizes the dihydropyridyl ring of α-pyridine nucleotides, that aris naturally as a small equilibrium component of NAD(P)H solutions, and manages to also epimerize the nicotinamide ribose to form β-NAD(P)+ products (Scheme 3.1). Importantly, renalase does this chemistry at least two orders of magnitude more rapidly than any reported turnover rate for catecholamine oxidation. The electrons

acquired from the α-NAD(P)H substrate are initially transferred to the enzyme's FAD cofactor and then to dioxygen to yield hydrogen peroxide. How and if this activity is linked to the reported physiological response to renalase has not been addressed, but the only known vasoactive molecule to be consumed or arise from this activity is H_2O_2. (*315, 316*) Coupling NAD(P)H oxidation to α-β anomerization and dioxygen reduction provides a large driving force for this chemistry and suggests the more pervasive physiological function for renalase is to drive the α/β NAD(P) ratio to zero. In this article we offer evidence for the kinetics and equillibria of the reductive and oxidative half reactions of human renalase reacting with α-NADPH.

Materials and Methods

Materials: Potassium phosphate, isopropyl-β-thiogalactopyranoside (IPTG) and sodium chloride were obtained from ACROS. Luria Bertani broth (Lennox) powder was from Fisher Scientific. Kanamycin and β-NADPH were purchased from Alexis. β-$NADP^+$ was purchased from Calbiochem and Axxora. β-NADH, β-NAD^+, xanthine, methyl viologen and epinephrine were from Sigma-Aldrich. Indigo carmine was from ICN. Xanthine oxidase was acquired from Calzyme. Renalase was expressed and purified according to our previously published methods. (*319*) α-NADPH was from the α/β-NAD(P)H equilibrium mixture (reliably 1.5% (NADPH) and 4% (NADH) alpha anomers at equilibrium). Anomer equilibrium was achieved by dissolving β-NADPH in PBS or HEPES pH 7.5 and placing this solution in a sealed vessel at 4°C for ~72 hours. (*309*) Prior to using stock solutions, the α-NAD(P)H concentration was determined by dioxygen electrode. Typically 1-2 μM renalase was added

to 1-3 mM of the NAD(P)H solution in PBS buffer at 25 ^{o}C. The observed amplitude of dioxygen consumption was used to define the fraction of the α-NAD(P)H component.

Quantitation: The concentration of NADPH and NADH solutions were determined using the published 340 nm extinction coefficient of 6200 $M^{-1}cm^{-1}$. (*309*) An extinction coefficient for renalase was determined in prior work (ε_{458nm} =11,330 $M^{-1}cm^{-1}$). (*319*) NADP+ and NAD+ solutions were quantified using published 260 nm extinction coefficients. (*311*)

Reduction Potentials Measurements and β-NADP^{+} Binding Affinity. Reduction potentials were measured for unliganded oxidized renalase and the Ren_{ox}•β-NADP^{+} complex using the xanthine/ xanthine oxidase reduction system of Massey. (*320*) A Hewlett Packard 8453 diode-array spectrophotometer was used to monitor the reduction of the enzyme in the presence of indigo carmine (E^{o} = -130 mV). The reaction mixture was placed in an anaerobic cuvette and consisted of 300 μM xanthine, 5 μM methyl viologen, 10 μM of indigo carmine, 10 μM renalase (with or without 30 mM β-NADP^{+}) in PBS buffer pH 7.5 at 25° C. Once the mixture was made anaerobic by 45 cycles of argon and vacuum (as above), xanthine oxidase (1-2 μM final) was added from a side arm to initiate the reduction of both the enzyme and dye. Spectra were recorded every two minutes until both species were fully reduced. The data were analyzed at wavelengths where the dye (610 nm) or the enzyme (470 nm) had absorption contributions that were spectrophotometrically independent of the other chromophore. At each of these wavelengths the ratio of oxidized and reduced species was determined. The log of the ratio of the oxidized and reduced

forms of indigo carmine was then plotted against the log of the same ratio for renalase and the indigo carmine midpoint was substituted into the pH-corrected Nernst equation(*321*) to obtain the reduction potential for the renalase flavin cofactor.

The dissociation constant for the Ren_{ox}•β-$NADP^+$ complex was measured by monitoring the spectrophotometric perturbation of the flavin cofactor between 400 and 600 nm when β-$NADP^+$ was titrated to the oxidized enzyme. Renalase (20 μM) in PBS buffer at 25°C was titrated with β-$NADP^+$ (0-8 mM). With each addition of β-$NADP^+$ the flavin absorption spectrum was measured. All spectra were corrected for dilution and the fractional occupancy assessed by the fraction of the extrapolated total perturbation observed at each β-$NADP^+$ concentration. This value was then used to obtain the concentration of unbound ligand. Plotting fractional occupancy versus unbound ligand gave a hyperbola that was fit to Equation 3.1, where f is fractional occupancy, $K_{β\text{-}NADP+}$ is the dissociation constant for the Ren_{ox}•β-$NADP^+$ complex and [β-$NADP^+_f$] is the concentration of unbound β-$NADP^+$.

Equation 3.1 $$f = [\beta\text{-}NADP^+_f]/(K_{β\text{-}NADP+} + [\beta\text{-}NADP^+_f])$$

Reductive Half-Reaction: The reduction of the renalase flavin cofactor was observed by mixing the anaerobic enzyme with anaerobic NADPH solutions at anomer equilibrium on a stopped flow spectrophotometer. Prior to the experiment the instrument was made anaerobic by introducing a solution of glucose (20 mM) and glucose oxidase (15.5 U/mL) for approximately 16 hrs. Renalase (4 μM) in PBS buffer with 1 mM glucose was made

anaerobic by placing it in a tonometer and exchanging the dissolved dioxygen for argon. Prior to sealing the vessel, ~16 U of glucose oxidase was added to the side arm of the tonometer. The tonometer was then sealed and connected to an anaerobic manifold where 45 cycles of argon and mild vacuum were applied. Between each three exchanges, the solution was gently agitated to promote exchange of gases in the headspace of the vessel. After this procedure the renalase/glucose solution was mixed with the glucose oxidase from the sidearm and then mounted onto a Hi-Tech (now TgK) DX-2 stopped-flow spectrophotometer. This solution was then reacted with varied concentrations of α-NADPH (~20-300 μM). Substrate solutions were prepared in PBS buffer with 1 mM glucose and sparged in an inverted glass syringe with purified Argon for 10 minutes before 8 U of glucose oxidase was added and the syringe was mounted to the stopped-flow instrument. The two solutions were then mixed and the bleaching of the flavin cofactor during reduction was observed at 458 nm. The data obtained was fit to a single exponential decay according to Equation 3.2, where k_{obs} is the observed rate constant for reduction of the FAD cofactor, ΔA is the amplitude for the absorbance change and C is the Abs_{458nm} endpoint.

Equation 3.2. $$A_{458nm} = \Delta A_1 e^{-k_{obs}t} + C$$

The dependence of the observed rate constant was then plotted against α-NADPH concentration and fit to Equation 3.3 to determine the limit of the rate constant of reduction (k_{red}) and the dissociation constant for α-NADPH ($K_{\alpha\text{-NADPH}}$).

Equation 3.3 $k_{obs} = k_{red}[\alpha\text{-NADPH}]/(K_{\alpha\text{-NADPH}} + [\alpha\text{-NADPH}])$

In order to observe potential NADP/FAD charge-transfer bands at longer wavelengths, the reductive process was also observed for 20 μM (final) renalase prepared in an equivalent manner and mixed with saturating α-NADPH (328 μM).

Oxidative Half-Reaction. The reoxidation of the renalase cofactor in the presence of dissolved dioxygen was observed in single turnover reactions by stopped-flow spectrophotometry. Renalase (14 μM) was prepared in tonometer in an equivalent manner to that described above. This solution was then mixed with α/β-NADPH mixture of known ratio to supply sufficient α-NADPH to achieve ~50% reduction. The dissolved oxygen concentration in this solution was defined by sparging an inverted syringe containing the α/β-NADPH mixture with blended nitrogen and oxygen gases of known partial pressures supplied by a Maxtec maxblend gas mixer. The concentration of dissolved oxygen was confirmed by first sparging the reaction chamber of a Hansatech dioxygen electrode filled with PBS buffer with the blended gases to define the equilibrium concentration of dissolved dioxygen. Once the molecular oxygen concentration was established, the gas blend was applied to the α/β-NADPH mixture and sparged for 10 minutes before mounting the solution on the stopped-flow instrument. The solutions were then mixed and the reduction and ensuing reoxidation were observed at 458 nm. The data were fit to Equation 3.4 in which k_{red} is the apparent rate constant for reduction and k_{ox} is the rate constant for

reoxidation, ΔA_1 and ΔA_2 are the amplitudes for the two phases, and C is the endpoint absorbance.

Equation 3.4. $$A_{458nm} = \Delta A_1 e^{-k_{red}t} + \Delta A_2 e^{-k_{ox}t} + C$$

The influence of exogenous β-$NADP^+$ on the kinetics of the oxidative half reaction was observed by reacting renalase (10 μM) with excess α-NADPH (20 μM) in the presence of 250 μM dioxygen and varied β-$NADP^+$ concentration (100-1600 μM). The reductive and oxidative processes were observed at 458 nm.

The Extent of Anomerization of an α/β-$NADP^+$ Mixture by Renalase: The capacity of renalase to catalyze anomerization independent of FAD cofactor reduction by α-NAD(P)H was assessed by incubation with an $NADP^+$ solution of known α/β ratio followed by high pressure liquid chromatography (HPLC). A 1/2.66 mixture of α/β-$NADP^+$ (275 μM total) was prepared by placing 40 mM β-NADPH in a solution of 10 mM sodium phosphate pH 7.4 and allowing it to age at room temperature for 14 days. The inherently lower reduction potential of α-NADP and the anomer bias for the β-form ensures that similar amounts of the α and β $NADP^+$ anomers accumulate. (*300*) The oxidized forms were separated from the reduced and other contaminants by loading the aged sample onto a 20 cm x 12.5 mm Q-sepharose column and eluting with a linear gradient of NaCl from 0-150 mM. The α/β-$NADP^+$ mixture was then diluted to 75 μM and 50 μL chromatographed using a 4.6 x 150 mm Xterra C18 reverse phase column coupled to a Waters 600 E HPLC pump and a Waters

2487 dual wavelength detector. The α and β-anomer mixture was then separated using an isocratic mobile phase of 10 mM sodium phosphate pH 7.5. Renalase (5.6 μM final) was then added to the α/β $NADP^+$ solution and 50 μL volumes were withdrawn periodically, filtered through a 0.5 mL Amicon 10 KDa centrifugal filter and chromatographed as above.

The propensity of the reduced enzyme to catalyze anomerization of $NAD(P)^+$ was assessed using similar methods but with prior reduction of renalase. The enzyme was reduced using an adaptation of the methods used to reduce the chromophores in the reduction potential measurements described above. The reaction mixture was placed in an anaerobic cuvette and consisted of 300 μM xanthine, 2 μM methyl viologen, 6.0 μM renalase in PBS buffer pH 7.5 at 25° C. The mixture was made anaerobic by 45 cycles of argon and vacuum (as above) and then xanthine oxidase (1-2 μM final) was added from a side arm to initiate the reduction of the enzyme. The extent of reduction was assessed spectrophotometrically using a Hewlett Packard 8453 spectrophotometer. 75 μM (final) of a 1/2.66 mixture of α/β-$NADP^+$ was then added from a second sidearm and the sample was allowed to incubate for 60 minutes before removing the protein components by filtering through a 10 KDa nominal molecular weight centrifugal filter. The chromatograms obtained were then compared to two controls, the first that included all reaction components minus the mixture of α/β-$NADP^+$ and the second that included only the α/β-$NADP^+$ mixture.

Results

Redox-Linked Measurement of β-NADP⁺ Binding Affinities. The renalase reduction potential was determined using a spectrophotometric method that compares the extent of reduction of the enzyme relative to a dye of known potential when electrons are supplied from xanthine oxidase reacting with xanthine under anaerobic conditions. (*320*) In this experiment the dye serves a similar function to that of a reference electrode. Figure 3.1A includes spectra obtained as renalase and indigo carmine are reduced by the xanthine/xanthine oxidase system. Figure 3.1B shows the midpoint for the dye compared to extent of reduction of renalase. This plot allowed a reduction potential for renalase of -155 mV to be calculated. The experiment was repeated with saturating β-NADP⁺ (*vide infra*) to obtain a reduction potential for the Ren_{ox}•β-NADP⁺ complex of -151 mV. No flavin semiquinone is observed to accumulate during reduction suggesting that the second one-electron potential is higher than the first. The reduction potential for α-NAD(P)H is -340 mV (*300*) indicating that the redox driving force (excluding the contribution of anomer equilibria) for the reduction of the flavin is -35.6 kJ/mole. Coupling this the reduction of dioxygen yields -122.5 kJ/mole driving force for the complete catalytic cycle.

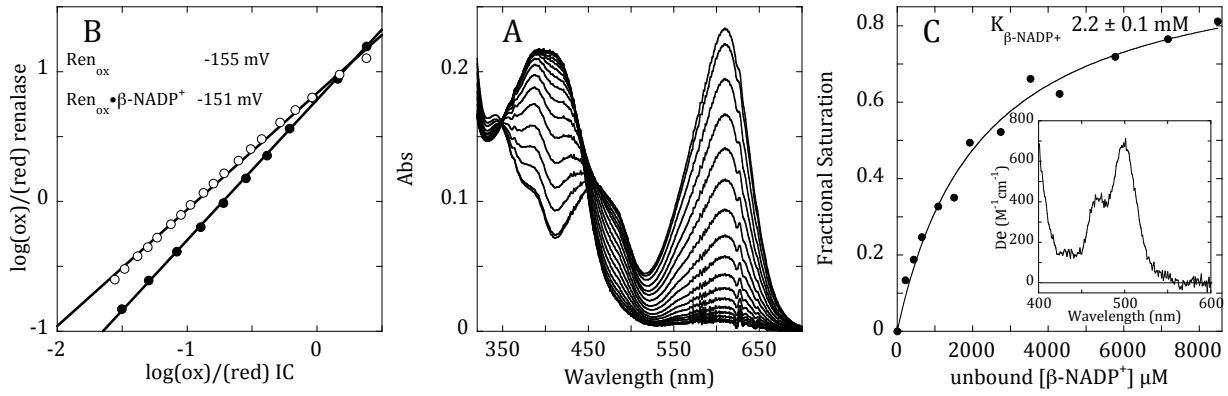

Figure 3.1. Redox States of Renalase. **A**: Simultaneous reduction of renalase (10 µM) and indigo carmine (10 µM) when reacted with 150 nM xanthine oxidase, 5 µM methyl viologen, 300 µM Xanthine in PBS buffer under anaerobic conditions. **B**: Analysis of the data in A. The extent reduced for the enzyme and the dye was assessed where neither had a changing contribution from the other; 470 nm for renalase and 610 nm for indigo carmine. The data for Ren_{ox} are depicted in open circles and that for Renox•β-NADP+ are shown as filled circles. **C**: Measurement of the dissociation constant for the Ren_{ox}•β-NADP+ complex. Renalase (20 µM) was titrated with β-NADP+ and the perturbation of the flavin spectrum observed. Inset depicts the ~80% saturation difference spectrum.

The dissociation constant for the renalase product complex (Ren_{ox}•β-NADP+) was measured using perturbation of the flavin absorption spectrum in the presence of the ligand (Figure 3.1C). These data indicate a relatively weak complex with a dissociation constant of 2.2 mM and are consistent with the prior work of Milani et al. who measured a value of 1.6 mM under similar conditions. (*60*) The reduction potentials of Ren_{ox} and the Ren_{ox}•β-NADP+ complex and the dissociation constant for the Ren_{ox}•β-NADP+ complex complete three sides of a thermodynamic box linking enzyme reduction and β-NADP+ complexation. The small difference in reduction potentials for Ren_{ox} and Ren_{ox}•βNADP+ indicate that the dissociation constants of the oxidized or reduced renalase β-NADP+ complexes are similar (Scheme 3.2). These data suggest that in the Ren_{ox}•β-NADP+ complex

the nicotinamide ring and the isoalloxazine ring of the renalase FAD cofactor are not in sufficient proximity to influence the cofactor's reduction potential.

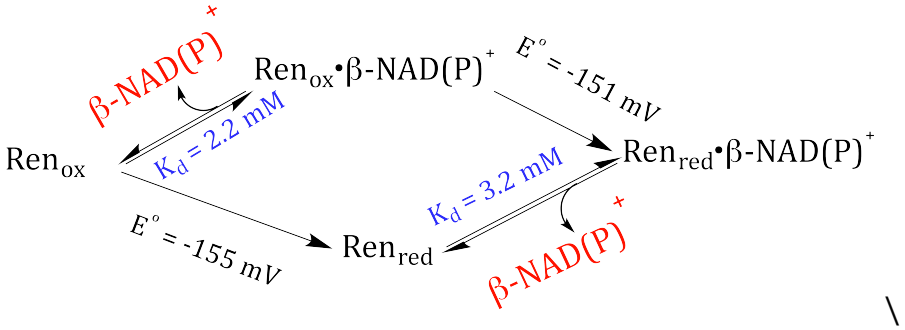

Scheme 3.2. Thermodynamic box linking renalase reduction and β-NADP+ complexation.

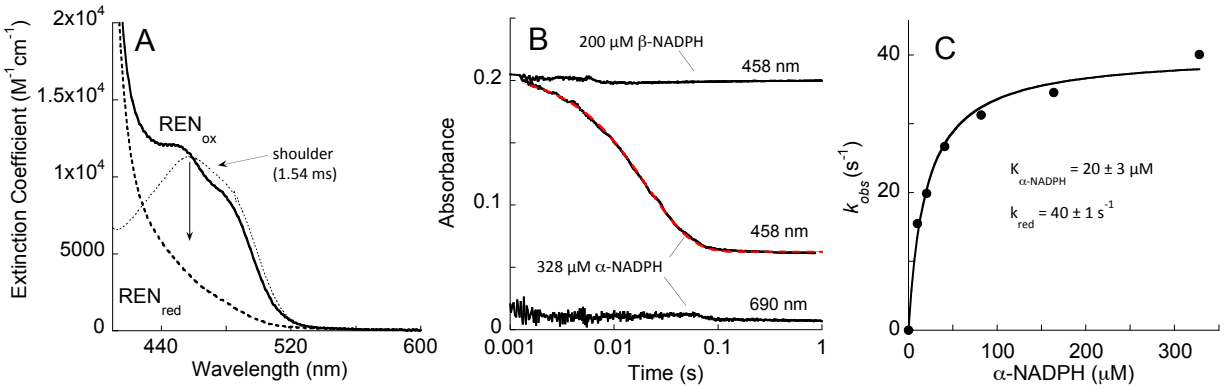

Figure 3.2. Reductive Half Reaction of Renalase. **A**: Initial (solid line) and final (dashed line) absorption spectra when 328 μM α-NADPH was reacted with 20 μM renalase under anaerobic conditions. The dotted line spectrum is the spectrum of resting oxidized renalase. **B**: Absorbance traces at 458 nm and 690 nm when 328 μM α-NADPH was reacted with 20 μM renalase under anaerobic conditions. The dashed line is the fit (red) to a single exponential phase (Equation 3.2) with a rate constant of 41 s^{-1}. Upper trace is for the reaction of 20 μM renalase with 200 μM solution freshly dissolved β-NADPH under anaerobic conditions. **C**: Dependence of the observed rate constant for reduction when when varied pseudo-first order concentrations of α-NADPH were reacted with 2 μM renalase under anaerobic conditions. The fit is to equation 3.3 and gave a limiting rate constant for reduction of 40±1 s^{-1} and a dissociation constant for α-NADPH of 19.8±2.6 μM.

Reductive Half-Reaction: The reductive half reaction of renalase was observed independent of oxidative chemistry by combining the enzyme with α-NADPH and excluding dioxygen (Figure 3.2). The α-NADPH substrate was supplied from a solution of NADPH at anomeric equilibrium (1.5% α-anomer). Under these conditions the α-NADPH substrate initiates reduction of the flavin observed as a decrease in the absorption transitions centered around 458 nm (Figure 3.2A & B). Freshly dissolved β-NADPH does not induce flavin reduction (Figure 3.2B). The dependence of the observed rate constant for reduction of the renalase flavin cofactor on the α-NADPH concentration could be fit to a rectangular hyperbola according to Equation 3.2 (Figure 3.2C). This equation assumes rapid equilibrium binding that diminishes the observed rate constant of reduction at subsaturating substrate concentrations. (*322*) The asymptote is thus the limit of the rate constant for reduction (k_{red} = 40.2±1.3 s^{-1}) and the concentration at which the observed rate constant for reduction is half maximal is the dissociation constant for α-NADPH ($K_{\alpha\text{-NADPH}}$ = 19.9±2.6 μM). These experiments required the use of low renalase concentration (2 μM) in order to be pseudo-first order with a range of α-NADPH concentrations that reasonably span the α-NADPH binding isotherm according to the $K_{\alpha\text{-NADPH}}$ value. A second experiment was also undertaken with relative high renalase concentration (20 μM) and α-NADPH (328 μM) concentrations in order to observe potential charge-transfer absorption transitions at longer wavelengths that would indicate proximity of the nicotinamide and FAD isoalloxazine rings (Figure 3.2, A & B). (*323, 324*) Figure 3.2B includes a long wavelength trace that indicates no significant accumulation of charge-transfer transitions before, during or after reduction. Figure 3.2A includes deconvoluted component spectra

obtained from single exponential fits to photo-diode array data for the reductive half reaction. These spectra also show that no significant new absorbance transitions indicative of charge-transfer absorption transitions were observed. It is therefore conceivable that neither α-NAD(P)H nor β-NAD(P)$^+$ nicotinamide rings stack with the flavin isoalloxazine ring (*vide infra*). The first spectrum acquired at 1.54 ms indicates that the flavin absorption transitions become resolved directly prior to reduction (Figure 3.2A – solid line). This perturbation may arise either in the Ren_{ox}•α-NADPH complex or potentially in a ribose ring-open iminium ion complex that forms rapidly prior to flavin reduction such as proposed in the hypothetical catalytic cycle depicted in Scheme 3.3.

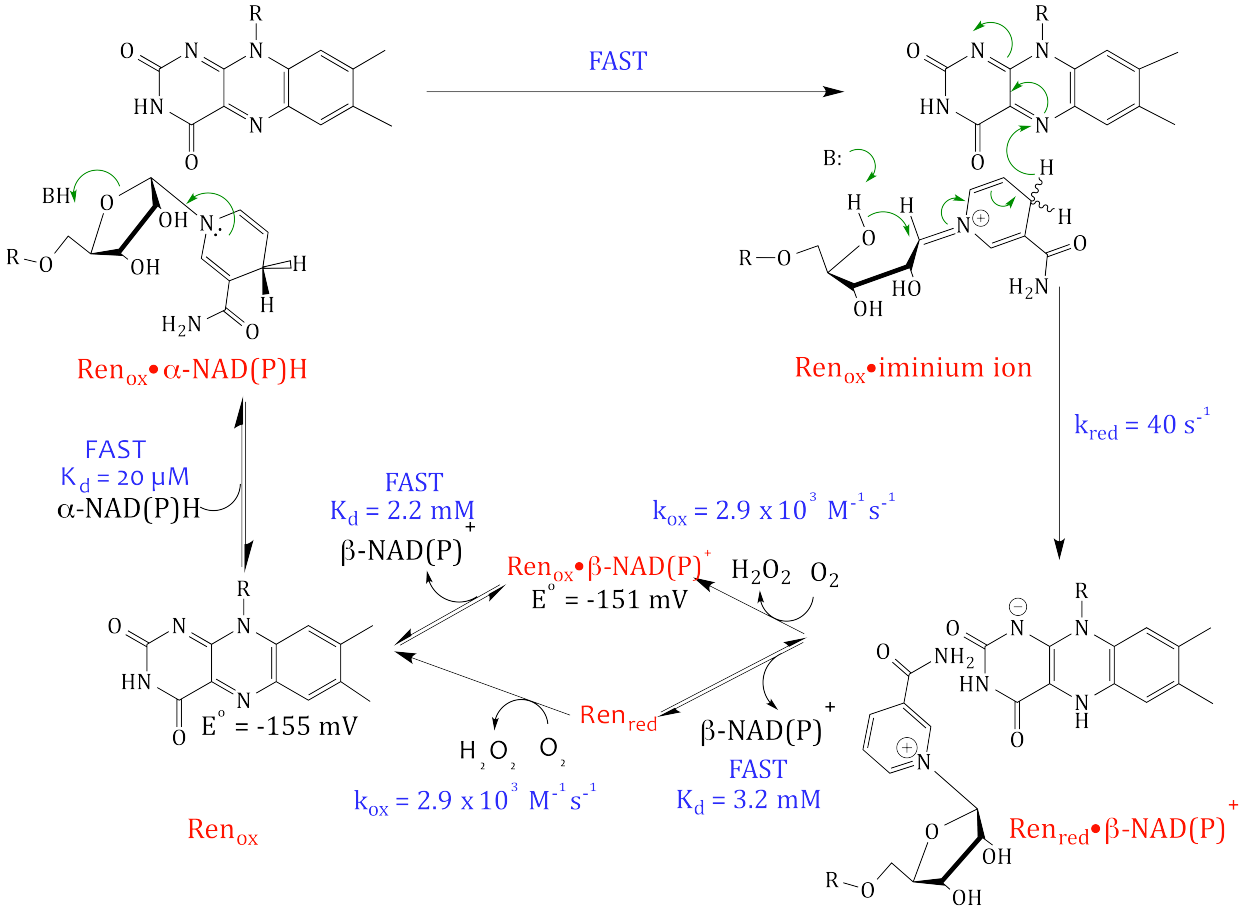

Scheme 3.3. The proposed catalytic cycle of renalase as and oxidase/anomerase.

Oxidative Half-Reaction. The oxidative half reaction of renalase is observed as a monophasic return to the oxidized state of the flavin cofactor. Figure 3.3A summarizes the data obtained when renalase was reduced by limiting concentrations of α-NADPH in the absence or presence of pseudo-first order concentrations of dioxygen. The reductive and oxidative processes differ sufficiently to allow both phases to be observed. When dioxygen concentration was titrated in successive reactions the observed rate constant for reoxidation had a linear dependence on the molecular oxygen concentration that passed through the origin (Figure 3.3B). This indicates that the reaction of reduced renalase with dioxygen is reliant on collision without prior complexation. The slope of the dependence indicated a rate constant of 2.95 $x10^3$ ± 70 $M^{-1}s^{-1}$, a value similar to that of autooxidation of FAD in solution (*325*) suggesting that renalase does not promote the reaction of its cofactor with dioxygen and dictating that reoxidation will generally be the rate-limiting process *in vitro* under conditions of atmospheric dioxygen (~250 μM).

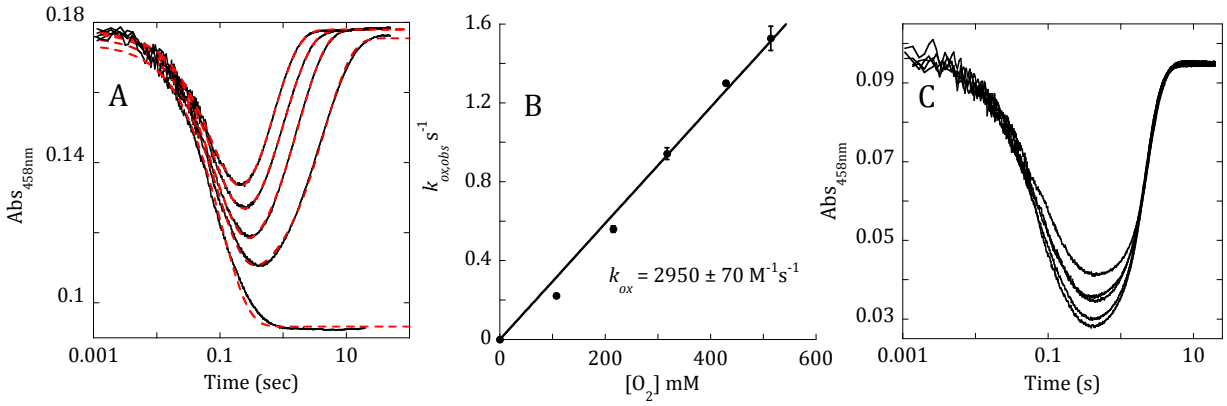

Figure 3.3. Single Turnover of Renalase with Limiting α-NADPH. **A**: Traces observed at 458 nm when 14 μM renalase was reacted with 5.7 μM α-NADPH in varied pseudo-first order concentrations of molecular oxygen. The traces shown in ascending order are for 0, 107, 215, 317, 514 μM dioxygen. Data obtained without dioxygen were fit to a single exponetial decay (Equation 3.2) and data obatined with dioxygen were fit to two exponential phases (Equation 3.4) (fits shown as dashed red lines). **B**: The dependence of the observed rate constant for reoxidation (k_2) on the concentration of molecular oxygen fit to a straight line that passes through the origin. The slope of the line indicates a second order rate constant for the addition of dioxygen of 2.9 x 10^3 $M^{-1}s^{-1}$. **C**: Influence of β-$NADP^+$ on Single Turnover Kinetics. Renalase (10 μM) was mixed with α-NADPH (20 μM) and varied β-$NADP^+$ (0-1600 μM) in the presence of 250 μM dioxygen. The traces in ascending order are for 100, 200, 400, 800, 1600 μM β-$NADP^+$.

In order to evaluate the timing of the release of the β-$NAD(P)^+$ product with respect to reoxidation of the flavin cofactor, exogenous β-$NAD(P)^+$ was titrated in single turnover reactions (Figure 3.3C). These data indicated that increasing concentrations of the β-nicotinamide product had no influence on the observed rate constant for reoxidation suggesting that reoxidation is not contingent on the release of β-$NAD(P)^+$. Consistent with the observed complexation of β-$NADP^+$ with the oxidized enzyme, our data show that this molecule is weakly competitive with α-NADPH as the observed rate of reduction slows with increasing β-$NADP^+$ concentration (observed as a decrease in the amplitude for the

reductive phase). Therefore we conclude that dioxygen and the nicotinamide ring of β-NAD(P)$^+$ do not compete for access to the reduced flavin cofactor during reoxidation. Overall the data are consistent with a kinetically ordered release of products with β-NAD(P)$^+$ dissociating prior the reoxidation of the enzyme. Exogenous β-NAD(P)$^+$ can populate the Ren_{ox}•β-NAD(P)$^+$ complex and hinder α-NADPH association to the oxidized enzyme, however, the physiological relevance of this observation is negligible as the concentration of β-NAD(P)$^+$ in the blood is low relative to its dissociation constant. (*326*)

Extent of Anomerization of α/β-NADP$^+$ by Oxidized Renalase: The ability of oxidized and reduced renalase to catalyze non-redox coupled anomerization was assessed by incubating oxidized or reduced renalase with an α/β-NADP$^+$ mixture of known anomer ratio. The ratio of both anomers was remeasured after incubations with oxidized or reduced renalase for defined times over an hour. Figure 3.4 illustrates that for renalase in either oxidation state the ratio of α- to β-NADP$^+$ is unchanged. This establishes that anomerization does not occur before FAD cofactor reduction, while it is reduced or after its reoxidation and suggests that the oxidative and epimerization activities of renalase are mechanistically linked via a common intermediate.

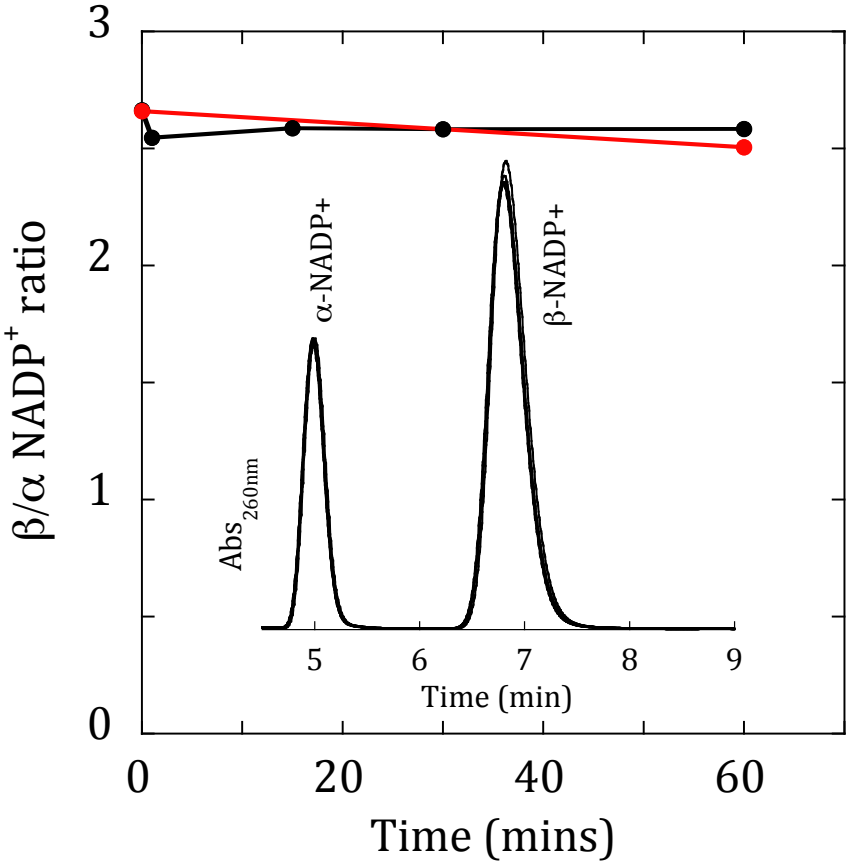

Figure 3.4. Extent of Anomerization by Renalase in the Oxidized and Reduced States. Data depict the extent of anomerization of a 75 μM mixture of 1/2.66 α/β-$NADP^+$ in the presence of 5.6 μM oxidized (black line) and 6.0 μM reduced (red line) renalase. The observed α/β $NADP^+$ ratio was based on HPLC peak area integration. The inset shows HPLC data for the oxidized enzyme experiment (four overlaid chromatograms are shown). Species were separated using a Xterra reerse phase C18 column running isocratically in 10 mM sodium phosphate buffer, pH 7.5.

Discussion

Renalase is a recently discovered flavoprotein that has been widely reported to be a kidney hormone whose endocrine function is to lower circulating concentrations of catecholamine neurotransmitters, such as epinephrine, thereby lowering blood pressure

and heart rate. (*1*) Reported slow rates of turnover with catecholamine substrates *in vitro* do not address catalytic enhancements, nor do they offer a definitive demonstration of the products formed or the reaction stoichiometry(*2, 11*). As such the claimed "monoamine oxidase C" activity of renalase continues to be challenged in the literature(*48-50, 59*). The identification of α-NAD(P)H oxidase/anomerase activity for renalase calls for re-evaluation of many of the reported physiological observations as the only known vasoactive molecule to be consumed or liberated by this activity is H_2O_2. (*314-316*) However, the concentration of this product is contingent on the low equilibrium concentration of α-NADPH that would be maintained near zero by renalase activity, meaning that the rate of H_2O_2 production by renalase would be dependent on the *in vivo* β to α NAD(P)H anomerization rate constant (ca 10^{-6} s^{-1}). (*309*)

Reconciling each of the observations and conclusions made for renalase is complicated by the use of different preparations of the enzyme. Renalase was initially expressed as a recombinant glutathione synthase fusion and isolated using glutathione sepharose. (*1*) Later preparations were isolated from urine using an anti-renalase affinity column.(*1, 11*) More recent preparations have used heterologous expression in *E. coli* from a synthetic codon-optimized renalase gene. Heterologous expression from the optimized gene yields a modest fraction of folded enzyme and a large fraction of inclusion body peptide. (*36*) The smaller, as expressed, soluble fraction can be purified by conventional methods (*60, 61, 319*) and was the form used to obtain the available X-ray crystal structure (*60*). It is likely that this is the native form of renalase as it is this form that exhibits the α-NAD(P)H oxidase/anomerase activity described herein. (*319*) The second reported

preparation method involves solubilizing inclusion body peptide and refolding by dilution and pH titration. (*36*) This form of renalase does not have the spectrophotometric properties of the soluble fraction and does not exhibit the α-NAD(P)H oxidase/anomerase activity (*319*) but has been used in a number of physiological studies of renalase that report vasoactivity(*2, 36*).

We have completed a preliminary examination of the catalytic cycle of the, as expressed, soluble renalase reacting with α-NADPH. We define substrate affinities, the rate constants for those steps that contribute to the turnover number and propose a hypothetical mechanism for the observed activity. Scheme 3,3 depicts an annotated chemical mechanism that accounts for each of the observations made in this study. The data suggest the redox and anomerization activities of renalase are coupled via a shared intermediate as neither the oxidized nor the reduced enzyme can catalyze anomerization of $NADP^+$ (Figure 3.4). Catalysis commences with the association of α-NAD(P)H to renalase to form the Ren_{ox}•α-NAD(P)H complex ($K_d \sim 20$ μM). The lack of charge-transfer absorbance transitions for this complex suggests that the nicotinamide base does not stack with the flavin isoalloxazine (Figure 3.2). (*327*) It is proposed instead that rapid delocalization of the dihydropyridine lone pair and protonation of the bridging oxygen atom of the ribose ring forms a iminium ion intermediate. The iminium ion then recyclizes at the ribose, simultaneously causing the formation the β-$NAD(P)^+$ product with concerted reduction of the flavin cofactor ($k_{red} \sim 40\ s^{-1}$). Much like the Ren_{ox}•α-NAD(P)H complex, the nicotinamide ring of the Ren_{red}•β-$NAD(P)^+$ complex is oriented with respect to the flavin isoalloxazine ring system such that it does not promote charge-transfer transitions (Figure 3.1C & Figure

3.2B). In this position, the β-nicotinamide of the product complex does not impede the reaction of the reduced flavin with dioxygen (k_{ox} ~2.9x10^3 M^{-1}s^{-1}) so that the β-NAD(P)$^+$ release and reoxidation steps occur independently (Figure 3.3C). Further evidence for this is that the reduction potentials of the unliganded oxidized enzyme and the Ren$_{ox}$•β-NAD(P)$^+$ complex are ostensibly the same. This also indicates that the dissociation constant of the Ren$_{ox}$•β-NAD(P)$^+$ complex (K_d ~2.2 mM) is similar to the Ren$_{red}$•β-NAD(P)$^+$ complex (Figure 3.1, Scheme 3.2, Scheme 3.3). In addition, the lack of influence of β-NAD(P)$^+$ on the observed rate constant for reoxidation indicates that the rate constant for reoxidation (k_{ox} ~ 2.9 x 10^3 M^{-1}s^{-1}) is the same for the unliganded reduced enzyme and the Ren$_{red}$•β-NAD(P)$^+$ complex (Figure 3.3C). A weak reassociation propensity of β-NADP$^+$ with oxidized renalase forms a dead-end complex that can retard binding of α-NAD(P)H (Figure 3.3C) suggesting that the nicotinamide substrate and product occupy the same or overlapping binding pockets.

Renalase turnover has two rate contributing chemistries, two-electron reduction of the flavin (~40 s^{-1}) and its subsequent re-oxidation (2.9 x 10^3 M^{-1}s^{-1}). The latter of these will typically have the greatest contribution to the turnover number *in vitro* under conditions of atmospheric oxygen (~250 μM O_2). However, in blood the concentration of available α-NAD(P)H will be negligible as a consequence of the large driving force for the renalase reaction (ΔG~120 kJ/mol) (*309*), while dissolved dioxygen will be approximately constant at ~140 μM. Under these conditions renalase activity will be primarily responsive to the α-NAD(P)H concentration, consistent with a role for renalase of minimizing the α/β-NAD(P) ratio.

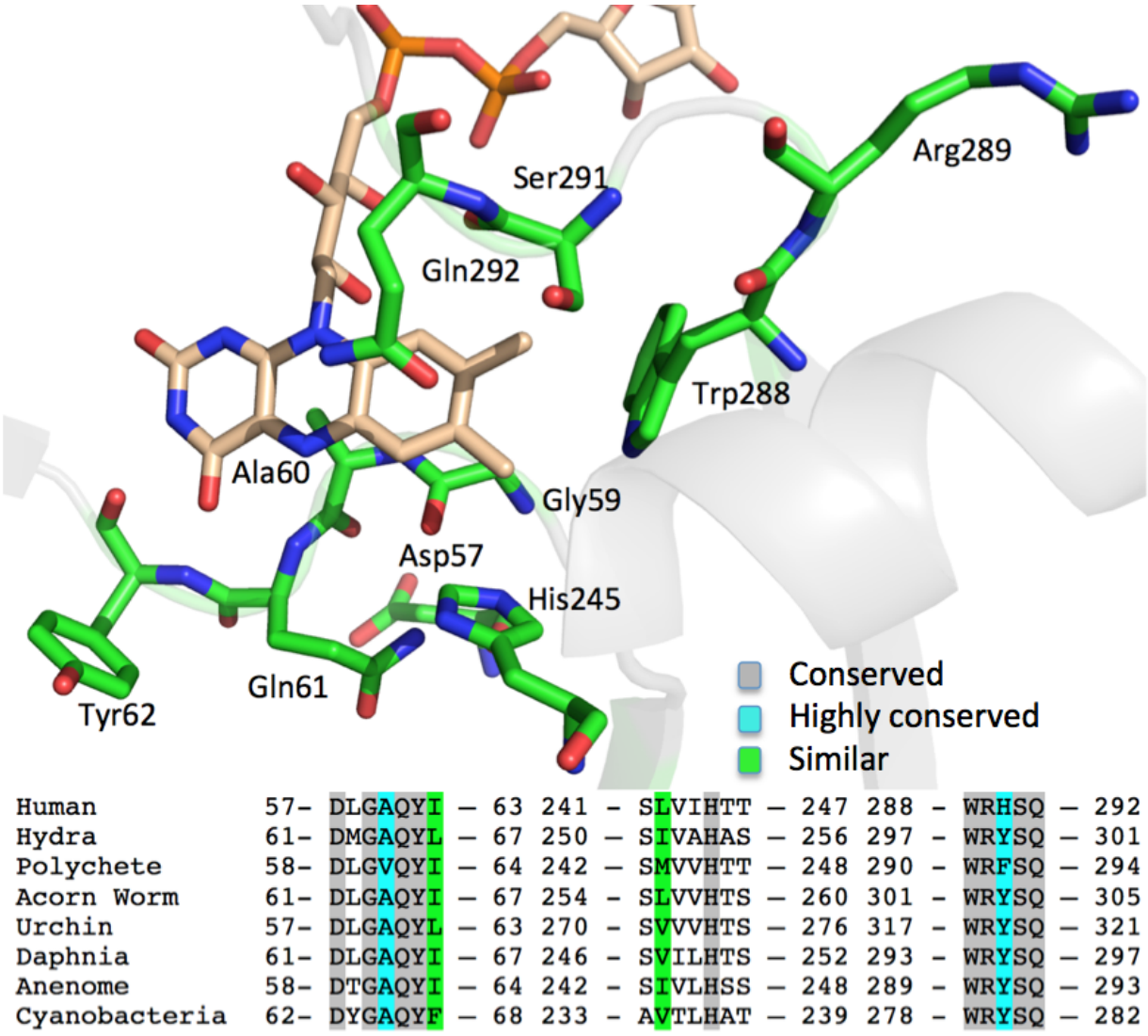

Human	57-	D	L	G	A	Q	Y	I	–	63	241	-	S	L	V	I	H	T	T	–	247	288	-	W	R	H	S	Q	–	292
Hydra	61-	D	M	G	A	Q	Y	L	–	67	250	–	S	I	V	A	H	A	S	–	256	297	-	W	R	Y	S	Q	–	301
Polychete	58-	D	L	G	V	Q	Y	I	–	64	242	–	S	M	V	V	H	T	T	–	248	290	-	W	R	F	S	Q	–	294
Acorn Worm	61-	D	L	G	A	Q	Y	I	–	67	254	-	S	L	V	V	H	T	S	–	260	301	-	W	R	Y	S	Q	–	305
Urchin	57-	D	L	G	A	Q	Y	L	–	63	270	-	S	V	V	V	H	T	S	–	276	317	-	W	R	Y	S	Q	–	321
Daphnia	61-	D	L	G	A	Q	Y	I	–	67	246	-	S	V	I	L	H	T	S	–	252	293	-	W	R	Y	S	Q	–	297
Anenome	58-	D	T	G	A	Q	Y	I	–	64	242	-	S	I	V	L	H	S	S	–	248	289	-	W	R	Y	S	Q	–	293
Cyanobacteria	62-	D	Y	G	A	Q	Y	F	–	68	233	-	A	V	T	L	H	A	T	–	239	278	-	W	R	Y	S	Q	–	282

Figure 3.5. Conservation Within the Renalase Active Site. Structure shown is for human renalase (PDB ID 3QJ4). Sequence data are for the primary structures of renalase and unconfirmed renalase-like proteins from a number of divergent phyla.

Renalase is reported to be expressed in numerous tissues (*1, 301*) and the conserved active site residue motif can be identified in homologous proteins from animals such as anemones, polycheates, daphnia and even single-celled organisms such as cyanobacteria (Figure 3.5). This implies that the root physiological role of renalase is more pervasive than vasodilation. The α-NAD(P)H oxidase/anomerase activity of renalase is significantly exothermic which implies that the purpose of this activity is to use the considerable oxidative power of dioxygen to deplete the α-NAD(P)H concentration. In the absence of renalase, the inherently lower reduction potential of α-NAD(P)H molecules (-340 mV) dictates that they will tend to oxidize by reducing β-NAD(P)$^+$ or other singlet molecules of higher potential and become isolated, unable to be reincorporated into metabolism. This would result in a steady but inexorable loss of function for a major fraction of available NAD(P) molecules. It is therefore reasonable to conclude that the renalase α-NAD(P)H oxidase/anomerase activity is important to all metabolism in order to maintain the α/β-NAD(P)H ratio at ostensibly zero such that the preponderance of nicotinamide dinucleotides remain available for redox cycling.

CHAPTER IV
A Metabolic Function for Human Renalase: Oxidation of Isomeric Forms of β-NAD(P)H that are Inhibitory to Primary Metabolism.

Brett A. Beaupre, Matt R. Hoag, Joseph Roman, F. Holger Försterling, Graham R. Moran

Abstract

Renalase is a recently identified flavoprotein that has been associated with numerous physiological maladies. There remains a prevailing belief that renalase functions as a hormone, imparting an influence on vascular tone and heart rate by oxidizing circulating catecholamines, chiefly epinephrine. This activity however, has not been convincingly demonstrated *in vitro*, nor has the stoichiometry of this transformation been shown. In prior work we demonstrated that renalase induced rapid oxidation of low-level contaminants of β-NAD(P)H solutions. (*54, 319*) Slow aqueous speciation of β-NAD(P)H resulted in the production of renalase substrate molecules whose spectrophotometric characteristics and equilibrium fractional accumulation closely matched those reported for α-anomers of NAD(P)H. The fleeting nature of these substrates precluded structural assignment. Here we structurally assign and identify two substrates for renalase. These molecules are 2-, and 6-dihydroNAD(P), isomeric forms of β-NAD(P)H that arise either by non-specific reduction of β-NAD(P)$^+$ or by tautomerization of β-NAD(P)H (4-dihydroNAD(P)). The pure preparations of these molecules induce rapid reduction of the renalase flavin cofactor (230 s^{-1} for 6-dihydroNAD, 850 s^{-1} for 2-dihydroNAD) but bind only a few fold tighter than β-NADH. We also show that 2-, and 6-dihydroNAD(P) are potent inhibitors of primary metabolism dehydrogenases and therefore conclude that the

metabolic function of renalase is to oxidize these isomeric NAD(P)H molecules to β-NAD(P)$^+$, eliminating the threat they pose to normal respiratory activity.

Introduction

Renalase is a flavoprotein that has been proposed to be an enzyme/hormone produced by the human kidney to attenuate blood pressure and slow the heart (*1*). It has been asserted that this physiological response is achieved by catabolizing circulating catecholamines (*11*). However, this claimed activity has never been convincingly demonstrated and a number of factors portend a more prevalent metabolic role for renalase. The first is that renalase transcripts have been detected in numerous mammalian tissues (*301, 328*). The second is that the X-ray crystal structure of renalase has revealed a unique constellation of conserved residues about an active site flavin isoalloxazine ring that form a structural motif that is identifiable in homologs as far removed as the cyanobacteria (*54, 60*). Despite numerous reports of physiological relevance, a definitive catalytic reaction for renalase has remained elusive (*22-25, 51, 329-332*). The most persistent claim is that renalase acts as the third monoamine oxidase (MAO C), oxidizing and cyclizing epinephrine and requiring NADH as a reductant to form the aminochrome molecule, adrenochrome (*2, 22*). The reported rates for this conversion, however, are exceedingly slow and the apparent odd stoichiometry of this reaction, in which four electrons are mobilized, has not been established.

In prior work, we identified fleeting minor contaminants of β-NAD(P)H solutions as substrates for renalase. These molecules induced rapid reduction of the active site flavin that then reoxidized by reduction of dioxygen. Product analysis indicated β-NAD(P)$^+$ and

hydrogen peroxide as products in 1:1:1:1 stoichiometry leading to the conclusion that renalase is an oxidase. On the basis of both spectrophotometric characteristics and aqueous equilibrium proportions we erroneously proposed that the substrates for renalase were the α-anomers of NAD(P)H (*54, 309, 319, 333*) and that the function of renalase was therefore to oxidize and epimerize α-NAD(P)H anomers to avoid an inexorable loss of cellular redox currency as α-NAD(P)$^+$ (molecules that have no known metabolic role in mammalian metabolism). This proposed activity seemed to satisfy a long standing conundrum whereby despite reported lower reduction potentials for α-anomers, α-NAD(P)$^+$ molecules are not observed to accumulate to any significant level in normal metabolism (*300*).

The purpose of this article is to correct the renalase literature, provide direct evidence for the structure of the renalase substrate(s) molecules described in our prior reports and link these molecules to an apparent important metabolic role for the activity observed. In this study we show that the substrate(s) for renalase are 2-dihyhdroNAD (2DHNAD(P)) and 6- dihydroNAD (6DHNAD(P)), both of which are isomeric forms of β-NAD(P)H where the hydride equivalent resides on either the 2 or the 6 position of the nicotinamide instead of the native 4 position. These molecules arise from non-specific (non-enzymatic) reduction of β-NAD(P)$^+$ or tautomerization of β-NAD(P)H and can multiple dehydrogenase enzymes of primary metabolic pathways. Renalase would therefore appear to alleviate this inhibition by oxidizing 2DHNAD(P) and 6DHNAD(P) to form β-NAD(P)+ (Scheme 4.1).

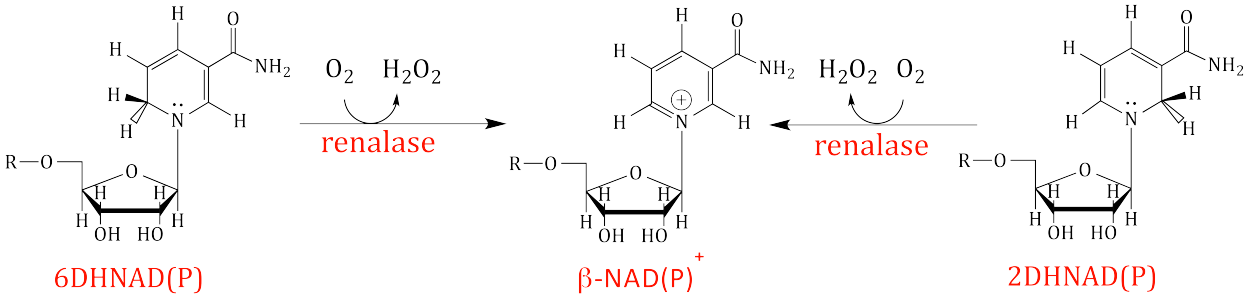

Scheme 4.1. Catalysis of renalse using isomers of β-NAD(P)H as substrates.

Materials and Methods

Materials. β-NADH (disodium salt, trihydrate) was obtained from Amresco. β-NAD$^+$, oxaloacetate, (±)-α-lipoamide and lactate dehydrogenase (LDH) (rabbit muscle) were each sourced from Sigma-Aldrich. Sodium borohydride, potassium phosphate (mono and dibasic), β-mercaptoethanol and pyruvate were from Acros. Deuterium oxide was from Cambridge Isotopes. Sep-Pak cartridges were purchased from Waters. Competent NEB5a and BL21 DE3 *Escherichia coli* cells were obtained from New England Biolabs. Q-sepharose was from Bio Rad. Lipoamide dehydrogenase (DLD) (porcine heart) was from Calzyme.

Malate dehydrogenase (MDH) was cloned from *E. coli*. Genomic DNA was isolated from 100 mL of log-phase cells (OD_{600nm} ~0.5) using a Qiagen Genomic DNA preparation kit and protocol. The MDH gene was amplified using oligonucleotides complementary to the 3' and 5' ends of the gene that incorporated respective Nde I and Xho I restriction sites (5' ATTATTATTATTCAT**ATG**AAAGTCGCAGTCCTCGCGT 3', 5' TTTTTTTTTTTTTTCTGGAG **TTATTA**CTTATTAACGAACTTCGCC 3'; start and stop codons are depicted bolded and restriction sites underlined). The amplified gene was then digested with the above two restriction enzymes and ligated with pET17b plasmid that had been digested in the same

way. The ligation was then transformed into competent NEB5a *E. coli* cells and plated onto Luria Bertani (LB) agar, 100 μg/mL ampicillin. Transformant cultures prepared from individual colonies were grown in LB broth, 100 μg/mL ampicillin and were screened for the correct plasmid insert by agarose gel electrophoresis. Plasmid DNA from each transformant was prepapred using the Qiagen Mini-prep kit and protocol followed by digestion with Nde I and Xho I restriction enzymes. The plasmid from verified cell lines were then prepared in sufficient quantity for DNA sequencing using the Qiagen Midi-prep kit and protocol. After sequence confirmation the plasmid, pECMDH, was then transformed into competent BL21(DE3) *E. coli*. A single colony was selected and grown in LB broth medium containing 100 μg/mL ampicillin. Cells from this culture were harvested in early log phase and mixed with 0.22 μm filter sterilized glycerol to a final concentration of 20% v/v and stored as 1 mL aliquots at -80 ^{o}C.

MDH was expressed and purified by thawing cell stocks and plating 100 μL per plate onto LB agar plates (100 μg/mL ampicillin) and grown at 37 ^{o}C for 16 hrs. The lawn of cells from two plates was then resuspended into 10 mL of LB broth and used as an inoculum for 1 L LB broth culture (100 μg/mL ampicillin) pre-warmed to 37 ^{o}C. The cell culture was then shaken at 220 rpm and the temperature maintained at 37 ^{o}C. When the density of the culture reached OD_{600nm}~1.0, 0.1 mM isopropyl-b-thiogalactopyranoside (IPTG) was added to induce over-expression of the MDH protein. After two hours the culture was harvested by centrifugation at 4000 g in an RC-3C Sorvall centrifuge and the cell pellet resuspended in 20 mL of ice-cold 20 mM HEPES buffer, 2 mM β-mercaptoethanol (βME), pH 7.0. All subsequent methods maintained the temperature of the sample at 4 ^{o}C, unless otherwise noted. The cell slurry was then sonicated for a total of 5 minutes at 20 Watts using a

Branson sonicator fit with a blunt tungsten tip. The resulting sonicate was then centrifuged at 15,600 g for 30 minutes using an Eppendorf 5804R centrifuge. The supernatant was then brought to 1.5% streptomycin over a period of 20 minutes and centrifuged at 12,850 g for 10 minutes. The supernatant obtained was decanted and brought to 45% ammonium sulfate saturation over 25 minutes and centrifuged again at 12,850 g for 10 minutes. The supernatant was retained and brought to 75% ammonium sulfate saturation over a period of 25 minutes and centrifuged at 12,850 g for 10 minutes. The pelleted protein was then redissolved in 20 mM HEPES, 2 mM bME, pH 7.0 (100 mL per liter of culture) and loaded onto a 2.5 x ~25 cm Q-sepharose column at a flow rate of 2 mL/min. Pure MDH protein was then eluted using a linear gradient to 200 mM NaCl spanning a volume of 400 mL supplied from a Biorad Biologic LC chromatographic system. The MDH obtained was then concentrated using 15 mL Amicon, 10 kDa nominal molecular weight cutoff centrifugal concentrator and stored at -80 ^{o}C. The pure enzyme was quantified using the calculated extinction coefficient for 280 nm of 6085 $M^{-1}cm^{-1}$ (*334*).

The gene for *Saccharomyces cerevisiae* old yellow enzyme (OYE, isoform 1) cloned into the Nde I and Xho I restriction sites of pET28a was obtained from Enzymax as an *E. coli* XL-1 blue transformant culture. Cloning into the Nde I restriction site fuses the OYE1 gene to an N-terminal His-Tag. A 50 μL aliquot of these cells was used to make cell stocks by culturing in 20 mL of LB broth (25 μg/mL kanamycin) incubated at 37 ^{o}C with shaking at 220 rpm for 6 hrs. Cells from this culture were stored in sterile 20% glycerol at -80 ^{o}C. Plasmid (pSCOYE) was prepared from 5 mL cultures of these cells using the Qiagen mini-prep kit and protocol and transformed into *E. coli* BL21(DE3) and prepared as cell stocks from a single colony as described above for pECMDH plasmid. OYE was expressed and

purified by spread plating onto LB agar (25 μg/mL kanamycin, 100 μL of cells per plate) and incubating at 37 ^{o}C for 20 hrs. The lawn of cells from two plates was resuspended in ~20 mL of LB broth and used as an inoculum for a 1 L culture of LB both (25 μg/mL kanamycin). Expression of the OYE protein and harvesting of the cells proceeded in an identical manner to that described above for *E. coli* MDH.

To prepare pure OYE the harvested cells were resuspended 20 mL/L of culture, 20 mM HEPES pH 7.5 and sonicated for ~10 min at 20 Watts. Thεe lysed cell slurry was then centrifuged at 15,600 g for 30 minutes and the supernatant (~25 mL/L of culture) was then loaded onto a Talon cobalt affinity column at a flow rate of 1 mL/min and the column was washed with 200 mL 50 mM HEPES, 10 mM imidazole, pH 7.5. OYE was then eluted with a 400 mL linear gradient to 50 mM HEPES, 300 mM imidazole, pH 7.5 using a Biorad Biologic liquid chromatography device. Fractions containing OYE activity were then pooled and the buffer exchanged to 10 mM potassium phosphate buffer, pH 7.5 using an Amicon 15 mL, 10,000 nominal molecular weight cutoff filter/concentrator. The pure OYE obtained was then aliquoted and stored at -80 ^{o}C. OYE was quantified using the 461 nm extinction coefficient of the flavin cofactor (10,400 $m^{-1}cm^{-1}$) that was determined using an SDS denaturation method based on the extinction coefficient of free flavin (*319*).

Preparation, Separation and Analysis of 2 & 6DHNAD. 2- & 6DHNAD were prepared by reduction of β-NAD^{+}. The ratio of reactants used was developed empirically such that the fractional accumulation of 2DHNAD (the less stable of the products) was comparable to that of 6DHNAD and β-NADH (4DHNAD). Initially, a 37 mM sodium borohydride solution was prepared in 20 mM potassium phosphate titrated to pH 11. A 200 μL aliquot of this

solution was then added to a freshly prepared 15.5 mM solution of β-NAD^+ in 100 mM potassium phosphate pH 7.5. Analytical high-pressure liquid chromatography (HPLC) separation of the products of β-NAD^+ reduction was achieved using an Xterra C18 reverse phase column (4.6 x 150 mm, 3.5 μM particle size) run isocratically at 0.5 mL/min in 10 mM potassium phosphate buffer pH 7.5. Purification of 2 & 6DHNAD was achieved by preparative HPLC. The partially reduced β-NAD^+ solution was injected (50-500 μL) onto a Phenomenex reverse-phase phenyl HPLC column (21.2 x 250 mm) run isocratically at 5 mL/min with a mobile phase of 10 mM potassium phosphate, pH 7.5. Both the analytical and preparative columns were coupled to a Waters 600E pump and Waters 2487 dual wavelength detector and the elution of component species was observed simultaneously at 260 and 340 (or 394) nm. To prepare samples for nuclear magnetic resonance (NMR) and mass spectrometry, reduced products were collected individually into 400 mL glass vessels immersed in liquid nitrogen. The pure dilute solutions were then thawed and desalted at 4 ^oC by loading onto a 35 cc C18 Sep-Pak cartridge (Waters) and eluted with a 200 mL gradient from 10 mM to 0 mM potassium phosphate pH 7.0 using a Biorad Biologic liquid chromatography device. The desalted samples were then dried by lyophilization (in order to minimize ambient temperature decomposition, the lyophilization vessels were embedded in ice throughout). Each of the desalted, dry and pure reduction products was then dissolved in cooled deuterium oxide (D_2O) and used immediately for NMR or dissolved in cooled water for mass spectrometry. For kinetic studies, the product identified as 6DHNAD was collected, desalted and concentrated and redissolved in D_2O as described above and stored at -80 ^oC. The product identified as 2DHNAD could not be stored due to

pronounced instability and was instead collected from the HPLC and used immediately (within 1-5 mins).

Spectrophotometric Quantification of NAD Molecules. The concentration β-NADH was determined using published 340 nm extinction coefficient of 6220 M^{-1} cm^{-1} *(309).* Dihydronicotinamide chromophore extinction coefficients for 2 & 6DHNAD (and the 260 nm extinction coefficient for β-NAD^+) were obtained using renalase to oxidize both molecules to β-NAD^+. Initially, the spectrum of each of the HPLC purified molecule (70-90 μM) was acquired using a Hewlett Packard 8453 spectrophotometer. The 2 & 6DHNAD were then oxidized to β-NAD^+ by adding 30 nM renalase. 4DHNAD (β-NADH) prepared in the same manner was oxidized to β-NAD^+ by the addition of 30 nM OYE. Under these conditions complete oxidation was achieved in 2-3 minutes. The pairs of fully reduced and fully oxidized spectra obtained from each reaction were then multiplied by the factor required to normalize the β-NAD^+ spectra and then all spectra were multiplied by the factor required to convert the β-NADH spectrum to equal its known extinction coefficient at 340 nm. This method gave extinction coefficient of ε_{394nm} = 5360 $M^{-1}cm^{-1}$ for 2DHNAD, ε_{345nm} = 6580 $M^{-1}cm^{-1}$ for 6DHNAD (*cf.* α-NADH ε_{345nm} = 6170 $M^{-1}cm^{-1}$) and ε_{260nm} = 18800 $M^{-1}cm^{-1}$ for β-NAD^+.

Mass Spectrometry. For both 2 & 6DHNAD, an HPLC purified and C^{18} Sep-Pak desalted sample (~50-100 μM, prepared as described above) was collected. This sample was injected via a Shimadzu LC-2010C liquid chromatography system onto a Shimadzu 2020

mass spectrometer. In each case, 10 μL of sample was delivered in a 1:1 mixture of water and methanol. Data were collected in negative ion mode in the mass range 100-800. This procedure was also followed for β-NADH, β-NAD^+ as controls.

Nuclear Magnetic Resonance. NMR experiments were carried out at 280 K in D_2O solvent using a Bruker DRX-500 NMR spectrometer equipped with a triple axis gradient inverse (BBI) probe operating at a frequency of 499.832389 MHz for proton and 125.6936644 MHz for ^{13}C. Chemical shifts are reported relative to the methyl signal of the sodium salt of 3-(trimethylsilyl) propanesulfonic acid using the residual HDO signal as indirect reference. One-dimensional experiments were performed by accumulating 128 scans using a spectral width of 10330 Hz (^1H) and 20161 Hz (^{31}P) and using relaxation delays of 1s and 3s, respectively. For a typical gradient selected DQF -COSY experiment 960 t_1 increments with 32 transients of 2048 points covering a spectral width of 5000 Hz were acquired. ^1H(*158*)-HSQC spectra were acquired with gradient selection and multiplicity editing, using 730 t_1 increments with 64 transients of 1600 points each, covering a spectral width of 5000 Hz and 22624 Hz in f2 and f1, respectively. A mixing time of 3.4 ms was used. ^1H(*158*)-HMBC spectra utilized gradient selection acquiring 820 t_1 increments with 160 transients of 4096 data points each with a spectral widths in f2 and f1 of 5000 Hz and 25140 Hz, respectively, and a mixing time of 50 ms. A low-pass filter was employed to suppress one bond J_{CH} couplings. All spectra were analyzed and assigned using Topspin 3.2 software (Bruker BioSpin).

Reductive Half-Reaction of Renalase with 2 & 6DHNAD. The reductive half-reaction of renalase could be observed independent of subsequent oxidative processes by exclusion of dioxygen. Renalase (5 mL, 20 μM) in 2 x PBS buffer containing 1 mM dextrose was added to the main chamber of a glass tonometer and glucose oxidase (25 μL, 25 units) was added to a detachable side arm. The tonometer was then assembled and embedded in ice and the renalase and glucose oxidase solutions were made anaerobic by exchanging argon for dissolved dioxygen. This was achieved by 45 alternating cycles of low-level vacuum followed by the introduction high-purity argon gas (at 5 psi). The argon was passed through an Alltech oxygen-reactive cartridge and sparged through anaerobic water. Throughout this procedure the sample was equilibrated with the argon atmosphere by gentle agitation after each set of three exchange cycles. Once anaerobic, the glucose oxidase was combined with the renalase/dextrose solution and mounted onto a Hitech (now TgK) DX2 stopped flow instrument. 6DHNAD samples were thawed (see above) and diluted to target concentrations in water containing 1 mM glucose. Each 6DHNAD sample was then placed in a glass syringe, inverted and sparged with argon gas for 5 minutes. Before capturing and mounting the substrate solution to the stopped flow instrument, 10 μL of glucose oxidase (10 units) was injected via the luer tip. 2DHNAD substrate solutions were prepared in an equivalent manner but were collected directly from preparative HPLC purification (50-90 μM) and used immediately (see above).

Renalase and substrate solutions were mixed and reduction of the renalase cofactor was observed at 458 nm. The stability of 6DHNAD substrate allowed it to be prepared in sufficient concentrations to achieve pseudo-first order reaction conditions. As such the data for this substrate was fit to a linear combination of two exponentials according to

Equation 4.1 using Kinetic Studio software (TgK Ltd). In this equation A_1 and A_2 are the amplitudes associated with the first and second rate constants, k_{1obs} and k_2, and C is the absorbance at end of the reaction. The dependence of the k_{1obs} values determined was then fit to the hyperbolic form of the single-site binding equation (Equation 4.2) according to Strickland, where k_{red} is the limiting rate constant for reduction and K_{6DHNAD} is the dissociation constant for 6DHNAD (*322*).

Equation 4.1 $$A_{458} = A_1(e^{-k_{1obs}t}) + A_2(e^{-k_2 t}) + C$$

Equation 4.2 $$k_{obs} = \frac{k_{red}[6DHNAD]}{(K_{6DHNAD}+[6DHNAD])}$$

For 2DHNAD, 100 μM was the approximate maximum concentration obtained from preparative HPLC; as such, the reductive half-reaction with this substrate was conducted under second-order reactant conditions and the data obtained were fit globally using Kintec Explorer to the model shown in Scheme 4.2. In this model the Ren_{ox}•2DHNAD complex k_{on} rate constant was arbitrarily assigned to ~10^8 $M^{-1}s^{-1}$, and the ratio of the k_3 and k_{-3} for the Ren_{red}•β-NAD^+ complex was confined to equal the measured dissociation constant for the Ren_{ox}•β-NAD^+ complex (for justification, see below).

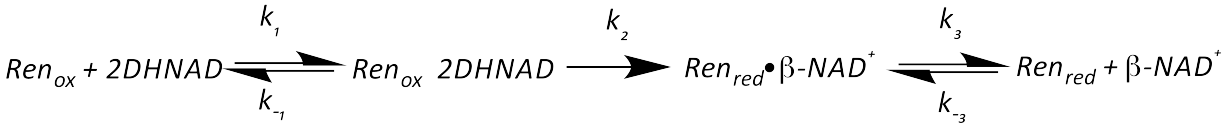

Scheme 4.2. Model of renlase reductive half-reaction of renalase using 2DHNAD as a substrate.

The Dissociation Constants for the Ren_{ox}•β-NADH and Ren_{ox}•β-NAD^+ Complexes. The dissociation constants for the Ren_{ox}•β-NADH and Ren_{ox}•β-NAD^+ complexes were measured by perturbation of the renalase flavin spectrum in the presence of each ligand. In order to avoid slow non-specific reduction of the renalase flavin by β-NADH during the experiment, a ~10 mL stock of renalase (15 μM) was prepared in PBS buffer at 25 °C. From this stock a 0.9 mL aliquot was added to a 1.5 mL quartz cuvette and 0.1 mL of β-NADH was added to this sample from a set of eight 2-fold serially diluted stocks. As such the spectrophotometric data are compiled from eight separate renalase samples observed shortly after the addition of β-NADH for concentrations that spanned the range 0 - 3.51 mM. The dissociation constant for the Ren_{ox}•β-NAD^+ complex was measured by preparing a single 20 μM solution of renalase in PBS buffer at 25 °C. To this solution β-NAD^+ was titrated such that a range of concentrations from 0-~6mM was achieved (higher concentrations induced marked precipitation of the enzyme).

For both β-NADH and β-NAD^+ titrations, spectra (250-900 nm) were acquired for each ligand concentration using a Shimadzu 1800 spectrophotometer. After correction for dilution, the change in absorption at 550 nm and 500 nm was used to determine the dissociation constant for the Ren_{ox}•β-NADH and the Ren_{ox}•β-NAD^+ complexes respectively. The changes in absorbance were fit to the hyperbolic form of the single site binding equation (Equation 4.3) in which f is fractional saturation and K_{ligand} is the dissociation constant for either β-NADH or β-NAD^+ for the respective Ren_{ox} complex.

Equation 4.3 $$f = \frac{[ligand]}{(K_{ligand}+[ligand])}$$

2 & 6DHNAD Dehydrogenase Inhibition. Inhibition of dehydrogenases from primary metabolism by 2 & 6DHNAD was assessed using two approaches. The relative stability of 6DHNAD allowed the collection of a series of nested Michealis-Menten curves each acquired in the presence of a different concentration of the candidate inhibitor. The relative instability of 2DHNAD dictated that the 50% inhibitory concentration (IC50) method of Cheng and Prusoff was used for determination of Ki (*335, 336*). Via this approach, 2DHNAD need only be separated from 6DHNAD and β-NADH using preparative HPLC, quantified and diluted to the target concentration before adding to the assay; as such the pure 2DHNAD is used within five minutes of purification.

6DHNAD and 2DHNAD Ki values were measured for three dehydrogenase enzymes of primary metabolism; malate dehydrogenase (MDH), lactate dehydrogenase (LDH), and lipoamide dehydrogenase (DLD). To limit the influence of enzyme instability encountered with the MDH and LDH enzymes, a solution of 0.3 U/mL was prepared in 10 mM potassium phosphate pH 7.5 and then frozen at -80 ^{o}C as 2 mL aliquots. These samples were then thawed and used as required. By contrast, DLD (0.3 U/mL) maintained activity when incubated at 4 ^{o}C and so was prepared in 100 mM potassium phosphate pH 7.5 and placed on ice until used in assays. For assessment of 6DHNAD inhibition of MDH and LDH a series of five Michaelis-Menten analyses were completed using β-NADH concentrations from 0-80 μM in the presence of saturating respective oxaloacetate (0.4 mM) and pyruvate (0.5 mM). For MDH and DLD, 6DHNAD were varied from 0-2 μM, while for LDH the range of 6DHNAD used was 0-20 μM. The data obtained for MDH and LDH were fit globally to the competitive

inhibition model using the non-linear least squares analysis provided by Prism 6 software (Graphpad Software Inc.).

Ki values for 2DHNAD with MDH, LDH, and DLD were assessed using the IC50 method. In this method the extent of inhibition for a range of 2DHNAD concentrations was measured at a concentration of β-NADH equivalent to the measured Michaelis constant for this substrate. This value was determined in the absence of inhibitor and at near saturating concentrations of the oxidized substrate (0.4 mM oxaloacetate, 0.5 mM pyruvate, 1 mM lipoamide acid for MDH, LDH and DLD respectively). All data were fit using non-linear least squares analysis available from KaleidaGraph software (Synergy Software Inc). The data obtained in the absence of the inhibitor was fit to Equation 4.4, the Michaelis-Menten equation, where v is the observed rate, V_{max} is the maximal rate of reaction and $K_{\beta\text{-NADH}}$ is the Michaelis constant for β-NADH. The extent of inhibition was then measured for a range of 2DHNAD concentrations and the data obtained was fit to the Hill equation (equation 4.5) to derive the IC50 mid-point as a measure of the Ki value for 2DHNAD.

Equation 4.4 $$v = \frac{V_{max}[\beta-NADH]}{(K_{\beta-NADH}+[\beta-NADH])}$$

Equation 4.5 $$v = V_{min} + \frac{V_{max}-V_{min}}{(1+(\frac{[2DHNAD]}{K_i})}$$

Results

Renalase Substrates are Generated by Non-Specific Reduction of β-NAD⁺. In prior work we identified small equilibrium proportions of molecules in β-NAD(P)H solutions that were

oxidized by renalase. The absorption maxima, extinction coefficients and apparent equilibrium proportions correlated well with those reported for α-anomers of NAD(P)H molecules, but the fleeting behavior of these molecules precluded rigorous structural assignment. We have since devised methods to both form larger fractional accumulations of these molecules by reduction of β-NAD^+ and prolong the decay half-life such that structural assignments can be made. Figure 4.1A illustrates the chromatographic separation of the reduced products obtained when β-NAD^+ is reduced by both hydrosulfite and borohydride. While hydrosulfite (E^o=-0.62 V) yields only β-NADH (4DHNAD), reduction by borohydride (E^o=-1.24 V) yields three products, two of which are substrates for renalase (Figure 4.1B). The third component, that was not a substrate for renalase, had a retention time identical to that of β-NADH. When reacted with renalase, the product from both substrate molecules was identified here (and in prior work) as β-NAD^+ and this product was made in near equimolar concentration to the amount of dioxygen consumed (Figure 4.1B inset)(*319*). The absorption spectra of the reduction products indicate distinct UV/Vis maxima at 345, 394, and 340 nm for the dihydro-nicotinamide moiety in each case (Figure 4.1C).

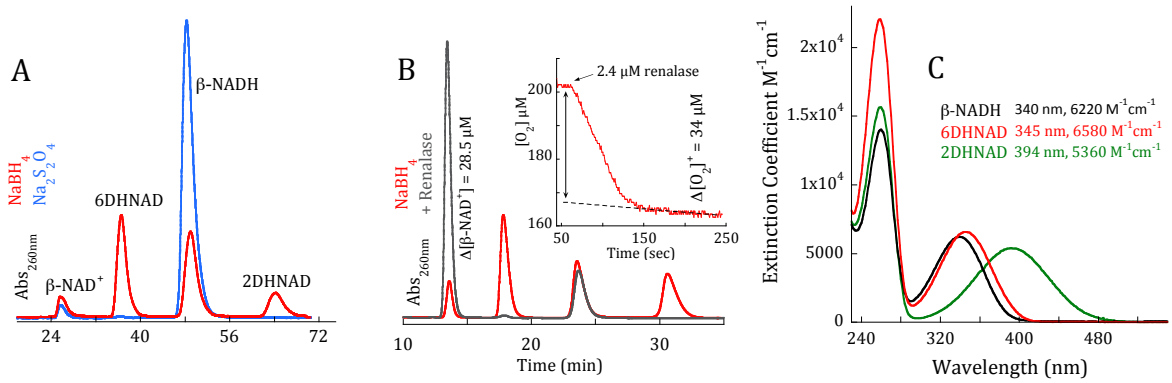

Figure 4.1. Generation of Renalase Substrates by Reduction of β-NAD⁺. **A**: Analytical HPLC chromatograms recorded after the reduction of 50 μM_β-NAD⁺ with 50 μM sodium hydrosulfite (blue line) or 50 μM sodium borohydride (red line). **B**: Analytical HPLC chromatograph demonstrating the consumption of two of the three products of sodium borohydride reduction by the addition of 2.4 μM renalase. The inset is taken from observation of the reaction shown in **B** using a Clark-type dioxygen electrode. After cessation of dioxygen consumption (~100 s) the sample was filtered using an Amicon 0.5 mL 10 kDa centrifugal filtration device and re-chromatographed as described (gray vs red chromatogram). **C**: Molar absorptivity absorption spectra of the purified reduction products.

Structural Assignment of Renalase Substrates. The unique absorption maxima of each borohydride reduction product were used to aid isolation of sufficient quantities by preparative HPLC for structural characterization. The mass of all reduction products was found to be 664.40±0.05, equal to the mass of the β-NADH control. The mass of the product formed from renalase activity was 662.40±0.00, equivalent to that of the β-NAD⁺ control. NMR spectra were recorded at 280 K in D_2O solvent. For each product, one-dimensional H^1 (1D), H^1 homonuclear correlation (COSY), H^1-C^{13} heteronuclear single quantum coherence (HSQC) and H^1-C^{13} heteronuclear multiple bond correlation (HMBC) spectra were obtained. Chemical shift and H^1 coupling assignments are included in Table 4.1. Figure 4.2 depicts the proton resonances assigned to the dihydronicotinamide rings of three products obtained

from borohydride reduction. In terms of homonuclear H^1 geminal and vicinal coupling, nicotinamide dinucleotides have four isolated sets of protons; those for the adenine and nicotinamide bases and two for the ribose moieties. Structural assignment of the nicotinamide bases therefore relies heavily on HMBC spectra to link the proton residing on the ribose anomeric carbon to the proximal N2 and N6 carbons and/or the protons residing on N2 and N6 to the anomeric carbon. These multi-bond heteronuclear couplings both orient the nicotinamide nuclear spin-system with respect to the ribose and also permit deconvolution of the individual ribose resonances that are then identified by sequential geminal homonuclear coupling. The pivotal geminal, vicinal homonuclear couplings and heteronuclear multiple bond couplings are indicated in Figure 4.2 by respective blue and red arrows. Correlations of this type were readily made for the 340 nm and 345 nm absorption maxima species, and these were assigned as 4- (β-NADH), and 6DHNAD respectively (Figure 4.2A & 4.2B). Note that the multiplet for the nicotinamide N5' proton of 6DHNAD is obscured by the residual water resonance and is instead depicted inset as the homonuclear coupling crosspeak to the N6' protons. The relative instability of the reduction product that exhibited the 394 nm absorption maximum precluded obtaining assignments by this approach. Control H^1 1D NMR spectra taken before and after two-dimensional heteronuclear spectra acquisition repeatedly indicated substantial degradation of the 394 nm species. As such the structural assignment of the 394 nm species as 2DHNAD is principally based on H^1 homonuclear couplings. For this species we observe a ~6-7 Hz geminal coupling for the N4' (d), N5'(m) and N6'(d) protons and a absence of geminal couplings in the resonances assigned to N2' protons that each exhibit only a vicinally coupled ~12 Hz doublet (Figure 4.2C, Table 4.1).

Table 4.1. NMR Chemical Shift Assignments for 2-, 4- and 6DHNAD.

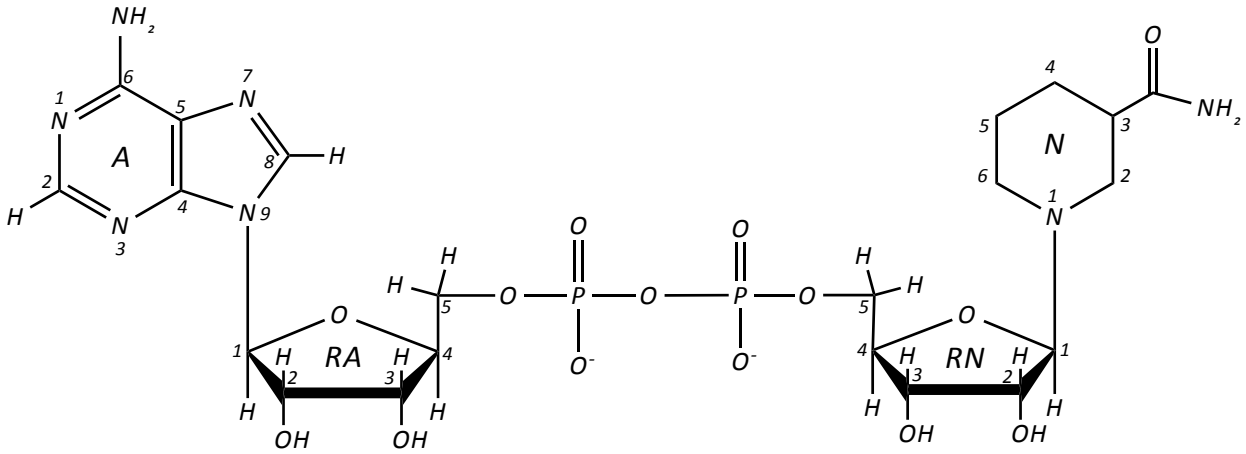

	β-NADH			6DHNAD			2DHNAD	
Position	^{1}H Shift (ppm)	multip.,J(Hz)	^{13}C Shift (ppm)	^{1}H Shift (ppm)	multip.,J(Hz)	^{13}C Shift (ppm)	^{1}HShift (ppm)	multip.,J (Hz)
N2	6.57	s	138.3	6.74	s	145.1	3.25 3.68	d, 12.4 d, 12.9
N4	2.38 2.22	dt,17.8, 2.2 dd, 18.4, 3.1	21.7	5.42	d	119.0	6.31	d, 6.1
N5	4.39	dd,	74.4	4.67	m*	112.6	4.45	t, 6.7
N6	5.61	d, 8.14	122.9	3.60 3.40	dd, 15.1, 2.9 dt, 15.1, 2.9	42.1	6.10	d, 7.1
R1 1	4.44	d, 7.48	94.7	4.51	d, 7.21	97.1	4.48	d, 7.48
R1 2	3.85	dd, 7.48, 6.73		3.98	dd, 7.26, 5.46	67.9	4.02	m, nm
R1 3	3.94	m	64.8	3.88	m	70.5	3.89	m, nm
R1 4	3.90	m	n/a	3.79	m	82.1	3.84	m
R1 5	3.766	m	65.8	3.74	m	65.6	3.62	m
R2 1	5.79	d, 5.4	86.6	5.78	d, 5.8	86.5	5.75	d, 5.7
R2 2	4.37	dd, 5.42, 5.16	74.4	4.41	dd, 5.39,5.99	74.2	4.38	t, 5.4
R2 3	4.17	dd, 5.16, 4.13	70.0	4.18	dd, 5.14, 3.58	70.0	4.17	m
R2 4	4.050	m, n/a	83.5	4.04	m	83.5	4.07	m
R2 5	3.90	dd,dd,	65.0	3.89	m	64.9	4.00	m
A2	7.87	s	152.3	7.88	s	152.3	7.89	s
A8	8.15	s	139.5	8.18	s	139.1	8.17	s

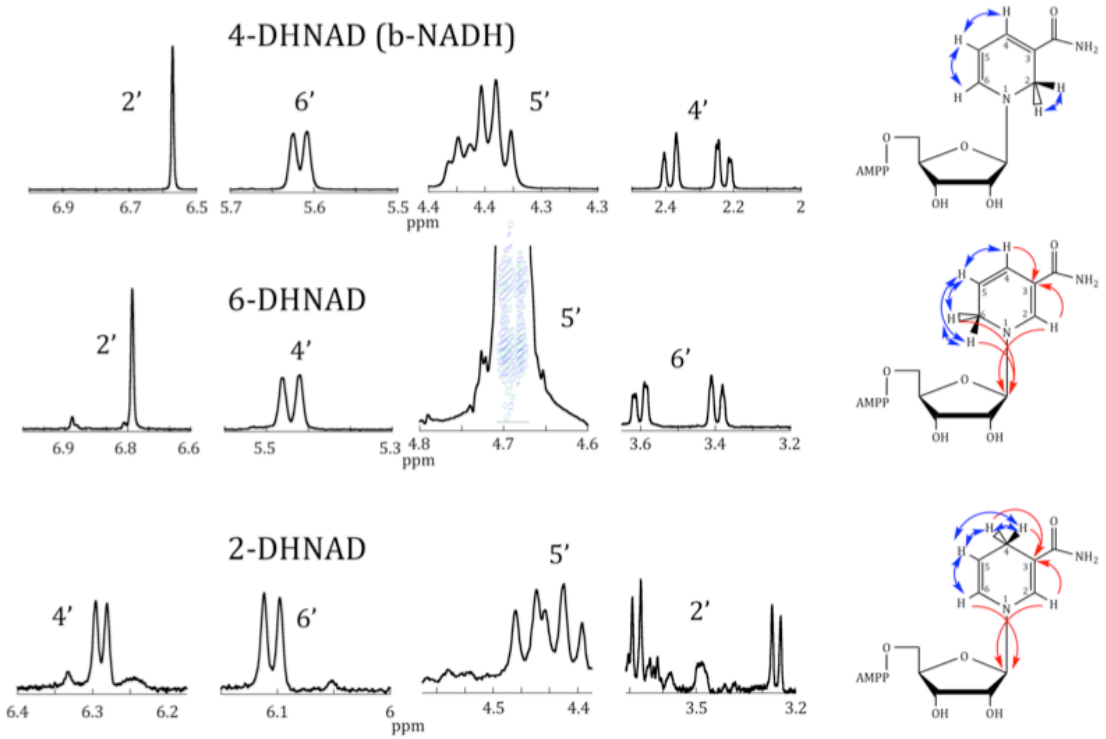

Figure 4.2. NMR Identification of the Purified Products of Sodium Borohydride reduction of β-NAD^+. Spectra were recorded at 280 K in deuterium oxide. Structures to the right depict the primary couplings used for identification of the β-NADH isomers. Blue arrows indicate homonuclear coupling, while red arrows indicate heteronuclear multi-bond coupling.

Renalase Reductive Half-Reaction. In prior work we published data for the reductive half-reaction of renalase (*54*). In these experiments the substrate was supplied to the enzyme in an apparent equilibrium mixture arising from aqueous speciation of β-NADPH (Scheme 4.3). As such the data obtained were not for a pure substrate molecule and included potential competitive inhibition effects from the β-NADPH background (see below). Here we show the reductive half-reactions for renalase with pure 2- and 6DHNAD. While 6DHNAD has sufficient stability to be purified and stored for use in such experiments,

2DHNAD does not and typically decomposes with a half-life of approximately 30 minutes. For this reason 2DHNAD was used immediately after preparative HPLC isolation and was limited to ~100 μM concentration by the capacity to resolve 2DHNAD from other reduction products with the preparative reverse-phase phenyl HPLC column used for purification. To observe reduction of the renalase flavin cofactor by 2- and 6DHNAD, anaerobic renalase (10 μM final) was mixed with varied concentrations of the anaerobic substrates. For 6DHNAD the range of substrate concentration used spanned approximate pseudo-first order reactant ratios (50-800 μM). The data obtained were thus fit to exponential decay(s) (Equation 4.1). Two phases were observed in the reduction traces. The first phase accounted for ~90% of the amplitude change and was indicative of flavin reduction. The rate constants for this phase (k_{1obs}) derived from fitting displayed a hyperbolic dependence that was fit to Equation 4.2 to derive the limiting rate constant for reduction from the asymptote (234 s^{-1}) and the dissociation constant for the Ren_{ox}•6DHNAD complex (173 μM). The rate constant for the second phase did not exhibit a 6DHNAD dependence, and was fit to ~20 s^{-1} in all traces. We propose that flavin reduction forms the Ren_{red}•β-NAD^+ complex whose flavin spectrum is altered by the proximity of the flavin and nicotinamide rings. This phase is thus tentatively assigned as the decay of the Ren_{red}•β-NAD^+ complex with the egress of β-NAD^+ from the active site. A complete mechanistic assignment of the reductive half-reaction is beyond the scope of this study.

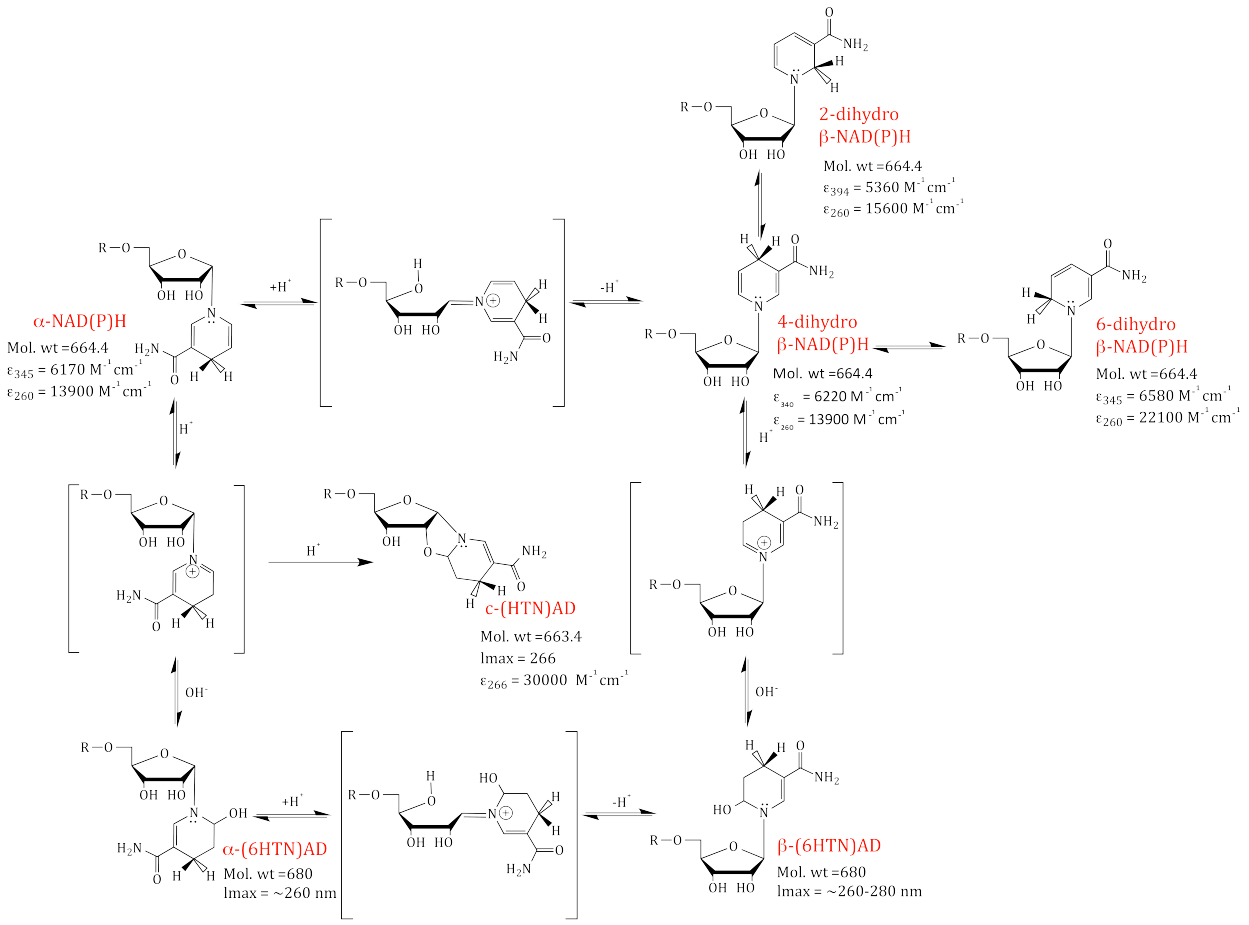

Scheme 4.3. Aquaeous speciation of nicotinamide dinucleotide species.

Our limited capacity to isolate and stabilize 2DHNAD dictated that the reductive half-reaction for renalase oxidizing this substrate was observed within a range of substrate concentrations that were second-order with respect to the enzyme concentration. As such the data obtained could only be analyzed by fitting the integrated rate expression for a more complete kinetic model as shown in Scheme 4.2. In this model the ratio of the β-NAD$^+$ dissociation and association rate constants (k_3:k_{-3}) was fixed to that defined by the dissociation constant for the Ren$_{ox}$•β-NAD$^+$ complex. This fitting restriction was based on our prior observation that the β-NAD$^+$ product does not modulate the reduction potential

of the flavin cofactor and therefore has equal affinity for the Ren_{ox} and Ren_{red} forms (see below) (*54*). In addition the reductive step (k_2) in which the hydride equivalent is transferred from 2DHNAD to the flavin was defined as irreversible in accord with the assumption that the difference in reduction potential of these two species is greater than 100 mV (ΔG>-20 kJ/mole). Lastly, the association rate constant for 2DHNAD (k_1) was confined as $\sim 10^8$ $M^{-1}s^{-1}$, close to the limit of diffusion. The fit obtained indicated a k_{red} for 2DHNAD of 860 s^{-1}, 3.6-fold faster than that measured for 6DHNAD but with a similar a dissociation constant of 166 μM.

Dissociation Constants for the Ren_{ox}•β-NADH and Ren_{ox}•β-NAD^+ Complexes. We propose that the metabolic function of renalase is to alleviate inhibition of primary metabolism by oxidizing isomers of β-NAD(P)H molecules that arise through tautomerization and/or non-specific reduction of β-NAD^+ (Scheme 4.4). As such renalase operates in an environment of near-isosteric non-substrate molecules such as β-NAD(P)H and β-$NAD(P)^+$ that are present in considerably higher concentration and presumably inhibitory. In order to gauge selectivity for 2- and 6DHNAD the dissociation constants for the Ren_{ox}•β-NADH and Ren_{ox}•β-NAD^+ complexes were measured using perturbation of the renalase flavin spectrum as physical evidence of association. These data fit well to a single site binding equation (Equation 4.3) and indicated that renalase is only three-fold selective against β-NADH ($K_{β\text{-NADH}}$ = 570±90 μM) (Figure 4.4A), but is 34-fold selective against β-NAD^+ ($K_{β\text{-NAD+}}$ = 5960±800 μM) (Figure 4B). Association of β-NADH induced new absorption transitions at

long wavelength indicative of charge-transfer presumably made possible by proximity of the dihydronicotinamide and flavin rings (*323*) (Figure 4.4A inset).

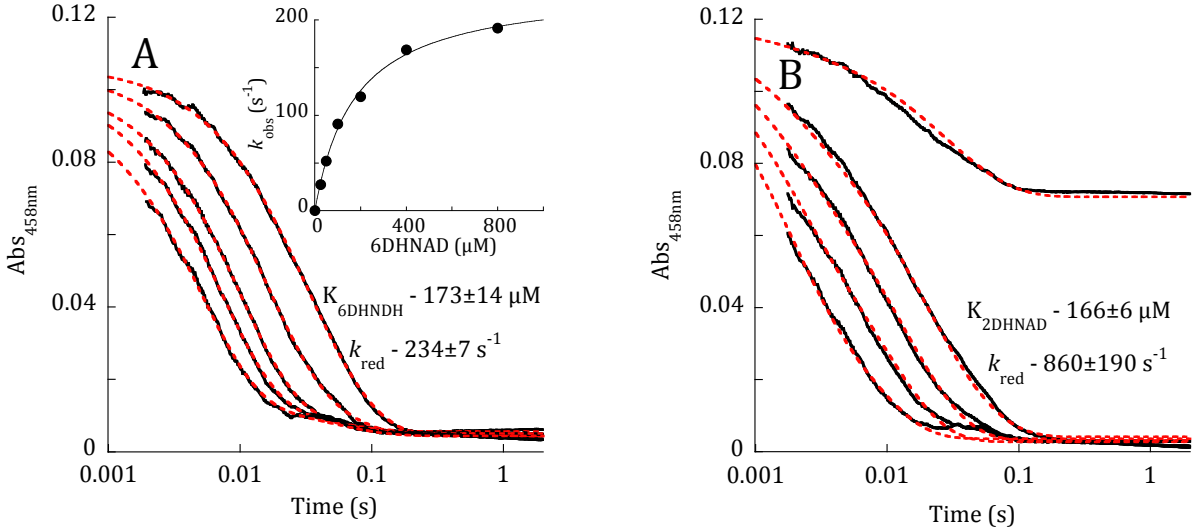

Figure 4.3. The Reductive Half-Reactions of Renalase with 2 & 6DHNAD**. A**: Reduction of the renalase cofactor (10 μM) in the presence of 6DHNAD. Traces shown are for 25, 50, 100, 200, 400, and 800 μM 6DHNAD. The data were fit (red dashed lines) to a linear combination of two exponential decays according to Equation 1. Inset shows the dependence of the observed rate constants on the concentration of 6DHNAD fit to Equation 4.2. **B**: Reduction of the renalase cofactor (10 μM) in the presence of 2DHNAD. Traces shown are for 3.7, 14.5, 21.3, 30.0, 43.5 μM 2DHNAD. These data were fit globally to the kinetic model depicted in Scheme 4.2.

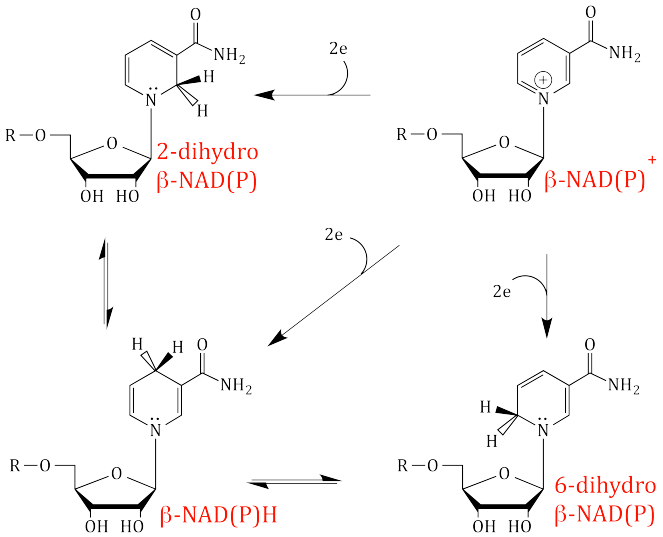

Scheme 4.4. Proposed metabolic function of renalase.

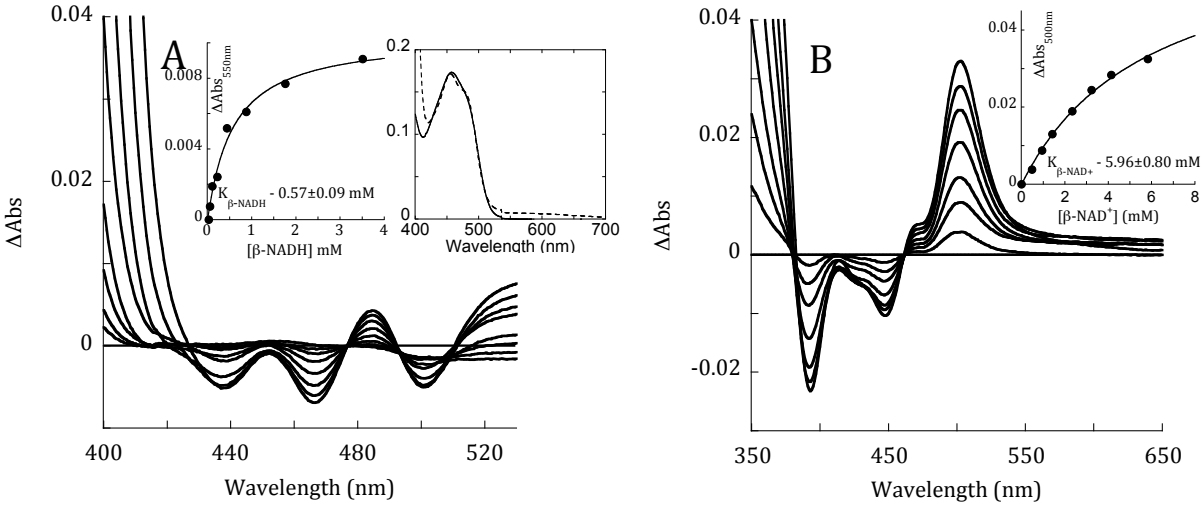

Figure 4.4. Measurement of the Dissociation Constants for the Ren_{ox}•β-NADH and Ren_{ox}•β-NAD+ Complexes. **A:** Difference absorption spectra for the renalase flavin at various concentrations of β-NADH. Inset (left) shows the charge transfer absorption band observed when 3.51 mM β-NADH was added (dashed line) to renalase. Inset(right) depicts the perturbation of the flavin spectrum at 550 nm as a function of β-NADH concentration fit to Equation 4.3. **B:** Difference absorption spectra for the renalase flavin at various concentrations of β-NAD^+. Inset depicts the perturbation of the flavin spectrum at 550 nm as a function of β-NADH concentration fit to Equation 4.3.

Dehydrogenase Inhibition. Lowry et al. and Dalziel reported that β-NADH preparations contained contaminants that were inhibitory to LDH (*67, 68*), and this observation has since been confirmed by numerous other authors (*66, 337-339*). In this study we measure K_i values for 2- and 6DHNAD to three dehydrogenase enzymes from primary metabolism. These data are summarized in Figure 4.5. Predictably, 6DHNAD inhibition was best fit to a competitive pattern with respect to β-NADH. The instability of 2DHNAD precluded categorization the inhibition pattern, though it can be reasonably assumed that 2DHNAD competes with β-NADH similarly. The data indicate that both 2- and 6DHNAD have high affinity for dehydrogenases and therefore pose a threat to primary metabolism. For *E. coli*

MDH, 6DHNAD has exceedingly high affinity (K_i = 34 ± 3 nM) while 2DHNAD has only modest inhibitory affinity for this enzyme (K_i = 3.05 ± 0.33 μM). LDH from rabbit muscle shows similar high affinity for both 2- and 6DHNAD (K_i ~ 500-600 nM). DLD is a β-NADH-dependent dehydrogenase component of both the pyruvate decarboxylase complex and the α-ketoglutarate decarboxylase complex. Curiously, this dehydrogenase does not appear to bind either 2- or 6DHNAD with significant affinity. Collectively these data establish a credible metabolic function for renalase; oxidation of NAD(P)H isomers that arise from tautomerization or non-specific reduction of β-NAD(P)$^+$ in order to alleviate stringent inhibition of essential dehydrogenase enzymes.

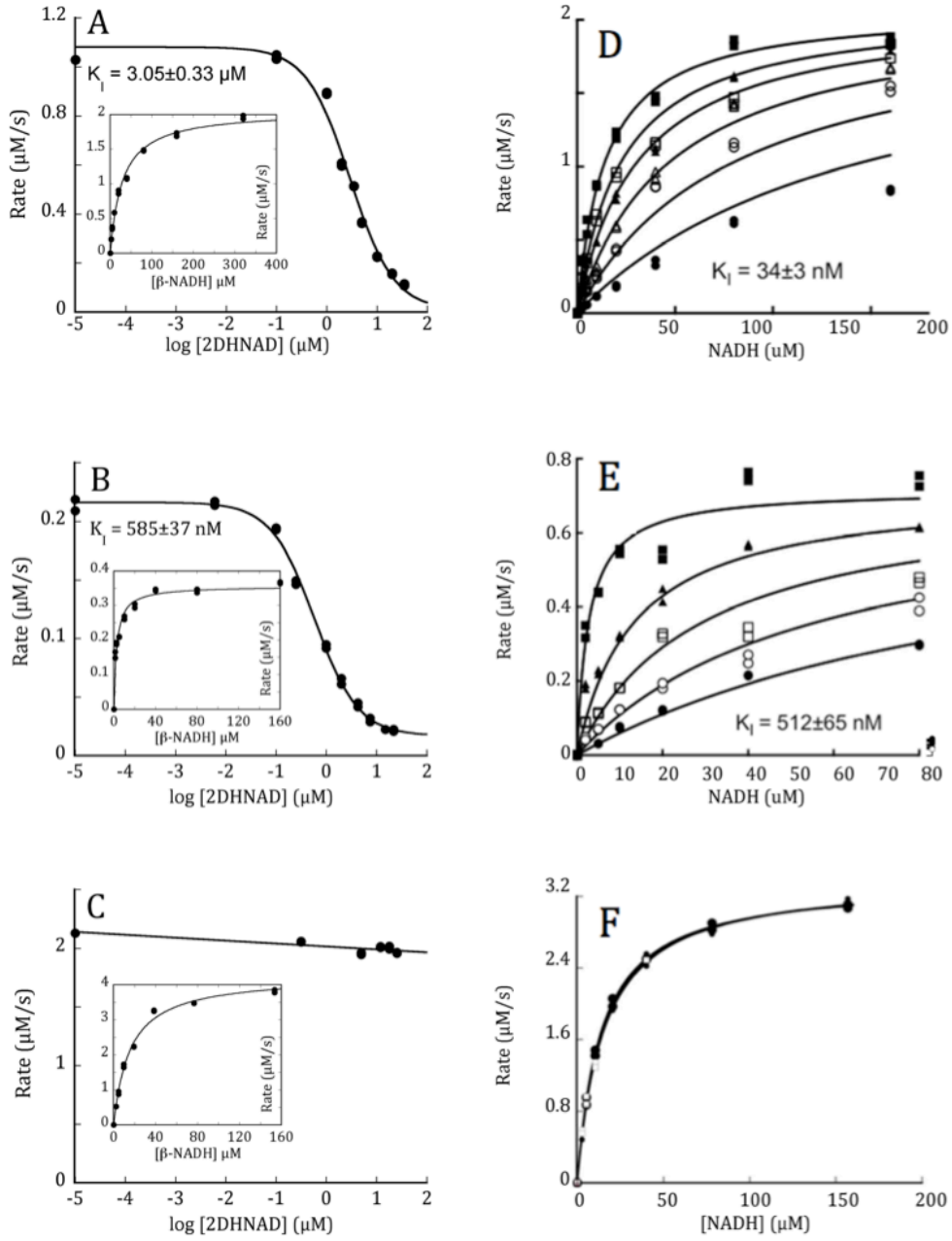

Figure 4.5. Inhibition of dehydrogenases from primary metabolism by 2- and 6DHNAD. Panels **A** and **D** depict evidence for the inhibition of E. coli malate dehydrogenase by 2DHNAD and 6DHNAD, respectively. In **D** the 6DHNAD concentrations used were 0, 20, 40, 80, 160, 320 nM. Panels **B** and **E** depict evidence for the inhibition of porcine heart lactate dehydrogenase by 2DHNAD and 6DHNAD. In panel **E** the 6DHNAD concentrations used were 0, 2, 5, 10, 20 μM. Panels C and F depict evidence for the absence of inhibition of rabbit muscle lipoamide dehydrogenase by 2DHNAD and 6DHNAD respectively.

Discussion

In this report we provide a credible thesis for the metabolic function of renalase. We assert that renalase oxidizes inhibitory isomers of β-NADH, forming β-NAD^+ and delivers the electrons harvested to dioxygen. We offer evidence for the structures of two substrate molecules that arise from non-specific reduction of β-NAD^+ and present an initial characterization of the kinetics of the reductive half-reaction observed with these substrates. This study also serves to correct our earlier erroneous claim that renalase oxidizes α-NADH molecules (*54, 319*). The data presented here indicate that the substrate molecule identified in prior work was not α-NAD(P)H but instead 6DHNAD(P), a species that has the same λmax (345 nm), ostensibly the same extinction coefficient and similar reported aqueous fractional accumulation at equilibrium (*309*).

In 1953 Mathews and Conn noted that the β-NADH prepared by borohydride reduction was only partially oxidized by LDH and proposed that in addition to β-NADH (4-DHNAD), 2-DHNAD and 6DHNAD were produced and that these forms were not able to react with enzymes (*340*). Later Chaykin and Meissner reported absorption spectra of the partially purified products of borohydride reduction and used tritium label elimination methods to establish the positions of reduction on the nicotinamide ring (*65*). A number of other studies have examined the properties of these non-specific reduction products (including a variety of misidentifications) (*63-66*), but it was Lowry et al. and Dalziel who first reported that β-NADH preparations contained contaminants that were inhibitory to LDH. Soon after, Godtfredsen and Ottesen described 6DHNAD as a humidity-induced lactate dehydrogenase inhibitor that arises in NADH powder (*339, 341*). Together, these and

numerous other studies establish that lactate dehydrogenase inhibitors arise by non-specific reduction of β-NAD^+ and/or via tautomerization of β-NADH (Scheme 4.3). The activity we have observed for renalase suggests that non-enzymatic redox and/or proton-movement mediated intercoversion of NAD(P)+/NAD(P)H isomers is also an *in vivo* phenomenon that suppresses primary metabolism.

We also show that renalase catalytically oxidizes both known isomeric forms of the β-NAD(P)H nicotinamide ring. Positionally, the 2 and 6 carbons of the nicotinamide ring are equivalent if the base is allowed to pivot about the glycosidic bond. This suggests that the nicotinamide amide substituent can be accommodated in two locations within the renalase active site and in these two binding modes the substrates are otherwise conformationally equivalent. Two orientations for the nicotinamide base implies there are also two binding modes for β-NAD(P)H and for β-$NAD(P)^+$ and that the dissociation constant measured for these molecules is an average of both binding modes. Moreover, it also follows that up to half of the binding events for 2- and 6DHNAD result in inhibitory complexes that cannot transfer the hydride equivalent to the renalase flavin; that we do not observe any inhibitory delay in the reductive half reaction suggests that binding and release of 2- and 6DHNAD from Ren_{ox} is rapid.

In prior studies we observed the reductive half-reaction of renalase by mixing the enzyme with an apparent equilibrium mixture of β-NADH and 6DHNAD (*54*). Here we use pure preparations of 2DHNAD and 6DHNAD to show that the rate constant for reduction is dramatically more rapid than previously reported. We observe rate constants for flavin reduction of 230 s^{-1} for 6DHNAD and 860 s^{-1} for 2DHNAD as opposed to ~40 s^{-1} observed

with the equilibrium mixture. We also show that renalase has only a modest ability to distinguish between the 2-, 4- and 6DHNAD molecules (Figure 4.3 & 4.4) as β-NADH (4DHNAD) binds to renalase forming a complex with a dissociation constant of ~600 μM, only ~3.5-fold weaker than that observed for 2- and 6DHNAD. However, renalase has a considerably greater capacity to distinguish between its substrates and β-NAD(P)$^+$ molecules, the renalase complex(es) of which has an order of magnitude higher dissociation constant (Figure 4.4B)(*54*). As such the relative high background of β-NAD(P)H and β-NAD(P)$^+$ in the cellular environment will populate and inhibit renalase to some extent. Given the ostensibly isosteric form of all three reduced isomers it is not unexpected that β-NAD(P)H would compete for access to the renalase active site. The apparent lack of β-NAD(P)H isomer binding stringency is only a limitation to the extent that 2- and 6DHNAD accumulate *in vivo*. The considerable driving force for the renalase reaction derived from the reduction of dioxygen provides a rather unrelenting capacity to scavenge these substrates. Provided renalase activity can scavenge both isomers at a rate that meets or exceeds their formation, its metabolic contribution is sufficient.

We have assessed the interaction of 2- and 6DHNAD with three dehydrogenases from primary metabolic pathways. 2- and 6DHNAD presumably act as inhibitors of these enzymes as they are highly similar in shape and electrostatic character to β-NADH, yet cannot associate in a manner that permits hydride transfer. These data indicate that both MDH and LDH are subject to inhibition by both 2- and 6DHNAD while DLD is not. Given the structural similarity of 2-, 4- and 6DHNAD it is interesting that DLD can select only the 4-

dihydro isomer while renalase, the enzyme apparently destined to rid the cell of 2- and 6DHNAD, cannot. The inhibition of MDH by 6DHNAD is an order of magnitude more potent suggesting that this interaction is the principal threat to primary metabolism from β-NAD(P)H isomers. While the *in vivo* concentrations of 2- and 6DHNAD are not known, such high affinity would suggest that, in the absence of renalase, even minute accumulations of 6DHNAD would undermine primary energy pathways. While, 2-DHNAD is much less stable than 6DHNAD, on a molecular timescale its half-life is more than sufficient to expect that it will also exert an influence over key dehydrogenase enzymes. The extent of the threat these molecules pose is likely to be organism specific and it cannot yet be stated that dehydrogenase inhibition of this type is a universal phenomenon. That porcine DLD is not inhibited by either 2- or 6DHNAD indicates that binding selectivity for these three forms of reduced β-NADH is possible. However, renalase is found throughout the *animalia* implying that key dehydrogenases found within all organisms of this kingdom, such as rabbit LDH shown here, are subject to inhibition by β-NADH isomers.

As stated, in prior work we mistakenly proposed that α-NAD(P)H anomers were substrates for renalase. It now seems appropriate to graft our earlier mechanistic observations with the data obtained in this study using pure 2- and 6DHNAD. Scheme 4.5 depicts the proposed mechanism for renalase based on prior and current observations. For simplicity this scheme depicts only the catalytic cycle for the 6DHNAD substrate though it is assumed that catalysis in the presence of 2DHNAD differs only in the position of the nicotinamide amide substituent (meta with respect to the position depicted). In this catalytic cycle 6DHNAD associates rapidly with a dissociation constant for the Ren_{ox}•β-

6DHNAD(P) complex of 170 μM. The nicotinamide locates in the active site such that the ortho positions with respect to the dihydropyridyl nitrogen are adjacent to the flavin N5 and oriented for conventional hydride transfer. Reduction of the flavin forms the Ren_{red}• β-$NAD(P)^+$ complex. Our prior studies indicated that the reoxidation of this complex occurs by a bimolecular reaction with dioxygen with a rate constant of $2.9x10^3$ $M^{-1}s^{-1}$ that forms hydrogen peroxide and is fully rate determining under conditions of normal mammalian physiological oxygen concentration (~ 140 μM) (*54*). The rate constant for reoxidation was not influenced by the addition of exogenous β-$NAD(P)^+$ indicating that the reaction with dioxygen is neither contingent on nor influenced by the release of β-$NAD(P)^+$. Consistent with this observation was that the reduction potential of the renalase flavin is the same within error for the unliganded oxidized enzyme and the Ren_{red}•β-$NAD(P)^+$ complex(*54*). As such the reoxidation/product release phase of catalysis is represented as random, but is kinetically ordered by the fact that β-$NAD(P)^+$ is released somewhat more rapidly (20 s^{-1}) than the reaction of the reduced enzyme with dioxygen under physiological conditions (0.4 s^{-1}).

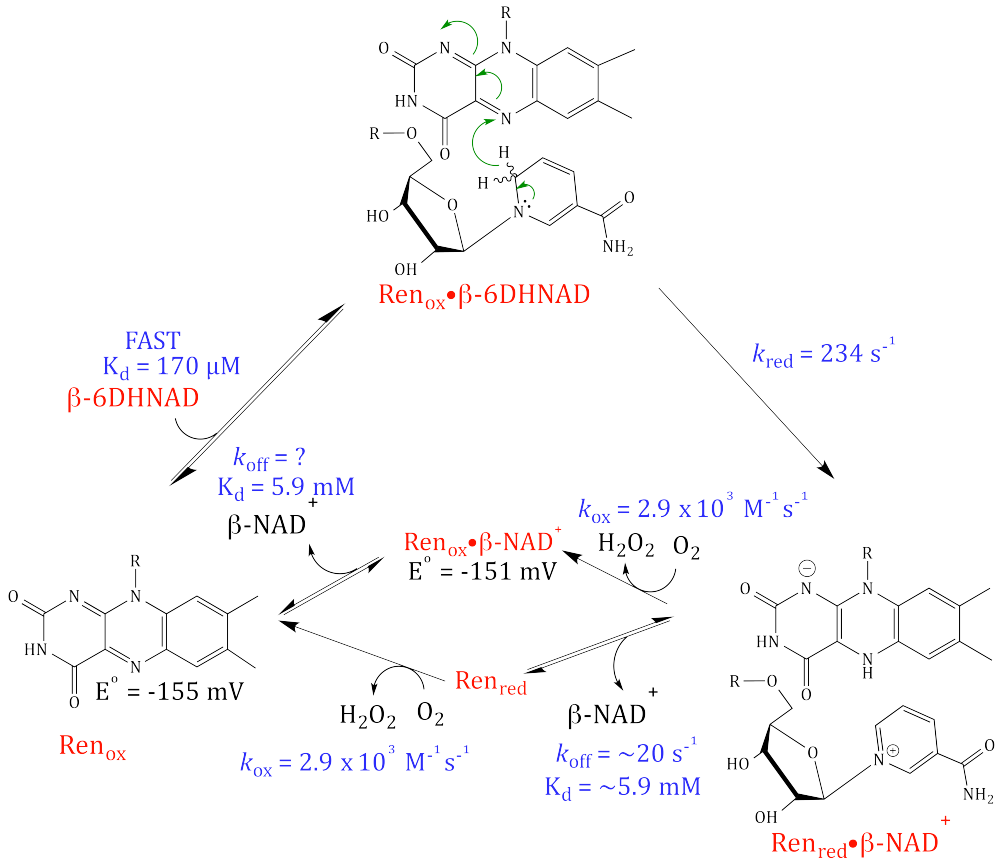

Scheme 4.5. The catalytic cycle of HsRen.

The number and breadth of physiological observations associated with renalase is expanding in an exponential manner. In addition to being linked to the control of blood pressure and heart rate(*1, 6*), renalase has also been associated with renal dopamine and phosphate metabolism (*24, 25*), diabetes (*15, 330, 342*), and amelioration of myocardial damage (*4*). Our earlier conclusions were based on recycling of α-anomers of NAD(P)H molecules and could not be linked to any known endocrine or other physiological role for renalase. While we make no attempt here to connect our current data to specific physiological responses, it does seem that the threat to normal primary metabolism posed

by β-NAD(P)H isomers does allow for renalase deficiencies to manifest as physiological abnormalities, in particular those associated with local ischemia.

CHAPTER V
Renalase Does Not Catalyze the Oxidation of Catacholamines

Brett A. Beaupre, Matthew R. Hoag and Graham R. Moran

Abstract

It is widely accepted that the function of human renalase is to oxidize catecholamines in blood. However, this belief is based on experiments that did not account for slow, facile catecholamine autoxidation reactions. Recent evidence has shown that renalase has substrates with which it reacts rapidly. The reaction catalyzed defines renalase is an oxidase, one that harvests two electrons from either 2-dihydroNAD(P) or 6-dihydroNAD(P) to form β-NAD(P)$^+$ and hydrogen peroxide. The apparent metabolic purpose of such a reaction is to avoid inhibition of primary dehydrogenase enzymes by these β-NAD(P)H isomers. This article demonstrates that renalase does not catalyze the oxidation of neurotransmitter catecholamines. Using high-performance liquid chromatography we show that there is no evidence of consumption of epinephrine by renalase. Using time-dependent spectrophotometry we show that the renalase FAD cofactor spectrum is unresponsive to added catecholamines, that adrenochromes are not observed to accumulate in the presence of renalase and that the kinetics of single turnover reactions with 6-dihydroNAD are unaltered by the addition of catecholamines. Lastly we show using an oxygen electrode assay that plasma renalase activity is below the level of detection and only when exogenous renalase and 6-dihydroNAD are added can dioxygen be observed to be consumed.

Introduction.

Renalase is widely defined to be a kidney-derived flavoprotein enzyme/hormone whose function is to oxidize circulating catecholamines in order to lower blood pressure and slow the rate of contraction of the heart (*1, 5, 6, 8, 10-12*). The initial basis of this claim for renalase activity was an exceedingly small accumulation of hydrogen peroxide in the presence of common neurotransmitter catecholamines when assayed using a generic Amplex Red-based oxidase assay. However, in these initial experiments no account, in the form of a control reaction, was made for background autoxidation (*1, 2, 5, 11, 36*). Catecholamines are prone to oxidation in the presence of dioxygen due to their capacity to form semiquinones (*343*). The superoxide ion that results rapidly disproportionates to dioxygen and hydrogen peroxide providing a steady non-enzymatic background signal for an Amplex Red assay (Scheme 5.1). The very low level of H_2O_2 production was subsequently rationalized by proposing that renalase is isolated in a quiescent state that can only be activated in blood in the presence of specific catecholamine neurotransmitters (*11, 36*). The chemical transformation ultimately claimed for renalase was that oxidized and cyclized aminochrome molecules were the native products and that the reaction was somewhat faster in the presence of NAD(P)H (*36*). However, even in these latter studies, no control was made for the addition of the catecholamine or the reductant, despite that NAD(P)H would greatly increase the complexity of the assay by increasing the number of non-enzymatic redox reactions that yield H_2O_2 (Scheme 5.1). That no control reactions were used to support any of the early catalytic claims emphasizes the overall tenuous foundation on which renalase catecholamine oxidase activity is based.

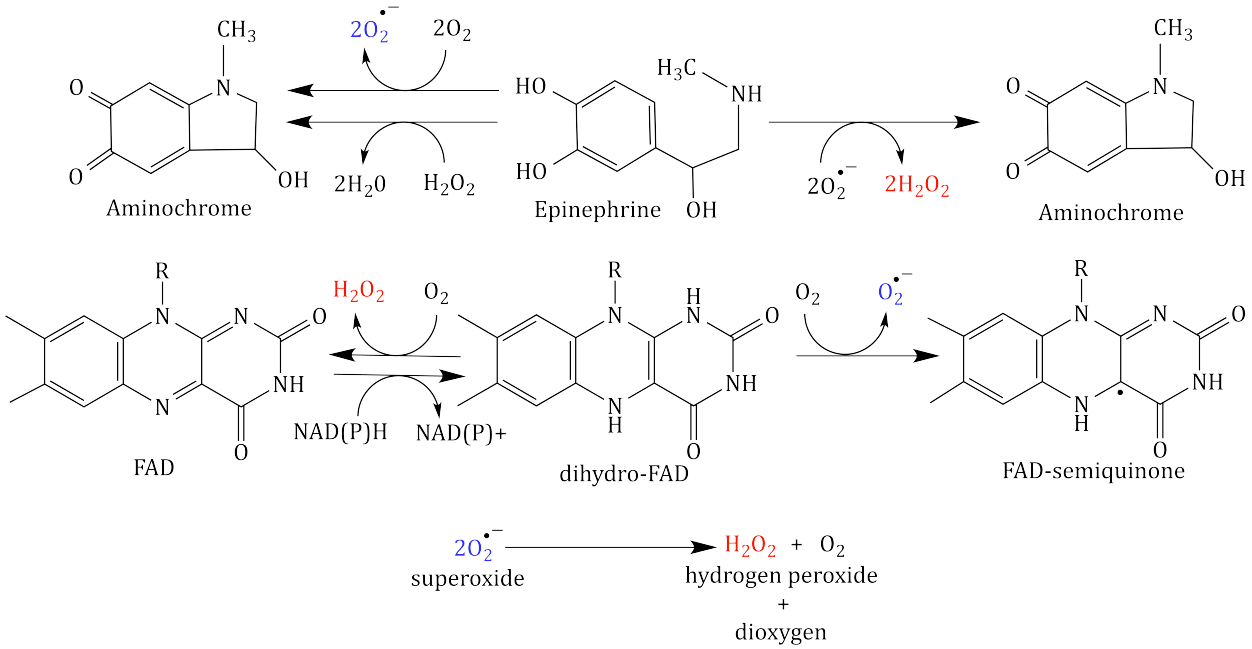

Scheme 5.1. Non-enzymatic redox reations in renalase catecholamine oxidase assays.

Boomsma and Tipton were first to register well-reasoned skepticism concerning a catecholamine oxidase role for renalase (*48*) and were joined by others expressing similar dissent and eventually direct experimental refutation was presented by Pandini et al. (*20, 51, 59*). However, the flawed initial *in vitro* evidence and counter evidence have been insufficient to quell the passive consensus that the function of renalase is to oxidatively consume catecholamine neurotransmitters from blood. Consequently, the early claims for catecholamine oxidase activity continue to be adduced and correlated with a wide variety of physiological measurements (*2-29, 31, 37, 39, 332*).

We recently demonstrated that 2-dihydroNAD (2DHNAD(P)) and 6-dihydroNAD(P) (6DHNAD(P)), both isomers of β-NAD(P)H (4DHNAD(P)), rapidly reduce the FAD coenzyme of renalase (230 s^{-1} for 6DHNAD, 850 s^{-1} for 2DHNAD) and in doing so become oxidized to β-NAD(P)$^+$. The reduced enzyme then reoxidizes by reducing molecular oxygen

to H_2O_2 (2.9 x 10^3 $M^{-1}s^{-1}$) (Scheme 5.2). Moreover, this genuinely catalytic reaction has an apparent metabolic purpose, as both 2DHNAD and 6DHNAD that are inhibitory to primary metabolism dehydrogenases (*55, 339*). The fundamental purpose of this study is corrective; using a verifiably active form of renalase, we demonstrate that no catalytic link exits between renalase and catecholamine oxidation. We show also that renalase it is not activated by blood plasma nor is, what we surmise to be, the native activity influenced by the presence catecholamines.

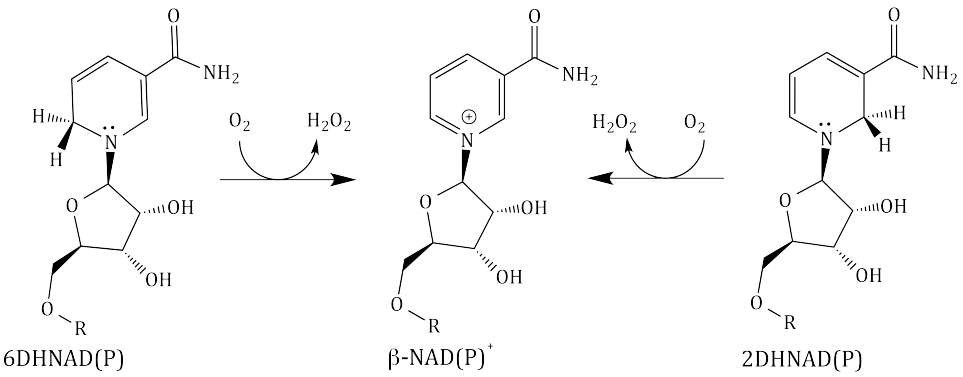

Scheme 5.2. Proposed native catalytic chemistry of renalase.

Materials and Methods.

Materials. Potassium phosphate, L-DOPA, epinephrine hydrochloride, and sodium chloride were obtained from ACROS. Dopamine hydrochloride was purchased from Alfa Aesar. Renalase was expressed and purified according to our previously published methods(*319*). β-NADH (disodium salt, trihydrate) was obtained from Amresco; β-NAD^+ was purchased from Sigma. 6DHNAD was prepared by reduction of β-NAD^+ as previously described (*55*). Human blood plasma was a gift from Dr. Julie A. Oliver (Biological Sciences Department-Univeristy of Wisconsin-Milwaukee). Freshly drawn blood was treated with 10 U/mL

heparin (Sagent Pharmaceuticals) to inhibit clotting. The sample was centrifuged at 2,200 rpm until blood cell pellet was formed (~15 minutes). The plasma was separated from the blood cell pellet and hematocrit and stored on ice until needed. Plasma samples were collected, purified, diluted (50% PBS), and used in experiments within 3 hours.

HPLC Product Analysis: In order to demonstrate the extent to which epinephrine, the catecholamine most often claimed or accepted as a substrate for renalase (*1, 3, 6, 10, 11*), is consumed by renalase, a mixture of β-NADH (50 μM) and epinephrine (150 μM) was prepared in PBS buffer at 25 ^{o}C. The sample was then divided into two and renalase (9 μM final) was added to one while the other served the role of a sample age control. A second set of mixtures were prepared in an identical manner, but FAD (9 μM final) was added in place of renalase. All samples were incubated for 10 minutes prior to ultrafiltration using a 0.5 mL Amicon 10 KDa centrifugal filter (removing renalase from the mixture). 50 μL of each filtrate was then chromatographed by HPLC using a Xterra C18 reversed phase column (4.6 x 150 mm, 3.5 μM particle size) run isocratically at 0.4 ml/min in 10 mM potassium phosphate pH 7.5 coupled to a 600 E HPLC pump and Waters 2487 dual wavelength detector (260nm and 340nm). Components eluting from the HPLC column were identified by their characteristic retention time compared to authentic compounds. The chromatograms derived from the renalase and FAD samples were corrected for the minor dilution that occurred with the addition of these components.

Spectrophotometric Evidence of Neurotransmitter Oxidation: Reactions were performed to assess the rates of autoxidation of catecholamines in the presence of renalase (or FAD control) when incubated with a reductant (β-NADH or 6DHNAD). Renalase was prepared

by dilution to 40 μM in 2x PBS buffer and mounted onto a onto a Hitech-DX2 (now TgK) stopped-flow spectrophotometer instrument. Reaction mixtures in which renalase (or FAD control) was combined with 100 μM catecholamine (epinephrine, dopamine or L-DOPA) and 15 μM β-NADH (or 6DHNAD control) in water were observed at 458 nm which allows observation of both the FAD redox state and the formation of aminochrome species (lmax~480 nm). All solutions were equilibrated with atmosphere at 25 ^{o}C and contained ~250 μM dioxygen.

To assess if catecholamine neurotransmitters (epinephrine, dopamine and L-DOPA) modulate the catalytic behavior of renalase, single turnover reactions with 6DHNAD were performed in the presence and absence of catecholamines with atmospheric dioxygen (~250 μM). Under these conditions the reduction and subsequent reoxidation of the renalase flavin coenzyme can be clearly observed. A native substrate solution, 6DHNAD (30 μM), was prepared in H_2O. This solution was mounted onto the stopped-flow spectrophotometer and mixed with the renalase (40 μM) sample described above and the turnover was observed at 458 nm, the visible absorption maximum for the FAD coenzyme bound to the enzyme. To determine if catecholamine neurotransmitters modulate the turnover of renalase, 200 μM of epinephrine, dopamine or L-DOPA was added to the 6DHNAD solution before mixing.

Dioxygen Consumption to Assess Renalase Activity in Blood and the Affect of Preincubation: In order to establish the constitutive level of renalase activity in human blood and the effect of preincubation with plasma and/or epinephrine as compared to PBS buffer control, a variety of assays were monitored by dioxygen consumption. Reactions were observed

using a Hansatech Oxygraph oxygen electrode and all reaction components were pre-equilibrated with atmospheric dioxygen (~250 μM) at 25°C. Reactants were added to the following final concentrations: 50% human blood plasma (diluted in PBS buffer), 10 μM epinephrine, 500 nM renalase and 30 μM 6DHNAD. Each assay was initiated by the addition of 6DHNAD, following either a 5 minute or 20 minute preincubation and then observed for an additional 700 seconds.

Results.

HPLC Product Analysis: Renalase is claimed to consume neuroactive catecholamines, chiefly epinephrine, in order to lower blood pressure(*36*). To demonstrate the extent to which verified active renalase can consume epinephrine in the presence of β-NADH, standardized HPLC chromatograms were collected and compared to controls that contained FAD in place of renalase (Figure 5.1). 150 μM Epinephrine was combined with 50 μM β-NADH (that has a β-NAD^+ impurity). The sample was divided into two and renalase added to one. Both samples were then incubated for 10 minutes (Figure 5.1A). Two similar mixtures were prepared as controls but with FAD substituted for renalase (Figure 5.1B). Analysis of the chromatograms showed that no significant consumption of epinephrine could be observed in the 10-minute window of the incubation. The renalase sample did show significant loss of β-NADH (11 μM) that was not entirely accounted for by a gain in the β-NAD^+ peak area (2 μM). This fraction of the β-NADH was accounted for by the modest dissociation constant for Ren_{ox}•β-NADH complex (K_d~600 μM) and the ~20-fold increase in the renalase concentration (180 μM) during filtration that together predict the 11 μM retention. (*55*). The FAD control chromatograms indicate no non-enzymatic chemistry has occurred within the 10 minute incubation window. Together these data definitively show that the

consumption of epinephrine cannot be detected in the presence of high concentrations (9 μM) of fully active renalase.

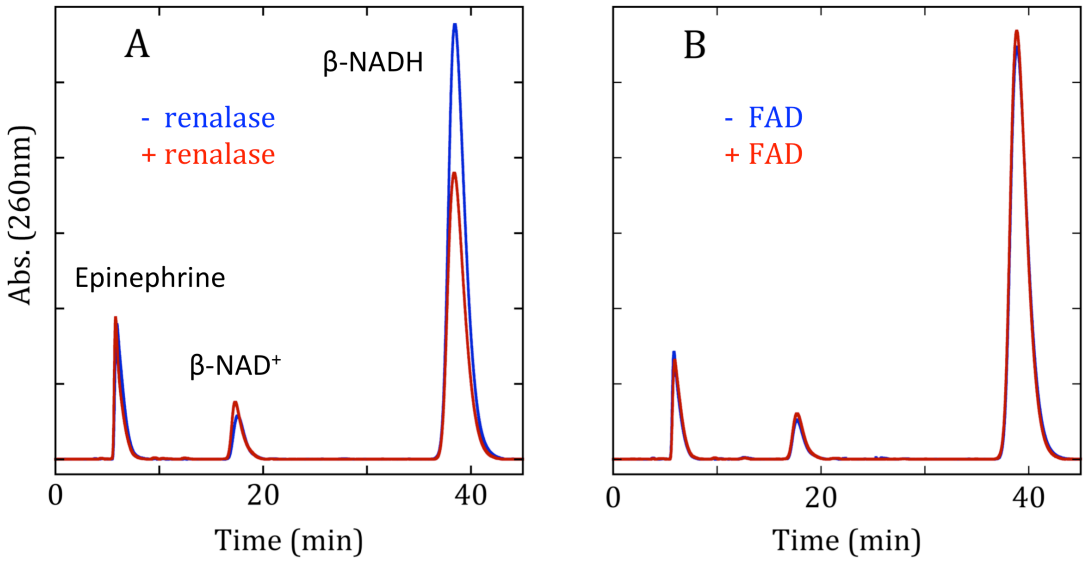

Figure 5.1. HPLC analysis of oxidation of epinephrine to adrenochrome by renalase. **A&B** were separated using a Xterra reverse phased C18 run isocratically in 10 mM Kpi, pH 7.5 and monitored at 260 nm. **A:** The blue line represents the mixture of 150 µM epinephrine and 50 µM β-NADH (4DHNAD) in PBS buffer at 25°C before the addition of 9 µM renalase and the red trace was taken after the addition of 9 µM renalase and incubation for 10 minutes at 25°C; renalase was removed from the sample by centrifugal (Amicon) ultra-filtration prior to injection. **B:** The reaction described in A was repeated except FAD was substituted for renalase.

Spectrophotometric Evidence of Neurotransmitter Oxidation: Renalase has been reported to oxidize catecholamines to aminochromes (Scheme 5.1)(*2*). It has also been proposed that catecholamines modulate the redox activity of renalase to the extent that the enzyme is largely inactive in the absence of epinephrine (*36*). In order to show the capacity of renalase to oxidize catecholamines to form aminochromes, two sets of reactions were performed one in the presence and one in the absence of renalase. Aminochromes are the oxidized and cyclized forms of catecholamines that have a puce color as a result of a broad absorption centered around 480 nm (ε_{480} ~4020 $M^{-1}cm^{-1}$) which provides a simple physical signal to observe their accumulation in solution. The absorption peak of aminochromes is

sufficiently broad that at 458 nm, the wavelength of observation used, the extinction coefficient is only 2% lower, permitting simultaneously assessment of the FAD coenzyme and the catecholamine oxidation/cyclization. Three common neuroactive catecholamines were mixed with reductant (β-NADH or 6DHNAD) and renalase (20 μM final) or FAD (20 μM final). In the first control β-NADH was combined with epinephrine, L-DOPA, or dopamine and subsequently mixed with renalase to determine if renalase could enhance the rate of oxidation of the catechols to their associated aminochromes in the presence of NADH. No change in absorbance was observed indicating that renalase does not promote the oxidation and cyclization catecholamines. As a control, FAD was substituted for renalase and the above experiment repeated. This data showed small accumulations of absorption (epinephrine, 0.0035; DOPA, 0.015; L-DOPA, 0.0025) equating to ~ 1-3 μM aminochrome after 300 seconds, indicating that a mixture of β-NADH and free FAD can enhance the rate of catecholamine autoxidation and that renalase actually provides some degree of protection from this chemistry presumably as a result of the active site flavin being inherently unreactive with β-NAD(P)H molecules in order to avoid wasteful diaphorase activity.

In our previous work we have demonstrated that renalase catalyzes rapid oxidation of 6DHNAD(P) and 2DHNAD(P) to β-NAD(P)$^+$ where a hydride equivalent is transfered from the nicotinamide base to the renalase flavin coenzyme that then reoxidizes by reducing dioxygen to form hydrogen peroxide (Scheme 5.2) (*54, 55, 319*). In order to show the extent of the influence of catecholamines on the kinetics of this chemistry, reduction and reoxidaton of the renalase flavin coenzyme that occurs in single turnover with 6DHNAD was observed at 458 nm (Figure 5.2B). The data obtained indicate that neither

epinephrine, L-DOPA, or dopamine have influence on the catalytic behavior of renalase. The FAD, 6DHNAD (± catecholamines) control for the single turnover reactions where ostensibly the same as those for FAD, β-NADH and catecholamine in Figure 5.1A (data not shown).

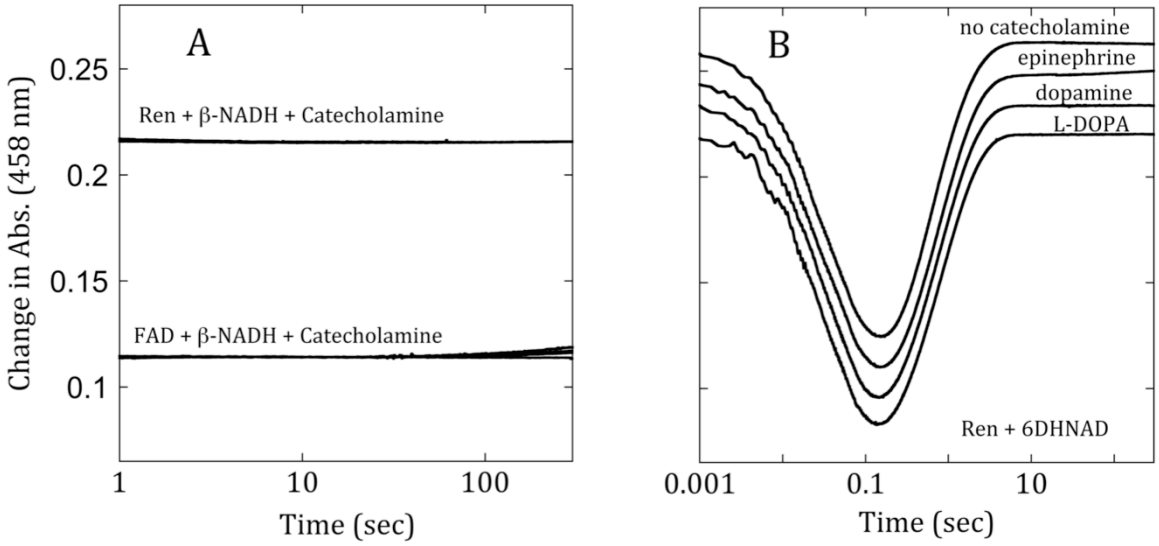

Figure 5.2. Catalytic turnover of renalase in the presence of neurotransmitters. **A&B:** Renalase single turnover(B) and control(A) stopped-flow spectrophotometer traces were observed at 458 nm for 200 sec. **A:** The extent of auto-oxidation of epinephrine was monitored; *top*, stopped-flow spectrophotometer trace of 20 μM renalase with 15 μM β-NADH(4DHNAD) in the absence and presence of 100 μM catecholamine of interest (epinephrine, DOPA, L-DOPA); *bottom;* stopped-flow spectrophotometer trace of 20 μM FAD with 15 μM β-NADH(4DHNAD) and 100 μM of catecholamine of interest (epinephrine, DOPA, L-DOPA). **B:** Single turnover of 20 μM renalase with 15 μM 6DHNAD in the absence and presence of 100 μM catecholamine of interest (epinephrine, DOPA, L-DOPA).

Dioxygen Consumption to Assess Renalase Activity in Blood and the Affect of Preincubation: There are three near constant elements in all scientific articles that pertain to renalase; all claims for activity involve the reduction of dissolved dioxygen, most report or cite that

catecholamines are substrates and the majority pivot their investigations on the role of renalase in blood(*51, 52*). Moroever, the low *in vitro* catecholamine oxidase activity has been claimed to be a consequence of a "prorenalase" form that is largely inactive when separated from some unidentified activator (*2, 11*). Given that renalase oxidizes 2- and 6DHNAD(P)(*55*), does renalase exhibit modified catalytic behavior in blood? In order to demonstrate the effects of preincubation with catecholamine and/or blood plasma we conducted a series of assays using an oxygen electrode (Figure 5.3). All assays had 6DHNAD added either after a short (5 min) or long (20 min) preincubation.

In Figure 5.3, assays 1 & 6, we see that epinephrine is slow to oxidize and does not promote significant consumption of dioxygen prior to or after the addition of 6DHNAD. In addition, assays 1 & 5 indicate that the basal level of renalase activity in blood is sufficiently low to be below the sensitivity of these methods. Using antibody detection, Zbroch et al. determined that the concentration of renalase in plasma was 4 μg/mL (100 nM) (*25*) approximately one fifth of the exogenous concentration added in assays 2, 3, 4, 7, 8 & 9. That each of these traces show marked dioxygen consumption with added renalase and those without show no dioxygen consumption (assays 1 & 5) suggests that there is very little renalase in blood or that the majority of it is inactive. Comparison of assays 2 & 4 to assays 7 & 9 indicates that preincubation of renalase in plasma does not alter its behavior. Both sets of assays indicate linear consumption of dioxygen that is equimolar to the amount of 6DHNAD added and then cessation of activity. Assays 2, 3 & 4 show recovery of approximately half the dioxygen consumed in the renalase catalytic phase presumably as a consequence of catalase activity in the plasma. Contrary to claims that epinephrine activates renalase (*36*), neither assay 1 or 6, those preincubated with epinephrine in

plasma and PBS respectively, show any evidence of activity, strongly suggesting that the circulating catecholamine does not activate a quiescent form of renalase.

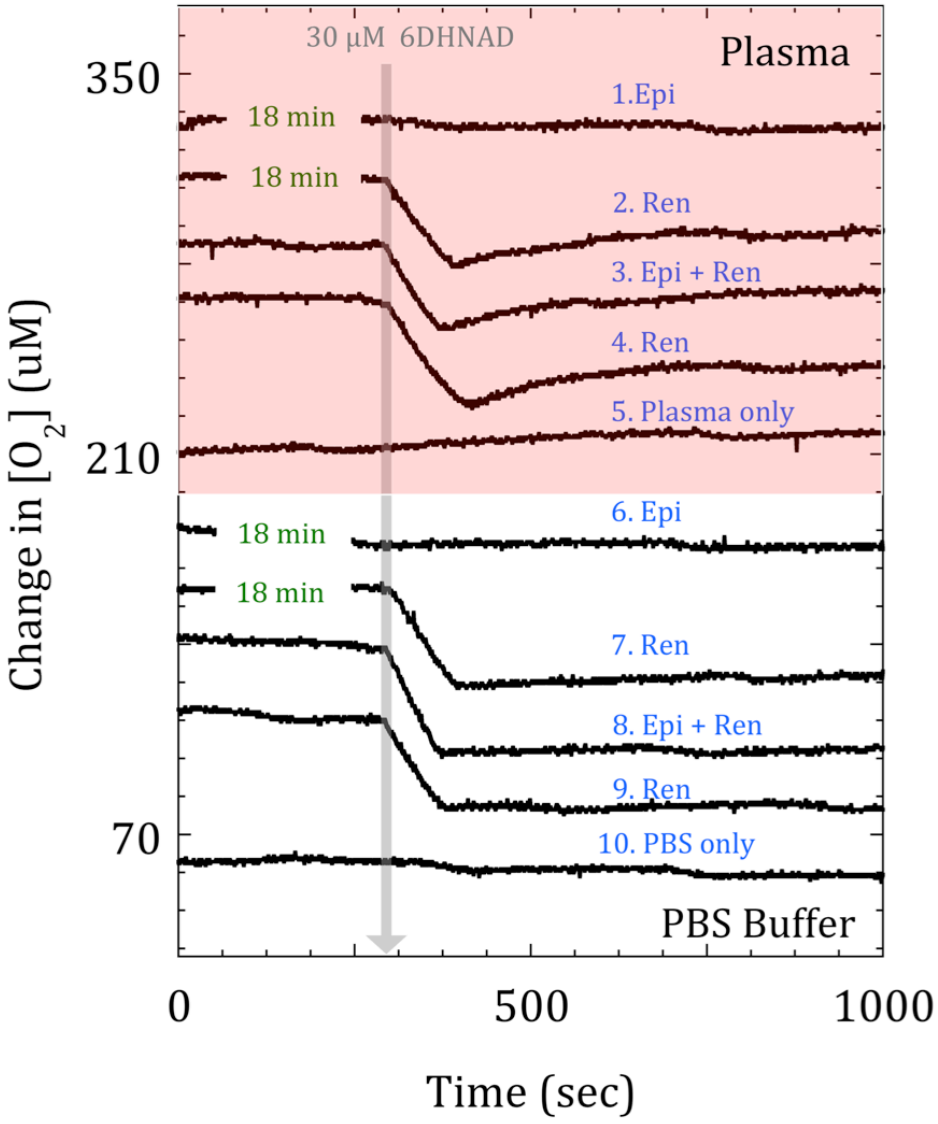

Figure 5.3. The Effect of Catecholamine and Plasma Preincubation. Renalase activity in 50% blood plasma and PBS buffer was determined by monitoring dioxygen consumption. Reactions were performed by reacting 30 µM 6DHNAD ion the absence or presence of 500 nM renalase and 10 µM epinephrine in either PBS buffer or 50 % blood plasma. Traces 1, 2, 6, and 7(from top) were incubated at 25°C for 20 minutes prior to the addition of 6DHNAD all other traces were incubated at 25°C for 5 minutes before 6DHNAD addition. Traces were aligned so the addition of 6DHNAD appears in the same time position in all reactions.

Discussion.

The chronology of reported activities for renalase elaborate the erroneous initial claim. In the progenitor article it was proposed that renalase is secreted by the kidney to oxidize circulating catecholamines and that the electrons mobilized are delivered to dioxygen (*1*). However, this was surmised only from the data obtained from a generic oxidase assay method and without the use of appropriate controls. Nonetheless, the association of renalase with catecholamines continues to become ever more conflated. Catecholamines are said to regulate the activity, secretion and synthesis of renalase (*11*). A variety of complex regulatory feedback pathways have been proposed (*3, 5, 11, 12, 14*). Aminochromes are claimed as the native products (*2*) and the active oxidizing agent is said to be superoxide (*36*). However, the extremely low levels of claimed *in vitro* catecholamine oxidase activity has been cited as a deficit by a number of researchers (*48, 51, 60*) and this was then rationalized by invoking "prorenalase" a claimed quiescent form of the enzyme that requires activation (*11, 12*) that occurs only in blood in the presence of a catecholamine (*11, 36*). It can now be stated with some certainty that this successive affirmative set of claims describes a compounding of an initial scientific deficit; the failure to employ appropriate control reactions to assess catalysis.

The purpose of this study is to clearly demonstrate that renalase is not the third monoamine oxidase. The apparently indelible mark of the early and recent activity claims for renalase must be dispelled if the field is to advance in a purposeful manner. We recently reported two isomeric forms of β-NAD(P)H as substrates for renalase that are clearly catalytically consumed (Figure 5.2B) and have redefined renalase as having a house-

keeping activity that is unrelated to blood pressure regulation. Renalase functions instead to oxidize reduced forms of nicotinamide adenine dinucleotides that harbor the hydride in non-metabolically accessible positions of the nicotinamide base (positions 2 & 6). We have proposed that this activity exists to relieve inhibition of primary metabolism by these molecules. A principal benefit of having identified native substrates for renalase is that we can now test the validity of previously proposed activities using a form of the enzyme that we have verified is fully active (Figure 5.2B) (*55*). In sum our data show that renalase does not consume catecholamines (Figures 5.1 & 5.2A), is not kinetically regulated by catecholamines (Figure 5.2B), is not isolated in an inhibited form and as such cannot be activated by blood plasma or catecholamines (Figure 5.3). In addition, our data suggests that blood has very little if any active renalase (Figure 5.3) an observation that is consistent with its newly identified activity that we would suggest has an exclusively intracellular/metabolic role.

Catecholamines form hydrogen peroxide as they oxidize in oxygenated media. That the initial accounts of renalase activity did not employ appropriate control reactions and reported vanishingly low activity undermines the subsequent affirmative claims. The case has also been made that in the absence of genuine substrates, no sample integrity measures have been established and as such there has been no means to discriminate natively folded and active renalase from misfolded inactive but soluble renalase (*51*). The vast majority of reports that describe direct use of the enzyme do not indicate the color of the protein (that is conspicuously yellow) or the unique absorption maxima of the flavin in the natively folded enzyme (*61*). Nonetheless, in the ten years since its initial discovery, the terms renalase and monoamine oxidase C have become somewhat synonymous (*14, 301, 344*) and

this has occurred despite sound argument and evidence to the contrary (*48, 51, 59*). In this article we have presented evidence that verifiably active renalase does not catalyze the oxidization of catecholamines.

CHAPTER VI
Bacterial Renalase: Structure and Kinetics of an Enzyme with 2- and 6-Dihydro-β-NAD(P) Oxidase Activity from *Pseudomonas phaseolicola.*

Matt R. Hoag, Joseph Roman, Brett A. Beaupre, Nicholas R. Silvaggi, Graham R. Moran

Abstract

Despite a lack of convincing *in vitro* evidence and a number of sound refutations, it is widely accepted that renalase is an enzyme unique to animals that catalyzes the oxidative degradation of catecholamines in blood in order to lower vascular tone. Very recently, we identified isomers of β-NAD(P)H as substrates for renalase. (*55*) These molecules carry the hydride equivalent on the two or six position of the nicotinamide base and presumably arise in non-specific redox reactions of nicotinamide dinucleotides. Renalase serves to rapidly oxidize these isomers to form β-NAD(P)$^+$ and then pass the electrons to dioxygen forming H_2O_2. We have also shown that these substrate molecules are highly inhibitory to dehydrogenase enzymes and thus have proposed an intracellular metabolic role for this enzyme. Here we identify a renalase from an organism without a circulatory system. This bacterial form of renalase has the same substrate specificity profile as human renalase but, in terms of binding constant (K_d), shows a marked preference for substrates derived from β-NAD$^+$. However, 2-dihydroNAD(P) substrates reduce the enzyme with rate constants (k_{red}) that greatly exceed those for 6-dihydroNAD(P) substrates. Taken together, k_{red}/Kd values indicate a minimum 20-fold preference for 2DHNAD. We also offer the first structures of a renalase in complex with the catalytically relevant ligands β-NAD$^+$ and β-NADH (the latter being an analog of the substrate(s)). These structures show

potential electrostatic repulsion interactions with the product and a unique binding orientation for the substrate nicotinamide base that is consistent with the identified activity.

Introduction

Renalase was discovered in 2005 and purported to be a flavoprotein hormone produced by the kidney that catalyzes the oxidation of catecholamines in order to lower blood pressure and slow the heart (*1, 6*). However, the initial experiments used to identify the substrates focused on only a handful of molecules and did not include control reactions to account for the inexorable oxidation of catecholamines in oxygenated buffer. Despite claimed physiological verifications of this activity (*6, 8-10, 12, 13*) no convincing *in vitro* evidence of catecholamine oxidase activity has been offered. The deficiencies in the original methods were compounded in subsequent claims that suggested an, as isolated, quiescent renalase state and ever more unlikely chemistries for which catalysis and the stoichiometry were not established (*11, 36*). A number of researchers have attempted to counter the expanding belief that renalase catalysis is associated with vascular tone, by either questioning the original methods used to establish activity (*48, 59*) or demonstrating that, relative to appropriate controls, there is no evidence of catecholamine consumption by the enzyme (*61*). These refutations have gone largely unheeded and the preponderance of scientific studies pertaining to renalase continue to be predicated on passive acceptance of an unproven catalytic role (*2-32, 37*).

We have recently shown that human renalase (HsRen) is indeed a flavoprotein oxidase, but one that catalyzes the oxidation of β-NAD(P)H isomers. These isomers carry

the hydride on the nicotinamide base in the non-canonical 2 and 6 positions (2- and 6-dihydroNAD(P)) (Scheme 6.1). The oxidation of these isomers occurs as much as five orders of magnitude more rapidly than any prior claim for renalase activity and the turnover reaction with these molecules has a defined stoichiometry and substrate specificity profile. Moreover, we have proposed that the purpose of this activity is to avoid inhibition of primary metabolism by these NAD(P)H isomers that have low nano-Molar Ki values for specific dehydrogenases (*55, 67, 68*). If 2- and 6-dihydroNAD(P) molecules are prone to form in non-enzymatic reduction reactions of β-NAD(P)$^+$ and are truly a detriment to respiratory activity, it is reasonable to assume that this is an intracellular enzymatic activity that will exist in organisms that do not have a circulatory system.

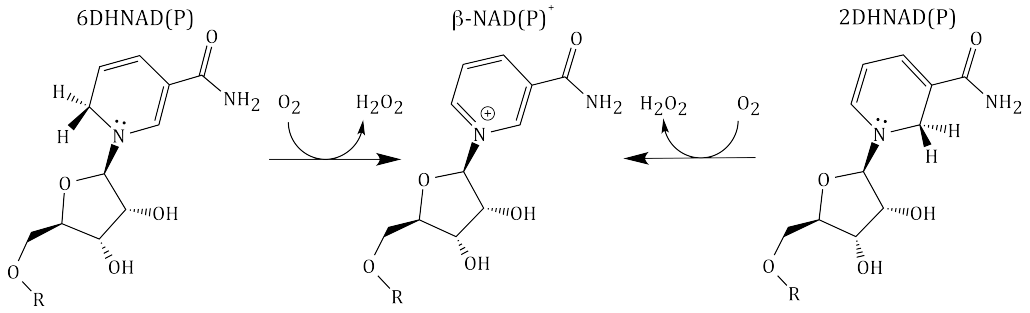

Scheme 6.1. Observed activities of renalase.

The structure of HsRen was determined by the Aliverti group in 2011(*60*) using the model of a generically assigned "amine oxidase" from *Pseudomonas syringae* (PDB ID 3KKJ) whose structure was solved and deposited in the Protein Data Bank (PDB) by the North East Structural Genomics Consortium (NESGC). While not highly homologous with the HsRen primary structure (19.5% identitical), this protein had the renalase fold (a topology

that is common to numerous redox-active flavoproteins (*303-306, 345, 346*)) and a very similar constellation of active site residues proximal to the FAD isoalloxazine (*60*). We surmised that this protein was likely a bacterial form of renalase. In this article we show that this "amine oxidase" from *Pseudomonas syringae* (van Hall pathovar *phaseolicola* strain 1448A) harbors the same catalytic activity observed for HsRen but with unique kinetic properties and stark substrate preferences. We also present the X-ray crystal structures of this enzyme in complex with nicotinamide dinucleotides that show a reductive pose of the nicotinamide base with respect to the flavin cofactor that is consistent with the proposed activity.

Materials and Methods

Materials. β-NAD^+ was sourced from Sigma-Aldrich. Sodium borohydride, potassium phosphate (mono and dibasic), sodium formate and glycerol were from Acros. Sep-Pak C18 (35 cc) cartridges were purchased from Waters. Competent NEB5a and BL21 DE3 *Escherichia coli* cells were obtained from New England Biolabs. Talon© metal affinity resin was from Thermo-Fisher Scientific. Sodium acetate was purchased from Mallinckrodt. 2- and 6-DHNAD and 2- and 6-DHNADP were prepared using an adaptation of our previously published methods (*55*). Both sets of substrates were formed by sodium borohydride reduction of β-NAD^+ or β-$NADP^+$. The products of reduction, β-NAD(P)H, 2-dihydroNAD(P) (2DHNAD(P)) and 6-dihydroNAD(P) (6DHNAD) (and residual β-NAD(P)+) were separated using a Waters X-Bridge 19 x 250 mm 5 μM C18 column. 6DHNAD(P) molecules were relatively stable and could be prepared as previously described and stored indefinitely at -

80 °C, whereas 2DHNAD(P) molecules were unstable and used immediately after collection from preparative HPLC.

Spectrophotometric Quantification. Dihydronicotinamide chromophore extinction coefficients were as follows: β-NADH, β-NADPH - ε_{340nm} = 6220 M^{-1} cm^{-1} *(309)*, 2DHNAD(P) - ε_{394nm} = 5360 $M^{-1}cm^{-1}$, 6DHNAD(P) - ε_{345nm} = 6580 $M^{-1}cm^{-1}$ and β-NAD^+ - ε_{260nm} = 18800 $M^{-1}cm^{-1}$(*55*). *Pseudomonas Syringae* renalase (PpRen) was quantified using the measured extinction coefficient for the enzyme-bound flavin (ε_{452nm} = 11,000 $M^{-1}cm^{-1}$), as determined using an SDS denaturation method as previously described (*347*).

Expression and Purification of PpRen: A plasmid derived from pET21a (pET21_NESG) containing the gene for PpRen was provided by the NESGC. This construct was prepared by PCR amplification of the PpRen gene from *Pseudomonas Syringae* (van Hall pathovar *phaseolicola* strain 1448A) followed by cloning into the Nde I and Xho I restriction sites, fusing the PpRen gene to a C-terminal 6His-tag. This construct has a single variant amino acid from what is reported for this *phaseolicola* strain; a serine is coded in place of glycine 145. The plasmid was transformed into competent BL21 DE3 cells and plated onto Luria Bertani (LB) agar (100 μg/mL Ampicillin) and grown overnight at 37 °C. Individual colonies were then selected and grown in LB broth with shaking (250 rpm) at 37 °C until growth reached early log phase. 1 mL cell stocks were made by adding filter sterilized glycerol to a final concentration of 20% and then storing at -80°C.

For expression, 1 mL cell stocks were thawed, plated onto LB agar, 100 μg/mL ampicillin, and grown overnight at 37°C (100 μL cells/plate). The lawn of cells obtained was resuspended in LB broth and transferred to LB broth cultures (two plates/L of broth) and grown at 37°C in a shaking incubator (220 rpm) until mid-log phase (OD_{600nm}=0.8). The temperature was then lowered to 17 °C and the culture was grown to OD_{600nm}~1.0 (~1-2 hr) and induced with 0.1 mM IPTG. 30 hrs after induction the cells were harvested by centrifugation (4,000 g for 30 min) and subjected to one freeze/thaw cycle. All purification steps were performed at 4°C. Cell pellets were resuspended in 20 mM sodium HEPES buffer pH 7.5 (approximately 20 mL/L culture) and placed in a stainless steel beaker and lysed by sonication using a Branson 450 sonicator (3 x 240 seconds at 50 W). During this procedure the cell suspension vessel was seated in a slurry of ice and water. Lysed cells were centrifuged at 12,800 x g for 30 min, the pellet was discarded and the supernatant loaded onto a 12.5 x 150 mm Co^{2+} Talon© affinity column equilibrated with 20 mM sodium HEPES buffer pH 7.5. Initially contaminating proteins were eluted with 150 mL of 10 mM imidazole, 50 mM sodium HEPES buffer adjusted to pH 7.5 with H_2SO_4, then a gradient from 10 mM to 300 mM imidazole in the same buffer was used to elute ostensibly pure PpRen as a single symmetrical peak. Distinctly yellow fractions were pooled. Imidazole was removed and the buffer exchanged to 10 mM potassium phosphate, pH 7.5 by dialysis using 10 kDa nominal molecular weight cut-off dialysis tubing to achieve a net ≥100,000-fold buffer exchange. Aliquots of purified concentrated renalase (<120 μM) were then stored at -80°C.

Analytical HPLC: Evidence of the substrate specificity profile was obtained by adding sodium borohydride (250 μM) to β-NAD(P)+ (250 μM). The sample was divided into two and PpRen (30 μM) was added to one and incubated for 3 minutes while the other was frozen in liquid nitrogen. PpRen was then removed from the first sample by centrifugal ultrafiltration using a 0.5 mL Amicon 10 kDa cutoff filter. Both samples were then chromatographed by analytical HPLC. Separation of the resulting mixtures was achieved using a Waters X-Bridge 4.6 x 150 mm, 3.5 μM C18 column coupled to a Waters 600E pump and Waters 2487 dual wavelength detector. Elution of components of the mixture was observed simultaneously at 260 and 340 (or 394) nm. The components were separated isocratically at 1.0 mL/min in either 10 mM (β-NAD^+ derived) or 50 mM (β-$NADP^+$ derived) potassium phosphate buffer pH 7.5.

Reductive Half-Reaction of PpRen with 6DHNAD(P): The reductive half-reaction of PpRen could be observed independent of subsequent oxidative processes by exclusion of dioxygen using previously published methods (*54*). Anaerobic PpRen (5 mL, 14-16 μM) in 20 mM potassium phosphate buffer containing 1 mM dextrose and 5 U/mL glucose oxidase (25 μL, 25 units) was mounted onto a Hitech (now TgK) DX2 stopped-flow instrument that had been scrubbed of residual dioxygen by incubation for 16 hr with a solution of 1 mM dextrose, 10 U/mL glucose oxidase. 6DHNAD(P) samples were thawed and diluted to target concentrations in water containing 1 mM glucose. 2DHNAD(P) was collected into a glass syringe (that had a small amount of concentrated dextrose added prior (≤1 mM final)) directly from preparative HPLC, diluted to approximate target concentration and used immediately. All substrate solutions were sparged with argon gas for 5 minutes. Before

capturing and mounting the substrate solution to the stopped flow instrument, 10 μL of glucose oxidase (10 units) was injected via the luer tip.

Anaerobic PpRen and substrate solutions were mixed and reduction of the renalase cofactor was observed at the absorption maximum of the PpRen FAD, 452 nm. The stability of the 6DHNAD substrate allowed for it to be prepared in sufficient quantity to achieve a high range of concentrations ranging from second order to pseudo-first order reaction conditions. The pseudo-first order data were fit to a linear combination of two exponentials according to Equation 6.1 using Kinetic Studio software (TgK Ltd). In this equation A_1 and A_2 are the amplitudes associated with the first and second rate constants, k_{1obs} and k_2 and C is the absorbance at end of the reaction. The dependence of the observed rate constants (k_{1obs}) for the largest amplitude phase (~90%) was fit to the hyperbolic form of the single-site binding equation (Equation 6.2) according to Strickland, where k_{red} is the limiting rate constant for reduction and $K_{6DHNAD(P)}$ is the binding constant for 6DHNAD (*322*). 2DHNAD(P) are prone to decompose within minutes. Reduction data for these substrates were obtained primarily from second order reactant ratios and as such could not be fit meaningfully to linear combinations of exponential terms. The data for 2DHNAD(P) substrates were fit to a the mechanism depicted in Scheme 6.2 using KinTek Explorer to obtain the dissociation constant for the substrate (k_{-1}/k_1) and the intrinsic rate constant for reduction (k_2). The concentration of these substrates was estimated by recording a spectrum immediately prior and immediately after each kinetic observation and averaging.

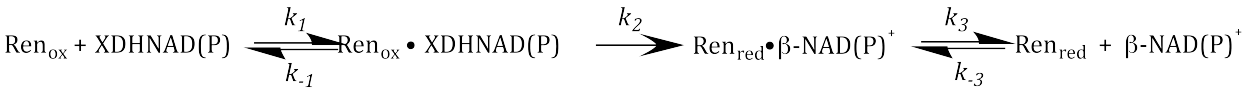

Scheme 6.2. Model for the reductive half-reaction.

Equation 6.1 $$A_{452nm} = A_1(e^{-k_{1obs}t}) + A_2(e^{-k_2t}) + C$$

Equation 6.2 $$k_{obs} = \frac{k_{red}[6DHNAD(P)]}{(K_{6DHNAD(P)} + [6DHNAD(P)])}$$

Oxidative Half-Reaction of PpRen: Reoxidation of the renalase cofactor in the presence of dissolved dioxygen was observed by double mixing stopped-flow spectrophotometry. PpRen (16 μM) was prepared in a tonometer in an equivalent manner to that of the reductive half reaction (though without dextrose or glucose oxidase). In the first mix, this solution was combined with 12 μM 6DHNAD. The reduction reaction was allowed to proceed for 150 seconds prior to the second mix that introduced dissolved dioxygen of defined concentration (Final concentrations after the second mix, 4 μM PpRen, 3 μM β-NAD$^+$, varied dioxygen). The dissolved oxygen concentration in this solution was defined by sparging an inverted syringe containing 10 mM phosphate buffer pH 7.5 with blended dinitrogen and dioxygen gases of known partial pressures supplied by a Maxtec Maxblend gas blender. The concentration of dissolved oxygen was confirmed by first sparging the reaction chamber of a Hansatech dioxygen electrode filled with the same buffer to define the equilibrium concentration of dissolved dioxygen. The reduced anaerobic PpRen solution was then mixed and the ensuing reoxidation observed at 452 nm. The data were fit to Equation 6.3 in which k_{oxobs} is the observed rate constant for reoxidation, A_1 is the

absorption amplitude for the phase observed, and C is the endpoint absorbance. The dependence of the observed rate constant was fit to a straight line that passed through the origin according to equation 6.4 where k_{ox} is the second order rate constant for reoxidation and $[O_2]$ is the concentration of dioxygen.

Equation 6.3 $$A_{452nm} = A_1(e^{-k_{oxobs}t}) + C$$

Equation 6.4 $$k_{oxobs} = k_{ox}[O_2]$$

The influence of β-NAD^+ on the rate constant for reoxidation was observed by similar methods to those described above using the double mixing facility of the stopped-flow instrument. PpRen (23.2 μM) was mixed with 6DHNAD (20 μM) and allowed to age for 150 seconds. This mixture was then mixed with 238 μM dioxygen and the reoxidation observed at 452 nm. β-NAD^+ (0-4 mM) was then added to the third solution and the experiment repeated. The dependence of the observed rate constant for reoxidation (k_{oxobs}) was then fit to Equation 6.5 to determine the extent of inhibition (Δk_{ox}) and the binding constant for β-NAD^+ to the reduced form of the enzyme (K_{NAD+}), where k^i_{ox} is the rate constant observed in the absence of exogenous β-NAD^+.

Equation 6.5 $$k_{oxobs} = k^i{}_{ox} - \left(\frac{\Delta k_{ox}[NAD+]}{(K_{NAD+}+[NAD+])}\right)$$

The Dissociation Constants for the PpRen$_{ox}$•b-NADH, PpRen$_{ox}$•β-NADPH and PpRen•SO$_3$ adduct Complexes: The dissociation constants for the PpRen$_{ox}$• β-NADH, PpRen$_{ox}$• β-NADPH and PpRen•SO_3 complexes were measured by perturbation of the renalase flavin spectrum when each ligand was titrated. For both the β-NADH and β-NADPH titrations, slow non-catalytic reduction of the PpRen flavin during the experiment (0.0008 s^{-1}) was avoided by preparing eleven 0.9 mL stocks (17 μM for β-NADH, 12 μM for β-NADPH) of the enzyme in 10 mM potassium phosphate buffer, pH 7.5 at 25 ^{o}C. To each 0.9 mL aliquot, 0.1 mL of a range of β-NADH or β-NADPH stocks were added and the spectrum recorded. As such, the spectrophotometric data are compiled from eleven PpRen renalase samples after the addition of β-NADH (0-1 mM) or β-NADPH (0-7 mM).

Titration of PpRen with sodium sulfite formed a labile sulfite adduct that is commonly observed with flavoprotein oxidases. In this experiment 7 μM PpRen in 10 mM potassium phosphate buffer pH 7.5 (25 ^{o}C) was titrated with sulfite by incremental additions spanning the range 0-310 mM. Spectra were recorded after each addition.

For β-NADH and sufite titrations, spectra were recorded using a Shimadzu 1800 UV-Vis spectrophotometer. For the β-NADPH titration, spectra were recorded using a Shimadzu 2600 UV-Vis spectrophotometer. After correction for dilution, the changes in absorption at 492 nm, 468 nm and 452 nm were used to determine the dissociation constants for the Ren$_{ox}$•β-NADH, Ren$_{ox}$•β-NADPH and the Ren$_{ox}$•β-NAD^+ complexes respectively. The changes in absorption were fit to the quadratic solution form of the single site binding equation (Equation 6.6) in which [E] is the PpRen concentration, [EL] is concentration of the PpRen•ligand complex and K_L is the dissociation constant of the PpRen•ligand complex. For both β-NADH, β-NADPH and sulfite, the raw data were fit. That

is, change in absorbance at defined wavelengths was used as a measure of [EL] and the maximal change in absorbance as a representation of [E].

Equation 6.6 $$[EL] = \frac{([L]+[E]+K_L)-\sqrt{([L]+[E]+K_L)^2-4([L]+[E])}}{2}$$

Crystallization, Structure Determination, and Model Refinement. Initial crystallization conditions were those identified by the NESGC and included 2 M sodium formate, 100 mM sodium acetate pH 4.6 at 20 °C. Diffraction-quality crystals were obtained by the hanging drop vapor diffusion method. The droplet was formed from three 1 µL additions; 1 µL of the well solution, 1 µL of PpRen (104 µM) and 1 µL of H_2O. Crystals appeared after 2–4 days and grew to maximal dimensions of ~200 µm x 50 µm x 10 µm. Crystals were harvested from the hanging drops, and soaked for 1-3 minutes in 2.5 M sodium formate, 120 mM sodium acetate pH 4.7 with 20% glycerol and 166 mM β-NAD^+ or 10 mM β-NADH. The mounted crystal was then flashed-cooled in liquid nitrogen. Crystals were initially screened for diffraction quality using the rotating anode X-ray source at Marquette University (Milwaukee, WI). X-ray diffraction data for PpRen•β-NAD+ were collected at beamline 21-ID-D of the Life Science Collaborative Access Team (LS-CAT) at the Advanced Photon Source (APS). Data for the PpRen·β-NADH complex were collected at LS-CAT beamline 21-ID-F. Data were processed with HKL2000 (*348*).

The structure of PpRen was determined by molecular replacement in PHASER (*349*) with a search model derived from chain A of the *P. syringae* Q888A4 renalase structure (PDB ID 3KKJ, Northeast Structural Genomics Consortium) with all non-protein atoms removed and all B-factors set to 20.0. After iterative cycles of manual model building in

COOT (*350*) and maximum likelihood based refinement using the PHENIX package (phenix.refine) (*351*), ordered solvent molecules were added in phenix.refine automatically and culled manually in COOT. After adding solvent atoms, the FAD cofactor and β-NAD+ or β-NADH were added to the model in COOT. During the last rounds of refinement, hydrogen atoms were added to the model using phenix.reduce (*352*) to improve the stereochemistry of the model. Positions of H atoms were refined using the riding model with a global B-factor. Regions of each model to be used in translation-libration-screw (TLS) refinement were identified using phenix.find_tls_groups and the TLS parameters were refined in phenix.refine. Once the refinement converged, the model was validated using the tools implemented in COOT and PHENIX (*353*), (*354*). Side chains with poor or missing electron density were modeled in favored rotameric conformations. The B-factors were allowed to refine without additional restraints, and the occupancies were held to 1.0. Data collection and model refinement statistics are listed in Table 6.1. Coordinates and structure factors for the PpRen·β-NAD^+ and PpRen·β-NADH complexes have been deposited in the Protein Data Bank with accession codes 4ZCD and 4ZCC, respectively.

Table 6.1. Crystallographic data collection and model refinement statistics.

	PpRen·β-NAD$^+$	**PpRen·β-NADH**
Space group	C 2	P 2_1
Unit cell parameters	a=144.7, b=37.6, c=138.2 Å α=γ=90, β=120 °	a=63.5, b=71.5, c=143.8 Å α=γ=90, β=97.5 °
Resolution (Å)	33.2-1.66	46.2-2.00
(last shell)a	(1.69-1.66)	(2.03-2.00)
Wavelength (Å)	0.97895	0.97872
No. of reflections		
Observed	286455 (12871)	328721 (15867)
Unique	76829 (3588)	86594 (4305)
Completeness (%)[a]	99.7 (94.0)	100.0 (100.0)
Rmerge (%)[a,b]	0.044 (0.336)	0.096 (0.628)
Multiplicity	3.7 (3.6)	3.8 (3.7)
$\langle I/\sigma(I)\rangle$[a]	26.3 (3.7)	13.7 (2.2)
Model Refinement Statistics		
Reflections in work set	73035	77722
Reflections in test set	2971	2892
R_{cryst} (R_{free})	0.151 (0.176)	0.170 (0.215)
No. of residues	651	1288
No. of solvent atoms	748	736
Number of TLS groups	4	28
Average B-factor (Å^2)[c]		
Protein atoms	16.0	33.1
Ligand atoms	15.5	32.5
Solvent	28.8	36.6
RMS deviations		
Bond lengths (Å)	0.012	0.014
Bond angles (°)	1.490	1.634
Coordinate error (Å)	0.15	0.19

[a] Values in parentheses apply to the high-resolution shell indicated in the resolution row.
[b] $R = \Sigma(||F_{obs}|\text{-scale}*|F_{calc}||) / \Sigma |F_{obs}|$.
[c] Isotropic equivalent B factors, including contribution from TLS refinement.

Results

Properties of PpRen and Substrate Identification: PpRen can be expressed by the above methods to yield ~17 mg of purified enzyme per liter of culture. The absorption spectrum of the purified enzyme indicates characteristic visible maxima indicative of bound flavin. The flavin maxima are observed at 380 nm (ε = 10.1 $mM^{-1}cm^{-1}$) and 452 nm (ε = 11 $mM^{-1}cm^{-1}$) distinct from those observed for HsRen (385 nm (ε = 10.9 $mM^{-1}cm^{-1}$), 458 nm (ε = 11.3 $mM^{-1}cm^{-1}$)) and free flavin (375 nm (ε = 9.7 $mM^{-1}cm^{-1}$), 450 nm (ε = 11.3 $mM^{-1}cm^{-1}$)). The enzyme is stable at 25 ^{o}C and below in phosphate buffer at pH 7.5, but prone to precipitate at concentrations above 4.5 mg/mL (~120 μM).

Borohydride reduction of β-NAD^+ or β-$NADP^+$ yields three reduced isomers of each: 2-dihydroNAD(P) (2DHNAD(P)), 4-dihydroNAD(P) (β-NAD(P)H) and 6-dihydroNAD(P) (6DHNAD(P)). We have shown that HsRen catalytically oxidizes both 2- and 6DHNAD(P) to form β-$NAD(P)^+$ (*55*). HPLC analysis indicated that when PpRen was added to the mixture of reduction products only 2- and 6DHNAD(P) molecules were consumed (Figure 6.1) indicating that this *Pseudomonas* form of renalase has the same substrate profile as the human. When chromatographed at 260 nm, where the adenine chromophore has maximal absorption, the net concentration lost from the 2- and 6DHNADP peaks (based on standard curves for each) was gained by the β-$NAD(P)^+$ peak indicating that the product formed from both types of substrate is the oxidized form of the nicotinamide dinucleotide (Scheme 6.1).

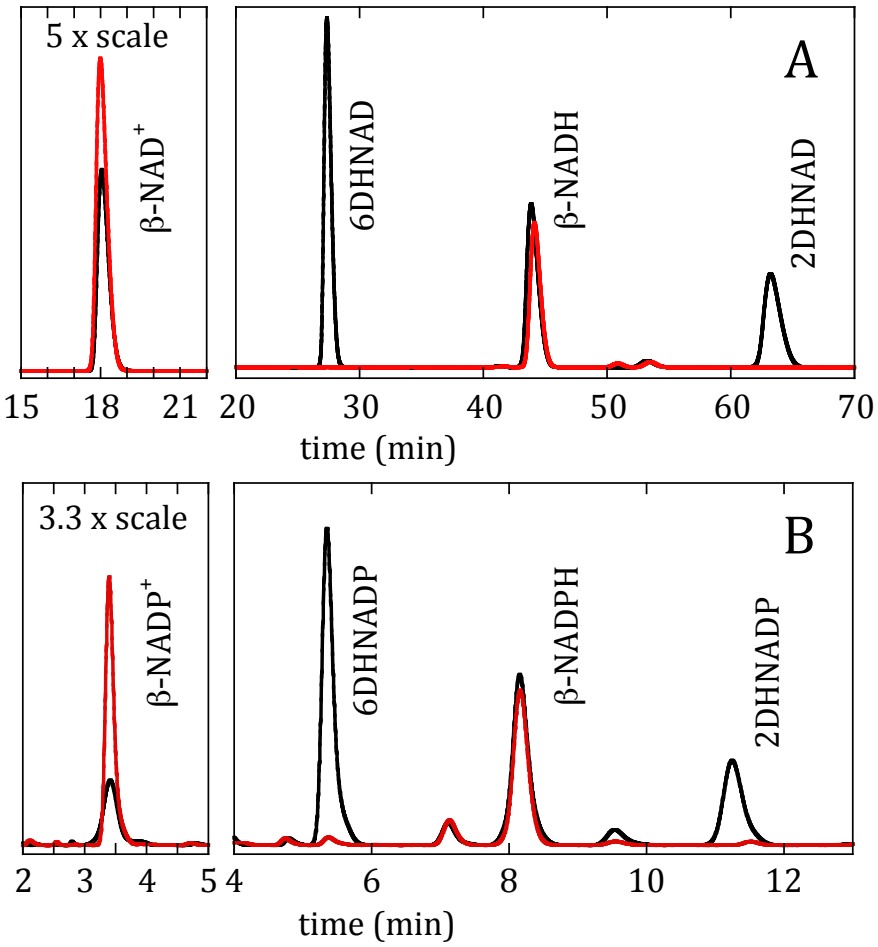

Figure 6.1. Analytical HPLC of Renalase Turnover Reactions of Borohydride Reduced Mixtures of β-NAD(P)H Isomers. HPLC separation was achieved using an analytical Waters X-bridge C18 column run isocratically in potassium phosphate buffer (10 mM for NAD derived mixtures, and 50 mM for NADP derived mixtures). All eluting species were detected at 260 nm, the absorption maximum for the NAD(P) adenine base. **A**: The black chromatogram is the separation of the components formed from borohydride reduction of β-NAD^+. The red chromatogram is three minutes after the addition of 30 μM PpRen. **B**: The black chromatogram is the separation of the components formed from borohydride reduction of β-$NADP^+$. The red chromatogram is three minutes after the addition of 30 μM PpRen.

Reductive Half-Reaction of PpRen with 6DHNAD(P): The reductive half-reaction was observed by mixing PpRen with varied concentrations of 6DHNAD, 6DHNADP, 2DHNAD and 2DHNADP, in the absence of molecular oxygen. The transfer of a hydride from the DHNAD(P) substrate to the PpRen flavin is observed as a large change in extinction coefficient of the flavin as it converts to the reduced state (Figure 6.2). The equilibrium and kinetic constants derived from these experiments are summarized in Table 6.2. Both 6DHNAD and 6DNADP substrates were titrated and the largely monophasic reduction and hyperbolic dependence of the observed rate constant for reduction indicated that these substrates bind rapidly and reversibly to the enzyme prior to hydride transfer. The substrate dissociation constants obtained from the reductive-half reaction data indicated relative higher binding affinity for β-NAD^+-derived substrates (K_{2DHNAD}~36 μM, K_{6DHNAD}~28 μM) compared to the β-$NADP^+$-derived substrates ($K_{2DHNADP}$~500 μM, $K_{6DHNADP}$~1400 μM). This apparent preference for β-NAD^+-derived substrates is consistent with our proposed function for renalase; to protect primary metabolism dehydrogenases from inhibition by 2- and 6DHNAD (*55*). However, both 6-dihydro substrates exhibited a relative slow reduction rate constant ($k_{red6DHNAD}$ =0.4 s^{-1} and $k_{red6DHNAP}$ =0.5 s^{-1}), approaching three orders of magnitude slower than those observed for the the 2-dihydro forms ($k_{red2DHNAD}$~180 s^{-1} and $k_{red2DHNAP}$~120 s^{-1}). When these data are viewed as a ratio they define a measure of substrate capture (k_{red}/Kd), it is apparent that PpRen has a twenty-fold preference for 2DHNAD over its next preferred substrate, 2DHNADP (Table 6.2). Both β-NAD^+- and β-$NADP^+$-derived substrates accelerate the reduction rate constant by 10^3-10^5 compared to that observed for β-NADH (~0.0008 s^{-1} at 2 mM β-NADH). A pronounced preference for the position of the nicotinamide hydride was not observed for HsRen that exhibited ostensibly

the same dissociation constant for either β-NAD^+-derived substrate isomers (K_{2DHNAD}, K_{6DHNAD}~170 μM) and only modest differences in the reduction rate constant (k_{red}6DHNAD ~230 s^{-1} and k_{red}2DHNAP ~850 s^{-1}) (*55*).

Table 6.2. Summary of Kinetic and Equilibrium Constants for PpRen.

Substrate/Ligand	K_d (μM)	k_{red} (s^{-1})	k_{red}/K_d ($\mu M^{-1}s^{-1}$)
2DHNAD	36 ± 8	134 ± 2	3.7 ± 0.8
2DHNADP	468 ± 71	84 ± 3	0.18 ± 0.02
6DHNAD	28 ± 3	0.39 ± 0.01	0.014 ± 0.002
6DHNADP	1380 ± 210	0.50 ± 0.05	3.6 ± 0.7 x 10^{-4}
β-NADH	81 ± 7	~0.0008 ± 0.00001	9.8 ± 0.8 x 10^{-6}
β-NADPH	1540 ± 370	n.m.[a]	

a- not measured

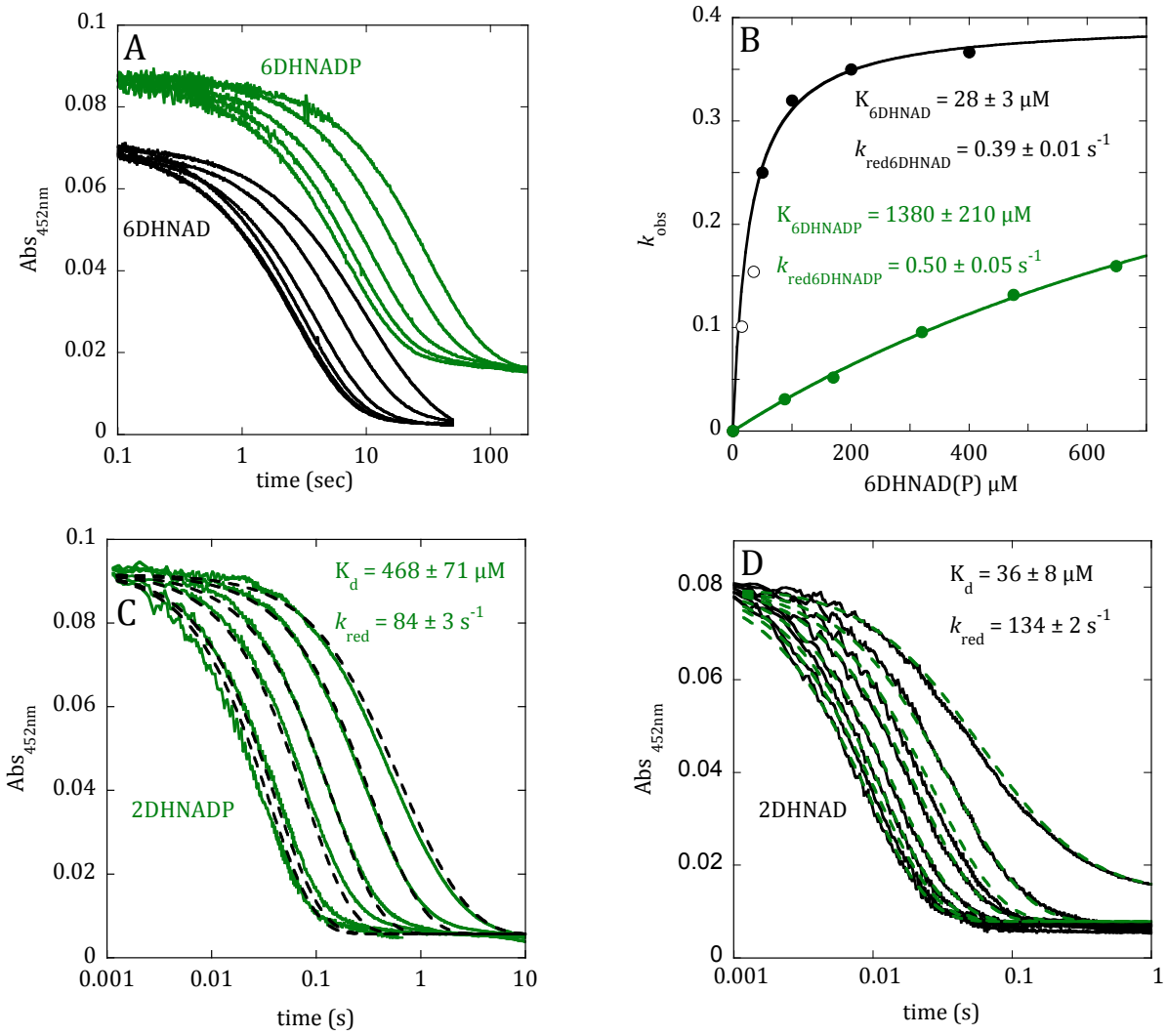

Figure 6.2. Kinetics of the Reductive Half-Reactions of PpRen with Nicotinamide Dinucletide Substrates. Oxidized anaerobic PpRen was mixed with varied concentrations of anaerobic substrates and the reduction of the enzyme's cofactor was observed at 452 nm. **A**: Reduction of the PpRen by 6DHNAD(P) substrates. Approximately 7 µM PpRen was reacted with either 6DHNAD (15, 35, 50, 100, 200, 400 µM) or 6DHNADP (88, 170, 320, 475, 613 µM). Traces for 6DHNAD are offset (down) for clarity. **B:** The dependence of the observed rate constant for reduction on the concentration of 6DHNAD and 6DHNADP fit to the hyperbolic form of the single site binding equation (equation 2). N**B:** observed rate constants obtained from exponential fits to non-pseudo first order reactant concentrations for 6DHNAD are shown as open circles. **C**: The reduction of PpRen (8 µM) by 2DHNADP (11.3, 21.5, 49.8, 93.0, 211.9, 263.8 µM) fit globally (dashed lines) to the model shown in Scheme 6.2. **D**: The reduction of PpRen (8 µM) by 2DHNAD (6.3, 13.0, 19.0, 26.4, 45.6, 72.1, 97.2, 163.2 µM) fit globally (dashed lines) to the model shown in Scheme 6.2. For **C** and **D** concentrations are based on the average of two spectra, one recorded immediately prior to and one immediately after collection of kinetic data.

Oxidative Half-Reaction of PpRen: The reoxidation of PpRen was observed by double mixing stopped flow. The anaerobic oxidized enzyme was first mixed with anaerobic 6DHNAD at a concentration sufficient to reduce 75% of the enzyme. After a 150 second age-time that accounted for >6 half-lives for the predicted reduction rate constant at the reactant concentrations used, the partially reduced enzyme was mixed with defined pseudo-first order concentrations of dioxygen and observed to reoxidize at 452 nm (Figure 6.3A). The dependence of the observed reoxidation rate constant on the concentration of dioxygen was linear with a zero intercept indicating a collision-based reaction (Figure 6.3A inset). The second order reoxidation rate constant was obtained from the slope of the dependence according to Equation 6.4 and was found to be $5x10^3$ $M^{-1}s^{-1}$, similar to that observed for HsRen ($2.9x10^3$ $M^{-1}s^{-1}$) (*54*).

Exogenous β-NAD^+ impeded the rate constant for reoxidation (Figure 6.3B). The dependence of the inhibition yielded a dissociation constant for the PpRen(red)•β-NAD^+ complex of 230 μM (Figure 6.3B inset), 7-fold higher affinity than the same complex in HsRen. Suppression of the reoxidation rate constant extrapolated to ~0 s^{-1}, indicating an ordered product release mechanism in which β-NAD^+ (and presumably β-$NADP^+$) must dissociate before dioxygen can react with the reduced flavin cofactor. This differs from HsRen whose reoxidation rate constant was not influenced by exogenous nicotinamide product and as such displayed a formally random product release mecnism (*54*).

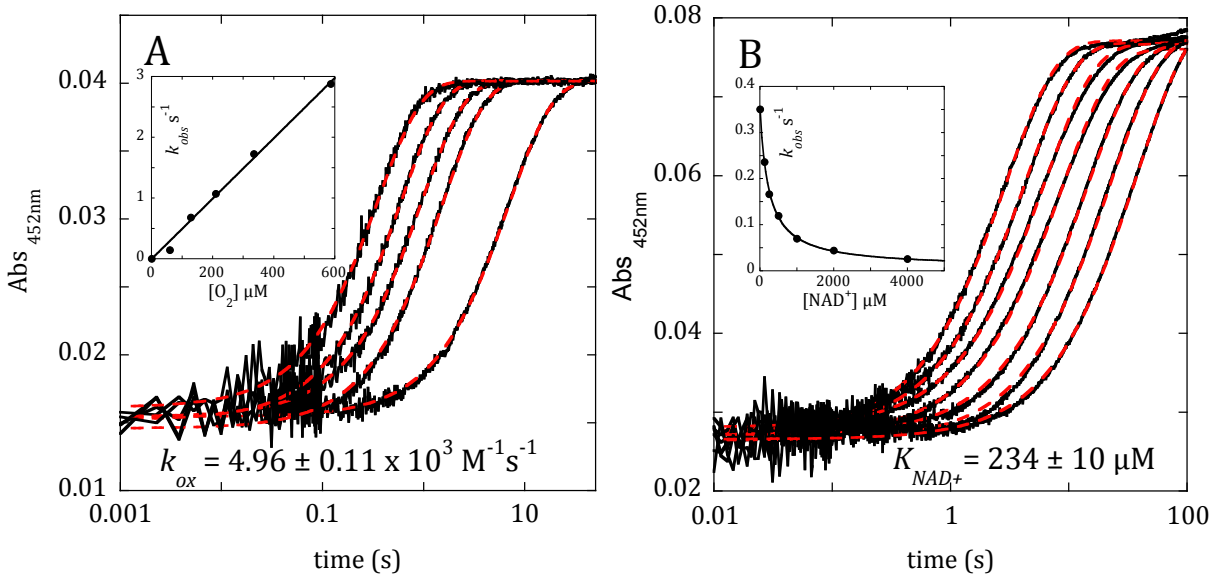

Figure 6.3. Kinetics of the Oxidative Half-Reaction of PpRen. **A:** Reoxidation of PpRen in the presence of varied concentrations of molecular oxygen observed at 452 nm. Reduced anaerobic PpRen (3 µM) was reacted with pseudo-first order concentrations (59, 128, 210, 335, 587 µM) of dioxygen. Traces were fit to Equation 6.3 (red dashes) Inset. The dependence of the observed rate constant for reoxidation fit to Equation 6.4. **B:** The dependence of the observed rate constant for reoxidation on the concentration of added β-NAD$^+$. Traces are shown for 5.8 µM PpRen reoxidizing in the presence of 119 µM dioxygen with 0, 125, 250, 500, 1000, 2000, 4000 µM added β-NAD$^+$ fit to Equation 6.3 (red dashes). Inset. The dependence of the observed rate constant for reoxidation on the concentration of exogenous β-NAD$^+$ fit to equation 6.5.

The Dissociation Constants for the PpRen$_{ox}$•β-NADH, PpRen$_{ox}$•β-NADPH and PpRen•SO$_3$ adduct Complexes: The dissociation constants for β-NADH and β-NADPH were measured by titration and observation of perturbation of the absorption spectrum of the PpRen FAD isoalloxazine moiety (Figure 6.4A). Consistent with the apparent preference for β-NAD$^+$-derived substrates, the dissociation constant for the PpRen•β-NADH complex was found to be ~80 µM, comparable to that for the 2DHNAD and 6DHNAD substrates (Figure 6.4). This low-level of β-NADH isomer selectivity was also observed in the human enzyme (*55*) and

indicates that renalases are not able to discriminate between each of the reduced forms of β-NADH and therefore function in a partially inhibitory ligand environment. However, the PpRen•β-NADH dissociation constant is seven-fold lower than that measured for the human enzyme, facilitating soaking strategies intended to form this complex in the crystal state (*vide infra*). Consistent with the dissociation constants measured in the reductive half reaction for 6DHNADP and 2DHNADP, the dissociation constant for β-NADPH was observed to be 19-fold larger than that for β-NADH.

Flavin-sulfite adduct formation is a peculiar characteristic of many oxidase enzymes. The Aliverti group showed that natively folded HsRen formed a dissociable sulfite adduct with the flavin cofactor (*60*). In order to offer an additional reactivity correlation to HsRen, we titrated sulfite to PpRen (Figure 6.4B). Characteristic bleaching of the long wavelength transitions of the flavin spectrum were observed along with the appearance of a UV-transition at ~320 nm. When the data obtained at 452 nm were fit to the quadratic solution of the single-site binding equation, a dissociation constant for sulfite of 105 mM was obtained, substantially weaker than the sulfite affinity observed for HsRen (K_{SO3} = 1.8 mM).

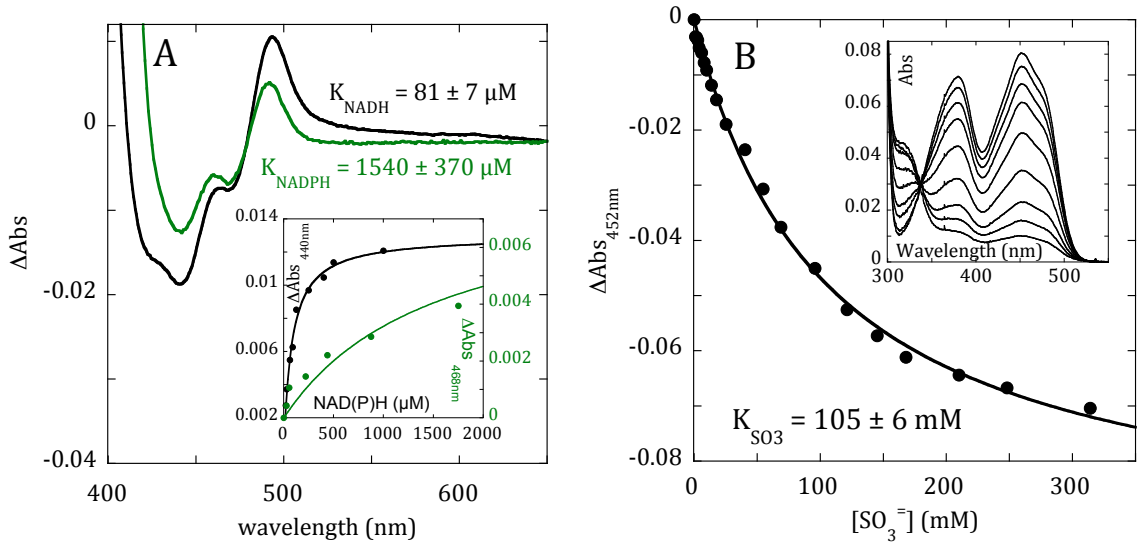

Figure 6.4. Measurement of the Dissociation Constants for the $PpRen_{ox}$•β-NADH, $PpRen_{ox}$•β-NADPH and PpRen•SO_3 Complexes. **A:** Flavin difference spectra and binding isotherms for the association of NADH and NADPH with PpRen. For the $PpRen_{ox}$•β-NADH titration (black), 17 µM PpRen was titrated with NADH (0-1 mM) and the spectrum at each ligand concentration recorded. The observed absorption changes in the spectrum at 494 nm were fit to Equation 5 (inset). For the $PpRen_{ox}$•β-NADPH titration (green), 12 µM PpRen was titrated with NADPH (0-7 mM) and the spectrum at each ligand concentration recorded. The observed absorption changes in the spectrum at 468 nm were fit to Equation 6.5 (inset). **B:** The titration of PpRen (10 µM) with sulfite (0-310 mM). The observed absorption changes in the spectrum at 452 nm were fit to Equation 5 (inset).

Structure of the PpRen•β-NAD⁺ and PpRen•β-NADH complexes: PpRen proved highly apt to form crystals. Both rectangular rods and hexagonal plates were obtained using the conditions that were provided with the PDB ID 3KKJ structure deposited by the NESGC. Only the plate-like crystals displayed uniform high diffraction. By soaking, structures of the PpRen•β-NAD^+ (1.78 Å) and PpRen•β-NADH (2.0 Å) complexes were obtained (Table 6.1). Respectively, these structures are the $PpRen_{ox}$•product (EP) complex and a close representation of the PpRen•substrate (ES) complex. For both structures two protomers of PpRen are arranged together with a large primarily Van der Waals contact interface of

~1100 Å^2 in which no ionic pairs and only 8 hydrogen bonds contribute to association of the protomers.

Despite low sequence identity (19%), the fold of PpRen is highly similar to that of HsRen (PDB ID 3QJ4) with an RMSD of 2.1 Å for 298/326 Cα carbons (Figure 6.5). It is interesting to note that the initial structure of PpRen deposited in the PDB (ID 3KKJ) was the search model used to solve the structure of HsRen by molecular replacement. This study therefore serves as the functional assignment of the 3KKJ protein, annotated previously as an amine oxidase. The renalase fold is not characteristic to renalase and is observed with numerous redox-active flavoproteins (*60*). However, the constellation of conserved active site residues is unique to renalase activity (Figure 6.6). Consistent with the observations of Milani et al, (that pertain to renalase sequences from *Animalia*) the active site opening is lined with three aromatic residues. In two of the three positions only the aromatic character of the side chain is conserved (PpRen W212, F204 corresponding to F223, Y214 in HsRen) whilst the third is a conserved tyrosine (PpRen Y57 corresponding to Y62 in HsRen). The inner surfaces of the active site pack closely to the *si* face of the flavin isoalloxazine and provide a substrate binding cavity adjacent to the *re* face. Conserved residues that line the substrate-binding cavity are H232 (HsRen H245) and W276 (HsRen W288). A guanidino group is supplied by R280 (HsRen Q292) and a similar placement of a guanidino group is accomplished in HsRen from R193 (PpRen T185) that is conserved in the *Animalia* and extends from a different element of secondary structure.

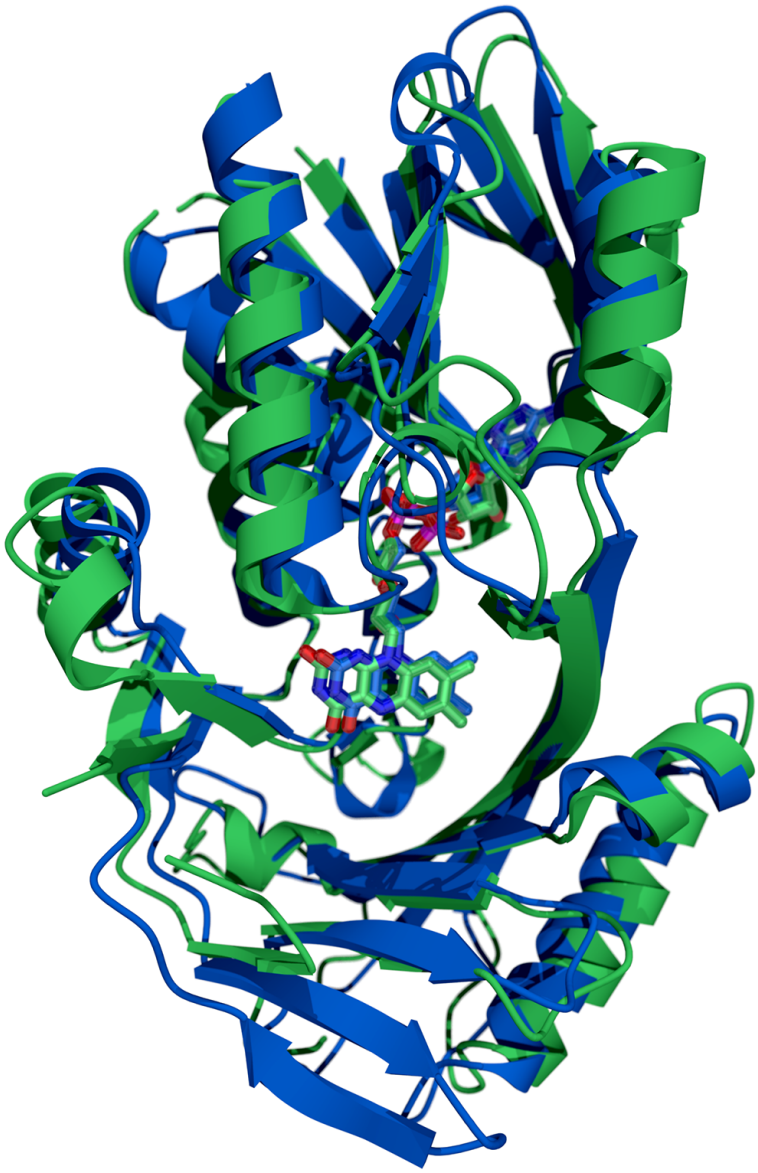

Figure 6.5. *Superposition of the PpRen•β-NADH and HsRen Tertiary Structures.* PpRen•β-NADH is depicted in blue and HsRen is depicted in green (PDB ID 3QJ4).

The primary advancement in understanding the chemistry of renalase was that the PpRen structures were solved with catalytically relevant ligands occupying the active site cavity. Stereo views of the active site with both ligands and representative ligand density are depicted in Figure 6.6. The PpRen•β-NADH complex structure provides a

representation of the ES complex. The reduced nicotinamide base of β-NADH has an overall neutral charge and is ostensibly isosteric with the bases of 2DHNAD(P) or 6DHNAD(P) and presumably localizes in a position similar to that of the native substrates. Evidence of this is that the 2-position of the base is most proximal to the N5 of the isoalloxazine (3.6 Å), the assumed position of hydride delivery, in an analogous position to that observed in other NAD(P)H/isoalloxazine complexes (*327, 355*) (Figure 6.7B & C). No evidence for partial occupancy of a 6-position reduction conformer is observed, suggestive of the apparent preference for 2DHNAD(P) isomers that were observed to reduce the enzyme ~500-fold more rapidly than 6DHNAD(P) isomers (Figure 6.2, Table 6.2). One possible explanation for this apparent conformer bias is that threonine 185 (that occupies the position of a conserved arginine in animal renalases, see below) donates an apparent hydrogen bond to the nicotinamide amide oxygen, stabilizing the pose that promotes donation of the hydride from the 2-position (Figure 6.6 & 6.7). Manually flipping the nicotinamide base in the PpRen•β-NADH model followed by additional refinement did not substantially alter the electron density for the pyridyl ring (data not shown). In this alternate pose a potential interaction is observed from the dihydronicotinamide amido nitrogen to the backbone carbonyl of G307. The PpRen•β-NAD^+ structure is that of the product complex. Despite 1.78 Å resolution, the electron density map for this complex indicated very low occupancy of the base and the ribose that form the nicotinamide nucleoside. It is suggested that the proximity of the R280 (R193 in HsRen) guanidino group plays an important role in ejecting the positively charged nicotinamide product (β-$NAD(P)^+$) from the active site. We observe that the guanidino group is displaced in the PpRen•β-NAD^+ structure from the position it

occupies in the PpRen•β-NADH complex structure by 2.6 Å, suggesting a charge repulsion interaction.

The ADP moiety of both ligands is anchored in the same position on the surface of the protein (Figure 6.7). In this binding pose the two ribose units emerge from the pyrophosphate moiety approximately parallel to one another, a position that places the respective 3'-hydroxyl groups within 2.9 Å. This conformation does not provide an obvious explanation for the observed substrate binding preference of PpRen where β-NAD^+-derived substrates bind ~50-fold more tightly than those derived from β-$NADP^+$.

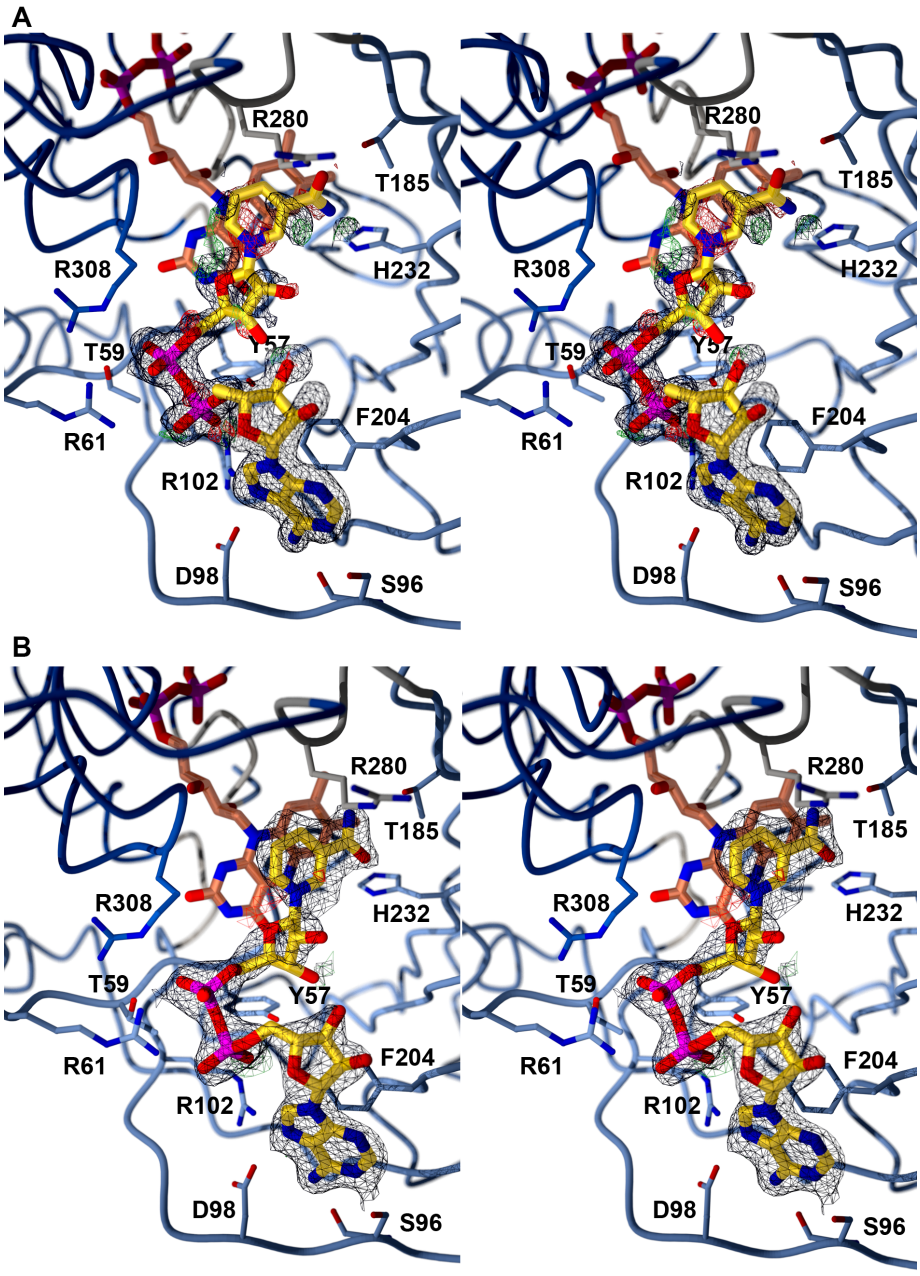

Figure 6.6. The Active Site of the PpRen β-NADH and β-NAD⁺ complexes**. A:** Stereoview for the PpRen•β-NAD⁺ complex showing the $2|F_o|-|F_c|$ simulated annealing composite omit electron density of the ligand (black) contoured at 1.0σ and $|F_o|-|F_c|$ electron density contoured at 3.0σ (green) and -3.0σ (red). **B:** Stereoview for the PpRen•β-NADH complex showing the $2|F_o|-|F_c|$ simulated annealing composite omit electron density of the ligand (black) contoured at 1.0σ and $|F_o|-|F_c|$ electron density contoured at 3.0σ (green) and -3.0σ (red).

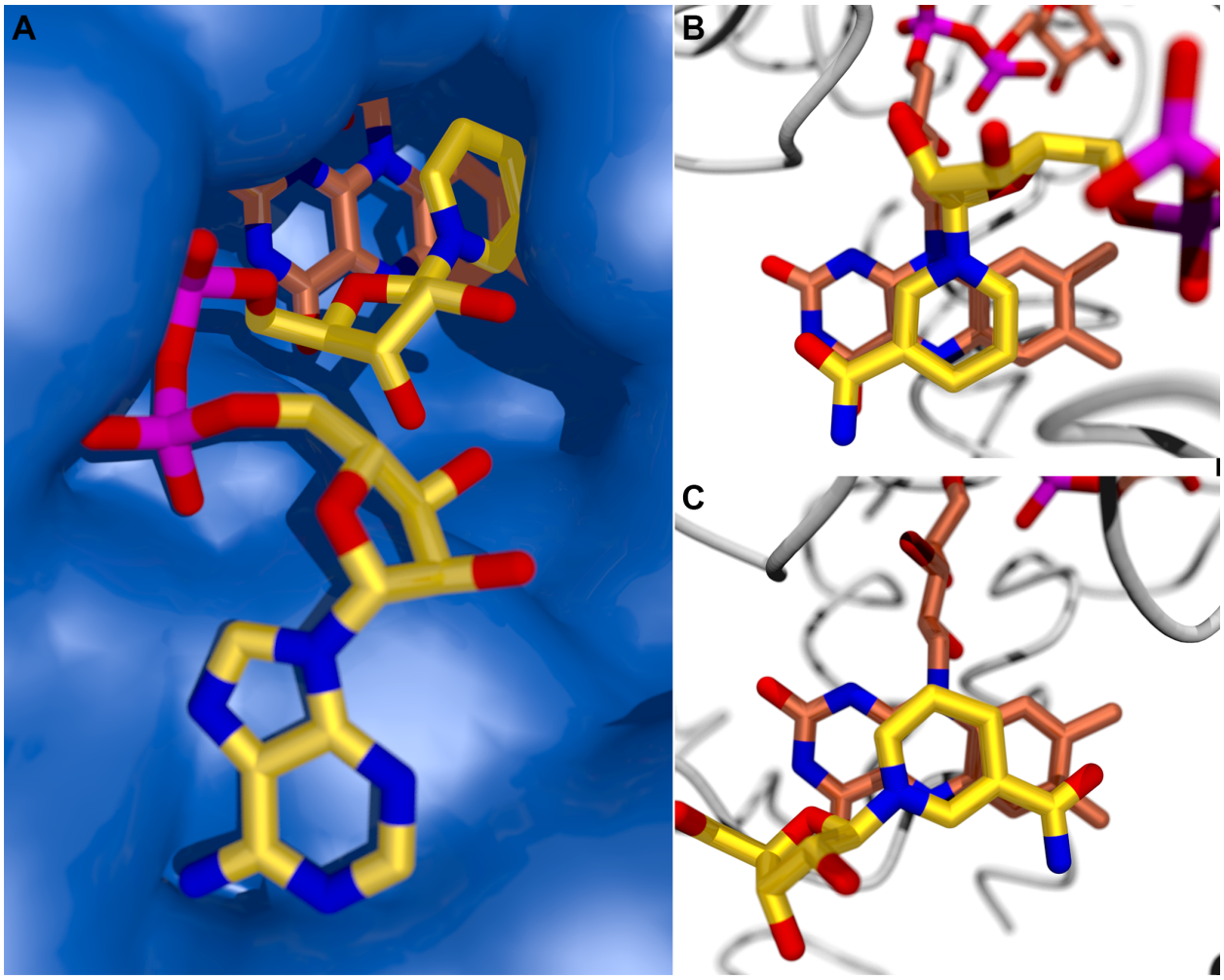

Figure 6.7. The Reductive Pose of Nicotinamide Dinucleotide Substrates. **A:** The relative positions of β-NADH and FAD on the solvent accessible surface of PpRen. **B:** The reductive complex of glutathione reductase in complex with β-NADH (PDB ID 1GRB) depicting the position of the nicotinamide 4-position 3.4 Å from the flavin isoalloxazine N5. **C:** The reductive complex of PpRen in complex with β-NADH (PDB ID 4ZCC) depicting the position of the nicotinamide 2-position 3.6 Å from the flavin isoalloxazine N5.

Discussion

The current consensus understanding for the function of renalase is that it is an animal enzyme/hormone whose catalytic activity lowers blood pressure and modulates the contraction rate of the heart by oxidative consumption of catecholamine substrates (critical evaluations of this claimed catalytic role are available (*356-358*)). This entrenched perception of the catalytic function of this enzyme has persisted in the literature since the progenitor article claimed to simultaneously discover the enzyme, its catalytic activity and its physiological role (*1*). We, and others, have disputed this claim and have offered evidence and counter arguments that undermine the link to catecholamines(*48, 51, 54, 55, 59, 61, 347*). Moreover, the recent discovery by our group that renalase has genuine catalytic behavior with two β-NAD(P)H isomers (*55*) casts further doubt over the extracellular catecholamine oxidase activity claim. This new activity for renalase is more consistent with an intracellular house-keeping metabolic function. In this role β-NAD(P)H isomers that we presume to arise in non-specific reduction events and inhibit dehydrogenase enzymes are recycled back to the nicotinamide dinucleotide pool by oxidation (forming β-NAD(P)$^+$). Such an activity would be expected to be generally advantageous to living organisms and therefore likely to be detectable in Kingdoms outside the *Animalia*. In this article we present the first account of a bacterial form of renalase. In addition to the substrate profile, kinetics of catalysis and substrate/ligand preferences, we also show the structures of the enzyme in complexes with catalytically relevant NAD ligands that have poses consistent with this newly identified activity.

PpRen was first identified in 2009 by the NESGC and in the absence of known function given a generic, amine oxidase designation (PDB ID 3KKJ). In 2011, the Aliverti

group solved the structure of HsRen using 3KKJ as a search model in a molecular replacement strategy (PDB ID 3Qj4) (*60*). The striking similarity of the apparent active sites of HsRen and 3KKJ led us to conclude that the 3KKJ structure was from a bacterial form of renalase. The data obtained with this enzyme support that it has the same function as HsRen. In the presence of a mixture of 2DHNAD(P), 4DHNAD(P) (β-NAD(P)H) and 6DHNAD(P) PpRen oxidizes only the 2- and 6-dihydro isomers as was observed for the human enzyme (Figure 6.1). Both β-NAD^+- and β-$NADP^+$-derived substrates induce relative rapid reduction of the PpRen flavin isoalloxazine ring and induce multiple turnovers indicating that they are genuine substrates for PpRen (Figure 6.2).

We have proposed that the true function of renalase is to scavenge NAD(P)H isomers to alleviate inhibition of primary metabolism. Solely in terms of dissociation constant, the substrate preference of PpRen would appear to be for β-NAD^+-derived substrates. Both 2DHNAD and 6DHNAD bind 10-50-fold more tightly than do 2DHNADP and 6DHNADP (Figure 6.2). However, substrate preference (or scavenging efficiency) is a function of both dissociation constant and the rate constant for the largely irreversible hydride transfer to the flavin and the 6-dihydro substrates reduce PpRen considerably more slowly than the 2-dihydro substrates. When the relative rate constants for reduction and dissociation constants are compared as a ratio (kred/Kd), PpRen has a 300-500–fold preference for 2-DHNAD(P) substrates. It is conceivable that this substrate preference mirrors a 2DHNAD(P) inhibitory susceptibility of one or more of the primary metabolism dehydrogenases in *P. phaseolicola*. The structures of PpRen•β-NADH and PpRen•β-NAD^+ do not reveal the basis of β-NAD^+-derived isomer binding selectivity (Figure 6.3 & 6.4A). In both the PpRen•β-NADH and PpRen•β-NAD^+ structures the oxygen atom of the 2-hydroxyl

of the adenine nucleotide riboside has no interacting residue or steric constraint within an 8 Å sphere (Figure 6.7A).

It would appear that renalase's primary catalytic purpose is to accept the hydride, as reoxidation of the enzyme occurs with a rate constant only 20-fold greater than that of free $FADH_2$ autoxidation and so is only modestly catalyzed (*308, 325*) (Figure 6.3). This is unlike most dioxygen-reactive flavoproteins that tend to have reoxidation rate constants at least two or three orders of magnitude more rapid than that of free flavin (*308, 359, 360*). There is no spectrophotometric evidence for the dissociation of the β-NAD(P)$^+$ product in the reductive half reaction, but its egress is assumed to be rapid compared to the rate constant for reoxidation at atmospheric levels of dioxygen (~1 s^{-1}) (Figures 6.3 & 6.6). Scheme 6.3 provides a summary of the kinetic and chemical mechanism conclusions for PpRen in turnover with the preferred substrate, 2DHNAD, that were made from our observations. In this scheme the substrates bind rapidly and transfers a hydride to the flavin isoalloxazine N5. The release of products has an obligate order in which β-NAD(P)$^+$ dissociates before dioxygen reacts with the reduced flavin. This ordered release of products is based on the observation that exogenous β-NAD$^+$ can completely suppress the reoxidation of the enzyme. Once β-NAD(P)+ has dissociated the flavin reoxidizes with a rate constant that would be the *in vitro* rate-limiting process under conditions of atmospheric dioxygen.

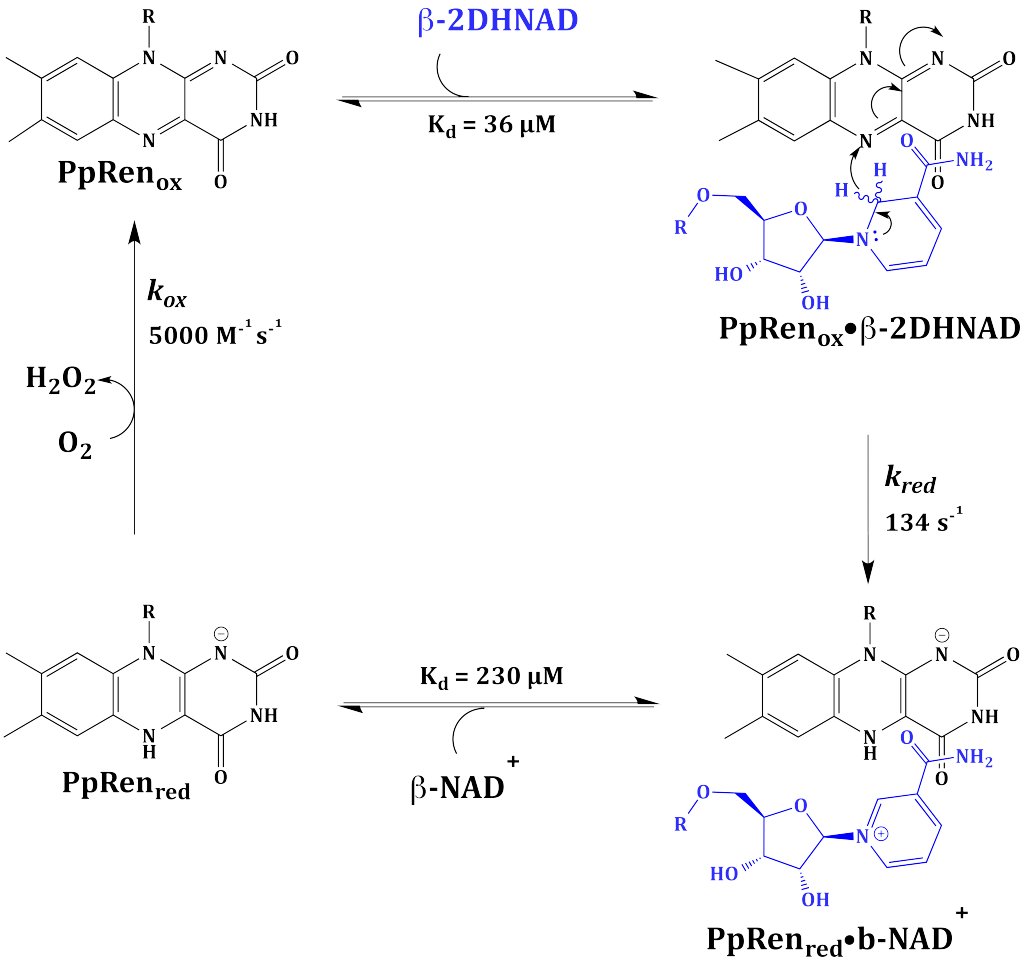

Scheme 6.3. Catalytic cycle of PpRen.

The PpRen structures represent a significant advancement in our understanding of the catalysis of this enzyme. Together, the PpRen•β-NADH and PpRen•β-NAD$^+$ structures offer evidence of the nature of the ES and EP complexes respectively. The reduction reaction catalyzed by renalase is exceedingly simple: the transfer of a hydride equivalent to the isoalloxazine of a flavin. The primary difference between this and numerous other enzymes is that the substrate nicotinamide is bound to afford hydride transfer from alternate positions of the pyridyl base (Figure 6.7). Possibly the most interesting aspect of renalase chemistry is that it accommodates reduction from both the 2 and 6 positions and

therefore must have binding modes for both substrate types. The structure of PpRen with β-NADH bound has the nicotinamide positioned such that the 2-position of the base is 3.6 Å from and directly over the N5 of the isoalloxazine ring (Figure 6.7C). No evidence of a flipped, 6-position reduction conformation, in the form of amide density in the alternate meta-position, in respect to the pyridyl nitrogen, is observed. Moreover, no density indicative of a lateral displacement of the nicotinamide to place the 6 position proximal to the flavin N5 is observed. As such it would appear that the rapid reduction rate constants observed with 2DHNAD(P) substrates are due to a more naturally optimized position whose conformer was selected in the crystalline state by the hydrogen bonding interaction with threonine 185.

Consistent with the relatively simple reaction being catalyzed, the number of conserved active site residues in renalase is small. The inner surface of the flavin re-face substrate cavity has only three fully conserved residues, H232, R280 and W276. Formally R280 is not positionally conserved, as it extends from a different secondary structural element in the bacterial enzyme (R193 in HsRen). However, the guanidino group of both residues resides in similar positions in the active site. It is posited that this charged residue is responsible for expulsion of the oxidized nicotinamide after hydride transfer and potentially facilitates the reduction chemistry by promoting the formation of the dihydroflavin anion. H232 is conserved in all known or annotated forms of renalase (H245 in HsRen). This residue is not required for acid/base chemistry in the reductive half reaction but may serve to add to the positive potential toward the internal reaches of the active site. H232 may participate in acid/base chemistry in the oxidative half reaction by shuttling protons to aid rapid elimination of hydrogen peroxide from a transient C4a-

(hydro)peroxyflavin during the oxidative half-reaction. This histidine is positioned 5.0 Å from the flavin N5 and C4a positions with both the β-NADH and β-NAD^+ ligands bound.

This study identifies the first known bacterial form of renalase. Defining true catalytic substrates for the human enzyme has both prompted re-evaluation of the true function of this enzyme and provided a means to definitively identify this activity in other organisms, including those without circulatory systems. In regard to the catalytic role of renalase, it has become very clear that claims concerning activity with catecholamines were quite incorrect, and were based on the propensity of such molecules to autoxidize in the presence of dioxygen. The elaboration of these claims throughout the last decade warrants some retrospection. While the observations included here and in prior work do not rule-out a non-catalytic moonlighting influence on vascular tone, they do argue strongly that the catalytic role of renalase serves an intracellular function that eliminates an inhibition of primary metabolism by β-NAD(P)H isomers.

References

1. Xu, J., Li, G., Wang, P., Velazquez, H., Yao, X., Li, Y., Wu, Y., Peixoto, A., Crowley, S., and Desir, G. V. (2005) Renalase is a novel, soluble monoamine oxidase that regulates cardiac function and blood pressure, *J Clin Invest 115*, 1275-1280.
2. Desir, G. V., Wang, L., and Peixoto, A. J. (2012) Human renalase: a review of its biology, function, and implications for hypertension, *J Am Soc Hypertens 6*, 417-426.
3. Desir, G. (2012) Novel insights into the physiology of renalase and its role in hypertension and heart disease, *Pediatr Nephrol 27*, 719-725.
4. Wu, Y., Xu, J., Velazquez, H., Wang, P., Li, G., Liu, D., Sampaio-Maia, B., Quelhas-Santos, J., Russell, K., Russell, R., Flavell, R. A., Pestana, M., Giordano, F., and Desir, G. V. (2011) Renalase deficiency aggravates ischemic myocardial damage, *Kidney Int 79*, 853-860.
5. Desir, G. V. (2011) Role of renalase in the regulation of blood pressure and the renal dopamine system, *Curr Opin Nephrol Hypertens 20*, 31-36.
6. Desir, G. V. (2007) Renalase is a novel renal hormone that regulates cardiovascular function, *J Am Soc Hypertens 1*, 99-103.
7. Li, X., Huang, R., Xie, Z., Lin, M., Liang, Z., Yang, Y., and Jiang, W. (2014) Renalase, a new secretory enzyme: Its role in hypertensive-ischemic cardiovascular diseases, *Med Sci Monit 20*, 688-692.
8. Xu, J., and Desir, G. V. (2007) Renalase, a new renal hormone: its role in health and disease, *Curr Opin Nephrol Hypertens 16*, 373-378.
9. Zhao, Q., Fan, Z., He, J., Chen, S., Li, H., Zhang, P., Wang, L., Hu, D., Huang, J., Qiang, B., and Gu, D. (2007) Renalase gene is a novel susceptibility gene for essential hypertension: a two-stage association study in northern Han Chinese population, *J Mol Med (Berl) 85*, 877-885.
10. Desir, G. V. (2008) Renalase deficiency in chronic kidney disease, and its contribution to hypertension and cardiovascular disease, *Curr Opin Nephrol Hypertens 17*, 181-185.
11. Li, G., Xu, J., Wang, P., Velazquez, H., Li, Y., Wu, Y., and Desir, G. V. (2008) Catecholamines regulate the activity, secretion, and synthesis of renalase, *Circulation 117*, 1277-1282.
12. Desir, G. V. (2009) Regulation of blood pressure and cardiovascular function by renalase, *Kidney Int 76*, 366-370.
13. Farzaneh-Far, R., Desir, G. V., Na, B., Schiller, N. B., and Whooley, M. A. (2010) A functional polymorphism in renalase (Glu37Asp) is associated with cardiac hypertrophy, dysfunction, and ischemia: data from the heart and soul study, *PLoS One 5*, e13496.
14. Medvedev, A. E., Veselovsky, A. V., and Fedchenko, V. I. (2010) Renalase, a new secretory enzyme responsible for selective degradation of catecholamines: achievements and unsolved problems, *Biochemistry (Mosc) 75*, 951-958.
15. Buraczynska, M., Zukowski, P., Buraczynska, K., Mozul, S., and Ksiazek, A. (2011) Renalase gene polymorphisms in patients with type 2 diabetes, hypertension and stroke, *Neuromolecular Med 13*, 321-327.

16. Gu, R., Lu, W., Xie, J., Bai, J., and Xu, B. (2011) Renalase deficiency in heart failure model of rats--a potential mechanism underlying circulating norepinephrine accumulation, *PLoS One 6*, e14633.
17. Przybylowski, P., Malyszko, J., Kozlowska, S., Koc-Zorawska, E., and Mysliwiec, M. (2011) Serum renalase depends on kidney function but not on blood pressure in heart transplant recipients, *Transplant Proc 43*, 3888-3891.
18. Baraka, A., and El Ghotny, S. (2012) Cardioprotective effect of renalase in 5/6 nephrectomized rats, *J Cardiovasc Pharmacol Ther 17*, 412-416.
19. Zbroch, E., Malyszko, J., Koc-Zorawska, E., and Mysliwiec, M. (2012) Renalase, kidney function, and markers of endothelial dysfunction in renal transplant recipients, *Pol Arch Med Wewn 122*, 40-44.
20. Zbroch, E., Malyszko, J., Malyszko, J. S., Koc-Zorawska, E., and Mysliwiec, M. (2012) Renalase, a novel enzyme involved in blood pressure regulation, is related to kidney function but not to blood pressure in hemodialysis patients, *Kidney Blood Press Res 35*, 395-399.
21. Czarkowska-Paczek, B., Zendzian-Piotrowska, M., Gala, K., Sobol, M., and Paczek, L. (2013) Exercise differentially regulates renalase expression in skeletal muscle and kidney, *Tohoku J Exp Med 231*, 321-329.
22. Lee, H. T., Kim, J. Y., Kim, M., Wang, P., Tang, L., Baroni, S., D'Agati, V. D., and Desir, G. V. (2013) Renalase protects against ischemic AKI, *J Am Soc Nephrol 24*, 445-455.
23. Przybylowski, P., Koc-Zorawska, E., Malyszko, J. S., Mysliwiec, M., and Malyszko, J. (2013) Renalase and endothelial dysfunction in heart transplant recipients, *Transplant Proc 45*, 394-396.
24. Sizova, D., Velazquez, H., Sampaio-Maia, B., Quelhas-Santos, J., Pestana, M., and Desir, G. V. (2013) Renalase regulates renal dopamine and phosphate metabolism, *Am J Physiol Renal Physiol 305*, F839-844.
25. Zbroch, E., Koc-Zorawska, E., Malyszko, J., and Mysliwiec, M. (2013) Circulating levels of renalase, norepinephrine, and dopamine in dialysis patients, *Ren Fail 35*, 673-679.
26. Desir, G. V., and Peixoto, A. J. (2014) Renalase in hypertension and kidney disease, *Nephrol Dial Transplant 29*, 22-28.
27. Sonawane, P. J., Gupta, V., Sasi, B. K., Kalyani, A., Natarajan, B., Khan, A. A., Sahu, B. S., and Mahapatra, N. R. (2014) Transcriptional regulation of the novel monoamine oxidase renalase: Crucial roles of transcription factors Sp1, STAT3, and ZBP89, *Biochemistry 53*, 6878-6892.
28. Wang, F., Huang, B., Li, J., Liu, L., and Wang, N. (2014) Renalase might be associated with hypertension and insulin resistance in Type 2 diabetes, *Ren Fail 36*, 552-556.
29. Wang, Y., Liu, F. Q., Wang, D., Mu, J. J., Ren, K. Y., Guo, T. S., Chu, C., Wang, L., Geng, L. K., and Yuan, Z. Y. (2014) Effect of salt intake and potassium supplementation on serum renalase levels in Chinese adults: a randomized trial, *Medicine (Baltimore) 93*, e44.
30. Wang, F., Li, J., Xing, T., Xie, Y., and Wang, N. (2014) Serum renalase is related to catecholamine levels and renal function, *Clin Exp Nephrol*.
31. Wybraniec, M. T., Mizia-Stec, K., Trojnarska, O., Chudek, J., Czerwienska, B., Wikarek, M., and Wiecek, A. (2014) Low plasma renalase concentration in hypertensive patients after surgical repair of coarctation of aorta, *J Am Soc Hypertens 8*, 464-474.

32. Quelhas-Santos, J., and Pestana, M. (2015) Plasma Renalase Expression in Chronic Kidney Disease: Differences and Similarities between Humans and Rats, *Curr Hypertens Rev*.
33. Guo, X., Hollander, L., MacPherson, D., Wang, L., Velazquez, H., Chang, J., Safirstein, R., Cha, C., Gorelick, F., and Desir, G. V. (2016) Inhibition of renalase expression and signaling has antitumor activity in pancreatic cancer, *Sci Rep 6*, 22996.
34. Quelhas-Santos, J., Serrao, M. P., Soares-Silva, I., Fernandes-Cerqueira, C., Simoes-Silva, L., Pinho, M. J., Remiao, F., Sampaio-Maia, B., Desir, G. V., and Pestana, M. (2015) Renalase regulates peripheral and central dopaminergic activities, *Am J Physiol Renal Physiol 308*, F84-91.
35. Qi, C., Wang, L., Zhang, M., Shao, X., Chang, X., Fan, Z., Cao, Q., Mou, S., Wang, Q., Yan, Y., Desir, G., and Ni, Z. (2015) Serum Renalase Levels Correlate with Disease Activity in Lupus Nephritis, *PLoS One 10*, e0139627.
36. Desir, G. V., Tang, L., Wang, P., Li, G., Sampaio-Maia, B., Quelhas-Santos, J., Pestana, M., and Velazquez, H. (2012) Renalase lowers ambulatory blood pressure by metabolizing circulating adrenaline, *J Am Heart Assoc 1*, e002634.
37. Guo, Y., and Jiang, W. (2012) [Research progress with renalase and cardiovascular disease], *Zhong Nan Da Xue Xue Bao Yi Xue Ban 37*, 537-540.
38. Wang, F., Li, J., Xing, T., Xie, Y., and Wang, N. (2015) Serum renalase is related to catecholamine levels and renal function, *Clin Exp Nephrol 19*, 92-98.
39. Quelhas-Santos, J., and Pestana, M. (2014) Plasma renalase in chronic kidney disease: differences and similarities between humans and rats, *Curr Hypertens Rev 10*, 166-170.
40. Ficek, J., Malyszko, J., and Chudek, J. (2015) [Renalase and its role in the development of hypertension in patients with chronic renal failure], *Przegl Lek 72*, 306-308.
41. Taranta-Janusz, K., Roszkowska, R., and Wasilewska, A. (2015) Renalase Levels in Children with Solitary Functioning Kidney, *Indian Pediatr 52*, 1047-1050.
42. Zheng, W. L., Wang, J., Mu, J. J., Liu, F. Q., Yuan, Z. Y., Wang, Y., Wang, D., Ren, K. Y., Guo, T. S., and Xiao, H. Y. (2016) Effects of salt intake and potassium supplementation on renalase expression in the kidneys of Dahl salt-sensitive rats, *Exp Biol Med (Maywood) 241*, 382-386.
43. Maciorkowska, D., Zbroch, E., and Malyszko, J. (2015) Circulating renalase, catecholamines, and vascular adhesion protein 1 in hypertensive patients, *J Am Soc Hypertens 9*, 855-864.
44. Shi, W. B., and Wang, H. Y. (2015) The association study on renalase polymorphism and hypertension: a meta-analysis, *Int J Clin Exp Med 8*, 9505-9511.
45. Zhou, M., Ma, C., Liu, W., Liu, H., Wang, N., Kang, Q., and Li, P. (2015) Valsartan Promoting Atherosclerotic Plaque Stabilization by Upregulating Renalase: A Potential-Related Gene of Atherosclerosis, *J Cardiovasc Pharmacol Ther 20*, 509-519.
46. Wang, F., Zhang, G., Xing, T., Lu, Z., Li, J., Peng, C., Liu, G., and Wang, N. (2015) Renalase contributes to the renal protection of delayed ischaemic preconditioning via the regulation of hypoxia-inducible factor-1alpha, *J Cell Mol Med 19*, 1400-1409.
47. Zhao, B., Zhao, Q., Li, J., Xing, T., Wang, F., and Wang, N. (2015) Renalase protects against contrast-induced nephropathy in Sprague-Dawley rats, *PLoS One 10*, e0116583.

48. Boomsma, F., and Tipton, K. F. (2007) Renalase, a catecholamine-metabolising enzyme?, *J Neural Transm (Vienna) 114*, 775-776.
49. Fava, C., Montagnana, M., Danese, E., Sjogren, M., Almgren, P., Engstrom, G., Hedblad, B., Guidi, G. C., Minuz, P., and Melander, O. (2012) The Renalase Asp37Glu polymorphism is not associated with hypertension and cardiovascular events in an urban-based prospective cohort: the Malmo Diet and cancer study, *BMC Med Genet 13*, 57.
50. Malyszko, J., Malyszko, J. S., Mikhailidis, D. P., Rysz, J., Zorawski, M., and Banach, M. (2012) Hypertension and kidney disease: is renalase a new player or an innocent bystander?, *J Hypertens 30*, 457-462.
51. Baroni, S., Milani, M., Pandini, V., Pavesi, G., Horner, D., and Aliverti, A. (2013) Is renalase a novel player in catecholaminergic signaling? The mystery of the catalytic activity of an intriguing new flavoenzyme, *Curr Pharm Des 19*, 2540-2551.
52. Malyszko, J., Bachorzewska-Gajewska, H., and Dobrzycki, S. (2015) Renalase, kidney and cardiovascular disease: are they related or just coincidentally associated?, *Adv Med Sci 60*, 41-49.
53. Beaupre, B. A., Carmichael, B. R., Hoag, M. R., Shah, D. D., and Moran, G. R. (2013) Renalase is an alpha-NAD(P)H oxidase/anomerase, *Journal of the American Chemical Society 135*, 13980-13987.
54. Beaupre, B. A., Hoag, M. R., Carmichael, B. R., and Moran, G. R. (2013) Kinetics and equilibria of the reductive and oxidative half-reactions of human renalase with alpha-NADPH, *Biochemistry 52*, 8929-8937.
55. Beaupre, B. A., Hoag, M. R., Roman, J., Forsterling, F. H., and Moran, G. R. (2015) Metabolic function for human renalase: oxidation of isomeric forms of beta-NAD(P)H that are inhibitory to primary metabolism, *Biochemistry 54*, 795-806.
56. Hoag, M. R., Roman, J., Beaupre, B. A., Silvaggi, N. R., and Moran, G. R. (2015) Bacterial Renalase: Structure and Kinetics of an Enzyme with 2- and 6-Dihydro-beta-NAD(P) Oxidase Activity from Pseudomonas phaseolicola, *Biochemistry 54*, 3791-3802.
57. Beaupre, B. A., Hoag, M. R., and Moran, G. R. (2015) Renalase does not catalyze the oxidation of catecholamines, *Arch Biochem Biophys 579*, 62-66.
58. Moran, G. R. (2016) The catalytic function of renalase: A decade of phantoms, *Biochim Biophys Acta 1864*, 177-186.
59. Eikelis, N., Hennebry, S. C., Lambert, G. W., and Schlaich, M. P. (2011) Does renalase degrade catecholamines?, *Kidney Int 79*, 1380; author reply 1380-1381.
60. Milani, M., Ciriello, F., Baroni, S., Pandini, V., Canevari, G., Bolognesi, M., and Aliverti, A. (2011) FAD-binding site and NADP reactivity in human renalase: a new enzyme involved in blood pressure regulation, *J Mol Biol 411*, 463-473.
61. Pandini, V., Ciriello, F., Tedeschi, G., Rossoni, G., Zanetti, G., and Aliverti, A. (2010) Synthesis of human renalase1 in Escherichia coli and its purification as a FAD-containing holoprotein, *Protein Expr Purif 72*, 244-253.
62. M.B. Mathews, E. E. C. (1953) The Reaction fo the Diphophopyridine Nucleotide with Sodium Borohydride, *Journal of the American Chemical Society 75*, 11.
63. Chakraverty, K., King, L., Watson, J. G., and Chaykin, S. (1969) Reduced 1,6-dihydrodiphosphopyridine nucleotide. Chemical properties and enzymatic modification, *J Biol Chem 244*, 4208-4217.

64. Chaykin, S., King, L., and Watson, J. G. (1966) The reduction of DPN+ and TPN+ with sodium borohydride, *Biochim Biophys Acta 124*, 13-25.
65. Chaykin, S., and Meissner, L. (1964) The borohydride reduction products of DPN, *Biochem Biophys Res Commun 14*, 233-240.
66. Chakraverty, K., and Chaykin, S. (1964) 1,6 DPNH, an enzymatically active form of reduced DPN, *Biochem Biophys Res Commun 15*, 262-268.
67. Lowry, O. H., Passonneau, J. V., and Rock, M. K. (1961) The stability of pyridine nucleotides, *J Biol Chem 236*, 2756-2759.
68. Dalziel, K. (1963) The purification of nicotinamide adenine dinucleotide and kinetic effects of nucleotide impurities, *J Biol Chem 238*, 1538-1543.
69. Burg, M. B., Kwon, E. D., and Kultz, D. (1997) Regulation of gene expression by hypertonicity, *Annu Rev Physiol 59*, 437-455.
70. Kempf, B., and Bremer, E. (1998) Uptake and synthesis of compatible solutes as microbial stress responses to high-osmolality environments, *Arch Microbiol 170*, 319-330.
71. McNeil, S. D., Nuccio, M. L., and Hanson, A. D. (1999) Betaines and related osmoprotectants. Targets for metabolic engineering of stress resistance, *Plant Physiol 120*, 945-950.
72. Bremer, E., and Kramer, A. (2000) Coping with Osmotic Chal- langes: Osmoregulation through Accumulation and Release of Compatible Solutes in Bacteria, in Bacterial Stress Response, *ASM Press*, 18.
73. Csonka, L. N., Epstein, W., Neidhart, F. C., Curtis, R., Ingraham, J. L., Lin, E. C., Low, K. B., Magasanik, B., Reznikoff, W. S., Riley, M., and Schaechter, D. C. (1996) Osmoregulation, in Escherichia coli and Salmonella: Cellular and Molecular Biology, *ASM Press*, 13.
74. Sakamoto, A., Valverde, R., Alia, Chen, T. H., and Murata, N. (2000) Transformation of Arabidopsis with the codA gene for choline oxidase enhances freezing tolerance of plants, *Plant J 22*, 449-453.
75. Sakamoto, A., Alia, and Murata, N. (1998) Metabolic engineering of rice leading to biosynthesis of glycinebetaine and tolerance to salt and cold, *Plant Mol Biol 38*, 1011-1019.
76. Ko, R., Smith, L. T., and Smith, G. M. (1994) Glycine betaine confers enhanced osmotolerance and cryotolerance on Listeria monocytogenes, *J Bacteriol 176*, 426-431.
77. Bayles, D. O., and Wilkinson, B. J. (2000) Osmoprotectants and cryoprotectants for Listeria monocytogenes, *Lett Appl Microbiol 30*, 23-27.
78. Sakamoto, A., and Murata, N. (2001) The use of bacterial choline oxidase, a glycinebetaine-synthesizing enzyme, to create stress-resistant transgenic plants, *Plant Physiol 125*, 180-188.
79. Ikuta, S., Imamura, S., Misaki, H., and Horiuti, Y. (1977) Purification and characterization of choline oxidase from Arthrobacter globiformis, *J Biochem 82*, 1741-1749.
80. Wright, J. R., and Clements, J. A. (1987) Metabolism and turnover of lung surfactant, *Am Rev Respir Dis 136*, 426-444.

81. Lisa, T. A., Casale, C. H., and Domenech, C. E. (1994) Cholinesterase, acid phosphatase, and phospholipase C of Pseudomonas aeruginosa under hyperosmotic conditions in a high-phosphate medium., *Curr. Microbiol. 28*, 5.
82. Peddie, B. A., Chambers, S. T., and Lever, M. (1996) Is the ability of urinary tract pathogens to accumulate glycine betaine a factor in the virulence of pathogenic strains?, *J Lab Clin Med 128*, 417-422.
83. Culham, D. E., Emmerson, K. S., Lasby, B., Mamelak, D., Steer, B. A., Gyles, C. L., Villarejo, M., and Wood, J. M. (1994) Genes encoding osmoregulatory proline/glycine betaine transporters and the proline catabolic system are present and expressed in diverse clinical Escherichia coli isolates, *Can J Microbiol 40*, 397-402.
84. Kunin, C. M., and Rudy, J. (1991) Effect of NaCl-induced osmotic stress on intracellular concentrations of glycine betaine and potassium in Escherichia coli, Enterococcus faecalis, and staphylococci, *J Lab Clin Med 118*, 217-224.
85. Landfald, B., and Strom, A. R. (1986) Choline-glycine betaine pathway confers a high level of osmotic tolerance in Escherichia coli, *J Bacteriol 165*, 849-855.
86. Lucht, J. M., and Bremer, E. (1994) Adaptation of Escherichia coli to high osmolarity environments: osmoregulation of the high-affinity glycine betaine transport system proU, *FEMS Microbiol Rev 14*, 3-20.
87. Finnegan, S., and Gadda, G. (2008) Substitution of an active site valine uncovers a kinetically slow equilibrium between competent and incompetent forms of choline oxidase, *Biochemistry 47*, 13850-13861.
88. Badger, J. L., and Kim, K. S. (1998) Environmental growth conditions influence the ability of Escherichia coli K1 to invade brain microvascular endothelial cells and confer serum resistance, *Infect Immun 66*, 5692-5697.
89. Schwan, W. R., Lee, J. L., Lenard, F. A., Matthews, B. T., and Beck, M. T. (2002) Osmolarity and pH growth conditions regulate fim gene transcription and type 1 pilus expression in uropathogenic Escherichia coli, *Infect Immun 70*, 1391-1402.
90. Rachid, S., Ohlsen, K., Witte, W., Hacker, J., and Ziebuhr, W. (2000) Effect of subinhibitory antibiotic concentrations on polysaccharide intercellular adhesin expression in biofilm-forming Staphylococcus epidermidis, *Antimicrob Agents Chemother 44*, 3357-3363.
91. Basso, H., Rharbaoui, F., Staendner, L. H., Medina, E., Garcia-Del Portillo, F., and Guzman, C. A. (2002) Characterization of a novel intracellularly activated gene from Salmonella enterica serovar typhi, *Infect Immun 70*, 5404-5411.
92. Leclerc, G. J., Tartera, C., and Metcalf, E. S. (1998) Environmental regulation of Salmonella typhi invasion-defective mutants, *Infect Immun 66*, 682-691.
93. Mohanty, A., Kathuria, H., Ferjani, A., Sakamoto, A., Mohanty, P., Murata, H., and Tyagi, A. K. (2002) Transgenics of an elite indica rice variety Pusa Basmati 1 harbouring the codA gene are highly tolerant to salt stress., *Theor. Appl. Genet. 106*, 6.
94. Ashraf, M., and Foolad, M. R. (2007) Roles of glycine betaine and proline in improving plant abiotic stress resistance, *Environmental and Experimental Botany 59*, 10.
95. Rhodes, D., and Hanson, A. D. (1993) Quaternary ammonium and tertiary sulfonium compounds in higher-plants., *Annu. Rev. Plant Physiol. Plant Mol. Biol 44*, 27.

96. Ohishi, N., and Yagi, K. (1979) Covalently bound flavin as prosthetic group of choline oxidase,\, *Biochem Biophys Res Commun 86*, 1084.
97. Ikuta, S., Imamura, S., Misaki, H., and Horiuti, Y. (1977) Purification and characterization of choline oxidase from Arthro- bacter globiformis, *J Biochem 82*, 8.
98. Fan, F., Ghanem, M., and Gadda, G. (2004) Cloning, sequence analysis, and purification of choline oxidase from Arthrobacter globiformis: a bacterial enzyme involved in osmotic stress tolerance, *Arch Biochem Biophys 421*, 149-158.
99. Gadda, G., Powell, N. L., and Menon, P. (2004) The trimethylammonium headgroup of choline is a major determinant for substrate binding and specificity in choline oxidase, *Arch Biochem Biophys 430*, 264-273.
100. Ghanem, M., Fan, F., Francis, K., and Gadda, G. (2003) Spectroscopic and kinetic properties of recombinant choline oxidase from Arthrobacter globiformis, *Biochemistry 42*, 15179-15188.
101. Gadda, G. (2003) pH and deuterium kinetic isotope effects studies on the oxidation of choline to betaine-aldehyde catalyzed by choline oxidase, *Biochim Biophys Acta 1650*, 4-9.
102. Gadda, G. (2003) Kinetic mechanism of choline oxidase from Arthrobacter globiformis, *Biochim Biophys Acta 1646*, 112-118.
103. Ghanem, M., and Gadda, G. (2005) On the catalytic role of the conserved active site residue His466 of choline oxidase, *Biochemistry 44*, 893-904.
104. Fan, F., and Gadda, G. (2005) On the catalytic mechanism of choline oxidase, *Journal of the American Chemical Society 127*, 2067-2074.
105. Fan, F., Germann, M. W., and Gadda, G. (2006) Mechanistic studies of choline oxidase with betaine aldehyde and its isosteric analogue 3,3-dimethylbutyraldehyde, *Biochemistry 45*, 1979-1986.
106. Gadda, G., Fan, F., and Hoang, J. V. (2006) On the contribution of the positively charged headgroup of choline to substrate binding and catalysis in the reaction catalyzed by choline oxidase, *Arch Biochem Biophys 451*, 182-187.
107. Fan, F., and Gadda, G. (2007) An internal equilibrium preorganizes the enzyme-substrate complex for hydride tunneling in choline oxidase, *Biochemistry 46*, 6402-6408.
108. Quaye, O., Lountos, G. T., Fan, F., Orville, A. M., and Gadda, G. (2008) Role of Glu312 in binding and positioning of the substrate for the hydride transfer reaction in choline oxidase, *Biochemistry 47*, 243-256.
109. Gadda, G. (2008) Hydride transfer made easy in the reaction of alcohol oxidation catalyzed by flavin-dependent oxidases, *Biochemistry 47*, 13745-13753.
110. Rungsrisuriyachai, K., and Gadda, G. (2008) On the role of histidine 351 in the reaction of alcohol oxidation catalyzed by choline oxidase, *Biochemistry 47*, 6762-6769.
111. Orville, A. M., Lountos, G. T., Finnegan, S., Gadda, G., and Prabhakar, R. (2009) Crystallographic, spectroscopic, and computational analysis of a flavin C4a-oxygen adduct in choline oxidase, *Biochemistry 48*, 720-728.
112. Quaye, O., and Gadda, G. (2009) Effect of a conservative mutation of an active site residue involved in substrate binding on the hydride tunneling reaction catalyzed by choline oxidase, *Arch Biochem Biophys 489*, 10-14.

113. Quaye, O., Cowins, S., and Gadda, G. (2009) Contribution of flavin covalent linkage with histidine 99 to the reaction catalyzed by choline oxidase, *J Biol Chem 284*, 16990-16997.
114. Xin, Y., Gadda, G., and Hamelberg, D. (2009) The cluster of hydrophobic residues controls the entrance to the active site of choline oxidase, *Biochemistry 48*, 9599-9605.
115. Quaye, O., Nguyen, T., Gannavaram, S., Pennati, A., and Gadda, G. (2010) Rescuing of the hydride transfer reaction in the Glu312Asp variant of choline oxidase by a substrate analogue, *Arch Biochem Biophys 499*, 1-5.
116. Rungsrisuriyachai, K., and Gadda, G. (2010) Role of asparagine 510 in the relative timing of substrate bond cleavages in the reaction catalyzed by choline oxidase, *Biochemistry 49*, 2483-2490.
117. Yuan, H., Fu, G., Brooks, P. T., Weber, I., and Gadda, G. (2010) Steady-state kinetic mechanism and reductive half-reaction of D-arginine dehydrogenase from Pseudomonas aeruginosa, *Biochemistry 49*, 9542-9550.
118. Salvi, F., and Gadda, G. (2013) Human choline dehydrogenase: medical promises and biochemical challenges, *Arch Biochem Biophys 537*, 243-252.
119. Ortega, E., de Marcos, S., Sanz-Vicente, I., Ubide, C., Ostra, M., Vidal, M., and Galban, J. (2016) Fluorescence of the Flavin group in choline oxidase. Insights and analytical applications for the determination of choline and betaine aldehyde, *Talanta 147*, 253-260.
120. Smitherman, C., Rungsrisuriyachai, K., Germann, M. W., and Gadda, G. (2015) Identification of the catalytic base for alcohol activation in choline oxidase, *Biochemistry 54*, 413-421.
121. Salvi, F., Rodriguez, I., Hamelberg, D., and Gadda, G. (2016) Role of F357 as an Oxygen Gate in the Oxidative Half-Reaction of Choline Oxidase, *Biochemistry 55*, 1473-1484.
122. Lambou, K., Pennati, A., Valsecchi, I., Tada, R., Sherman, S., Sato, H., Beau, R., Gadda, G., and Latge, J. P. (2013) Pathway of glycine betaine biosynthesis in Aspergillus fumigatus, *Eukaryot Cell 12*, 853-863.
123. Li, J., Vrielink, A., Brick, P., and Blow, D. M. (1993) Crystal structure of cholesterol oxidase complexed with a steroid substrate: implications for flavin adenine dinucleotide dependent alcohol oxidases, *Biochemistry 32*, 11507-11515.
124. Wohlfahrt, G., Witt, S., Hendle, J., Schomburg, D., Kalisz, H. M., and Hecht, H. J. (1999) 1.8 and 1.9 A resolution structures of the Penicillium amagasakiense and Aspergillus niger glucose oxidases as a basis for modelling substrate complexes, *Acta crystallographica. Section D, Biological crystallography 55*, 969-977.
125. Albrecht, M., and Lengauer, T. (2003) Pyranose oxidase identified as a member of the GMC oxidoreductase family, *Bioinformatics 19*, 1216-1220.
126. Bannwarth, M., Bastian, S., Heckmann-Pohl, D., Giffhorn, F., and Schulz, G. E. (2004) Crystal structure of pyranose 2-oxidase from the white-rot fungus Peniophora sp, *Biochemistry 43*, 11683-11690.
127. Cavener, D. R. (1992) GMC oxidoreductases. A newly defined family of homologous proteins with diverse catalytic activities, *J Mol Biol 223*, 811-814.

128. Hallberg, B. M., Henriksson, G., Pettersson, G., and Divne, C. (2002) Crystal structure of the flavoprotein domain of the extracellular flavocytochrome cellobiose dehydrogenase, *J Mol Biol 315*, 421-434.
129. Hallberg, B. M., Leitner, C., Haltrich, D., and Divne, C. (2004) Crystal structure of the 270 kDa homotetrameric lignin-degrading enzyme pyranose 2-oxidase, *J Mol Biol 341*, 781-796.
130. Hecht, H. J., Kalisz, H. M., Hendle, J., Schmid, R. D., and Schomburg, D. (1993) Crystal structure of glucose oxidase from Aspergillus niger refined at 2.3 A resolution, *J Mol Biol 229*, 153-172.
131. Henriksson, G., Johansson, G., and Pettersson, G. (2000) A critical review of cellobiose dehydrogenases, *J Biotechnol 78*, 93-113.
132. Kiess, M., Hecht, H. J., and Kalisz, H. M. (1998) Glucose oxidase from Penicillium amagasakiense. Primary structure and comparison with other glucose-methanol-choline (GMC) oxidoreductases, *Eur J Biochem 252*, 90-99.
133. Yue, Q. K., Kass, I. J., Sampson, N. S., and Vrielink, A. (1999) Crystal structure determination of cholesterol oxidase from Streptomyces and structural characterization of key active site mutants, *Biochemistry 38*, 4277-4286.
134. Finnegan, S., Yuan, H., Wang, Y. F., Orville, A. M., Weber, I. T., and Gadda, G. (2010) Structural and kinetic studies on the Ser101Ala variant of choline oxidase: catalysis by compromise, *Arch Biochem Biophys 501*, 207-213.
135. Finnegan, S., Agniswamy, J., Weber, I. T., and Gadda, G. (2010) Role of valine 464 in the flavin oxidation reaction catalyzed by choline oxidase, *Biochemistry 49*, 2952-2961.
136. Salvi, F., Wang, Y. F., Weber, I. T., and Gadda, G. (2014) Structure of choline oxidase in complex with the reaction product glycine betaine, *Acta crystallographica. Section D, Biological crystallography 70*, 405-413.
137. Rand, T., Halkier, T., and Hansen, O. C. (2003) Structural characterization and mapping of the covalently linked FAD cofactor in choline oxidase from Arthrobacter globiformis, *Biochemistry 42*, 7188-7194.
138. Baron, R., Riley, C., Chenprakhon, P., Thotsaporn, K., Winter, R. T., Alfieri, A., Forneris, F., van Berkel, W. J., Chaiyen, P., Fraaije, M. W., Mattevi, A., and McCammon, J. A. (2009) Multiple pathways guide oxygen diffusion into flavoenzyme active sites, *Proc Natl Acad Sci U S A 106*, 10603-10608.
139. Yuan, H., and Gadda, G. (2011) Importance of a serine proximal to the C(4a) and N(5) flavin atoms for hydride transfer in choline oxidase, *Biochemistry 50*, 770-779.
140. Leon, C. M., Barbosa, C. M., Justo, G. Z., Borelli, P., Resende, J. D., Jr., de Oliveira, J. S., Ferreira, A. T., and Paredes-Gamero, E. J. (2011) Requirement for PLCgamma2 in IL-3 and GM-CSF-stimulated MEK/ERK phosphorylation in murine and human hematopoietic stem/progenitor cells, *J Cell Physiol 226*, 1780-1792.
141. Wongnate, T., Sucharitakul, J., and Chaiyen, P. (2011) Identification of a catalytic base for sugar oxidation in the pyranose 2-oxidase reaction, *Chembiochem 12*, 2577-2586.
142. Rotsaert, F. A., Renganathan, V., and Gold, M. H. (2003) Role of the flavin domain residues, His689 and Asn732, in the catalytic mechanism of cellobiose dehydrogenase from phanerochaete chrysosporium, *Biochemistry 42*, 4049-4056.

143. Romero, E., and Gadda, G. (2014) Alcohol oxidation by flavoenzymes, *Biomol Concepts 5*, 299-318.
144. Ghanem, M., and Gadda, G. (2006) Effects of reversing the protein positive charge in the proximity of the flavin N(1) locus of choline oxidase, *Biochemistry 45*, 3437-3447.
145. Wencewicz, T. A., and Walsh, C. T. (2012) Pseudomonas syringae self-protection from tabtoxinine-beta-lactam by ligase TblF and acetylase Ttr, *Biochemistry 51*, 7712-7725.
146. Chaiyen, P., Fraaije, M. W., and Mattevi, A. (2012) The enigmatic reaction of flavins with oxygen, *Trends Biochem Sci 37*, 373-380.
147. Hemmerich, P., Nagelschneider, G., and Veeger, C. (1970) Chemistry and molecular biology of flavins and flavoproteins, *FEBS Lett 8*, 69-83.
148. Sobrado, P. (2012) Noncanonical reactions of flavoenzymes, *Int J Mol Sci 13*, 14219-14242.
149. Mansoorabadi, S. O., Thibodeaux, C. J., and Liu, H. W. (2007) The diverse roles of flavin coenzymes--nature's most versatile thespians, *J Org Chem 72*, 6329-6342.
150. Massey, V. (1994) Activation of molecular oxygen by flavins and flavoproteins, *J Biol Chem 269*, 22459-22462.
151. Palfey, B. A., and McDonald, C. A. (2010) Control of catalysis in flavin-dependent monooxygenases, *Arch Biochem Biophys 493*, 26-36.
152. Teufel, R., Miyanaga, A., Michaudel, Q., Stull, F., Louie, G., Noel, J. P., Baran, P. S., Palfey, B., and Moore, B. S. (2013) Flavin-mediated dual oxidation controls an enzymatic Favorskii-type rearrangement, *Nature 503*, 552-556.
153. Teufel, R., Stull, F., Meehan, M. J., Michaudel, Q., Dorrestein, P. C., Palfey, B., and Moore, B. S. (2015) Biochemical Establishment and Characterization of EncM's Flavin-N5-oxide Cofactor, *Journal of the American Chemical Society 137*, 8078-8085.
154. Piel, J., Hertweck, C., Shipley, P. R., Hunt, D. M., Newman, M. S., and Moore, B. S. (2000) Cloning, sequencing and analysis of the enterocin biosynthesis gene cluster from the marine isolate 'Streptomyces maritimus': evidence for the derailment of an aromatic polyketide synthase, *Chem Biol 7*, 943-955.
155. Cheng, Q., Xiang, L., Izumikawa, M., Meluzzi, D., and Moore, B. S. (2007) Enzymatic total synthesis of enterocin polyketides, *Nat Chem Biol 3*, 557-558.
156. Hertweck, C., Xiang, L., Kalaitzis, J. A., Cheng, Q., Palzer, M., and Moore, B. S. (2004) Context-dependent behavior of the enterocin iterative polyketide synthase; a new model for ketoreduction, *Chem Biol 11*, 461-468.
157. Xiang, L., Kalaitzis, J. A., and Moore, B. S. (2004) EncM, a versatile enterocin biosynthetic enzyme involved in Favorskii oxidative rearrangement, aldol condensation, and heterocycle-forming reactions, *Proc Natl Acad Sci U S A 101*, 15609-15614.
158. Seto, H., Sato, T., Urano, S., Uzawa, J., and Yonehara, H. (1976) Utilization of 13C-13C coupling in structural and biosynthetic studies. VII. The structure and biosynthesis of vulgamycin., *Tetrahedron Letters 48*, 3.
159. Crosby, J., and Crump, M. P. (2012) The structural role of the carrier protein--active controller or passive carrier, *Nat Prod Rep 29*, 1111-1137.
160. Entsch, B., Ballou, D. P., and Massey, V. (1976) Flavin-oxygen derivatives involved in hydroxylation by p-hydroxybenzoate hydroxylase, *J Biol Chem 251*, 2550-2563.

161. Entsch, B., and Ballou, D. P. (1989) Purification, properties, and oxygen reactivity of p-hydroxybenzoate hydroxylase from Pseudomonas aeruginosa, *Biochim Biophys Acta 999*, 313-322.
162. Rastetter, W. H., Gadek, T. R., Tane, J. P., and Frost, J. W. (1979) Oxidations and oxygen transfers effected by a flavin N(5)-oxide. A model for flavin-dependent monooxygenases., *Journal of the American Chemical Society 101*, 3.
163. Orf, H. W., and Dolphin, D. (1974) Oxaziridines as possible intermediates in flavin monooxygenases, *Proc Natl Acad Sci U S A 71*, 2646-2650.
164. Howlett, B. J., and Bar-Tana, J. (1980) Polyprenyl p-hydroxybenzoate carboxylase in flagellation of Salmonella typhimurium, *J Bacteriol 143*, 644-651.
165. Leppik, R. A., Young, I. G., and Gibson, F. (1976) Membrane-associated reactions in ubiquinone biosynthesis in Escherichia coli. 3-Octaprenyl-4-hydroxybenzoate carboxy-lyase, *Biochim Biophys Acta 436*, 800-810.
166. Cox, G. B., Young, I. G., McCann, L. M., and Gibson, F. (1969) Biosynthesis of ubiquinone in Escherichia coli K-12: location of genes affecting the metabolism of 3-octaprenyl-4-hydroxybenzoic acid and 2-octaprenylphenol, *J Bacteriol 99*, 450-458.
167. Meganathan, R. (2001) Ubiquinone biosynthesis in microorganisms, *FEMS Microbiol Lett 203*, 131-139.
168. Aussel, L., Pierrel, F., Loiseau, L., Lombard, M., Fontecave, M., and Barras, F. (2014) Biosynthesis and physiology of coenzyme Q in bacteria, *Biochim Biophys Acta 1837*, 1004-1011.
169. Gulmezian, M., Hyman, K. R., Marbois, B. N., Clarke, C. F., and Javor, G. T. (2007) The role of UbiX in Escherichia coli coenzyme Q biosynthesis, *Arch Biochem Biophys 467*, 144-153.
170. Zhang, H., and Javor, G. T. (2000) Identification of the ubiD gene on the Escherichia coli chromosome, *J Bacteriol 182*, 6243-6246.
171. Stratford, M., Plumridge, A., and Archer, D. B. (2007) Decarboxylation of sorbic acid by spoilage yeasts is associated with the PAD1 gene, *Appl Environ Microbiol 73*, 6534-6542.
172. Mukai, N., Masaki, K., Fujii, T., Kawamukai, M., and Iefuji, H. (2010) PAD1 and FDC1 are essential for the decarboxylation of phenylacrylic acids in Saccharomyces cerevisiae, *J Biosci Bioeng 109*, 564-569.
173. Richard, P., Viljanen, K., and Penttila, M. (2015) Overexpression of PAD1 and FDC1 results in significant cinnamic acid decarboxylase activity in Saccharomyces cerevisiae, *AMB Express 5*, 12.
174. Clausen, M., Lamb, C. J., Megnet, R., and Doerner, P. W. (1994) PAD1 encodes phenylacrylic acid decarboxylase which confers resistance to cinnamic acid in Saccharomyces cerevisiae, *Gene 142*, 107-112.
175. Zhang, H., and Javor, G. T. (2003) Regulation of the isofunctional genes ubiD and ubiX of the ubiquinone biosynthetic pathway of Escherichia coli, *FEMS Microbiol Lett 223*, 67-72.
176. Liu, J., and Liu, J. H. (2006) Ubiquinone (coenzyme Q) biosynthesis in Chlamydophila pneumoniae AR39: identification of the ubiD gene, *Acta Biochim Biophys Sin (Shanghai) 38*, 725-730.

177. Jacewicz, A., Izumi, A., Brunner, K., Schnell, R., and Schneider, G. (2013) Structural insights into the UbiD protein family from the crystal structure of PA0254 from Pseudomonas aeruginosa, *PLoS One 8*, e63161.
178. Do, H., Lee, J. H., Kwon, M. H., Song, H. E., An, J. Y., Eom, S. H., Lee, S. G., and Kim, H. J. (2013) Purification, characterization and preliminary X-ray diffraction analysis of a cold-active lipase (CpsLip) from the psychrophilic bacterium Colwellia psychrerythraea 34H, *Acta Crystallogr Sect F Struct Biol Cryst Commun 69*, 920-924.
179. Do, H., Kim, S. J., Lee, C. W., Kim, H. W., Park, H. H., Kim, H. M., Park, H., and Lee, J. H. (2015) Crystal structure of UbiX, an aromatic acid decarboxylase from the psychrophilic bacterium Colwellia psychrerythraea that undergoes FMN-induced conformational changes, *Sci Rep 5*, 8196.
180. Larsson, S., Nilvebrant, N. O., and Jonsson, L. J. (2001) Effect of overexpression of Saccharomyces cerevisiae Pad1p on the resistance to phenylacrylic acids and lignocellulose hydrolysates under aerobic and oxygen-limited conditions, *Appl Microbiol Biotechnol 57*, 167-174.
181. Lin, F., Ferguson, K. L., Boyer, D. R., Lin, X. N., and Marsh, E. N. (2015) Isofunctional enzymes PAD1 and UbiX catalyze formation of a novel cofactor required by ferulic acid decarboxylase and 4-hydroxy-3-polyprenylbenzoic acid decarboxylase, *ACS Chem Biol 10*, 1137-1144.
182. White, M. D., Payne, K. A., Fisher, K., Marshall, S. A., Parker, D., Rattray, N. J., Trivedi, D. K., Goodacre, R., Rigby, S. E., Scrutton, N. S., Hay, S., and Leys, D. (2015) UbiX is a flavin prenyltransferase required for bacterial ubiquinone biosynthesis, *Nature 522*, 502-506.
183. Payne, K. A., White, M. D., Fisher, K., Khara, B., Bailey, S. S., Parker, D., Rattray, N. J., Trivedi, D. K., Goodacre, R., Beveridge, R., Barran, P., Rigby, S. E., Scrutton, N. S., Hay, S., and Leys, D. (2015) New cofactor supports alpha,beta-unsaturated acid decarboxylation via 1,3-dipolar cycloaddition, *Nature 522*, 497-501.
184. Majer, F., Schmid, D. G., Altena, K., Bierbaum, G., and Kupke, T. (2002) The flavoprotein MrsD catalyzes the oxidative decarboxylation reaction involved in formation of the peptidoglycan biosynthesis inhibitor mersacidin, *J Bacteriol 184*, 1234-1243.
185. Blaesse, M., Kupke, T., Huber, R., and Steinbacher, S. (2003) Structure of MrsD, an FAD-binding protein of the HFCD family, *Acta crystallographica. Section D, Biological crystallography 59*, 1414-1421.
186. Blaesse, M., Kupke, T., Huber, R., and Steinbacher, S. (2000) Crystal structure of the peptidyl-cysteine decarboxylase EpiD complexed with a pentapeptide substrate, *Embo J 19*, 6299-6310.
187. Huang, J., He, Z., and Wiegel, J. (1999) Cloning, characterization, and expression of a novel gene encoding a reversible 4-hydroxybenzoate decarboxylase from Clostridium hydroxybenzoicum, *J Bacteriol 181*, 5119-5122.
188. Rangarajan, E. S., Li, Y., Iannuzzi, P., Tocilj, A., Hung, L. W., Matte, A., and Cygler, M. (2004) Crystal structure of a dodecameric FMN-dependent UbiX-like decarboxylase (Pad1) from Escherichia coli O157: H7, *Protein Sci 13*, 3006-3016.
189. Christendat, D., Yee, A., Dharamsi, A., Kluger, Y., Savchenko, A., Cort, J. R., Booth, V., Mackereth, C. D., Saridakis, V., Ekiel, I., Kozlov, G., Maxwell, K. L., Wu, N., McIntosh, L. P., Gehring, K., Kennedy, M. A., Davidson, A. R., Pai, E. F., Gerstein, M., Edwards, A. M.,

and Arrowsmith, C. H. (2000) Structural proteomics of an archaeon, *Nat Struct Biol 7*, 903-909.
190. Kopec, J., Schnell, R., and Schneider, G. (2011) Structure of PA4019, a putative aromatic acid decarboxylase from Pseudomonas aeruginosa, *Acta Crystallogr Sect F Struct Biol Cryst Commun 67*, 1184-1188.
191. Steinbacher, S., Hernandez-Acosta, P., Bieseler, B., Blaesse, M., Huber, R., Culianez-Macia, F. A., and Kupke, T. (2003) Crystal structure of the plant PPC decarboxylase AtHAL3a complexed with an ene-thiol reaction intermediate, *J Mol Biol 327*, 193-202.
192. Kupke, T., Hernandez-Acosta, P., Steinbacher, S., and Culianez-Macia, F. A. (2001) Arabidopsis thaliana flavoprotein AtHAL3a catalyzes the decarboxylation of 4'-Phosphopantothenoylcysteine to 4'-phosphopantetheine, a key step in coenzyme A biosynthesis, *J Biol Chem 276*, 19190-19196.
193. Manoj, N., and Ealick, S. E. (2003) Unusual space-group pseudosymmetry in crystals of human phosphopantothenoylcysteine decarboxylase, *Acta crystallographica. Section D, Biological crystallography 59*, 1762-1766.
194. Gao, Y., Honzatko, R. B., and Peters, R. J. (2012) Terpenoid synthase structures: a so far incomplete view of complex catalysis, *Nat Prod Rep 29*, 1153-1175.
195. Doud, E. H., Perlstein, D. L., Wolpert, M., Cane, D. E., and Walker, S. (2011) Two distinct mechanisms for TIM barrel prenyltransferases in bacteria, *Journal of the American Chemical Society 133*, 1270-1273.
196. Lupoli, T. J., Tsukamoto, H., Doud, E. H., Wang, T. S., Walker, S., and Kahne, D. (2011) Transpeptidase-mediated incorporation of D-amino acids into bacterial peptidoglycan, *Journal of the American Chemical Society 133*, 10748-10751.
197. Walsh, C. T., and Wencewicz, T. A. (2013) Flavoenzymes: versatile catalysts in biosynthetic pathways, *Nat Prod Rep 30*, 175-200.
198. Koehn, E. M., and Kohen, A. (2010) Flavin-dependent thymidylate synthase: a novel pathway towards thymine, *Arch Biochem Biophys 493*, 96-102.
199. Huisgen, R. (1963) 1,3-Dipolar Cycloadditions. Past and Future, *Angew. Chem. Int. Ed. Engl 2*.
200. Prantz, K., and Mulzer, J. (2010) Synthetic applications of the carbonyl generating Grob fragmentation, *Chem Rev 110*, 3741-3766.
201. Macheroux, P., Schmid, J., Amrhein, N., and Schaller, A. (1999) A unique reaction in a common pathway: mechanism and function of chorismate synthase in the shikimate pathway, *Planta 207*, 325-334.
202. Bornemann, S., Lowe, D. J., and Thorneley, R. N. (1996) Escherichia coli chorismate synthase, *Biochem Soc Trans 24*, 84-88.
203. Hill, R. K., and Newkome, G. R. (1969) Stereochemistry of chorismic acid biosynthesis, *Journal of the American Chemical Society 91*, 5893-5894.
204. Onderka, D. K., and Floss, H. G. (1969) Steric course of the chorismate synthetase reaction and the 3-deoxy-D-arabino-heptulosonate 7-phosphate (DAHP) synthetase reaction, *Journal of the American Chemical Society 91*, 5894-5896.
205. Morell, H., Clark, M. J., Knowles, P. F., and Sprinson, D. B. (1967) The enzymic synthesis of chorismic and prephenic acids from 3-enolpyruvylshikimic acid 5-phosphate, *J Biol Chem 242*, 82-90.

206. Welch, G. R., Cole, K. W., and Gaertner, F. H. (1974) Chorismate synthase of Neurospora crassa: a flavoprotein, *Arch Biochem Biophys 165*, 505-518.
207. Hasan, N., and Nester, E. W. (1978) Purification and properties of chorismate synthase from Bacillus subtilis, *J Biol Chem 253*, 4993-4998.
208. Floss, H. G., Onderka, D. K., and Carroll, M. (1972) Stereochemistry of the 3-deoxy-D-arabino-heptulosonate 7-phosphate synthetase reaction and the chorismate synthetase reaction, *J Biol Chem 247*, 736-744.
209. Bornemann, S., Ramjee, M. K., Balasubramanian, S., Abell, C., Coggins, J. R., Lowe, D. J., and Thorneley, R. N. (1995) Escherichia coli chorismate synthase catalyzes the conversion of (6S)-6-fluoro-5-enolpyruvylshikimate-3-phosphate to 6-fluorochorismate. Implications for the enzyme mechanism and the antimicrobial action of (6S)-6-fluoroshikimate, *J Biol Chem 270*, 22811-22815.
210. White, P. J., Millar, G., and Coggins, J. R. (1988) The overexpression, purification and complete amino acid sequence of chorismate synthase from Escherichia coli K12 and its comparison with the enzyme from Neurospora crassa, *Biochem J 251*, 313-322.
211. Mousdale, D. M., and Coggins, J. R. (1986) Rapid chromatographic purification of glyphosate-sensitive 5-enolpyruvylshikimate 3-phosphate synthase from higher plant chloroplasts, *J Chromatogr 367*, 217-222.
212. Schaller, A., van Afferden, M., Windhofer, V., Bulow, S., Abel, G., Schmid, J., and Amrhein, N. (1991) Purification and Characterization of Chorismate Synthase from Euglena gracilis: Comparison with Chorismate Synthases of Plant and Microbial Origin, *Plant Physiol 97*, 1271-1279.
213. Schaller, A., Schmid, J., Leibinger, U., and Amrhein, N. (1991) Molecular cloning and analysis of a cDNA coding for chorismate synthase from the higher plant Corydalis sempervirens Pers, *J Biol Chem 266*, 21434-21438.
214. Bornemann, S., Lowe, D. J., and Thorneley, R. N. (1996) The transient kinetics of Escherichia coli chorismate synthase: substrate consumption, product formation, phosphate dissociation, and characterization of a flavin intermediate, *Biochemistry 35*, 9907-9916.
215. Macheroux, P., Petersen, J., Bornemann, S., Lowe, D. J., and Thorneley, R. N. (1996) Binding of the oxidized, reduced, and radical flavin species to chorismate synthase. An investigation by spectrophotometry, fluorimetry, and electron paramagnetic resonance and electron nuclear double resonance spectroscopy, *Biochemistry 35*, 1643-1652.
216. Macheroux, P., Bornemann, S., Ghisla, S., and Thorneley, R. N. (1996) Studies with flavin analogs provide evidence that a protonated reduced FMN is the substrate-induced transient intermediate in the reaction of Escherichia coli chorismate synthase, *J Biol Chem 271*, 25850-25858.
217. Osborne, A., Thorneley, R. N., Abell, C., and Bornemann, S. (2000) Studies with substrate and cofactor analogues provide evidence for a radical mechanism in the chorismate synthase reaction, *J Biol Chem 275*, 35825-35830.
218. Fitzpatrick, T. B., Killer, P., Thomas, R. M., Jelesarov, I., Amrhein, N., and Macheroux, P. (2001) Chorismate synthase from the hyperthermophile Thermotoga maritima combines thermostability and increased rigidity with catalytic and spectral properties similar to mesophilic counterparts, *J Biol Chem 276*, 18052-18059.

219. Maclean, J., and Ali, S. (2003) The structure of chorismate synthase reveals a novel flavin binding site fundamental to a unique chemical reaction, *Structure 11*, 1499-1511.
220. Kitzing, K., Auweter, S., Amrhein, N., and Macheroux, P. (2004) Mechanism of chorismate synthase. Role of the two invariant histidine residues in the active site, *J Biol Chem 279*, 9451-9461.
221. Rauch, G., Ehammer, H., Bornemann, S., and Macheroux, P. (2007) Mutagenic analysis of an invariant aspartate residue in chorismate synthase supports its role as an active site base, *Biochemistry 46*, 3768-3774.
222. Rauch, G., Ehammer, H., Bornemann, S., and Macheroux, P. (2008) Replacement of two invariant serine residues in chorismate synthase provides evidence that a proton relay system is essential for intermediate formation and catalytic activity, *Febs J 275*, 1464-1473.
223. Gaertner, F. H., and Cole, K. W. (1973) Properties of chorismate synthase in Neurospora crassa, *J Biol Chem 248*, 4602-4609.
224. Gaertner, F. H. (1987) Chorismate synthase: a bifunctional enzyme in Neurospora crassa, *Methods Enzymol 142*, 362-366.
225. Fraaije, M. W., and Mattevi, A. (2000) Flavoenzymes: diverse catalysts with recurrent features, *Trends Biochem Sci 25*, 126-132.
226. van Berkel, W. J., Kamerbeek, N. M., and Fraaije, M. W. (2006) Flavoprotein monooxygenases, a diverse class of oxidative biocatalysts, *J Biotechnol 124*, 670-689.
227. Macheroux, P., Schonbrunn, E., Svergun, D. I., Volkov, V. V., Koch, M. H., Bornemann, S., and Thorneley, R. N. (1998) Evidence for a major structural change in Escherichia coli chorismate synthase induced by flavin and substrate binding, *Biochem J 335 (Pt 2)*, 319-327.
228. fukui, K. (1965) Stereoselectivity associated with noncycloaddition, *Tetrahedron Letters 28*, 5.
229. Hill, R. K. (1978) Stereochemistry of 1,4-conjugate elimination reactions, *Journal of the American Chemical Society 100*, 2.
230. Anh, N. (1968) Stereochemistry of some reactions: SN2¢, SE2¢, and E2 additions to polyenes., *Chemical Communications*, 2.
231. Viola, C. M., Saridakis, V., and Christendat, D. (2004) Crystal structure of chorismate synthase from Aquifex aeolicus reveals a novel beta alpha beta sandwich topology, *Proteins 54*, 166-169.
232. Quevillon-Cheruel, S., Leulliot, N., Meyer, P., Graille, M., Bremang, M., Blondeau, K., Sorel, I., Poupon, A., Janin, J., and van Tilbeurgh, H. (2004) Crystal structure of the bifunctional chorismate synthase from Saccharomyces cerevisiae, *J Biol Chem 279*, 619-625.
233. Shindyalov, I. N., and Bourne, P. E. (1998) Protein structure alignment by incremental combinatorial extension (CE) of the optimal path, *Protein Eng 11*, 739-747.
234. Berman, H. M., Westbrook, J., Feng, Z., Gilliland, G., Bhat, T. N., Weissig, H., Shindyalov, I. N., and Bourne, P. E. (2000) The Protein Data Bank, *Nucleic Acids Res 28*, 235-242.
235. Nassau, P. M., Martin, S. L., Brown, R. E., Weston, A., Monsey, D., McNeil, M. R., and Duncan, K. (1996) Galactofuranose biosynthesis in Escherichia coli K-12:

identification and cloning of UDP-galactopyranose mutase, *J Bacteriol 178*, 1047-1052.
236. Beverley, S. M., Owens, K. L., Showalter, M., Griffith, C. L., Doering, T. L., Jones, V. C., and McNeil, M. R. (2005) Eukaryotic UDP-galactopyranose mutase (GLF gene) in microbial and metazoal pathogens, *Eukaryot Cell 4*, 1147-1154.
237. Koplin, R., Brisson, J. R., and Whitfield, C. (1997) UDP-galactofuranose precursor required for formation of the lipopolysaccharide O antigen of Klebsiella pneumoniae serotype O1 is synthesized by the product of the rfbDKPO1 gene, *J Biol Chem 272*, 4121-4128.
238. Weston, A., Stern, R. J., Lee, R. E., Nassau, P. M., Monsey, D., Martin, S. L., Scherman, M. S., Besra, G. S., Duncan, K., and McNeil, M. R. (1997) Biosynthetic origin of mycobacterial cell wall galactofuranosyl residues, *Tuber Lung Dis 78*, 123-131.
239. Novelli, J. F., Chaudhary, K., Canovas, J., Benner, J. S., Madinger, C. L., Kelly, P., Hodgkin, J., and Carlow, C. K. (2009) Characterization of the Caenorhabditis elegans UDP-galactopyranose mutase homolog glf-1 reveals an essential role for galactofuranose metabolism in nematode surface coat synthesis, *Dev Biol 335*, 340-355.
240. Pan, F., Jackson, M., Ma, Y., and McNeil, M. (2001) Cell wall core galactofuran synthesis is essential for growth of mycobacteria, *J Bacteriol 183*, 3991-3998.
241. Latge, J. P. (1999) Aspergillus fumigatus and aspergillosis, *Clin Microbiol Rev 12*, 310-350.
242. Schmalhorst, P. S., Krappmann, S., Vervecken, W., Rohde, M., Muller, M., Braus, G. H., Contreras, R., Braun, A., Bakker, H., and Routier, F. H. (2008) Contribution of galactofuranose to the virulence of the opportunistic pathogen Aspergillus fumigatus, *Eukaryot Cell 7*, 1268-1277.
243. Turco, S. J., and Descoteaux, A. (1992) The lipophosphoglycan of Leishmania parasites, *Annu Rev Microbiol 46*, 65-94.
244. Kleczka, B., Lamerz, A. C., van Zandbergen, G., Wenzel, A., Gerardy-Schahn, R., Wiese, M., and Routier, F. H. (2007) Targeted gene deletion of Leishmania major UDP-galactopyranose mutase leads to attenuated virulence, *J Biol Chem 282*, 10498-10505.
245. Richards, M. R., and Lowary, T. L. (2009) Chemistry and biology of galactofuranose-containing polysaccharides, *Chembiochem 10*, 1920-1938.
246. Partha, S. K., Sadeghi-Khomami, A., Slowski, K., Kotake, T., Thomas, N. R., Jakeman, D. L., and Sanders, D. A. (2010) Chemoenzymatic synthesis, inhibition studies, and X-ray crystallographic analysis of the phosphono analog of UDP-Galp as an inhibitor and mechanistic probe for UDP-galactopyranose mutase, *J Mol Biol 403*, 578-590.
247. Veerapen, N., Yuan, Y., Sanders, D. A., and Pinto, B. M. (2004) Synthesis of novel ammonium and selenonium ions and their evaluation as inhibitors of UDP-galactopyranose mutase, *Carbohydr Res 339*, 2205-2217.
248. Itoh, K., S., H. Z., and Liu, H. W. (2007) *Organic letters 9*, 3.
249. Kuppala, R., Borrelli, S., Slowski, K., Sanders, D. A., Ravindranathan Kartha, K. P., and Pinto, B. M. (2015) Synthesis and biological evaluation of nonionic substrate mimics of UDP-Galp as candidate inhibitors of UDP galactopyranose mutase (UGM), *Bioorg Med Chem Lett 25*, 1995-1997.

250. El Bkassiny, S., N'Go, I., Sevrain, C. M., Tikad, A., and Vincent, S. P. (2014) Synthesis of a novel UDP-carbasugar as UDP-galactopyranose mutase inhibitor, *Organic letters 16*, 2462-2465.
251. Mahdavi-Amiri, Y., Mohan, S., Borrelli, S., Slowski, K., Sanders, D. A., and Pinto, B. M. (2016) Mechanism-based candidate inhibitors of uridine diphosphate galactopyranose mutase (UGM), *Carbohydr Res 419*, 1-7.
252. Borrelli, S., Zandberg, W. F., Mohan, S., Ko, M., Martinez-Gutierrez, F., Partha, S. K., Sanders, D. A., Av-Gay, Y., and Pinto, B. M. (2010) Antimycobacterial activity of UDP-galactopyranose mutase inhibitors, *Int J Antimicrob Agents 36*, 364-368.
253. Dykhuizen, E. C., May, J. F., Tongpenyai, A., and Kiessling, L. L. (2008) Inhibitors of UDP-galactopyranose mutase thwart mycobacterial growth, *Journal of the American Chemical Society 130*, 6706-6707.
254. Soltero-Higgin, M., Carlson, E. E., Phillips, J. H., and Kiessling, L. L. (2004) Identification of inhibitors for UDP-galactopyranose mutase, *Journal of the American Chemical Society 126*, 10532-10533.
255. Sanders, D. A., Staines, A. G., McMahon, S. A., McNeil, M. R., Whitfield, C., and Naismith, J. H. (2001) UDP-galactopyranose mutase has a novel structure and mechanism, *Nat Struct Biol 8*, 858-863.
256. Oppenheimer, M., Poulin, M. B., Lowary, T. L., Helm, R. F., and Sobrado, P. (2010) Characterization of recombinant UDP-galactopyranose mutase from Aspergillus fumigatus, *Arch Biochem Biophys 502*, 31-38.
257. Goni, G., Serrano, A., Frago, S., Hervas, M., Peregrina, J. R., De la Rosa, M. A., Gomez-Moreno, C., Navarro, J. A., and Medina, M. (2008) Flavodoxin-mediated electron transfer from photosystem I to ferredoxin-NADP+ reductase in Anabaena: role of flavodoxin hydrophobic residues in protein-protein interactions, *Biochemistry 47*, 1207-1217.
258. Oppenheimer, M., Valenciano, A. L., and Sobrado, P. (2011) Isolation and characterization of functional Leishmania major virulence factor UDP-galactopyranose mutase, *Biochem Biophys Res Commun 407*, 552-556.
259. Zhang, Q., and Liu, H. W. (2000) Studies of UDP-Galactopyranose Mutase from Escherichia coli: An Unusual Role of Reduced FAD in Its Catalysis, *Journal of the American Chemical Society 122*, 5.
260. Zhang, Q., and Liu, H. W. (2001) Chemical synthesis of UDP-beta-L-arabinofuranose and its turnover to UDP-beta-L-arabinopyranose by UDP-galactopyranose mutase, *Bioorg Med Chem Lett 11*, 145-149.
261. Oppenheimer, M., Valenciano, A. L., Kizjakina, K., Qi, J., and Sobrado, P. (2012) Chemical mechanism of UDP-galactopyranose mutase from Trypanosoma cruzi: a potential drug target against Chagas' disease, *PLoS One 7*, e32918.
262. Dhatwalia, R., Singh, H., Solano, L. M., Oppenheimer, M., Robinson, R. M., Ellerbrock, J. F., Sobrado, P., and Tanner, J. J. (2012) Identification of the NAD(P)H binding site of eukaryotic UDP-galactopyranose mutase, *Journal of the American Chemical Society 134*, 18132-18138.
263. Fonseca, I. O., Kizjakina, K., and Sobrado, P. (2013) UDP-galactopyranose mutases from Leishmania species that cause visceral and cutaneous leishmaniasis, *Arch Biochem Biophys 538*, 103-110.

264. Tanner, J. J., Boechi, L., Andrew McCammon, J., and Sobrado, P. (2014) Structure, mechanism, and dynamics of UDP-galactopyranose mutase, *Arch Biochem Biophys 544*, 128-141.
265. Barlow, J. N., Marcinkeviciene, J., and Blanchard, J. S. (1999) The enzymatic conversion of UDP-galactopyranose to UDP-galactofuranose, *Biomedical and Health Research 27*, 8.
266. Gusarov, I., Starodubtseva, M., Wang, Z. Q., McQuade, L., Lippard, S. J., Stuehr, D. J., and Nudler, E. (2008) Bacterial nitric-oxide synthases operate without a dedicated redox partner, *J Biol Chem 283*, 13140-13147.
267. van Straaten, K. E., Kuttiyatveetil, J. R., Sevrain, C. M., Villaume, S. A., Jimenez-Barbero, J., Linclau, B., Vincent, S. P., and Sanders, D. A. (2015) Structural basis of ligand binding to UDP-galactopyranose mutase from Mycobacterium tuberculosis using substrate and tetrafluorinated substrate analogues, *Journal of the American Chemical Society 137*, 1230-1244.
268. Gruber, T. D., Westler, W. M., Kiessling, L. L., and Forest, K. T. (2009) X-ray crystallography reveals a reduced substrate complex of UDP-galactopyranose mutase poised for covalent catalysis by flavin, *Biochemistry 48*, 9171-9173.
269. Partha, S. K., van Straaten, K. E., and Sanders, D. A. (2009) Structural basis of substrate binding to UDP-galactopyranose mutase: crystal structures in the reduced and oxidized state complexed with UDP-galactopyranose and UDP, *J Mol Biol 394*, 864-877.
270. van Straaten, K. E., Routier, F. H., and Sanders, D. A. (2012) Structural insight into the unique substrate binding mechanism and flavin redox state of UDP-galactopyranose mutase from Aspergillus fumigatus, *J Biol Chem 287*, 10780-10790.
271. van Straaten, K. E., Routier, F. H., and Sanders, D. A. (2012) Towards the crystal structure elucidation of eukaryotic UDP-galactopyranose mutase, *Acta Crystallogr Sect F Struct Biol Cryst Commun 68*, 455-459.
272. Sun, H. G., Ruszczycky, M. W., Chang, W. C., Thibodeaux, C. J., and Liu, H. W. (2012) Nucleophilic participation of reduced flavin coenzyme in mechanism of UDP-galactopyranose mutase, *J Biol Chem 287*, 4602-4608.
273. Huang, Z., Zhang, Q., and Liu, H. W. (2003) Reconstitution of UDP-galactopyranose mutase with 1-deaza-FAD and 5-deaza-FAD: analysis and mechanistic implications, *Bioorg Chem 31*, 494-502.
274. Mehra-Chaudhary, R., Dai, Y., Sobrado, P., and Tanner, J. J. (2016) In Crystallo Capture of a Covalent Intermediate in the UDP-Galactopyranose Mutase Reaction, *Biochemistry 55*, 833-836.
275. Gruber, T. D., Borrok, M. J., Westler, W. M., Forest, K. T., and Kiessling, L. L. (2009) Ligand binding and substrate discrimination by UDP-galactopyranose mutase, *J Mol Biol 391*, 327-340.
276. Soltero-Higgin, M., Carlson, E. E., Gruber, T. D., and Kiessling, L. L. (2004) A unique catalytic mechanism for UDP-galactopyranose mutase, *Nat Struct Mol Biol 11*, 539-543.
277. Barlow, J. N., Girvin, M. E., and Blanchard, J. S. (1999) Positional Isope Exchange Catalyzed by UDP-galactopyranose Mutase, *Journal of the American Chemical Society 121*, 11.

278. Zhang, Q., and Liu, H. (2001) Mechanistic investigation of UDP-galactopyranose mutase from Escherichia coli using 2- and 3-fluorinated UDP-galactofuranose as probes, *Journal of the American Chemical Society 123*, 6756-6766.
279. Fullerton, S. W., Daff, S., Sanders, D. A., Ingledew, W. J., Whitfield, C., Chapman, S. K., and Naismith, J. H. (2003) Potentiometric analysis of UDP-galactopyranose mutase: stabilization of the flavosemiquinone by substrate, *Biochemistry 42*, 2104-2109.
280. Huang, W., and Gauld, J. W. (2012) Tautomerization in the UDP-galactopyranose mutase mechanism: a DFT-cluster and QM/MM investigation, *J Phys Chem B 116*, 14040-14050.
281. Poulin, M. B., Shi, Y., Protsko, C., Dalrymple, S. A., Sanders, D. A., Pinto, B. M., and Lowary, T. L. (2014) Specificity of a UDP-GalNAc pyranose-furanose mutase: a potential therapeutic target for Campylobacter jejuni infections, *Chembiochem 15*, 47-56.
282. Dhatwalia, R., Singh, H., Oppenheimer, M., Sobrado, P., and Tanner, J. J. (2012) Crystal structures of Trypanosoma cruzi UDP-galactopyranose mutase implicate flexibility of the histidine loop in enzyme activation, *Biochemistry 51*, 4968-4979.
283. Dhatwalia, R., Singh, H., Oppenheimer, M., Karr, D. B., Nix, J. C., Sobrado, P., and Tanner, J. J. (2012) Crystal structures and small-angle x-ray scattering analysis of UDP-galactopyranose mutase from the pathogenic fungus Aspergillus fumigatus, *J Biol Chem 287*, 9041-9051.
284. Beis, K., Srikannathasan, V., Liu, H., Fullerton, S. W., Bamford, V. A., Sanders, D. A., Whitfield, C., McNeil, M. R., and Naismith, J. H. (2005) Crystal structures of Mycobacteria tuberculosis and Klebsiella pneumoniae UDP-galactopyranose mutase in the oxidised state and Klebsiella pneumoniae UDP-galactopyranose mutase in the (active) reduced state, *J Mol Biol 348*, 971-982.
285. Kincaid, V. A., London, N., Wangkanont, K., Wesener, D. A., Marcus, S. A., Heroux, A., Nedyalkova, L., Talaat, A. M., Forest, K. T., Shoichet, B. K., and Kiessling, L. L. (2015) Virtual Screening for UDP-Galactopyranose Mutase Ligands Identifies a New Class of Antimycobacterial Agents, *ACS Chem Biol 10*, 2209-2218.
286. Da Fonseca, I., Qureshi, I. A., Mehra-Chaudhary, R., Kizjakina, K., Tanner, J. J., and Sobrado, P. (2014) Contributions of unique active site residues of eukaryotic UDP-galactopyranose mutases to substrate recognition and active site dynamics, *Biochemistry 53*, 7794-7804.
287. Cristescu, M. E., and Egbosimba, E. E. (2009) Evolutionary history of D-lactate dehydrogenases: a phylogenomic perspective on functional diversity in the FAD binding oxidoreductase/transferase type 4 family, *J Mol Evol 69*, 276-287.
288. Krissinel, E., and Henrick, K. (2004) Secondary-structure matching (SSM), a new tool for fast protein structure alignment in three dimensions, *Acta crystallographica. Section D, Biological crystallography 60*, 2256-2268.
289. Penman, G. A., Lockhart, D. E., Ferenbach, A., and van Aalten, D. M. (2012) Purification, crystallization and preliminary X-ray diffraction data of UDP-galactopyranose mutase from Aspergillus fumigatus, *Acta Crystallogr Sect F Struct Biol Cryst Commun 68*, 705-708.
290. Derewenda, Z. S. (2004) Rational protein crystallization by mutational surface engineering, *Structure 12*, 529-535.

291. Goldschmidt, L., Cooper, D. R., Derewenda, Z. S., and Eisenberg, D. (2007) Toward rational protein crystallization: A Web server for the design of crystallizable protein variants, *Protein Sci 16*, 1569-1576.
292. Bottoms, C. A., Smith, P. E., and Tanner, J. J. (2002) A structurally conserved water molecule in Rossmann dinucleotide-binding domains, *Protein Sci 11*, 2125-2137.
293. Kleiger, G., and Eisenberg, D. (2002) GXXXG and GXXXA motifs stabilize FAD and NAD(P)-binding Rossmann folds through C(alpha)-H... O hydrogen bonds and van der waals interactions, *J Mol Biol 323*, 69-76.
294. Luft, F. C. (2005) Renalase, a catecholamine-metabolizing hormone from the kidney, *Cell Metab 1*, 358-360.
295. Humes, H. D. (1995) Acute renal failure: prevailing challenges and prospects for the future, *Kidney Int Suppl 50*, S26-32.
296. Stec, A., Semczuk, A., Furmaga, J., Ksiazek, A., and Buraczynska, M. (2012) Polymorphism of the renalase gene in end-stage renal disease patients affected by hypertension, *Nephrol Dial Transplant 27*, 4162-4166.
297. Zhang, R., Li, X., Liu, N., Guo, X., Liu, W., Ning, C., Wang, Z., Sun, L., and Fu, S. (2013) An association study on renalase polymorphisms and ischemic stroke in a chinese population, *Neuromolecular Med 15*, 396-404.
298. Alhasan, R., and Njus, D. (2008) The epinephrine assay for superoxide: why dopamine does not work, *Anal Biochem 381*, 142-147.
299. Misra, H. P., and Fridovich, I. (1972) The role of superoxide anion in the autoxidation of epinephrine and a simple assay for superoxide dismutase, *J Biol Chem 247*, 3170-3175.
300. Oppenheimer, N. J. (1982) Chemistry and Solution Confromation of Pyridine Nucleotides, In *The Pyridine Nucletide coenzymes* (Everse, J., Anderson, B., and You, K.-S., Eds.), pp 51-90, Academic Press Inc., New York.
301. Hennebry, S. C., Eikelis, N., Socratous, F., Desir, G., Lambert, G., and Schlaich, M. (2010) Renalase, a novel soluble FAD-dependent protein, is synthesized in the brain and peripheral nerves, *Mol Psychiatry 15*, 234-236.
302. Anand, R., and Marmorstein, R. (2007) Structure and mechanism of lysine-specific demethylase enzymes, *J Biol Chem 282*, 35425-35429.
303. Chen, Y., Yang, Y., Wang, F., Wan, K., Yamane, K., Zhang, Y., and Lei, M. (2006) Crystal structure of human histone lysine-specific demethylase 1 (LSD1), *Proc Natl Acad Sci U S A 103*, 13956-13961.
304. Schreuder, H. A., Prick, P. A., Wierenga, R. K., Vriend, G., Wilson, K. S., Hol, W. G., and Drenth, J. (1989) Crystal structure of the p-hydroxybenzoate hydroxylase-substrate complex refined at 1.9 A resolution. Analysis of the enzyme-substrate and enzyme-product complexes, *J Mol Biol 208*, 679-696.
305. Faust, A., Niefind, K., Hummel, W., and Schomburg, D. (2007) The structure of a bacterial L-amino acid oxidase from Rhodococcus opacus gives new evidence for the hydride mechanism for dehydrogenation, *J Mol Biol 367*, 234-248.
306. Pawelek, P. D., Cheah, J., Coulombe, R., Macheroux, P., Ghisla, S., and Vrielink, A. (2000) The structure of L-amino acid oxidase reveals the substrate trajectory into an enantiomerically conserved active site, *Embo J 19*, 4204-4215.

307. Tan, T. C., Pitsawong, W., Wongnate, T., Spadiut, O., Haltrich, D., Chaiyen, P., and Divne, C. (2010) H-bonding and positive charge at the N5/O4 locus are critical for covalent flavin attachment in trametes pyranose 2-oxidase, *J Mol Biol 402*, 578-594.
308. Gadda, G. (2012) Oxygen activation in flavoprotein oxidases: the importance of being positive, *Biochemistry 51*, 2662-2669.
309. Klemm, A., Steiner, T., Flotgen, U., Cumme, G. A., and Horn, A. (1997) Determination, purification, and characterization of alpha-NADH and alpha-NADPH, *Methods Enzymol 280*, 171-186.
310. Freire, E., Mayorga, O. L., and Straume, M. (1990) Isothermal Titration Calorimetry, *Anal Chem 62*, A950-A959.
311. Pfleiderer, v.-G., and Woenckhaus, C. (1965) alpha-Nicotinamid-adenin-dinucletid, *Ann Chem 690*, 170-175.
312. Suzuki, K., Nakano, H., and Suzuki, S. (1967) Natural occurrence and enzymatic synthesis of alpha-nicotinamide adenine dinucleotide phosphate, *J Biol Chem 242*, 3319-3325.
313. Neumann, J. M., Borrel, J., Thiery, J. M., Guschlbauer, W., and Tran-Dinh, S. (1977) PMR-relaxation and steric computations give unequivocal nucleoside conformations, *Biochim Biophys Acta 479*, 427-440.
314. Fujimoto, S., Asano, T., Sakai, M., Sakurai, K., Takagi, D., Yoshimoto, N., and Itoh, T. (2001) Mechanisms of hydrogen peroxide-induced relaxation in rabbit mesenteric small artery, *Eur J Pharmacol 412*, 291-300.
315. Miura, H., Bosnjak, J. J., Ning, G., Saito, T., Miura, M., and Gutterman, D. D. (2003) Role for hydrogen peroxide in flow-induced dilation of human coronary arterioles, *Circ Res 92*, e31-40.
316. Kokusho, Y., Komaru, T., Takeda, S., Takahashi, K., Koshida, R., Shirato, K., and Shimokawa, H. (2007) Hydrogen peroxide derived from beating heart mediates coronary microvascular dilation during tachycardia, *Arterioscler Thromb Vasc Biol 27*, 1057-1063.
317. Weir, M. R., and Dzau, V. J. (1999) The renin-angiotensin-aldosterone system: a specific target for hypertension management, *Am J Hypertens 12*, 205S-213S.
318. Boyer, R. F. (1977) A spectrophotometric assay of polyphenoloxidase activity. A special project in enzyme characterization, *J Chem Educ 54*, 585-586.
319. Beaupre, B. A., Carmichael, B. R., Hoag, M. R., Shah, D. D., and Moran, G. R. (2013) Renalase is an α-NAD(P)H Oxidase/Anomerase, *J. Am. Chem. Soc. In press*.
320. Massey, V. (1990) A Simple Method for the Determination of Redox Potentials, In *Flavins and flavoproteins* (Curti, B., S., R., and G., Z., Eds.), pp 59-66, Walter de Gruyter & Co, New York.
321. Prince, R. C., Linkletter, S. J., and Dutton, P. L. (1981) The thermodynamic properties of some commonly used oxidation-reduction mediators, inhibitors and dyes, as determined by polarography, *Biochim Biophys Acta 635*, 132-148.
322. Strickland, S., Palmer, G., and Massey, V. (1975) Determination of dissociation constants and specific rate constants of enzyme-substrate (or protein-ligand) interactions from rapid reaction kinetic data, *J.Biol.Chem. 250*, 4048-4052.
323. Crozier-Reabe, K. R., Phillips, R. S., and Moran, G. R. (2008) Kynurenine 3-monooxygenase from Pseudomonas fluorescens: substrate-like inhibitors both

stimulate flavin reduction and stabilize the flavin-peroxo intermediate yet result in the production of hydrogen peroxide, *Biochemistry 47*, 12420-12433.
324. Moran, G. R., Entsch, B., Palfey, B. A., and Ballou, D. P. (1997) Electrostatic effects on substrate activation in para-hydroxybenzoate hydroxylase: studies of the mutant lysine 297 methionine, *Biochemistry 36*, 7548-7556.
325. Valton, J., Mathevon, C., Fontecave, M., Niviere, V., and Ballou, D. P. (2008) Mechanism and regulation of the Two-component FMN-dependent monooxygenase ActVA-ActVB from Streptomyces coelicolor, *J Biol Chem 283*, 10287-10296.
326. Creeke, P. I., Dibari, F., Cheung, E., van den Briel, T., Kyroussis, E., and Seal, A. J. (2007) Whole blood NAD and NADP concentrations are not depressed in subjects with clinical pellagra, *J Nutr 137*, 2013-2017.
327. Pai, E. F., and Schulz, G. E. (1983) The catalytic mechanism of glutathione reductase as derived from x-ray diffraction analyses of reaction intermediates, *J Biol Chem 258*, 1752-1757.
328. Fedchenko, V., Globa, A., Buneeva, O., and Medvedev, A. (2013) Renalase mRNA levels in the brain, heart, and kidneys of spontaneously hypertensive rats with moderate and high hypertension, *Med Sci Monit Basic Res 19*, 267-270.
329. Malyszko, J., Koc-Zorawska, E., Malyszko, J. S., Kozminski, P., Zbroch, E., and Mysliwiec, M. (2012) Renalase, stroke, and hypertension in hemodialyzed patients, *Ren Fail 34*, 727-731.
330. Guo, X., Wang, L., Velazquez, H., Safirstein, R., and Desir, G. V. (2014) Renalase: its role as a cytokine, and an update on its association with type 1 diabetes and ischemic stroke, *Curr Opin Nephrol Hypertens 23*, 513-518.
331. Dziedzic, M., Petkowicz, B., Bednarek-Skublewska, A., Solski, J., Buczaj, A., and Choina, P. (2014) Relationship between renalase and N-terminal pro-B-type natriuretic peptide (NT pro-BNP) in haemodialysis patients, *Ann Agric Environ Med 21*, 132-135.
332. Wang, S., Lu, X., Yang, J., Wang, H., Chen, C., Han, Y., Ren, H., Zheng, S., He, D., Zhou, L., Asico, L. D., Wang, W. E., Jose, P. A., and Zeng, C. (2014) Regulation of renalase expression by D5 dopamine receptors in rat renal proximal tubule cells, *Am J Physiol Renal Physiol 306*, F588-596.
333. Oppenheimer, N. J., and Kaplan, N. O. (1975) The alpha beta epimerization of reduced nicotinamide adenine dinucleotide, *Arch Biochem Biophys 166*, 526-535.
334. Pace, N. C., Vajdos, F., Fee, L., Grimsley, G., and Gray, T. (1995) How to measure and predict the molar absorption coefficient of a protein, *Prot.Sci. 4*, 2411-2423.
335. Cheng, Y., and Prusoff, W. H. (1973) Relationship between the inhibition constant (K1) and the concentration of inhibitor which causes 50 per cent inhibition (I50) of an enzymatic reaction, *Biochem Pharmacol 22*, 3099-3108.
336. Cortes, A., Cascante, M., Cardenas, M. L., and Cornish-Bowden, A. (2001) Relationships between inhibition constants, inhibitor concentrations for 50% inhibition and types of inhibition: new ways of analysing data, *Biochem J 357*, 263-268.
337. Biellmann, J. F., Lapinte, C., Haid, E., and Weimann, G. (1979) Structure of lactate dehydrogenase inhibitor generated from coenzyme, *Biochemistry 18*, 1212-1217.

338. Wenz, I., Loesche, W., Till, U., Petermann, H., and Horn, A. (1976) Purification and characterization of commercial NADH and accompanying dehydrogenase inhibitors, *J Chromatogr 120*, 187-196.
339. Godtfredsen, S. E., and Ottesen, M. (1978) 1,6-Dihydro-NAD as an Humidity-Induced Lactate Dehydrogenase Inhibitor in NADH Preparations, *Carlesberg Research Communications 43*, 171-175.
340. Mathews, M. B., and Conn, E. E. (1953) The Reaction of Diphosphopyridine Nucleotide with Sodium Borohydride, *Journal of the American Chemical Society 75*, 5428-5430.
341. Godtfredsen, S. E., Ottesen, M., and Andersen, N. R. (1979) On the Mode of Formation of 1,6-Dihydro-NAD in NADH Preparations, *Carlesberg Research Communications 44*, 65-75.
342. Koc-Zorawska, E., Malyszko, J., Zbroch, E., and Mysliwiec, M. (2012) Vascular adhesion protein-1 and renalase in regard to diabetes in hemodialysis patients, *Arch Med Sci 8*, 1048-1052.
343. Napolitano, A., Manini, P., and d'Ischia, M. (2011) Oxidation chemistry of catecholamines and neuronal degeneration: an update, *Curr Med Chem 18*, 1832-1845.
344. Wang, J., Qi, S., Cheng, W., Li, L., Wang, F., Li, Y. Z., and Zhang, S. P. (2008) Identification, expression and tissue distribution of a renalase homologue from mouse, *Mol Biol Rep 35*, 613-620.
345. Birchfield, N. B., Latli, B., and Casida, J. E. (1998) Human protoporphyrinogen oxidase: Relation between the herbicide binding site and the flavin cofactor, *Biochemistry 37*, 6905-6910.
346. Mizutani, H., Miyahara, I., Hirotsu, K., Nishina, Y., Shiga, K., Setoyama, C., and Miura, R. (1996) Three-dimensional structure of porcine kidney D-amino acid oxidase at 3.0 Å resolution, *J.Biochem. 120*, 14-17.
347. Beaupre, B. A., Carmichael, B. R., Hoag, M. R., Shah, D. D., and Moran, G. R. (2013) Renalase Is an alpha-NAD(P)H Oxidase/Anomerase (JACS Spotlight Article), *Journal of the American Chemical Society 135*, 13980-13987.
348. Otwinowski, Z., and Minor, W. (1997) Processing of X-ray diffraction data collection in oscillation mode., *Methods Enzymol 276*, 307-325.
349. McCoy, A. J., Grosse-Kunstleve, R. W., Adams, P. D., Winn, M. D., Storoni, L. C., and Read, R. J. (2007) Phaser crystallographic software, *Journal of applied crystallography 40*, 658-674.
350. Emsley, P., Lohkamp, B., Scott, W. G., and Cowtan, K. (2010) Features and development of Coot, *Acta crystallographica. Section D, Biological crystallography 66*, 486-501.
351. Afonine, P. V., Mustyakimov, M., Grosse-Kunstleve, R. W., Moriarty, N. W., Langan, P., and Adams, P. D. (2010) Joint X-ray and neutron refinement with phenix.refine, *Acta crystallographica. Section D, Biological crystallography 66*, 1153-1163.
352. Word, J. M., Lovell, S. C., Richardson, J. S., and Richardson, D. C. (1999) Asparagine and glutamine: using hydrogen atom contacts in the choice of side-chain amide orientation, *J Mol Biol 285*, 1735-1747.
353. Urzhumtseva, L., Afonine, P. V., Adams, P. D., and Urzhumtsev, A. (2009) Crystallographic model quality at a glance, *Acta Crystallogr D 65*, 297-300.

354. Chen, V. B., Arendall, W. B., 3rd, Headd, J. J., Keedy, D. A., Immormino, R. M., Kapral, G. J., Murray, L. W., Richardson, J. S., and Richardson, D. C. (2010) MolProbity: all-atom structure validation for macromolecular crystallography, *Acta crystallographica. Section D, Biological crystallography 66*, 12-21.
355. Karplus, P. A., and Schulz, G. E. (1987) Refined structure of glutathione reductase at 1.54 A resolution, *J Mol Biol 195*, 701-729.
356. Malyszko, J., Malyszko, J. S., Rysz, J., Mysliwiec, M., Tesar, V., Levin-Iaina, N., and Banach, M. (2013) Renalase, hypertension, and kidney - the discussion continues, *Angiology 64*, 181-187.
357. Malyszko, J., Bachorzewska-Gajewska, H., and Dobrzycki, S. (2014) Renalase, kidney and cardiovascular disease: Are they related or just coincidentally associated?, *Adv Med Sci 60*, 41-49.
358. Moran, G. R. (2015) The Catalytic Function of Renalase: A Decade of Phantoms, *Biochim Biophys Acta in press*.
359. Entsch, B., Massey, V., and Ballou, D. P. (1974) Intermediates in flavoprotein catalyzed hydroxylations, *Biochem Biophys Res Commun 57*, 1018-1025.
360. Crozier-Reabe, K., and Moran, G. R. (2012) Form follows function: structural and catalytic variation in the class a flavoprotein monooxygenases, *Int J Mol Sci 13*, 15601-15639.

Brett A. Beaupre

Curriculum Vitea

Education

Doctorate of Philosophy in Chemistry (Ph D) *Expected Graduation: 21 June 2016*
University of Wisconsin-Milwaukee
Thesis: The Catalytic Function of Renalase
Major: Biochemistry Minor: Organic Chemistry

Bachelor of Science (BS) *December 2012*
University of Wisconsin-Milwaukee
Major: Biochemistry

Bachelor of Business Administration (BBA) December 2009
University of Wisconsin-Milwaukee
Major: Finance

Publications

1. **Beaupre BA,** Hoag MR, MoranGR, Renalase does not Catalyze the Oxidation of Catecholamines. Arch Biochem Biophys. 2015 Jun 3; 579:62-6

2. **Beaupre BA**, Hoag MR, Roman J, Försterling FH, Moran GR. *Metabolic Function for Human Renalase: Oxidation of Isomeric Forms of β-NAD(P)H that Are Inhibitory to Primary Metabolism.* Biochemistry. 2015 Jan 8.

3. Hoag MR, Roman J, **Beaupre BA**, Silvaggi NR, Moran GR. *Bacterial Renalase; Structure and Kinetics of an Enzyme with 2- and 6-Dihydro-b-NAD(P) Oxidase Activity from Pseudomonas phadeolicola.*

4. **Beaupre BA**, Hoag MR, Carmichael BR, Moran GR. *Kinetics and Equilibria of the Reductive and Oxidative Half-reactions of Human Renalase with α-NADPH.* Biochemistry. 2013 Dec 10;52(49):8929-37.

5. **Beaupre BA**, Carmichael BR, Hoag MR, Shah DD, Moran GR. *Renalase is an α-NAD(P)H Oxidase/anomerase.* J Am Chem Soc. 2013 Sep 18;135(37):13980-7

Research Experience

University of Wisconsin-Milwaukee *May 2014-present*
Research Assistant

- Responsible for carrying out enzyme purification and expression, large-scale culture preparation and various types of column chromatography.
- Designed methods for analytical separation, quantification, purification and identification using high-pressure liquid chromatography (HPLC), absorbance spectroscopy, florescence spectroscopy, isothermal calorimetric (ITC), mass spectrometry (MS, MS-MS) and nuclear magnetic resonance (1D, COSY, HETCORE, HMBC).
- Molecular biology experience in electroporation, transformation, site-directed mutagenesis, and polymerase chain reactions (PCR).
- Measured enzyme kinetics using stopped-flow spectroscopy and designed methods of measurement using controlled molecular oxygen concentrations.
- Collaborate with others in a larger study that will provide the manuscript for catalytic activity of specific enzymes.

University of Wisconsin-Milwaukee *December 2011- July 2012*
Research Assistant - Consultant

- Measured enzyme kinetics using UV spectroscopy and dissolved oxygen.
- Responsible for designing experiments to measure enzyme inhibition using multiple biochemical techniques

National Sea Grant College Program of Wisconsin
Invasive Species Monitoring *May 2008- August 2009*

- Responsible for enforcing DNR recreational vehicle guidelines for proper invasive species sanitation.
- Independently responsible for collecting and reporting numerical samples for invasive species research.

Teaching Experience

University of Wisconsin-Milwaukee *August 2012- May 2014*
Teaching Assistant

- Chemistry 501, Intro to Biochemistry
- Chemistry 603, Biochemistry Lab
- Chemistry 102, General Chemistry I
- Chemistry 102, General Chemistry Lab I

A**wards**

- Outstanding Graduate Student Award — Spring 2016
- UW-Milwaukee Chancellors Graduate Award — August 2012 - May 2014
- Support for Undergraduate Research (SURF) — *May 2012 – August 2012*

Conferences & Activities

- **Enzyme Mechanisms Conference.** Galveston, TX — *January, 2015*
  Presented research poster

- **Midwest Enzyme Chemistry Conference.** Chicago, IL — *October 2014*
  Presented research poster

- **Young Chemists Committee.** Milwaukee, WI — *November 2013*
  Presented research

- **Midwest Enzyme Chemistry Conference.** Chicago, IL — *October 2013*
  Presented research poster